Université Pierre et Marie Curie

Ecole doctorale n°138

- Cerveau Cognition comportement -

Institut du Fer à Moulin, équipe « Plasticité des réseaux corticaux et épilepsie »

Rôle du transporteur neuronal Potassium/Chlore KCC2 dans la plasticité des synapses glutamatergiques

Involvement of the neuronal K/Cl cotransporter KCC2 in the plasticity of glutamatergic synapses

Par Quentin Chevy

Thèse de doctorat de Neurosciences

Dirigée par Jean-Christophe Poncer

Présentée et soutenue publiquement le 16 janvier 2015

Devant un jury composé de :

Dr David DiGregorio	Président du Jury
Pr Colin Akerman	Rapporteur
Pr José Esteban	Rapporteur
Dr Gilles Huberfeld	Examinateur
Dr Nathalie Sans	Examinateur
Dr Jean-Christophe Poncer	Directeur de thèse

ABSTRACT

The polarity and efficacy of GABAergic synaptic transmission are both influenced by the intra-neuronal chloride concentration. In mature neurons, chloride extrusion through the neuronal K/Cl cotransporter KCC2 allows an inhibitory influx of chloride upon activation of $GABA_A$ receptors. Nevertheless, KCC2 is enriched in the vicinity of excitatory synapses within the dendritic spines that are actin-rich protrusions emerging from dendritic shafts. Expression of KCC2 is tightly regulated throughout development and by both normal and pathological neuronal activities. Thus, KCC2 expression is strongly inhibited in a variety of neurological disorders. While it has become clear that KCC2 suppression alters chloride homeostasis and GABA signaling, little is known on its impact on glutamatergic transmission. In the laboratory, we have previously demonstrated that KCC2 suppression in mature neurons leads to decreased glutamatergic transmission efficacy through an ion-transport independent function of KCC2. During my PhD, I have explored how KCC2 may also impact LTP of glutamatergic synapses. My work reveals that KCC2 suppression compromises both functional and structural LTP at these synapses. This effect is associated with inhibition of the actin-severing protein cofilin and enhanced mobilization of F-actin in dendritic spines. Since LTP can be rescued by preventing cofilin inhibition upon KCC2 suppression, I suggest KCC2 might influence LTP through altered actin cytoskeleton dynamics. My results demonstrate that KCC2 function extends beyond the mere control of neuronal chloride homoeostasis and suggest regulation of KCC2 membrane stability may act as a metaplastic switch to gate long term plasticity at excitatory synapses in cortical neurons.

RÉSUMÉ

La polarité et l'efficacité de la transmission synaptique GABAergique sont influencées par la concentration intracellulaire en ions chlorure. Dans les neurones matures, l'extrusion de ces ions par le transporteur neuronal potassium chlore de type 2 (KCC2) permet l'influx d'ions chlorure lors de l'activation des récepteurs du GABA de type A. Néanmoins, KCC2 est également enrichi à proximité des synapses excitatrices portées par les épines dendritiques qui correspondent à des protrusions dendritiques enrichies en actine. De plus, l'expression de KCC2 est finement régulée lors du développement et par l'activité neuronale, aussi bien physiologique que pathologique. L'expression de ce transporteur a ainsi été observée comme étant inhibée dans différentes pathologies neurologiques. Alors que l'effet d'une suppression de KCC2 sur l'homéostasie neuronale des ions chlorure et la transmission GABAergique est largement documenté, peu de choses sont connues sur l'impact qu'une telle suppression peut avoir sur la transmission glutamatergique. Au laboratoire, nous avons précédemment démontré que la suppression de KCC2 dans des neurones matures entraine une diminution de l'efficacité de la transmission glutamatergique par un mécanisme indépendant de la fonction de KCC2. Lors de ma thèse, j'ai exploré le rôle de ce mécanisme dans la potentialisation à long terme (LTP) de la transmission glutamatergique à l'origine des phénomènes d'apprentissage et de mémorisation. Ce travail a révélé que la suppression de KCC2 compromet les modifications fonctionnelles et structurales sous-tendant la LTP. Cet effet est associé à une inhibition de la cofilin, protéine responsable de la dépolymérisation de l'actine, qui corrèle avec une augmentation de la quantité d'actine filamenteuse dans les épines dendritiques. En empêchant l'inhibition de la cofilin liée à l'absence de KCC2, il m'a alors été possible de restaurer la LTP suggérant que KCC2 pourrait influencer cette forme de plasticité en régulant la dynamique de polymérisation du cytosquelette d'actine. Mes résultats démontrent que la fonction de KCC2 va au-delà du contrôle de l'homéostasie des ions chlorure et suggèrent que la régulation de la stabilité membranaire de ce transporteur pourrait influencer les mécanismes de plasticité à long terme de la synapse excitatrice.

TABLE OF CONTENTS

TABLE OF FIGURES

ABBREVIATIONS

2PLSM	Two-photon laser-scanning microscope
aCSF	Artificial cerebrospinal fluid
AIS	Axon initial segment
AKAP	A-kinase anchor proteins
AMPAR	α-Amino-3-hydroxy-5-methyl-4-isoxazolepropionic acid receptor
AP-2	Adaptator protein-2
Arc	Activity-regulated cytoskeleton-associated protein
BDNF	Brain-derived neurotrophic factor
Beta-PIX	Beta-PAK interacting exchange factor
CaMKII	Ca2+/Calmoduline Kinase II
CCC	Chloride co-transporters
CIP1	CCC-interacting protein 1
CKB	Brain-type creatine kinase
CLSM	Confocal light-scanning microscope
cLTP	Chemical LTP
CNS	Central nervous system
CREB	C-AMP Response Element-binding protein
CTD	Carboxy terminal domain
Egr4	Early growth response transcription factor 4
EPSC	Excitatory postsynaptic currents
EPSP	Excitatory post synaptic potential
ERK	Extracellular signal-regulated kinase
F-actin	Filamentous actin
FERM	Four.one, Ezrin, Radixin, Moesin
FLIM	Fluorescence lifetime imaging microscopy
FRAP	Fluorescence recovery after photobleaching
FRET	Förster Resonant Energy Transfer
FRS-2	FGF receptor substrate 2
FWHM	Full width at half maximum
GABA	γ-Amino Butyric Acid
GABAAR	Receptor subtype A for GABA
F/G-actin	Filamentous/Globular-actin
GDPs	Giant depolarization potentials
GEF	Guanine-nucleotide-exchange factors
GFP	Green fluorescent protein
GIT1	G protein-coupled receptor kinase-interacting protein1
GlyR	Glycine receptor
GRIP	Glutamate Receptor Interacting Proteins
HFS	High frequency stimulation
iGluR	Ionotropic glutamate receptor
IPSC	Inhibitory postsynaptic current
IPSP	Inhibitory post synaptic potential
KB	Ketone body
KCC	K+/Cl- co-transporters

LIMK	Lin-11, Isl-1, and Mec-3 Kinase
LIMKi	LIMK inhibitor
LTD	Long term depression
LTP	Long term potentiation
MAGUK	Membrane-associated guanylate kinase proteins
mGluR	Metabotropic glutamate receptor
MSD	Mean square displacement
NA	Numerical aperture
NCC	Na+/Cl- co-transporter
Neto2	Neuropilin and tolooid like-2 protein
NKCC	Na+/K+/Cl- co-transporters
NMDAR	N-methyl-D-Aspartate receptor
NRSE	Neuron-restrictive silencing elements
NSF	N-ethylmaleimide-sensitive factor
NTD	Amino terminal domain
OSR1	Oxidative stress-responsive kinase-1
PAK	p21-activated kinase
PAM	Protein associated with Myc
PICK1	Protein Interacting with C-Kinase 1
PKA	Protein kinase A
PKC	Protein kinase C
PLCγ	Phospholipase C gamma
PP	Protein phosphatases
PSD	Postsynaptic density
PSF	Point-spread function
RCC1	Regulator of Chromatin Condensation
ROCK	RhoA-specific kinase
SCI	Spinal cord injury
SEP	SuperEcliptic pHluorin
Sh3	SRC homology domain 3
Shc	SRC homology 2 domain containing transforming protein
shRNA	Short-hairpin RNA
SNARE	Soluble N-ethylmaleimide-sensitive-factor attachment protein Receptor
SPAK	Ste20p-related proline/alanine-rich kinase
STDP	Spike timing dependent plasticity
STED	Stimulated Emission Depletion
TARP	Transmembrane AMPAR regulatory proteins
TEA	Tetraethylamonium
Tiam1	T-cell lymphoma invasion and metastasis 1
TIRF	Total internal reflection fluorescence
TLE	Temporal lobe epilepsies
TMS	Transmembrane segments
TrKB	Tropomyosin receptor kinase B
TTX	Tetrodotoxin
uEPSC	Uncaging-induced excitatory postsynaptic current
VDCC	Voltage-dependent Ca2+ channels
WNK	With no lysine

INTRODUCTION

INTRODUCTION

In the central nervous system (CNS), information processing relies on temporally organized emission of action potentials by neurons. Action potential firing allows fast propagation of information between synaptically connected neurons. Synaptic activity may then promote or inhibit postsynaptic neuronal activity depending of the neurotransmitter released by the presynaptic neuron. In the mature CNS, synaptic activation of glutamate-gated channels promotes action potential emission whereas release of γ-Amino Butyric Acid (GABA) or glycine usually inhibits postsynaptic neuronal firing (Figure 1).

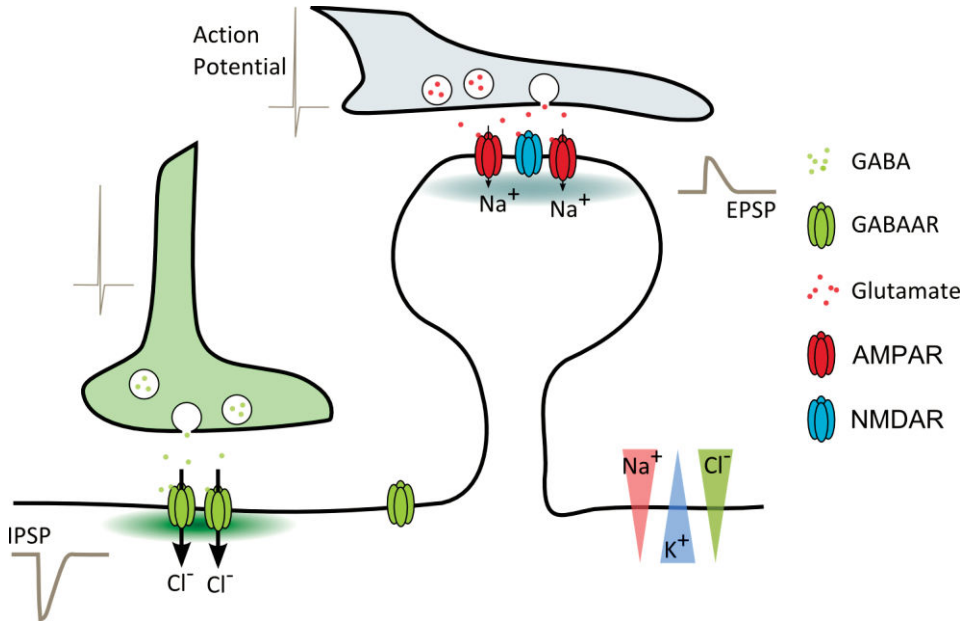

Figure 1 Central nervous system inhibitory and glutamatergic synapses
Opening of GABA-gated channels, GABAARs, leads to a hyperpolarizing current induced by chloride influx. Glutamatergic synapses are found in a bulbous membrane protrusion called dendritic spine. In basal conditions, action potential-dependent glutamate release from presynaptic terminals leads to the opening of AMPARs and to a depolarizing influx of sodium. Note the respective electrochemical gradients of Na^+, K^+ and Cl^- on the bottom right of the figure. (IPSP & EPSP: inhibitory & excitatory post synaptic potential).

Synaptic inhibition and excitation or action potential emission by neurons arise from the particular electrical properties of neurons. At rest (V_{rest}), the neuronal cytoplasmic membrane is electrically polarized with a net negative charge on the inside of the membrane. An action potential corresponds to an abrupt depolarization in the membrane potential due to activation of voltage-gated sodium channels once the membrane potential exceeds their

activation threshold. Fast excitatory transmission results from glutamate receptor activation and is mediated by a net depolarizing influx of cations (Na^+, Ca^{2+}) through the membrane, that underlie excitatory postsynaptic currents (EPSCs). On the other hand, ionotropic receptor subtype A for GABA (GABAAR) or Glycine receptor (GlyR) activation mediates both an electrical shunting due to an increased membrane conductance and a net hyperpolarizing influx of anions (inhibitory postsynaptic current, IPSC) which prevent action potential emission (Figure 1).

The direction of ion fluxes relies on the ability of neurons to maintain electrochemical ion gradients across their membrane (Figure 2). Intraneuronal K^+ and Na^+ concentrations are respectively maintained high and low primarily by the Na/K ATPase pump. Na/K ATPase pump together with leak potassium conductances greatly participates to the generation and the maintenance of V_{rest}. Neuronal chloride homeostasis is mainly regulated by two secondary active cation chloride co-transporters (CCC), the Na/K/Cl cotransporter NKCC1 and the K/Cl cotransporter KCC2. These transporters use the Na^+ and K^+ electrochemical gradients to respectively load and extrude chloride from the cell. In most mature neurons, KCC2 activity is larger than NKCC1 activity resulting in a low intraneuronal chloride concentration. This predominant KCC2 activity accounts for the hyperpolarizing response upon synaptic GABAAR activation. Hence, changes in the activity of these transporters directly impact synaptic transmission and have been involved in various pathological conditions.

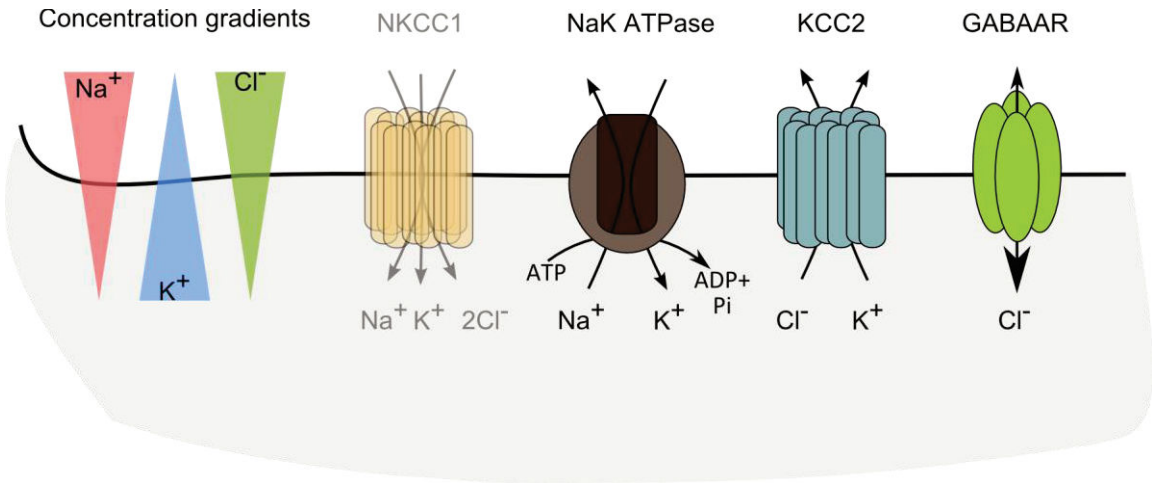

Figure 2 Chloride influx through GABAARs is influenced by CCC activity
KCC2 extrudes chloride from the cell using the potassium electrochemical gradient maintained by the NaK ATPase. NKCC1, in contrast, loads chloride into neurons using the electrochemical sodium gradient. In mature neurons, KCC2 function dominates over NKCC1 function leading to low neuronal chloride concentration. Hence, opening of GABAARs leads to a hyperpolarizing influx of chloride.

Nevertheless, modulation of synaptic transmission is also observed under physiological conditions. In several brain structures or neuronal types, synaptic efficacy is modulated in response to neuronal activity. This so-called “synaptic plasticity” includes short term modifications as well as long term- depression (LTD) or potentiation (LTP) of synaptic transmission. Long term changes in synaptic efficacy are thought to represent the molecular basis of learning and memory. LTP of excitatory transmission has been extensively studied and several mechanisms of induction and expression have been proposed. Notably, Ca^{2+} influx via the N-methyl-D-Aspartate receptor (NMDAR) leads to the addition of α-Amino-3-hydroxy-5-methyl-4-isoxazolepropionic acid receptor (AMPAR) in the postsynaptic density (PSD) resulting in an increased response to the same glutamate release. Similarly plasticity of inhibitory transmission may also involve changes in synaptic GABAAR content. In addition modulation of the CCCs activity has been proposed to modulate inhibitory transmission. Interestingly KCC2 function and expression are strongly regulated by neuronal and glutamatergic synaptic activity. Thus, KCC2 may act as a link between plasticity of excitatory glutamatergic and inhibitory GABAergic synapses. Recently, a non-canonical function of KCC2, independent of its chloride transport role, has been identified and shown to directly influence the efficacy of glutamatergic synapses.

My PhD thesis focuses on the interplay between KCC2 and the plasticity of glutamatergic transmission. Before presenting these results in a form of a submitted research article that lies in the center of this manuscript (Chevy et al., submitted), I will introduce the function and the regulation of KCC2 as well as the postsynaptic mechanisms sustaining long term potentiation of the excitatory synapses. The obtained results will then be discussed in the third part of the manuscript.

I. THE K/CL COTRANSPORTER KCC2: A MULTIFUNCTIONAL PROTEIN AT THE CROSS-ROADS BETWEEN EXCITATORY AND INHIBITORY TRANSMISSION

Fast excitatory and inhibitory synaptic transmissions require maintenance of an electrochemical gradient of sodium and chloride respectively. The activity of the Na/K ATPase pump maintains a low intracellular sodium concentration and allows its depolarizing effect while flowing through glutamate-gated channels. On the other hand chloride neuronal concentration is mainly constrained by secondary active **cation chloride co-transporters** that use either the K^+ or Na^+ electrochemical gradient to respectively extrude or load the cell with chloride (Blaesse et al., 2009; Gamba, 2005). Although they will not be described in this manuscript, it should be mentioned that anion exchangers, Na^+ dependent anion exchangers and Chloride Channel family also participate, to some extent, in neuronal chloride homeostasis.

Members of the CCC family, encoded by genes *Slc12a1-9*, are usually categorized in four different subtypes according to the counter ion they use to transport chloride (Figure 2):

- Na^+/Cl^- co-transporter (NCC): expressed selectively in kidney;
- $Na^+/K^+/Cl^-$ co-transporters (NKCC1-2): NKCC1 is the only NKCC found in the CNS;
- K+/Cl- co-transporters (KCC1-4): including the neuronal specific KCC2;
- CIP1 and CC9 with an unknown function.

NKCC1 and KCC2 have been strongly implicated in the maturation of GABAergic transmission (Plotkin et al., 1997; Rivera et al., 1999). Intracellular chloride concentration in **immature neurons** is higher than in mature ones due to a high NKCC1 and low KCC2 expression. This leads to a chloride electrochemical gradient depolarized relative to resting membrane potential. Hence, **GABAAR-mediated synaptic activity depolarizes the cell**. A strong increase in KCC2 expression in **mature neurons** leads to a decrease in intraneuronal chloride concentration and thereby to the appearance of the classical **hyperpolarizing chloride-mediated currents** upon GABAAR opening (Figure 3).

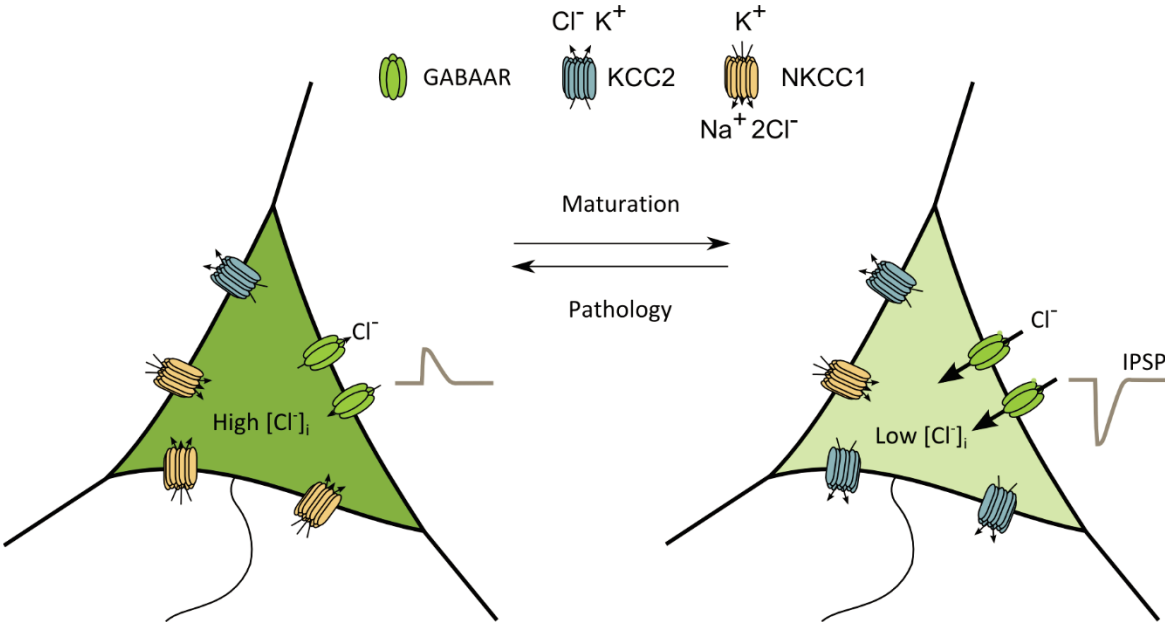

Figure 3 Maturation of GABAergic transmission is mediated by changes in CCC expression
In immature or pathological neurons (left), high NKCC1 expression and low KCC2 expression result in decreased chloride gradient such that GABAergic transmission may be depolarizing. In mature neurons (right), the low neuronal chloride concentration is due to an increase in KCC2 expression that extrudes chloride from the cell. Chloride influx through GABARs would then hyperpolarize the neuron.

Moreover KCC2 expression and function are rapidly modulated by physiological and pathophysiological activities (Chamma et al., 2013; Lee et al., 2011). Recent evidence links KCC2 to glutamatergic transmission through a non-canonical mechanism: in addition to its transport function, KCC2 interacts with several proteins, some of them being critical for glutamatergic synapse development and function.

Historically, Thompson et al. made the first observation that intraneuronal concentration of chloride was lower than what a passive distribution of this ion would predict (Thompson et al., 1988). Hence, they hypothesized the existence of a neuron specific K^+-driven export of chloride specific to neuron. Few years later, Cherubini and Ben-Ari. observed the so-called "developmental switch" of GABAergic transmission polarity, from depolarizing in immature neurons to solely hyperpolarizing at the end of the first postnatal week in the rat hippocampus (Cherubini et al., 1991). Only in the late 90s was KCC2 was identified (Payne, 1997; Payne et al., 1996) and implicated in the maturation and the control of GABAergic transmission (Rivera et al., 1999). Since then, hundreds of research articles have been published exploring the mechanisms of regulation of KCC2 as well as its role in inhibitory transmission and more

recently at the glutamatergic synapse (for reviews Blaesse et al., 2009; Chamma et al., 2012; Kahle et al., 2013; Medina et al., 2014). The loss of this transporter has been suggested to be at the origin of numerous pathological conditions due to subsequent changes in neuronal excitability (for reviews Cellot and Cherubini, 2014; Miles et al., 2012; Payne et al., 2003; Price et al., 2009; Vinay and Jean-Xavier, 2008). The study of this electroneutral transporter and of chloride homeostasis remains technically challenging. Nevertheless, the development of new pharmacological and genetic tools to study the causal impact of its suppression (Gauvain et al., 2011; Hübner et al., 2001; Seja et al., 2012; Tornberg et al., 2005) and the recent identification of KCC2 human mutations (Kahle et al., 2014; Puskarjov et al., 2014a) may help clarify the function of KCC2 in synaptic transmission and pathologies of the CNS.

1. Overview of KCC2 structure and phylogeny

KCC2 belongs to the CCC family. Within the CCC family, only the topology of NKCC1 has been elucidated so far (Gerelsaikhan and Turner, 2000). Despite low sequence homology (Gamba, 2005), KCC2 as well as the other CCCs are predicted to share the same **secondary structure** described for NKCC1. Hence, this structure consists of a 140kDa glycoprotein with 12 transmembrane segments (TMS) with glycosylated extracellular loops (Ding et al., 2013; Williams et al., 1999a) and flanked by a short amino terminal (NTD, amino acids 1-103) and long carboxy terminal domain (CTD, the last 500 amino acids), both intracellular (Figure 4). The long carboxy terminal domain of KCC2 hosts many regulatory sites important for its membrane localization and its functional regulation as well as protein-binding domains. Less is known about the **tertiary structure** of KCC2 due to the lack of a crystallographic model although the carboxy terminal domain of a bacterial CCC has recently been crystallized (Warmuth et al., 2009). As a **quaternary structure**, the functional relevance of KCC2 dimers, as observed in western blot, is still a matter of debate (Medina et al., 2014; Warmuth et al., 2009). Immunocytofluorescence stainings also suggest KCC2 forms clusters in the plasma membrane that could rely on the same mechanisms than those required for oligomerization.

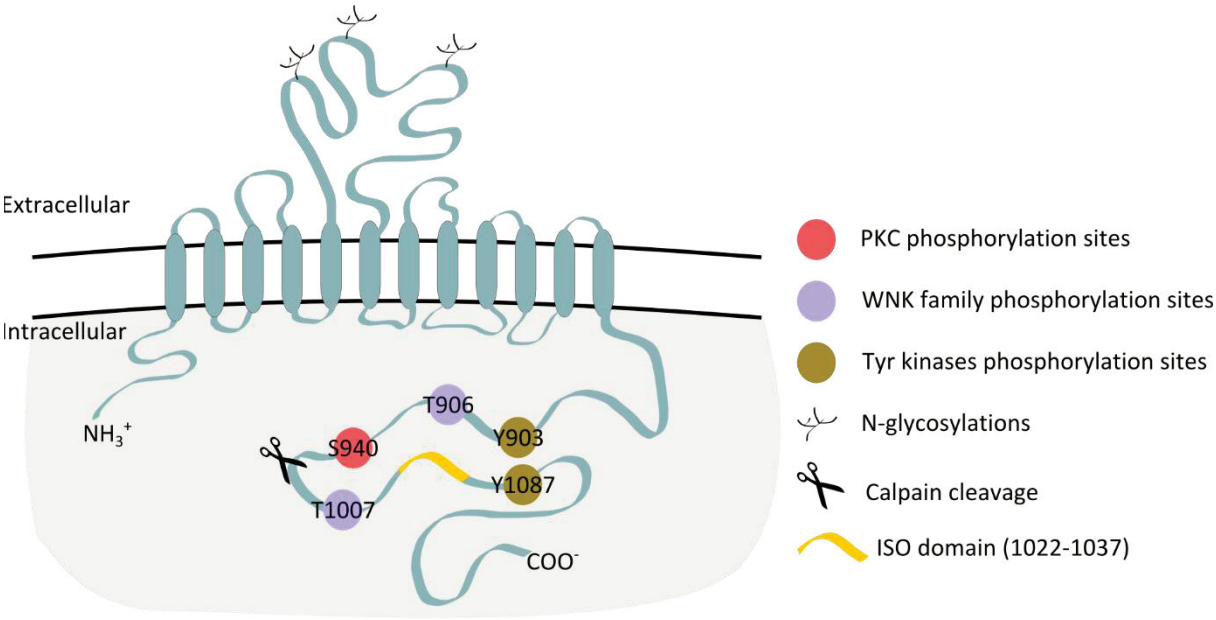

Figure 4 Structure of the transmembrane protein KCC2
Predicted KCC2 secondary structure consists of a glycoprotein with 12 transmembrane segments flanked by a short amino terminal and a long carboxy terminal domain. The carboxy terminal domain of KCC2 hosts many regulatory phosphorylation sites (not exhaustively represented), putative calpain sites between amino acid 929 and 1043 and an ISO domain underpinning the KCC2 function under isotonic condition.

a) Amino terminal domain of KCC2

The two splicing isoforms of KCC2, KCC2a and KCC2b, differ only by their he N-terminus domain (KCC2-NTD) (Uvarov et al., 2007). Specifically, **KCC2a- but not KCC2b-NTD shows a putative phosphorylation site for SPAK/OSR1 kinases** (Uvarov et al., 2007) which are involved in osmotic regulation (see introduction I.2.c). It should be also mentioned that although these two isoforms have similar transport activity, KCC2b expression progressively increases during post-natal development and is predominant over KCC2a expression in mature rodent cortical neurons (>90%). Except when otherwise stated, KCC2 will refer to both isoforms in the following manuscript.

Based on work on KCC2 homologue KCC1 (Casula et al., 2001), the cytosolic KCC2-NTD has been proposed to include residues mandatory for **KCC2 transport function** (Li et al., 2007). Several groups have therefore synthesized and used a nonfunctional, NTD deleted form of KCC2, KCC2-ΔNTD (Fiumelli et al., 2013; Horn et al., 2010; Li et al., 2007). This truncated form was assumed to be non-functional and used to study ion transport-independent role of KCC2 (see introduction I.5).

However, a recent work presented at the 9th FENS Forum (Milano 2014) by the group of Igor Medina as well as personal observations (Figure 5) are questioning the role of KCC2-NTD. Thus, the truncation of the **KCC2-NTD seems to affect primarily KCC2 membrane expression**. Our observations suggest that KCC2-ΔNTD was retained in the endoplasmic reticulum. Experiments using a phluorin-tagged KCC2 (KCC2-SEP that allowed the visualization of the membrane pool of KCC2) performed by the group of Medina described that exocytosis was also altered by the truncation. Among the papers that used KCC2-ΔNTD construct, only Horn et al. verified its expression (Horn et al., 2010). But both the image resolution and the presence of potential endogenous KCC2 make these observations difficult to interpret. Thus, the exact role of KCC2-NTD in function and trafficking of KCC2 needs more investigation.

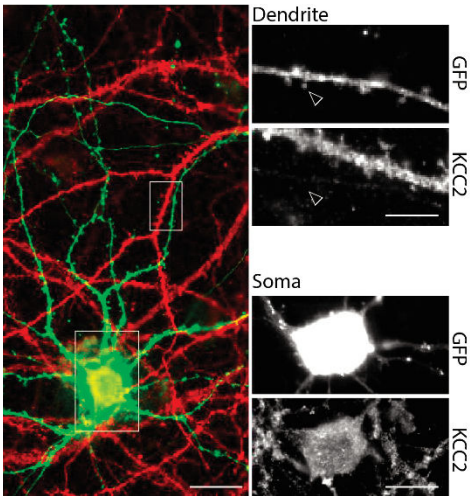

Figure 5 Deletion of KCC2-NTD impacts its expression in hippocampal neurons
Endogenous KCC2 was suppressed by RNA interference (shKCC2). 21 DIV hippocampal neurons were co-transfected with an shRNA-proof, N-terminal deleted KCC2, shKCC2 and GFP (green). No KCC2 immunoreactivity was detected in dendrites (red; empty arrow head). Note the immunoreactivity of KCC2-ΔNTD in the soma, potentially trapped in intracellular compartments. (Scale, left: 10µm, right: 5µm and 5µm)

b) Carboxy terminal domain of KCC2: home sweet home of regulation sites and protein interactions.

The cytosolic carboxy terminal domain of KCC2 (KCC2-CTD) contains both inhibitory and excitatory regulation sites as well as protein-protein interaction domains.

- The **complete truncation of KCC-CTD** has been shown to abolish membrane expression of KCC1 (Casula et al., 2001), KCC2 (Payne, 1997) and KCC3 (Howard et al., 2002). In addition, during sustained neuronal activity, partial truncation of KCC2-CTD by the Ca^{2+}-dependent protease calpain leads to KCC2 internalization (Puskarjov et al., 2012; Zhou et al., 2012).

Moreover, using an extracellular tagged-KCC2, Zhao et al. showed that KCC2 undergoes a constitutive dynamin-dependent clathrin-mediated endocytosis due to an interaction between its carboxy terminal domain and the clathrin-binding adaptator protein-2 (AP-2) (Zhao et al., 2008).

- KCC2-CTD also hosts phosphorylatable residues that are involved in both membrane expression and KCC2 transport function (Figure 4). Among them, **phosphorylation of Ser940 by the protein kinase C** (PKC) has been described to increase KCC2 activity and membrane stability through decreased endocytosis (Bos et al., 2013; Lee et al., 2007, 2011). **Thr906 and Thr1007** residues are substrates for With No Lysine (WNK) Kinases and/or Ste20p-related proline/Alanine-rich kinase (SPAK) as well as oxidative stress-responsive kinase-1 (OSR1) (de Los Heros et al., 2014) which are thought to represent a pathway for cellular volume regulation (see introduction: I.2.c). Finally, the **Tyr903 and Tyr1087** residues are targeted by yet unidentified tyrosine kinases (Lee et al., 2010a). Using phospho-mimetic (Y1087D) or dephosphorylated-like mutants (Y1087F) investigators have shown that the phosphorylation of Tyr1087 inactivates KCC2 in heterologous systems (Strange et al., 2000; Watanabe et al., 2009) and in neurons (Akerman and Cline, 2006; Chudotvorova et al., 2005; Pellegrino et al., 2011) without affecting its membrane expression.

- KCCs activity appears to increase following swelling of red blood cells and have therefore been described as swelling-activated K^+ efflux transporters. Interestingly KCC2, which is absent from red blood cells, is the only CCC that elicits a transport activity at **isotonic conditions**. A short amino-acid sequence (1022-1037) in the KCC2-CTD is thought to confer this specific feature (Acton et al., 2012; Mercado et al., 2006). This “ISO domain” is however not sufficient alone to confer isotonic activity to KCC4 and is not involved in swelling-induced activation of KCC2. The mechanisms conferring this particular isotonic activity remain to be explored although putative targets for serine kinases have been identified within the ISO-sequence (Figure 4).

- KCC2 **interacts with numerous proteins** through its long carboxy terminal domain (Figure 6). Specifically, KCC2-CTD binds the FERM domain of the **actin-interacting protein 4.1N** as shown by co-immunoprecipitation assays (Li et al., 2007). This interaction is thought to be

relevant for spinogenesis (Li et al., 2007), AMPAR (Gauvain et al., 2011) and KCC2 diffusions (Chamma et al., 2013). More recently, the team of Claudio Rivera described a direct interaction between KCC2 and the beta isoform of the Rac/PAK guanine nucleotide exchange factor, Beta-PIX (Medina et al., 2014). **Beta-PIX** is involved in a molecular cascade which regulates actin polymerization (Bosch et al., 2014; Okamoto et al., 2009; Saneyoshi et al., 2010) (see introduction I.5 and II.3.c) for complementary information on 4.1N and Beta-Pix).

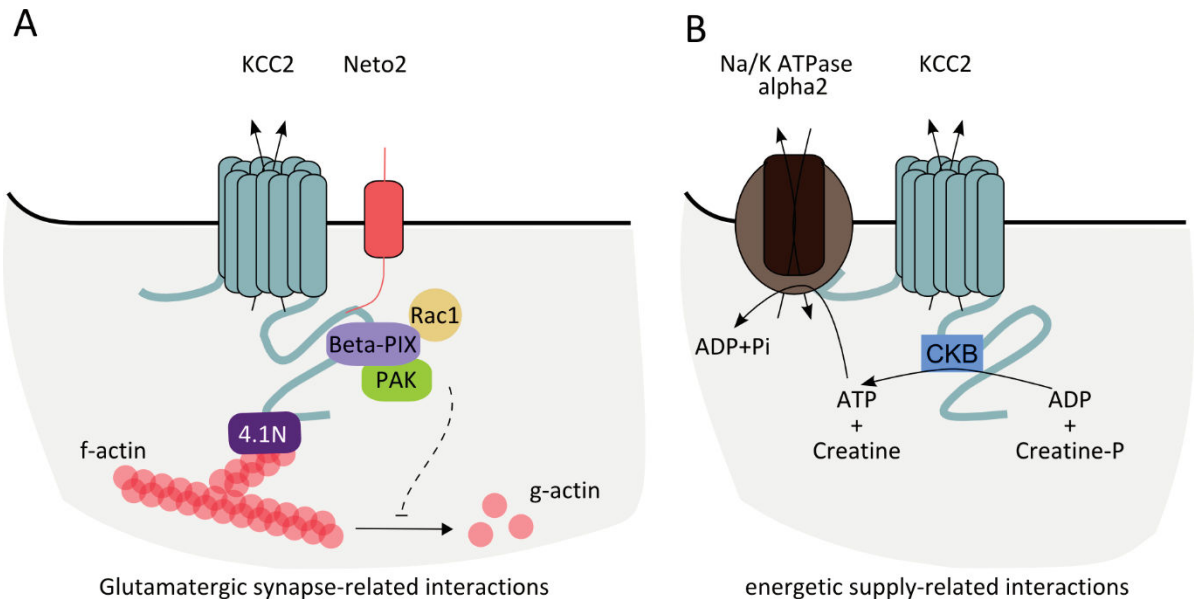

Figure 6 KCC2 interactome
KCC2 is involved in several putative macrocomplexes. (A) KCC2-CTD interacts with the kainate receptor-related protein Neto2 and with actin-interacting protein 4.1N. A 4.1N-Kainate receptor interaction has also been described (not represented). The newly described KCC2-Beta-PIX interaction is thought to affect actin polymerization. (B) KCC2 interacts with the alpha2 subunit of the Na/K ATPase and with the brain-type creatine kinase (CKB). These interactions are thought to increase the energetic coupling between primary and secondary-types of active transporters as well as to promote ATP replenishment.

In addition, a **KCC2-Neto2** (neuropilin and tolooid like-2 protein) interaction has been described and may be required for normal KCC2 membrane expression and activity (Ivakine et al., 2013). Neto2 is a single membrane-spanning protein and presents an up-regulation during development in parallel to KCC2 (Michishita et al., 2004). Neurons from mice invalidated for Neto2 expression exhibits depolarizing GABAergic synaptic currents resulting from a decrease in KCC2 function (Ivakine et al., 2013). Further investigations by the same group showed that KCC2 also interacts with glutamatergic **kainate receptors** (Mahadevan et al., 2014) for which Neto2 has been shown to be a critical auxiliary subunit (Copits et al., 2011).

Conversely, a genetic ablation or an acute knock down of GluK2, a subunit of the kainate receptor, induces a decrease of KCC2 expression (Mahadevan et al., 2014). Interestingly, kainate receptors (Copits and Swanson, 2013) and the GluA1 subunit of the AMPAR (Li et al., 2007) interact with the protein 4.1N. Thus, one could hypothesize the existence of a KCC2-containing macromolecular complex important for glutamate-related transmission and cytoskeleton interaction (Figure 6A).

KCC2 interacts also with non actin-related proteins. KCC2 binds the **brain-type creatine kinase (CKB)**, an enzyme that used the energy contained in phosopho-creatine to regenerate ATP (Inoue et al., 2004). According to the authors, this link participates to provide ATP to the regulatory kinases of KCC2. The same team showed two years later that CKB inhibition affects KCC2 transport function (Inoue et al., 2006) suggesting a phosphorylation of KCC2 by CKB. Although they reported no difference in global ATP concentration, this last result rather suggests a decrease in local ATP supplied to the primary active transporter that secondarily affects KCC2 function. Nevertheless, KCC2 seems to be entangled in a bigger macromolecular complex involved in energy and electrochemical gradient regulation since it also interacts with the **alpha2-subunit of the Na/K ATPase** (Ikeda et al., 2004). In addition to the link with CKB, this interaction could represent a way to functionally increase the coupling between primary active generation of K^+ gradient with secondary active transport of chloride by KCC2 (Figure 6B). In a recent review, Kai Kaila proposed that association between KCC2, Na/K ATPase and CKB may form what he called an “ion-transport metabolon” (Kaila et al., 2014).

Last, the **RCC1** (Regulator of Chromatin Condensation) domain of the protein associated with Myc (**PAM**) (Garbarini and Delpire, 2008) or the CCC **CIP1** (Wenz et al., 2009) are other known partners of KCC2. Both interactions positively regulates KCC2 activity in HEK-293.

Altogether, these data suggest that in addition to host regulatory residues for KCC2 function, KCC2-CTD underpins a structural role of KCC2 through many binding partners. The suppression of KCC2 could therefore impact not only neuronal chloride homeostasis but also could weaken and/or disorganize macromolecular complexes.

c) Oligomerization and clustering of KCC2

In addition to these interactions, KCC2 can interact with itself as well as other members of the CCC family and thereby form multimeric clusters or structures. Several mechanisms can account for cluster formation including oligomerization, accumulation into lipid rafts and/ specific interaction with cytoskeleton. The importance of this quaternary organization for KCC2 transport function remains however debatable.

Putative di-, tri- and tetrameric KCC2 complexes are detected by biochemical assay from neuronal or heterologous cell lysates (Blaesse et al., 2006; Uvarov et al., 2009). Regulation of these complexes is supposed to be age-dependent with a progressive increase of the oligomeric forms over time (Blaesse et al., 2006). In the same study, it was suggested that **KCC2 is active when clustered**. In neurons from post-natal day 3 (P3) mice, KCC2 was detected only in its monomeric form (120kDa). Monomeric KCC2 expression was associated with low chloride extrusion capacity (i.e. non functional KCC2, see Materials and Methods). On the contrary, expression of oligomeric KCC2 in P12 neurons was associated with an increase in chloride extrusion capacity, reflecting a functional KCC2 (Blaesse et al., 2006). Supporting this hypothesis, Casula et al. observed that oligomerization of KCC1 through its CTD was requiered for its function (Casula et al., 2001).

Two groups have suggested that **lipid rafts may influence KCC2 oligomerization, clustering and function** (Hartmann et al., 2009; Watanabe et al., 2009). However, they reached opposite conclusions regarding the direction of this lipid-raft dependent modulation of KCC2 clustering. Watanabe et al. observed that increased lipid raft-associated KCC2 led to a decrease in oligomerization and clustering of KCC2 and thereby of KCC2 function (Watanabe et al., 2009). On the contrary, Hartmann et al. reported an increase in KCC2 clustering and transport activity in the absence of lipid rafts (Hartmann et al., 2009). Hence, the precise implication of lipid raft in KCC2 clustering and function remains largely to be explored in non heterologous system. The study of Watanabe et al. also suggested a link between the mechanisms of KCC2 oligomerization, observed in western blot, and clustering, observed in immunocytochemistry (Doyon et al., 2011; Watanabe et al., 2009).

Both KCC2 clustering and function are modulated by neuronal activity through changes in diffusion properties and/or membrane trafficking of KCC2 (Chamma et al., 2013). In this study, we showed that KCC2 was less clustered and functional upon an increase in neuronal activity.

We also showed that KCC2 diffusion and clustering were constrained by KCC2-CTD-dependent interactions with 4.1N protein and actin cytoskeleton (see introduction I.5). However, the decrease in cluster size upon KCC2-CTD overexpression (Chamma et al., 2013), which likely hinders interaction between KCC2 and 4.1N (Li et al., 2007), was not correlated with a decrease in neuronal chloride extrusion capacity (Gauvain et al., 2011). This last observation questions the hypothesis of a direct link between KCC2 oligomerization/clustering and function. Moreover, some **limitations regarding the assessment of KCC2 oligomerization** itself by western blot were recently raised (Medina et al., 2014). Thus, formation of KCC2 dimer-like complexes that resist SDS treatment seem to depend on protein extraction protocols.

It seems however unlikely that KCC2 is fully devoid of oligomerization capacity. The structure of the CTD of an ancestral CCC protein has been determined by X-ray crystallography. In this study, the authors showed that CTD forms dimers in solution through a specific interaction domain (Warmuth et al., 2009). The phylogenetic relation between ancestral CCCs and eukaryotic CCCs has been also investigated.

d) Evolution of KCC2 within the CCCs family

Intragenic duplication of genes encoding transmembrane proteins with small numbers of transmembrane segments might be at the origin of 12 membrane-spanning segments proteins (Saier, 2003) like KCC2. Several studies already addressed the question of CCC phylogeny but most of them were focusing on specific taxons (mammals, plants, insects or nematode). In a recent publication, Hartmann et al. extracted important insights into the CCC phylogeny by comparing genes coding for putative CCC from Archeae and Eukaryota taxons (Hartmann et al., 2014). One of their main conclusions was the existence of a **single ancestral CCC gene in Archaea**. In addition, they concluded that the diversity of the CCC family among and between species arose from **consecutive duplication** events (Figure 7).

Analysis of amino acid sequence identity allowed to split ***Slc12a* genes in two major branches**: the Na^+-dependent (NCC and NKCC) and Na^+-independent carriers (KCC) (Figure 7A). This separation is supported by the low degree of identity between these two groups. Conversely, the percentage of identical residues within the two branches is large (>50% for NCC/NKCCs

and >70% for KCCs). Furthermore, the existence of one NKCC and two KCC orthologs within a protozoa genome participates to the hypothesis of an ancient genetic separation event between NCC/NKCC and KCCs coding genes.

Coding sequences for KCCs paralogs are found in many non-vertebrates species such as cyanobacteria, c. Elegans (Xu et al., 1994), drosophila (Hekmat-Scafe et al., 2006). Nevertheless, it seems that these KCCs are independent of KCCs variants solely found in vertebrates. Genes encoding modern KCCs (genes *Slc12a*4-7) are observed in many species of vertebrates (fish, birds, mammals…). In a recent review, Gagnon and Delpire have generated a dendogram representing the possible evolution of the KCC family (Gagnon and Delpire, 2013). This phylogenetic tree was computed using alignment similarities of amino acid sequences of the different KCCs. From this analysis, they concluded that an ancestral KCC coding gene underwent two consecutives duplications in early and late vertebrate evolution. These two duplications gave rise to *Slc12a5* and *a7* (KCC2 and 4) on one hand and to *Slc12a4* and *a6* (KCC1 and 3) on the other hand (Figure 7B).

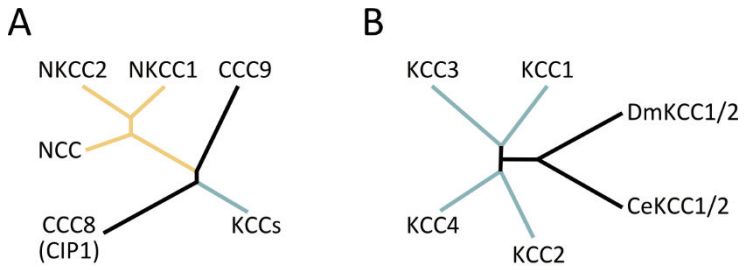

Figure 7 Phylogenetic tree of CCC family
CCC diversity originates from consecutive duplication events. (A) Slc12a genes are separated in two major phylogenetic branches: the Na^+-dependent (NCC and NKCC, yellow) and Na^+-independent carriers (KCC, blue). (B) Within the KCC family, two consecutive duplications of Slc12a genes led to the appearance of KCC1/3 and KCC2/4. Note that KCCs observed in Caenorhabtidis Elegans (CeKCC1/2) and Drosophila Melanogester (DmKCC1/2) are separated from the vertebrate KCC family. (Adapted and simplified from Gagnon and Delpire, 2013. The length of the branches does not contain information)

How were KCCs and more generally CCCs naturally selected? This question is difficult to address since CCC function is not only important for neuronal chloride homeostasis but also for kidney function, osmotic regulation etc. KCC2 is the only isoform that exhibits a neuronal specificity and transport activity under isotonic conditions. The combination of these two properties makes KCC2 an ideal candidate to serve and participate to the emergence of a stable but tunable inhibitory GABAergic transmission. In a recent review, Blaesse and Schmidt highlighted the **multifunctional properties of KCC2** referring to its transport function and to

the protein interactions that KCC2 is engaged in. They proposed that KCC2 belongs to the group of **"moonlighting" proteins** (Blaesse and Schmidt, 2014) which gathers proteins with multiple functions (Copley, 2012; Jeffery, 2009). Moonlighting proteins are assumed to represent putative intermediate steps of protein evolution. The coding gene sequence of which might be promised for duplication, each of the paralog genes keeping one function. It seems however unlikely that, as stated by the authors, by KCC2 may have been not primarily "used" as a transporter as stated by the authors. Although seducing, this hypothesis neglects that KCC2 phylogenetically belongs to CCC family that all have an ion-transport function.

In conclusion, the study of KCC2 structure provides insights into the tight regulation of its membrane expression and transport function. The numerous KCC2 partners also predict KCC2 function may not be restricted to chloride extrusion but that KCC2 could be part of larger molecular complexes the role of which can as yet only be speculated. Despite the lack of a transport model or crystallographic structure of the various ion-bound states of KCC2, more is known regarding the transport kinetics of KCC2.

2. KCC2 transport activity: a key regulator of chloride homeostasis

In the forebrain, inhibitory transmission relies on both a shunting effect (Staley and Mody, 1992) that dampens membrane depolarization through an increase in membrane conductance and a hyperpolarizing influx of chloride through GABA-ligand gated-channel. GABAARs nevertheless are not only permeable to chloride but also to some extent to bicarbonate, the reversal potential of which is around -10mV (Staley et al., 1995). The reversal potential of GABAAR current (E_{GABA}) is therefore a combination of chloride and bicarbonate conductances. Hence, depolarizing currents due to HCO_3^- outflow through GABAAR are observed upon collapse of electrochemical chloride gradient and has been sometimes predicted to promote neuronal excitability. Although shunting inhibition persists in these conditions (Staley and Mody, 1992), it highlights the importance for the neuron to control chloride homeostasis in order to maintain fully inhibitory GABAergic transmission. Interestingly, GABA-mediated depolarizing currents are observed in rodent pups and progressively disappear with age as intracellular chloride is lowered (Ben-Ari, 2002). Following

the identification of KCC2 (Payne et al., 1996), a pioneer study by Claudio Rivera and collaborators in the laboratory of Kai Kaila demonstrated that the changes in the polarity of the GABAAR-mediated current was due to an increase in KCC2 expression and chloride extrusion activity (Rivera et al., 1999). Since then, the crucial role of KCC2 function for GABAergic signaling has been demonstrated in many different physiological (development, ionic plasticity, axonal GABAergic current), theoretical or pathophysiological (spaticity, epilepsy…) models.

a) Thermodynamics of chloride co-transport

Under physiological conditions, KCC2 extrudes chloride from the cell using the electrochemical gradient of potassium, maintained by the Na/K ATPase. This feature has three important consequences:

- Simple calculation leads to the minimal, maximal and passive intraneuronal chloride concentrations, assuming that KCC2, NKCC1 and GABAAR are respectively the main sources of chloride extrusion and uptake. These values can be obtained when the net current through the transporter or the channel is equal to zero. The ionic concentrations are then computed using the Nernst equation for chloride:

$$E_{Cl^-} = -\frac{RT}{zF}\ln\left(\frac{[Cl^-]_i}{[Cl^-]_e}\right)$$

With the ideal gas constant R=8.31 $J.K^{-1}.mol^{-1}$, the temperature T=310°K, the Faraday constant F=$9.65*10^4$ $C.mol^{-1}$ and the ionic valence z=-1. Since ln(X) = 2.3026 log(X), we can replace and simplify the equation as follow:

$$E_{Cl^-} = 60mV \times \log\left(\frac{[Cl^-]_i}{[Cl^-]_e}\right)$$

With an experimentally fixed value of $[Cl^-]_e = 140mM$, we can obtain $[Cl^-]_i$ as a function of E_{Cl^-}:

$$[Cl^-]_i = 140mM \times 10^{\frac{E_{Cl^-}}{60}}$$

The **minimal chloride concentration,** $[\boldsymbol{Cl^-}]_{i,min}$, corresponds to the value of $[Cl^-]_i$ for which chloride export through KCC2 is stopped:

$$I_{KCC2} = 0 = I_{K^+} - I_{Cl^-} = \gamma_{K^+}(V_m - E_{K^+}) - \gamma_{Cl^-}(V_m - E_{Cl^-})$$

Since $\gamma_{K^+} = \gamma_{Cl^-}$, this state is obtained when $E_{K^+} = E_{Cl^-}$.

E_{K^+} is usually assumed to fluctuate around -90mV, therefore:

$$[Cl^-]_{i,min} = 140mM \times 10^{\frac{-90mV}{60mV}} = 4.4mM$$

Conversely, the **maximal chloride concentration,** $[\boldsymbol{Cl^-}]_{\boldsymbol{i,max}}$ is obtained when NKCC1 only is functional at the neuronal membrane and can be calculated using $I_{NKCC1} = 0$ with a $1K^+$:$1Na^+$:$2Cl^-$ stoichiometry:

$$I_{NKCC1} = 0 = I_{K^+} + I_{Na^+} - 2I_{Cl^-}$$
$$= \gamma_{K^+}(V_m - E_{K^+}) + \gamma_{Na^+}(V_m - E_{Na^+}) - 2\gamma_{Cl^-}(V_m - E_{Cl^-})$$

As for KCC2, since $\gamma_{K^+} = \gamma_{Na^+} = \gamma_{Cl^-}$, $I_{NKCC1} = 0$ is reached when $E_{Cl^-} = \frac{1}{2}(E_{K^+} + E_{Na^+})$. With $E_{Na^+} = +70mV$, one can estimate $[Cl^-]_{i,max}$:

$$[Cl^-]_{i,max} = 140 \times 10^{\frac{\frac{1}{2}\times(-90+70)}{60}} = 95.4mM$$

It is also interesting to calculate the **chloride concentration when the chloride gradient is collapsed,** $[\boldsymbol{Cl^-}]_{\boldsymbol{i,eq}}$**,** as it would happen upon high frequency activation of GABAARs (see below). This value is reached when $E_{Cl^-} = V_{rest}$ (which is assumed to be around -60mV) and corresponds to a passive distribution of chloride ions. Therefore:

$$[Cl^-]_{i,eq} = 140 \times 10^{\frac{-60}{60}} = 14mM$$

Although these values represent approximations, they inform about boundary values for internal chloride concentrations. Interestingly, chloride concentration measurements performed using MQAE-based fluorescence measurement (see Materials and Methods) showed similar values (Doyon et al., 2011): at rest $[Cl^-]_{i,rest}$=7mM while KCC2 inhibition using the specific antagonist VU0240551 leads to an increase in $[Cl^-]_{i,VU}$ up to 13mM, with slightly different extracellular chloride concentrations than the one used for the calculation based on electrophysiological data. This comparison between theoretical and experimental values for $[Cl^-]_i$ indicates that KCC2 is one of the main source for chloride extrusion since $[Cl^-]_{i,VU}$ is close to $[Cl^-]_{i,eq}$. Moreover it seems that KCC2 is working near its maximal capacity since $[Cl^-]_{i,rest}$ is close to $[Cl^-]_{i,min}$. This last hypothesis is in agreement with computational-based results

showing that an increase in KCC2 activity from 100% to 200% has little effect on E_{Cl} (Doyon et al., 2011). Similar chloride concentrations values were reported by the team of Kevin Staley using genetically-encoded chloride sensor mice (Glykys et al., 2009) (see Materials and Methods).

- The $1K^+$:$1Cl^-$ transport stoichiometry renders the transporter **electroneutral** (as for all the CCC family members). Hence, it is impossible to directly assess its function using classical electrophysiological measurements. To override this limitation, investigators have developed and used different tools to indirectly measure the activity of the transporter either *in vitro* or *in vivo*. The first developed methods that have allowed KCC2 identification were mostly based on the measurement of radioactive-labeled cations which are transported by KCC2. Electrophysiological measurement of the reversal potential of GABAAR-mediated currents, which depends on KCC2 function, has then been used extensively as a measure of KCC2 activity. The development of non-invasive, optical tools to assess internal chloride concentrations is promising but some limitations remain that could lead to misinterpretation (see Materials & Methods).

- KCC2 is working near its thermodynamic equilibrium under physiological conditions leading to three potential scenarios (Figure 8):

Case 1 (Figure 8B): Due to a rise in extracellular potassium concentration $[K^+]_e$, **KCC2 chloride extrusion can be reversed**. Increased extracellular potassium concentration may be a consequence of intense neuronal activity and would then lead to an increase in neuronal chloride concentration due to reversed transport of chloride by KCC2. This in turn induces a decrease in the efficacy of synaptic inhibition and therefore the appearance of a positive feedback loop that further increases neuronal activity.

Case 2 (Figure 8C): KCC2-mediated chloride extrusion protects neurons from **GABA-mediated depolarization** resulting from rise in neuronal chloride concentration (Cherubini et al., 1991; Kaila et al., 1997; Marty and Llano, 2005; Staley et al., 1995; Zhu et al., 2005). High frequency activation (HFS) of synaptic GABAARs induces a biphasic postsynaptic response

with a delayed postsynaptic depolarization. In this situation, upon HFS, a collapse of E_{Cl-} would reveal the depolarizing HCO_3^- current carried by GABAARs.

Case 3 (Figure 8D): An increase in neuronal chloride concentration upon sustained activation of GABAergic synapse leads to an **increase of KCC2 extrusion rate** and a subsequent increase in extracellular potassium concentration. Under this condition, KCC2 would then promote neuronal excitation (Viitanen et al., 2010).

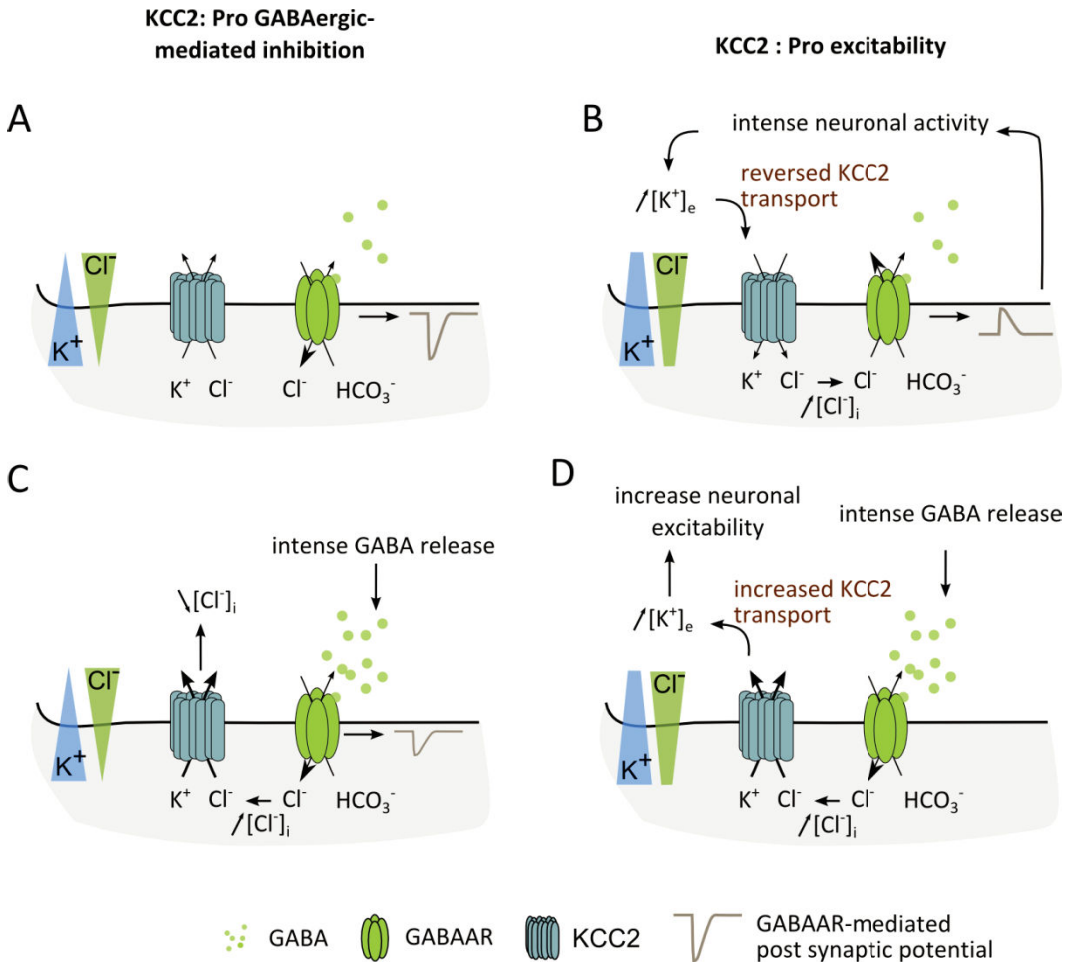

Figure 8 Thermodynamic modulation of KCC2 transport
(A*) In normal conditions, KCC2 extrudes chloride and thereby ensures that GABAAR-mediated current is hyperpolarizing. (B) Activity-dependent rise in extracellular potassium can reverse KCC2 transport activity leading to a pro-excitatory feedback loop. (C) Intense GABA release increases neuronal chloride concentration. KCC2 function protects from a switch in GABAergic polarity due to a rise in intracellular chloride. (D) The increase in intracellular chloride due to intense GABA release leads to an increase in KCC2-mediated potassium extrusion and thereby to an increase in neuronal excitability due to accumulation of extracellular K^+. In (A) and (C), KCC2 function maintains a hyperpolarizing GABAergic transmission while in (B) and (D), KCC2 function promotes excitability.*

The relative importance of the last two cases in influencing ongoing neuronal activity has been evaluated using computational models.

b) Computational modeling of chloride transport and homeostasis

The use of theoretical models allows one to test hypotheses that assume a precise spatio-temporal integration of chloride homeostasis as well as the influence of other ions or electrical parameters. The drawback of computational studies is that they are constrained by our current knowledge. Since all the models intermingled KCC2 function, chloride homeostasis and GABAAR function, it is not surprising that many computational studies reached the same, somewhat expected conclusion that **KCC2 mediated-chloride extrusion influences GABAergic transmission** (Doyon et al., 2011; Jedlicka et al., 2010; Lewin et al., 2012).

In 2010, Jedlicka et al. developed a multicompartmental *in silico* neuron in which they computed GABAAR-mediated HCO_3^- and chloride conductances, chloride extrusion and diffusion along dendrites. This model allowed them to demonstrate a clear dependence of the GABAergic synapse position along the dendritic axes on the strength of **GABA-mediated depolarization**. Chloride accumulation was larger in thin distal dendrites than in the soma, predicting that inhibitory inputs on distal dendrites may be less robust to high frequency stimulation of inhibitory synapses. This result was further confirmed by two others computational studies with more detailed models (Doyon et al., 2011; Lewin et al., 2012). Furthermore, in accordance with the case 2 explaining the GABA-mediated depolarization, an increase in the relative GABAAR permeability to HCO_3^- logically increases the depolarization upon sustained GABAAR activation (Doyon et al., 2011; Jedlicka et al., 2010).

As previously mentioned in the case 3, the group of Kaila and Voipio proposed that **KCC2 could promote an excitatory action of GABA** (Viitanen et al., 2010). In addition to the delayed synaptic-mediated depolarization, HFS of GABAergic transmission or application of a GABAAR agonist (isoguvacine), lead to a **presynaptic-independent increase in $[K^+]_e$**. As an explanation for this effect, the authors proposed that the collapse of chloride gradient induced an increase in KCC2 activity (i.e. export of K^+/Cl^-), leading to a 3mM $[K^+]_e$ increase. Lewin et al. investigated this phenomenon using a theoretical model. They decreased the activity of KCC2 by 60% and evaluated the amplitude of GABAAR-mediated depolarization amplitude and the increase in $[K^+]_e$ (Lewin et al., 2012). Overall, they concluded that KCC2 function primarily protects neurons from GABA-mediated depolarization without much of an effect on neuronal excitability through changes in $[K^+]_e$.

Another study reached a similar conclusion regarding the interdependence between extracellular K^+, GABAergic transmission and KCC2 activity (Doyon et al., 2011). Importantly, they showed that the relative position of KCC2-mediated chloride extrusion with respect to the inhibitory synapse does not influence the capacity of the cell to counteract the collapse of chloride gradient upon HFS of GABAergic transmission. At this micro-domain scale, diffusion of chloride is predominant over chloride extrusion through KCC2. KCC2 is then important to maintain **steady state levels of intracellular chloride** and produce a somato-dendritic gradient of chloride (Doyon et al., 2011).

c) Water transport extrusion and osmotic regulation

In addition to chloride transport, KCC2 also extrudes water. This feature has been shown both to influence neuronal firing by computational study (Berndt et al., 2011) and, empirically, to influence osmotic regulation.

KCCs were first described as **swelling-activated K+ efflux transporters** in red blood and epithelial cells, two non-neuronal cell types facing large osmotic challenges (Dunham and Ellory, 1981; Hoffmann et al., 2009; Lauf and Theg, 1980; Zeuthen and MacAulay, 2002). In these cells, chloride homeostasis maintenance is directly linked to osmotic and volume regulation. Together with water transport through aquaporins, CCCs are also key players in kidney function, which requires maintenance of strong osmotic gradients. It appears that **chloride co-transport by CCCs** is directly or indirectly (cytoplasmic membrane is to some extent permeable to water) **coupled to water transport** (Zeuthen, 2010; Zeuthen and MacAulay, 2002). This flow of water through CCC is thought to partially compensate and equilibrate osmolarity changes arising from ion co-transport. Hence, it has been estimated that KCC2 and NKCC1 activity triggers respectively a net outflow and inflow of approximately 500 water molecules per transported ion (MacAulay and Zeuthen, 2010).

In the CNS, large net influxes of cations and anions due to glutamate and GABA/Glycine receptor activity respectively are accompanied by water influx that maintains intracellular osmolarity. Intense synaptic activity may consequently lead to **neuronal swelling** and, if not compensated, to cell death. In this context, the complete absence of aquaporin in neurons is quite striking (Amiry-Moghaddam and Ottersen, 2003; Andrew et al., 2007). Water transport

through CCCs could therefore represent a way for neurons to perform volume regulation. Recently, experiments using digital holographic microscopy evaluated the contribution of KCC2 and NKCC1 to neuronal volume regulation (Jourdain et al., 2011). Briefly, this technique measures changes in phase signal that mainly reflects intracellular refractive index due to nonaqueous material. Therefore, a shift in refractive index reflects a change in osmolite concentration. Experiments revealed that bath-applied glutamate triggered water fluxes through both NMDAR and NKCC1. Consistent with its role in water transport, delayed **activation of KCC2 compensated this influx of water** by mediating a net outflow of water. In addition, we have shown that KCC2 transport also influenced dendritic spine volume (Gauvain et al., 2011). Knock down of the protein or pharmacological blockage of KCC2 transport induced an increase in spine volume. This led us to hypothesize that the suppression of water extrusion through KCC2 was likely responsible for this effect.

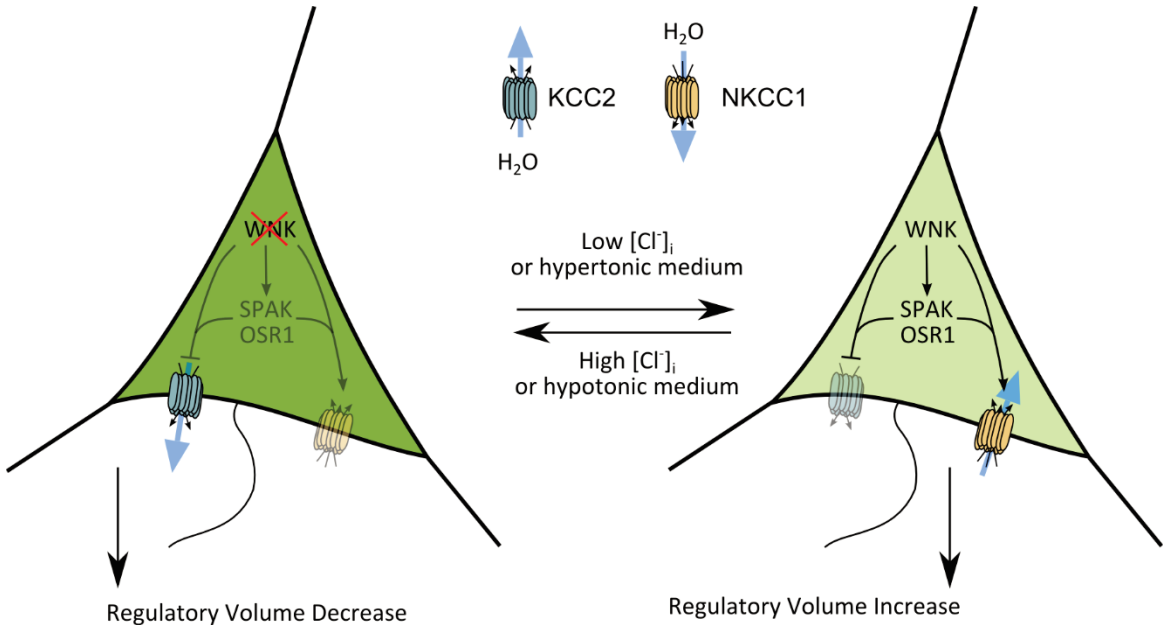

Figure 9 Cation chloride cotransporters in osmotic regulation
Salts transported by KCC2 and NKCC1 are accompanied by water outflux and influx, respectively. Thereby, KCC2 and NKCC1 participate in cellular osmotic regulation. Osmotic challenges and/or changes in neuronal chloride concentration regulate CCC activity. The chloride sensor WNK is activated by low neuronal chloride concentration or in hypertonic conditions (Right). Activation of WNK directly or indirectly, through SPAK and OSR1, increases and decreases NKCC1 and KCC2 function, respectively. Elevation of chloride concentration – e.g. intense GABAAR activation – inhibits the WNK pathway (Left).

Whereas we reported an effect reflecting an endogenous activity of the transporter, likely due to presence of the ISO domain (Acton et al., 2012), Jourdain et al. described a swelling-induced activation of KCC2 (Jourdain et al., 2011). The intracellular pathway leading to this activiation is partially identified. **WNK kinase family** together with **SPAK and OSR1** kinases have been

identified as CCC regulators upon osmolarity challenge (for review on WNK kinases: Kahle et al., 2010, 2013). WNK1/3 kinase are serine/threonine kinases acting as osmosensors potentially through a chloride sensitivity (Piala et al., 2014).

Extracellular hyperosmotic challenge or intracellular chloride decrease induce an activation of WNK1 through phosphorylation of Ser383. Activated WNK1 then phosphorylates SPAK on residues Thr233 and Ser373 resulting in SPAK activation. Stimulation of this pathway then induces activation of NKCC1 as well as inhibition of KCC2 through phosphorylation of Thr906 and Thr1006 KCC2 residues (Gagnon et al., 2006; Rinehart et al., 2009). This finally leads to a net influx of water and therefore to an increase in cell volume. This phenomenon called **Regulatory Volume Increase** allows compensation of the original hyperosmotic challenge. Conversely, upon a rise in internal chloride concentration or hypoosmotic challenge, inhibition of NKCC1 and activation of KCC2 due to inhibition of WNK / SPAK OSR1 kinase pathway lead to a **Regulatory Volume Decrease**.

Down regulation of human WNK3 expression and dephosphorylation of KCC2 on Thr906 and Thr1007 parallel KCC2 activity during development, suggesting a **possible implication of WNK kinase pathway in the maturation of GABAergic transmission** (Kahle et al., 2013). I would like to finish this section by briefly mentioning two puzzling observations regarding this last hypothesis. WNK3 mRNA expression increases in rodent between P15 and P21 (Kahle et al., 2005) contrary to what has been reported in human by the same team (Kahle et al., 2013). It remains unknown whether this discrepancy arose from interspecies difference or if we should reconsider the results of the first study (Kahle et al., 2005). Moreover, it seems unlikely that WNK kinases-dependent phosphorylation could play a role in developmental regulation of KCC2 and steady-state chloride homeostasis. Indeed, in immature neurons, intracellular chloride concentration is high due to the absence of KCC2 and the presence of NKCC1 (Figure 3). Therefore WNK kinases should be inhibited, leading to an activation of KCC2 (Figure 9). Such regulation would be going against the proposed developmental pattern of KCC2 and WNK kinase activation. Conversely, in mature neurons, low chloride concentration is due to KCC2 activation and the prediction is going toward an activation of WNK kinase and a negative feedback loop on KCC2 activity (Figure 3 vs. Figure 4). In conclusion, whereas the WNK kinases are good candidates to explain volume regulation through CCC, their role in developmental regulation of KCC2 remains less clear.

d) Controversies: does GABAergic transmission depend on KCC2 ?

- *Role of energetic substrates on the polarity of GABAergic transmission.*

In a set of papers, the group of Yuri Zilberter argued that the polarity of GABAergic transmission may be primarily determined by energy substrates and the presence of **ketone bodies** at early developmental stages: upon addition of ketone bodies (KB) to glucose-based artificial cerebrospinal fluid (aCSF), hyperpolarizing but not depolarizing GABAAR-mediated currents could be observed in immature neocortical neurons (Rheims et al., 2009). They further showed that supplying aCSF with KB (DL-3-hydroxybutyrate 4mM) or other energy substrates (Lactate 4mM or Pyruvate 5mM) suppressed giant depolarization potentials (GDPs) (Holmgren et al., 2010). This GDPs correspond to early network oscillations and are thought to depend on interneuron activity and depolarizing GABAergic transmission (Ben-Ari et al., 2007).

Later on, Bregestovski and Bernard claimed that depolarizing GABAergic transmission could be entirely explained by an artifact resulting from brain slices preparation and maintenance (Bregestovski and Bernard, 2012). This argument was based on studies by the group of Zilberter as well as a more recent study by Dzhala and colleagues. The latter showed that "injured" neurons at the slice surface have an unsatisfied high-energy requirement that yield to an increase in intracellular chloride concentration as observed using the genetically-encoded chloride sensor, clomeleon (Dzhala et al., 2012).

A really well-documented review has gathered concerns and evidences against or discrepancies in the arguments raised by the group of Zilberter or by Bregestovksi and Bernard (Ben-Ari et al., 2012). Multiple papers failed to reproduce the results from Zilberter and colleagues on the KB dependency of GABAergic transmission polarity or GDPs generation (Ruusuvuori et al., 2010; Tyzio et al., 2011). Furthermore, the concentrations of the various additional energy substrates used by Zilberter and colleagues were from 4 to more than 10 times higher than that observed in the plasma level from rat pups (Tyzio et al., 2011). Finally, GDPs have been observed both *in vivo* and *in vitro* in a whole hippocampus preparation in which deficit in energetic supply or slicing artifact cannot account for the appearance of GDPs (Ben-Ari et al., 2012).

- *How is neuronal chloride concentration controlled?*

Recently the group of Kevin Staley proposed that chloride concentration may not be determined by CCC activity but instead may be primarily constrained by **intracellular and extracellular impermeant anions**. Gradients of impermeable charged molecules can influence the transmembrane diffusion of membrane permeable ions such as chloride. This effect is known as the **Gibbs-Donnan Effect**: the gradient of impermeable charged molecules forms an electrical gradient across the membrane that is compensated by diffusion of permeable ions. This can therefore lead to the appearance of an ion gradient in the absence of an active transporter. Hence, Glykys and coworkers observed a negative correlation between the neuronal chloride concentration and both the intra- and extracellular concentrations of impermeant anions, $[A]_i$ and $[A]_e$. Moreover, they reported no effect of KCC2 or NKCC1 antagonists on neuronal chloride concentration using chloride imaging. They concluded that steady-state concentration of chloride is mainly constrained by impermeant anions and that modulation of $[A]_i$ could participate in the maturation and plasticity of inhibitory transmission.

In support of their hypotheses, they made and tested different predictions that I shall refer to and highlight some intriguing points.

In prediction 2, they applied 20mM gluconate, pyruvate and D-Lactate. These weak acids are transported across the cytoplasmic membrane in their uncharged form and dissociate inside the cell. Hence, they argued that addition of these weak acids would increase $[A]_i$. They observed a 5 to 10% decrease in $[Cl^-]_i$ upon application of these weak acids. Interestingly, they applied the same compounds as the group of Zilberter and observed similar effects: a decrease in $[Cl-]_i$ (as in Glykys et al., 2014) leads to a decrease in the reversal potential of GABAAR-mediated response (as in Rheims et al., 2009). Then, it is unclear which observations could explain the other or whether both observations are due to the same unknown side effect.

Furthermore, the overall effect on $[A]_i$ has been questioned: the protons released by the dissociation will be buffered intracellularly leading to a decrease in the concentration of endogenous buffer anions and therefore a maintenance of total anions concentration (Luhmann et al., 2014). However, it is not clear whether the endogenous anions that Luhmann

et al. are referring to, are impermeant or not (i.e. if they are participating to the Gibbs-Donnan effect).

Intriguingly, $[Cl^-]_i$ is influenced in the same way by variation of $[A]_i$ and $[A]_e$: in predictions 1 and 2 the authors reported that $[Cl^-]_i$ varies inversely with $[A]_i$ to maintain a constant $[A]_i+[Cl^-]_i$ and in prediction 3 and 4 they predicted that "$[A]_e$ should vary inversely with $[Cl^-]_i$". Hence, the direction of the electrical gradient imposed by the impermeant anions leading to the Gibbs-Donnan effect is not clear.

In text books, we learn that for an isolated cell, impermeant anions are mainly represented by proteins in the intracellular space and absent in extracellular space. This gradient of impermeant anions ($[A]_i>[A]_e$) is compensated by an outflux of anions and an influx of cations due to the Gibbs-Donnan effect. In the present study, the presence of the negatively charged sulfated extracellular matrix makes it difficult to predict the direction of the anionic electrical gradient. Moreover, the measurement of $[A]_i$ was only based on staining of nucleic acids: although they reported that their signal was mainly cytoplasmic (RNA). How nuclear DNA could participate to a Gibbs-Donnan effect across the cytoplasmic membrane is far from clear.

Finally, the entire study is based on the surprising observation that pharmacological inhibition of either KCC2 or NKCC1 does not affect $[Cl^-]_i$, either in immature or in mature neurons. This contradicts twenty years of research, including from the same authors, demonstrating the predominant role of CCC in setting the steady-state concentration of chloride as well as the neuronal capacity to face an increase in neuronal chloride concentration (Doyon et al., 2011; Dzhala et al., 2010; Gauvain et al., 2011; Glykys et al., 2009; Hübner et al., 2001; Li et al., 2007; Rivera et al., 1999; Seja et al., 2012; Zhu et al., 2005). Instead, they proposed that "local $[A]_i$ and $[A]_e$ determine $[Cl^-]_i$", "CCCs serve to maintain $[Cl^-]_i$ at this set point.", and that "The species of CCC and other cellular features are likely to correlate with $[A]_i$ and $[Cl-]_i$ [e.g, (14,24)]". How are CCCs regulated by these parameters remains undetermined. References 14 and 24 reported a cell-type specific and developmental regulation of GABAergic transmission through NKCC1 expression (Martina et al., 2001; Plotkin et al., 1997). It is therefore surprising that the authors refered to these publications since they cannot stand *examplia gratia* of their effect.

The authors report that epileptic-like activity leads to an increase in both chloride concentration and cellular volume. They suggest that these two observations may reflect NKCC1-dependent influx of chloride and water (see introduction I.2.c). How could NKCC1 activity be responsible for a transient nature of the increase in chloride concentration or volume? At most, NKCC1 activity could favor initiation of epileptic seizure due to a decrease in GABAergic transmission efficacy. Moreover, they completely eluded that increase in chloride concentration could arise from intense GABAergic activity likely to happen upon epileptic seizure (see introduction I.2 and I.4.a). Increase in cell volume upon intense neuronal activity, also called spreading depression, is a complex mechanism involving glutamatergic transmission and appearance of osmotic challenge due to both synaptic and neuronal activities (Andrew and MacVicar, 1994; Basarsky et al., 1999). Although CCCs have been recently involved in osmotic regulation upon increase in neuronal activity (Jourdain et al., 2011), the view of CCCs being at the center of activity-dependent neuronal increase in both chloride concentration and volume is way too simplistic.

In conclusion, the study by Glykys and colleagues certainly raises interesting theoretical predictions on the role of impermeant anions but mostly falls down by over-interpreting intriguing observations disproved by twenty years of experiments.

3. Regulation of KCC2 expression and function

KCC2 is expressed in almost all neurons throughout the CNS. However, its expression and localization at the membrane are tightly regulated during brain development and by neuronal activity. Rapid membrane turnover makes KCC2 a good candidate to allow for fast modulation of GABAergic transmission through changes in E_{Cl-} (Rivera et al., 2004; Zhao et al., 2008). In this section, I will present some of the mechanisms that contribute to influence KCC2 expression and function.

a) Cellular and Subcellular patterns of expression

KCC2 expression is **neuron specific** due to the presence of neuron-restrictive silencing elements (NRSE) and early growth response transcription factor 4 (Egr4) binding sites in its promoter sequence (Uvarov et al., 2006; Yeo et al., 2009). Hence, KCC2 expression is observed

throughout the CNS including spinal cord (Hübner et al., 2001) cerebellum (Williams et al., 1999b), thalamus (Barthó et al., 2004), auditory brainstem (Blaesse et al., 2006) and cortical structures (Gulyás et al., 2001; Rivera et al., 1999) (Figure 10).

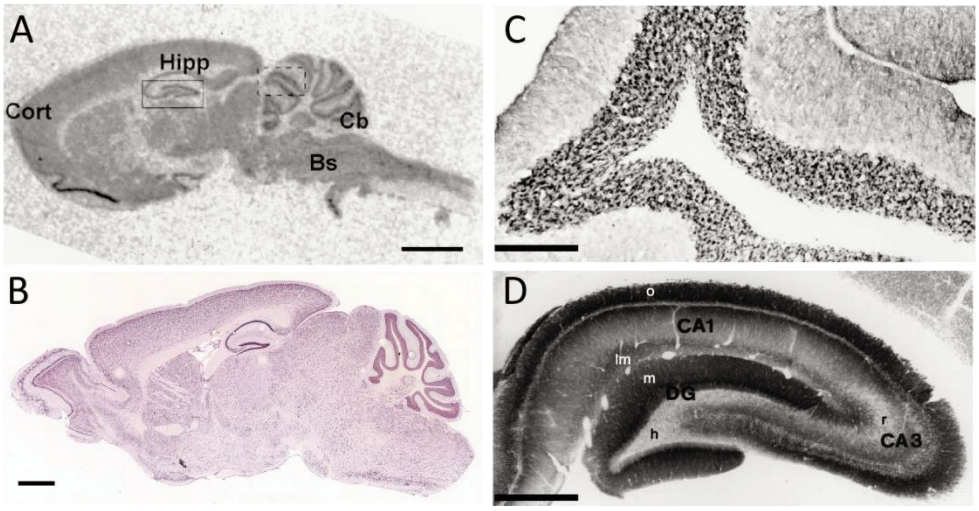

Figure 10 KCC2 in the adult brain
Left: First in situ hybridization of KCC2 mRNA from Payne et al., 1996 (A, scale, 3mm) and Allen Brain Atlas (B, scale, 1mm). Right: immunohistochemistry revealing KCC2 protein expression in the cerebellum (C, scale, 200µm, Williams et al., 1999b) and in the hippocampus (D, scale, 1mm, Rivera et al., 1999).

Although KCC2 expression appears to be ubiquitous, **E_{GABA} varies among brain structures and neuronal population** suggesting a modulation of KCC2 expression levels or activity. For instance, E_{GABA} in interneurons is more depolarized than in principal cells in amygdala, neo- or peri-rhinal cortices (Martina et al., 2001) as well as in cerebellum (Chavas and Marty, 2003). These variations are thought to reflect differences in chloride homeostasis mechanisms due to KCC2 function but also to changes in other CCCs such as NKCC1, as well as other chloride transporters/channels. It should be mentioned that differences in HCO_3^- metabolism or intrinsic membrane properties could also account for these differences. Nevertheless, GABAergic transmission will have different impacts on neuronal networks according to the value of E_{GABA} and by extension of the GABAergic driving force, since V_{rest} also varies between the different cell types.

At the **subcellular level**, KCC2 expression is restricted to the somato-dendritic compartment and excluded from the axon (Figure 11). Leterrier and Dargent proposed that axon initial segment (AIS) participates to protein exclusion from axon by acting as a gatekeeper to

maintain axonal identity (Leterrier and Dargent, 2014). At the level of the AIS, accumulation of actin cytoskeleton tethered by voltage-dependent channels and transmembrane adhesion proteins mainly through ankyrin G / βIV spectrin cortical cytoskeleton represents both a membrane and cytoplasmic diffusion barrier that control axonal identity. It has been hypothesized that actin motor proteins participates to protein exclusion (Myosin V) or targeting (Myosin IV) to the axon. Axonal microtubules and motor-related protein might also be involved in this process. KCC2 axonal exclusion mechanism is however unknown. As a physiological consequence of this axonal exclusion, intracellular chloride concentration appears higher in axons than in somato-dendritic compartment (Price and Trussell, 2006). Therefore, activation of GABAARs at axoaxonic GABAergic synapses or GABA spillover cause a paradoxical increase in axonal excitability (Pugh and Jahr, 2011, 2013).

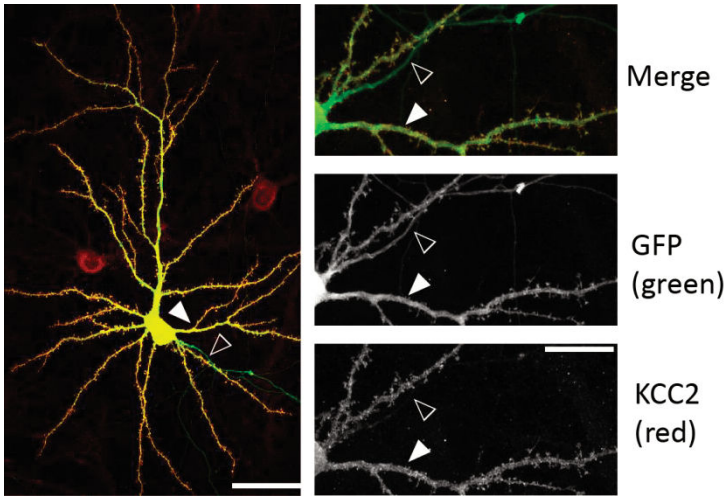

Figure 11 Subcellular segregation of KCC2
Immunocytochemistry of KCC2 in mature hippocampal cultured neurons. KCC2 is excluded from axon (empty arrow head) compared to somato-dendritic compartments (filled arrow head). Right insets are details from left image (scale, 40µm and 10µm respectively). Original data from Chamma et al., 2013.

Bipolar retinal cells show a peculiar and as yet unexplained subcellular and intercellular pattern of KCC2 expression. In the retina, light stimulation leads to a decrease in the tonic glutamate release from cone cells onto bipolar cells. Two types of bipolar cells can be distinguished based on their glutamate receptors content and response to light stimulation. ON-bipolar cells are activated by light due to the decreased activation of the inhibitory metabotropic receptor for glutamate, mGluR6 (Duebel et al., 2006). In contrast, OFF-cell activity is inhibited upon light stimulation due to the decrease in glutamatergic activation of ionotropic receptors. In addition to this heterogeneous expression of glutamate receptors,

these cells do not respond in the same way to dendro-somatic GABA release from horizontal cells and axonal GABA release from amarcrine cells. While KCC2 expression is observed in OFF-cell somato-dendritic compartment, ON-cell dendrites lack KCC2 and instead express NKCC1 (Vardi et al., 2000). This intercellular heterogeneity in CCC expression leads to inward and outward chloride current through GABAAR in OFF- and ON-bipolar cells respectively (Billups and Attwell, 2002; Duebel et al., 2006). The similar KCC2 segregation is observed between the dendritic branches of ON-OFF retinal ganglion cells of zebrafish that respond both to the onset and the offset of light stimulation (Zhang et al., 2013). Both these heterogeneities in glutamate receptors and CCC expression have been proposed to enhance contrast through lateral inhibition. Surprisingly, both axonal boutons of ON- and OFF-bipolar cells express KCC2 and have a depolarizing response to GABA release from amacrine cells (Vardi et al., 2000). Hence polarity of GABAergic transmission is both cellular- and layer-specific due to respectively intra- and inter-neuronal heterogeneities in CCCs expression.

Although mechanisms of axonal KCC2 exclusion or of the particular pattern of CCCs expression in the retina are not known, several mechanisms have been identified to control KCC2 expression and function.

b) Developmental regulation of KCC2

During development, the increase in KCC2 expression is observed throughout the forebrain (Clayton et al., 1998; Rivera et al., 1999) with some exceptions, as depicted in the previous section. Noteworthy only the KCC2b isoform undergoes this up-regulation while KCC2a expression remains constant over brain development (Yeo et al., 2009). However, while full KCC2 knock out mice die at birth due to respiratory failure (Hübner et al., 2001), KCC2b selective knock out mice are viable until up to P15 (Woo et al., 2002), suggesting both KCC2 isoforms may be important for the inhibitory synaptic transmission.

KCC2 ontogenic up-regulation can be closely linked to the **neurotrophic action of GABAergic transmission** in the immature brain (Ben-Ari et al., 2007). GABAergic synapses are formed and active before glutamatergic transmission. In immature neurons, vesicular-independent GABA release, possibly through the reverse action of GABA transporters, is thought to act as a cue for cell migration (Bortone and Polleux, 2009), as well as axon elongation and guidance (Ageta-

Ishihara et al., 2009). Depolarizing currents mediated by GABAARs lead to voltage-dependent Ca^{2+} channels (VDCC) activation or facilitates NMDA-mediated glutamatergic transmission (Akerman and Cline, 2006), and therefore allow to positively inform the neuron of its environment (Figure 12). Conversely, the absence of KCC2 in immature brain is crucial for interneuron migration (Bortone and Polleux, 2009) as well as for the GABAergic-dependent giant depolarization potential observed in the hippocampus *in vitro* (Ben-Ari et al., 2007) and for the maturation of the retinotectal network (Akerman and Cline, 2006).

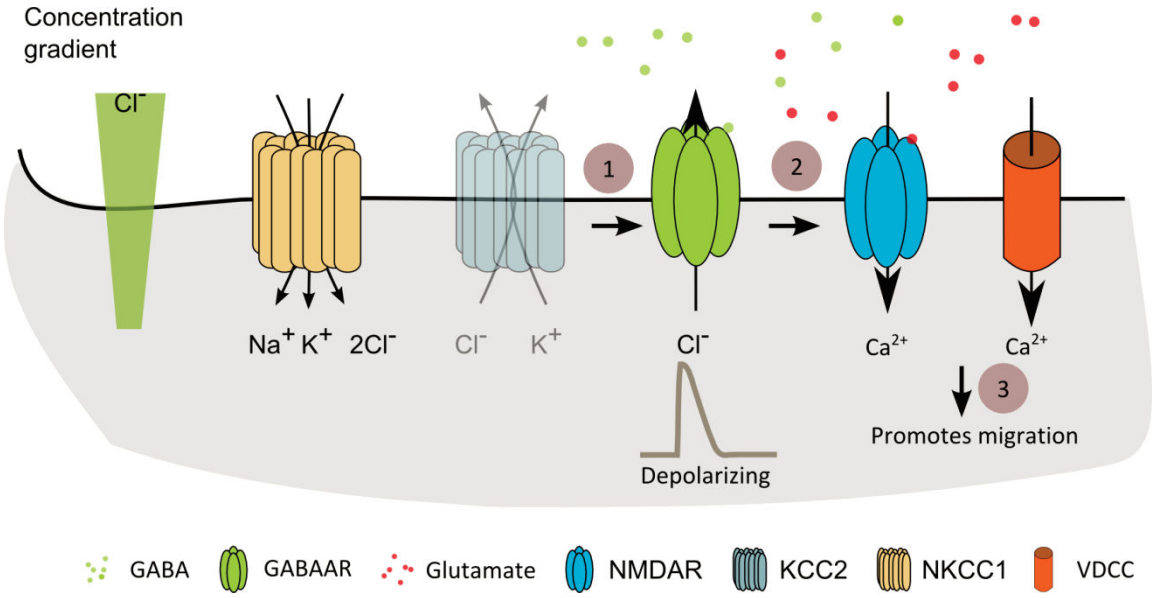

Figure 12 Ontogenic role of GABA in immature neurons
(1) The absence of KCC2 in immature neurons leads to membrane depolarization through GABAARs. (2) This depolarization allows Ca^{2+} influx through NMDARs and opening of voltage-gated Ca^{2+} channels (VDCC). (3) Rise in Ca^{2+} then promotes migration and neuronal development. Adapted from Bortone and Polleux, 2009.

Interestingly, recent evidence implicated KCC2 partners in neuronal maturation (Horn et al., 2010) as well as in tumoral cell migration and invasion (Wei et al., 2011). Hence, KCC2 involvement in neuron migration during development might not solely due to its chloride extrusion function.

The progressive up-regulation of KCC2 during development is promoted by **Brain-derived neurotrophic factor (BDNF)** release (Aguado et al., 2003). BDNF binding to tropomyosin receptor kinase B (TrKB) leads to activation of the extracellular signal-regulated kinases 1 and 2 (ERK1/2) pathway. Activation of ERK1/2 increases the expression of KCC2 through Egr4-dependent KCC2 transcription (Ludwig et al., 2011). This observation has however never been confirmed at the protein level. Interestingly, BDNF also promotes the maturation of GABAergic

neurons (Yamada et al., 2002) and the formation of GABAergic synapses (Vicario-Abejón et al., 1998). Conversely, in immature but not in mature hippocampal neurons, GABA increases BDNF mRNA levels (Berninger et al., 1995), suggesting a synergic effect of BNDF and maturation of GABAergic transmission.

Intriguingly, BDNF actions on both KCC2 gene expression and membrane protein localization as well as function (Boulenguez et al., 2010; Rivera et al., 2002, 2004) and GABAergic transmission (Mizoguchi et al., 2003) change during neuronal maturation. Whereas BDNF promotes KCC2 expression in immature neurons, BDNF incubation for 2 to 3h decreases chloride extrusion capacity of CA1 pyramidal neurons (Rivera et al., 2004). In the same type of neuron from P6 rat, BDNF application leads to a reversible potentiation of GABAergic transmission dependent on TrkB receptor activation and intracellular Ca^{2+} increase. In contrast, in P14 animals, application of BDNF leads to a long lasting depression of inhibitory post synaptic current (Mizoguchi et al., 2003) possibly through GABAAR internalization (Brünig et al., 2001). More generally, overall effects of BDNF does not only differ in time but also in function of the cell type (pyramidal neurons vs. interneuron, Rutherford et al., 1998) or according to the delivery mode (acute vs. gradual release of BDNF, Ji et al., 2010). These sometimes opposing actions of BDNF on KCC2 and GABAergic transmission are thought to represent differences in spatio-temporal integration of TrkB signaling (Ji et al., 2010; Rivera et al., 2004).

Post-translational modifications also influence KCC2 function in the immature brain. In immature neurons from primary culture of hippocampus but not from acute slice, application of the broad-spectrum kinase inhibitor staurosporine induces an activation of KCC2 function indirectly suggesting that KCC2 is already expressed but not functional (Khirug et al., 2005). Moreover experiments performed in rat hippocampal brain slices showed that KCC2 was solely expressed in mature hippocampus as revealed by northern blots (Rivera et al., 1999) and immunohistofluorescence (Gulyás et al., 2001; Rivera et al., 1999). Although it seems unlikely that developmental regulation of KCC2 solely depends on post-translational modifications, some KCC2 residues have been proposed to undergo age-dependent phosphorylation.

As previously mentioned, KCC2 **Thr906 and Thr1006** are phosphorylated by WNK1/3 kinase at early stages of development and their dephosphorylation parallels the maturation of

GABAergic transmission (Kahle et al., 2013; Rinehart et al., 2009). In line with the first observation of Kelsch and colleagues in 2001 who showed that KCC2 function upregulation was dependent on tyrosine kinase (Kelsch et al., 2001), phosphorylation of **Tyr1087** has been proposed to be required for KCC2 function (Wake et al., 2007; Watanabe et al., 2009) as it favors oligomerization (Blaesse et al., 2006), I.1.c). Although experimental evidence is lacking, the activity-driven phosphorylation of Ser940 could also represent a way to activate KCC2 during development (Banke and Gegelashvili, 2008; Bos et al., 2013; Lee et al., 2007, 2010a).

c) Activity-dependent regulation

Activity-dependent regulation of KCC2 participates in ionic plasticity of inhibitory transmission (Buzsáki et al., 2007; Ling and Benardo, 1995) to maintain neuronal activity homeostasis (Wang et al., 2006; Yang et al., 2010) or to support potential learning-related function (Fiumelli and Woodin, 2007; Kullmann et al., 2012). Different mechanisms have been proposed to undergo these changes. In particular, numerous residues implicated in the developmental up-regulation of KCC2 are also thought to modulate KCC2 function following increases in neuronal activity (Figure 13).

At the transcriptional level, I already mentioned that action of **BDNF on KCC2 expression** is age-dependent. While BDNF application favors KCC2 expression in immature hippocampal neurons (Ludwig et al., 2011), sustained activity-induced BDNF release (Rivera et al., 2004) or exogenous BDNF application (Rivera et al., 2002) leads to a down regulation of KCC2 in mature neurons through activation of TrkB receptors. TrkB-induced phospholipase C gamma (PLCγ) activation is ultimately responsible for CREB (C-AMP Response Element-binding protein*)* activation and down-regulation of *Slc12a5* gene expression. TrkB receptor is also coupled to the Src homology 2 domain containing transforming protein (Shc) and FGF receptor substrate 2 (FRS-2) which are responsible for ERK1/2 pathway activation. The concomitant activation of Shc and PLC pathways is necessary for the down-regulation of KCC2 expression. However, BDNF-mediated KCC2 upregulation, as observed in immature brain, arises solely from activation of Shc signaling (Rivera et al., 2002).

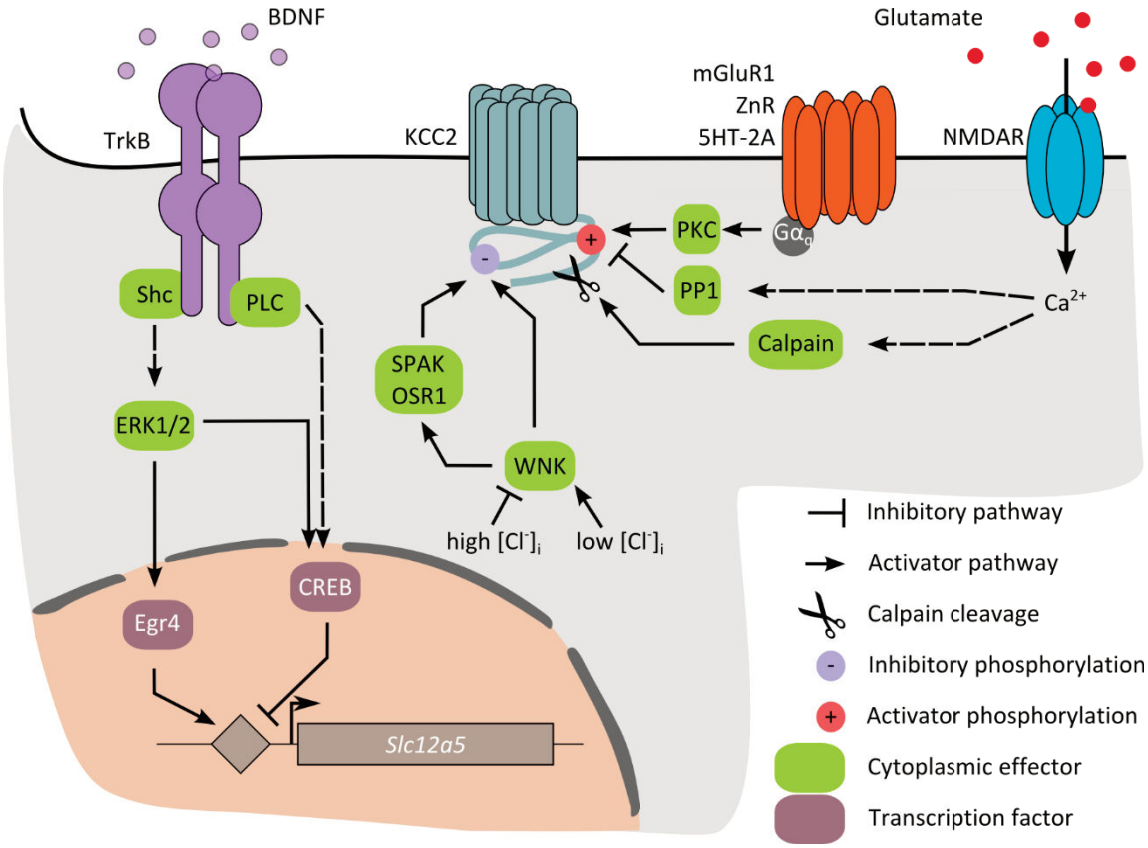

Figure 13 Transcriptional and post-translational modulation of KCC2
During neuronal development, only Shc is stimulated leading to the transcription of Slc12a5. On the contrary, in mature neurons, BDNF binding to TrkB induces the co-stimulation of Shc and PLC leading to the inhibition of KCC2 gene expression. Multiple post-translational pathways regulate KCC2 membrane localization and function. (Dash line means "indirect activation")

Rivera and colleagues used a 0-Mg^{2+}-based solution to increase neuronal activity of hippocampal slices. This paradigm also favors activation of NMDAR and increase in intracellular Ca^{2+} (Rivera et al., 2002). Increase in intracellular Ca^{2+} through activation of NMDAR, Voltage-Dependent Ca2+ Channels (VDCC) or release from internal stores (ryanodine receptors) is a common mechanism modulating protein expression and function as well as synaptic plasticity induction (see introduction II). The role and the origin of Ca^{2+} transients that affects KCC2 expression and function have been investigated.

In the early 2000s, the group of Mu-Ming Poo published two papers on a KCC2-dependent GABAergic plasticity (Fiumelli et al., 2005; Woodin et al., 2003). Woodin and colleagues used a spike timing dependent plasticity (STDP) protocol that was already characterized for glutamatergic transmission (for review, Debanne and Poo, 2010). Using gramicidin perforated-patch, they showed that concomitant (±20ms) activation of inhibitory synapse and postsynaptic spiking induced a **L-type VDCC-dependent** potentiation of inward GABAergic

currents. This potentiation was due to a depolarizing shift in E_{Cl} that was restricted to the stimulated synapse. Finally, this effect was both furosemide- and $[K^+]_e$–dependent and led the authors to conclude that it relied on a down regulation of KCC2 (Woodin et al., 2003). Conversely, the second study reported a VDCC-dependent decrease of outward GABAergic currents upon postsynaptic firing (Fiumelli et al., 2005). This effect was also explained by a down regulation of KCC2 leading to a depolarizing shift in E_{Cl}. In addition, the second study proposed that these effects were mediated by PKC.

Nevertheless, this PKC requirement is unlikely to be a direct effect since the only described KCC2 residue phosphorylated by PKC (Ser940) has been shown to increase KCC2 function when phosphorylated (Banke and Gegelashvili, 2008; Bos et al., 2013; Lee et al., 2011). Ser940-dependent upregulation of KCC2 function has been observed following activation of the subtype I metabotropic glutamate receptor, mGluR1 (Banke and Gegelashvili, 2008), metabotropic zinc-sensing receptor, mZnR (Chorin et al., 2011) or the serotonin receptor 5HT-2A (Bos et al., 2013). These transporters are all G protein-coupled receptors and are coupled to the $G\alpha_q$ protein that ultimately leads to the activation of PKC (Figure 13).

VDCC activation is not either strictly necessary for Ca^{2+}-dependent regulation of KCC2. Bath application of glutamate in mature dissociated culture of hippocampus or repetitive activation of excitatory synapses in hippocampal organotypic slices leads to a NMDA-, but not VDCC-, dependent decrease in KCC2 activity (Kitamura et al., 2008). Mechanisms underlying **NMDA-dependent regulation of KCC2** have been investigated by four different groups, including ours (Figure 13). Chronologically, the group of Stephen Moss first showed that Ca^{2+} influx mediated by NMDAR activation leads to the inhibitory dephosphorylation of the Ser940 residue. This dephosphorylation was long lasting, relied on protein phosphatase 1 activation and was therefore prevented by okadaic acid, a phosphatase inhibitor (Lee et al., 2011). In 2012, two independent studies have implicated KCC2 cleavage by the calcium activated protease calpain as a mechanism for NMDA-induced down regulation of KCC2 (Puskarjov et al., 2012; Zhou et al., 2012). Finally, in a recent paper, we showed that an increase in excitatory synaptic activity leads to a decrease in KCC2 function and clustering dependent on both Ser940 dephosphorylation and cleavage by calpain (Chamma et al., 2013). We also demonstrated that changes in KCC2 clustering were partially correlated with a change in KCC2 lateral diffusion. KCC2 membrane diffusion was constrained by its interaction with cytoskeleton. Disruption of

actin cytoskeleton by latrunculin A, suppression of the actin- and KCC2-linked protein 4.1N or overexpression of the KCC2-CTD that interacts with 4.1N, all lead to an increased diffusion of the transporter. This last study in which I participated can be found in the additional publication section of this manuscript.

4. Chloride homeostasis dysregulation in pathology

As we have seen above, KCC2 is a key regulator of chloride homeostasis and its tight regulation is necessary for the maturation and plasticity of GABAergic transmission. It is therefore not surprising that defects in KCC2 function have been proposed to be involved in neurological disorders often associated with hyperexcitability and alterations of inhibitory transmission.

a) Excitation/inhibition balance in epilepsies

Epilepsies represent a broad spectrum of neurological disorders with a large range of etiologies and symptoms. However, all epilepsies reflect an excessive, hypersynchronous neuronal discharge. Epileptic activities produce different electroencephalographic signatures that may either remain focal or spread to multiple regions. Defects in excitatory/inhibitory balance within networks with recurrent connections such as the hippocampus or the thalamocortical loop are suspected to generate epileptic activity. Many anti-epileptic drugs are promoting GABAergic transmission in order to increase the inhibitory tone. For instance, positive allosteric modulators of GABAARs such as benzodiazepines, are commonly used as anticonvulsive drugs for absence-type epilepsy.

In contrast, mesial temporal lobe epilepsies (TLE) are often pharmacoresistant with an unexpected pro convulsive effect of drugs that promotes GABAergic activity. A pioneer study by the group of Richard Miles shed light on this apparent paradox (Cohen et al., 2002). Using human hippocampal resection tissue from TLE patients, they demonstrated that both excitatory and inhibitory signaling contribute to interictal-like events, since they were blocked by either GABAergic or glutamatergic antagonists. Subicular pyramidal cells showed an excitatory GABAergic transmission that was hypothesized to be due to a loss of KCC2 expression. This hypothesis was partially confirmed in 2007 when Huberfeld and colleagues

showed that KCC2 mRNA and protein were absent from a subset of pyramidal neurons in subiculum (Huberfeld et al., 2007).

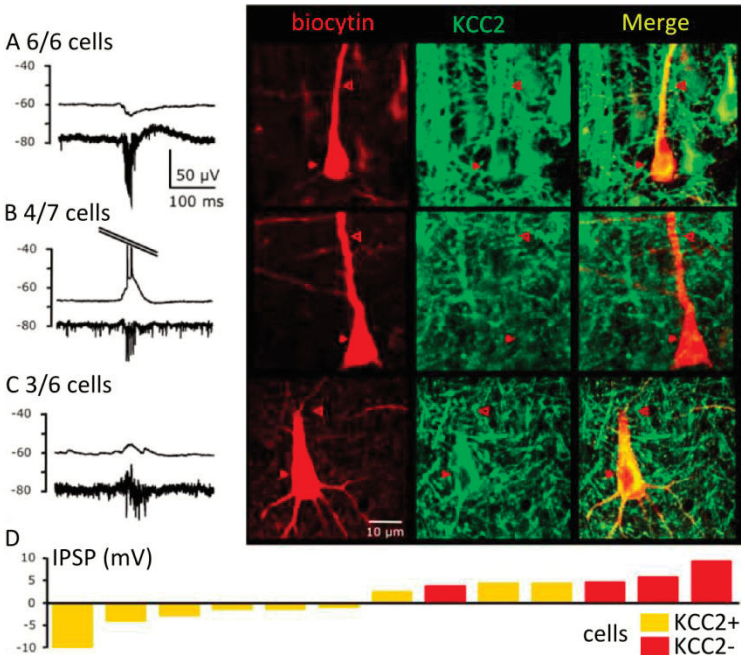

Figure 14 Correlation between KCC2 protein expression and the polarity of IPSPs during intercital activity
(A-C left) Simultaneous intracellular (top, thin traces) and extracellular (bottom, thick traces) recordings during interictal-like activity in resected hippocampus from an epileptic patient. Immunostaining reveal the absence of KCC2 in 4 out of 7 recorded cells eliciting a depolarizing GABAergic transmission (A-C right). (D) Correlation between KCC2 protein expression and the polarity of GABAergic transmission. From Huberfeld et al., 2007.

Interestingly, depolarizing GABAergic transmission was observed in all KCC2 immunonegative neurons but also in some KCC2-expressing pyramidal neurons (Figure 14). This suggests either that KCC2 was present but inactive due to posttranslational modifications or that depolarizing GABAAR-mediated potential had a different origin.

Bumetanide, a specific NKCC1 antagonist, was able to stop interictal activity further suggesting that a pathological neuronal chloride load could explain the generation of these pathological activities (Huberfeld et al., 2007). Accumulation of chloride by a NKCC1-dependent mechanism is also thought to be at the origin of neonatal seizures in rodent neocortex (Dzhala et al., 2010; Glykys et al., 2009). It is not clear however whether bumetanide can block itcal events *in vivo* (Kaila et al., 2014). Moreover, whereas KCC2 has been surprisingly proposed to be pro-convulsive as its activity raises extracellular K^+ concentration (Viitanen et al., 2010, but see introduction I.2.b), NKCC1 function has been proposed to be anti-epileptic (Zhu et al., 2008), likely through extracellular K^+ clearance.

One major question remains on the role of KCC2 in epilepsy: is KCC2 down-regulation a cause or a consequence of epileptic activity? The working hypothesis is that in epileptic patients, an original trauma leads to weakened inhibitory transmission (e.g. activity-dependent KCC2 down-regulation). This decrease in inhibitory transmission efficacy may thus set the ground for the development of an epileptic condition. This hypothesis is based on different observations. On one hand, the different mouse models of KCC2 function deficits show increased excitability (Woo et al., 2002) and susceptibility to seizures (Tornberg et al., 2005). On the other hand, KCC2 activity is strongly down-regulated by neuronal activity (see introduction I.3.c). Experimental models of epilepsy in rodents show decreased KCC2 expression after lithium-pilocarpine induced status epilepticus (Li et al., 2008; Pathak et al., 2007) or after kindling-induced seizures (Rivera et al., 2002). On the contrary, single-seizure activity in neonates induces BDNF-dependent up-regulation of KCC2 (Khirug et al., 2010; Puskarjov et al., 2014b).

Overall, it remains not clear whether 1) KCC2 expression could be decreased upon an original trauma in early developmental stage, 2) KCC2 suppression due to epileptic activity participates to interictal event generation. Recent development of a floxed KCC2 mouse line (Seja et al., 2012) or lentiviral-based suppression of KCC2 by RNA interference (Chevy et al., submitted) may help answering this conundrum.

b) Alteration of chloride homeostasis in spinal cord: Spasticity and Neuropathic pain

Chronic pain and spasticity (hypertonia) are a direct consequence of spinal cord injury (SCI) affecting the sensory-motor system directly at the spinal cord level. These conditions seem to share some features with epilepsy since anticonvulsant drugs can be used to treat neuropathic pain. As for TLE patients, some patients suffering from neuropathic pain are resistant to pro-GABAergic drugs. Rodent SCI models of spasticity and neuropathic pain show a **decreased KCC2 expression in motoneurons**, in the case of spasticity (Bos et al., 2013; Boulenguez et al., 2010), and in **neurons of the lamina I** of the superficial dorsal horn in chronic pain models (Coull et al., 2003). Down-regulation of KCC2 in both conditions is dependent of the BDNF/TrkB pathway described earlier (Boulenguez et al., 2010; Coull et al., 2003).

Hypotheses for neuropathic pain are based on the **gate control theory of pain** and have been well described in different reviews (Kaila et al., 2014; Price et al., 2009; Vinay and Jean-Xavier, 2008). Lamina I of spinal cord neurons receive inputs from **pain-conducting C-fibers** and project the pain signal to the brain. The presynaptic terminals of C-fibers are contacted by GABAergic interneurons that receive **tactile information from A-beta fibers**. These terminals do not express KCC2 and only low level of NKCC1, leading to relatively small changes of the membrane potential upon GABAAR stimulation. This depolarization is however sufficient to **inactivate sodium voltage-gated channel** and thereby inhibit transmitter release from C-fibers. In contrast, upon SCI, an increase in NKCC1 expression in the C-fiber presynaptic terminal leads to an augmentation of neurotransmitter release following GABAAR activation. Thus, upon SCI, tactile-conducting fibers will lead to an activation of pain-conducting fibers inducing hyperalgesia (Price et al., 2009).

c) Other pathologies

Alteration of chloride homeostasis has also been implicated in stress-related pathology (Hewitt et al., 2009). Stress-dependent endocrine response requires the activity of hypothalamic parvocellular neurons that receive strong synaptic inhibition. Down-regulation of KCC2 in restraint, stressed animals leads to a decrease in the efficacy of this inhibitory tone that can even be transformed in GABA-mediated depolarization due to the sustained activation of GABAAR (see introduction I.2).

KCC2/NKCC1 imbalance has also been proposed to contribute to human psychiatric disorders such as schizophrenia (Hyde et al., 2011) and autism (Lemonnier and Ben-Ari, 2010). The recent results obtained by the group of Yezekhel Ben-Ari on the positive effect of bumetanide on autism are based on studies using rodent models (Tyzio et al., 2006, 2014). They showed that during delivery, maternal oxytocin triggers a transient hyperpolarizing shift in GABA transmission in the fetal brain (Tyzio et al., 2006). This transient shift is abolished in pups from valproate and fragile X rodent models of autism. Autistic phenotypes can be attenuated by pretreatment of the mother with bumetanide. Conversely, blocking oxytocin signaling in naïve mothers induces the appearance of autistic-like behaviors in newborn rats (Tyzio et al., 2014). However, the exact mechanisms underlying the effect of bumetanide treatment on autistic patients remains unclear. Obviously, this treatment in children does not affect oxytocin-

induced transient shift in GABAergic transmission upon delivery. More intriguingly, bumetanide does not cross the blood brain barrier. Nevertheless, the benefit of bumetanide treatment starts to be well-documented for autistic patients (Cellot and Cherubini, 2014; Grandgeorge et al., 2014; Hadjikhani et al., 2013; Lemonnier and Ben-Ari, 2010; Lemonnier et al., 2012).

5. Emerging role of KCC2 at the glutamatergic synapse

In 2001, Gulyas and collaborators made the first paradoxical observation that KCC2 is present in dendritic spines (Gulyás et al., 2001) that host glutamatergic synapses (Hering and Sheng, 2001; Kasai et al., 2010). In a visionary way, they proposed that this intriguing position of KCC2 could be related to compensation of osmotic challenges induced by excitatory synaptic activity (see introduction I.2.c). Indeed our group recently showed that knock down of KCC2 in mature neurons induces a swelling of dendritic spine heads, likely resulting from a loss in water extrusion mediated by KCC2 (Gauvain et al., 2011).

The putative role of KCC2 in excitatory synapse function was first investigated by precocious overexpression of KCC2. KCC2 overexpression in tectal neurons of Xenopus embryos reduced excitatory transmission (Akerman and Cline, 2006). This effect was however reflecting the ontogenic role of depolarizing GABAergic transmission, leading to activation of NMDAR at AMPAR-lacking excitatory synapses (silent synapses). On the other hand, overexpression of KCC2 in immature cultured hippocampal neurons did not impact excitatory transmission but instead promoted the maturation of inhibitory synapses (Chudotvorova et al., 2005). This discrepancy may result from differences in network organization or from differentially positioned inhibitory relative to excitatory synapses in the two models. Indeed, Akerman and Cline clearly showed that the feedforward GABAergic connectivity was temporally structured to influence silent glutamatergic synapses. The development of genetic tools to suppress KCC2 expression further led to the emergence of several new hypotheses on how KCC2 could directly influence glutamatergic transmission.

a) An ion transport-independent role of KCC2 in spinogenesis

In 2007, the group of Claudio Rivera took advantage of the **KCC2 knock-out mouse** developed by Vilen et al. ($KCC2^{-/-}$, Vilen et al., 2001) to study the role of KCC2 within dendritic spines (Li et al., 2007). Although pups are not viable after birth, Rivera's group was able to study neuronal maturation and synaptic function using primary cultures of dissociated neurons from embryonic hippocampus. Unexpectedly, genetic ablation of KCC2 led to an **aberrant maturation of dendritic spines** that was accompanied by a decrease in the number of functional synapses (Figure 15A-B). This defect was not attributable to a homeostatic effect due to a decrease in the efficacy of GABAergic transmission. It was partially reproduced in vivo using hypomorphic KCC2-deficient mice ($KCC2^{hyp/null}$, Tornberg et al., 2005). Interestingly, functional and structural spine maturation were rescued upon overexpression of a KCC2 non-functional form, indicating a **transport-independent mechanism**. Conversely, overexpression in wild type neurons of the carboxy terminal domain of KCC2, likely acting in a dominant negative manner on KCC2-protein interactions, replicated the phenotype observed in $KCC2^{-/-}$ neurons.

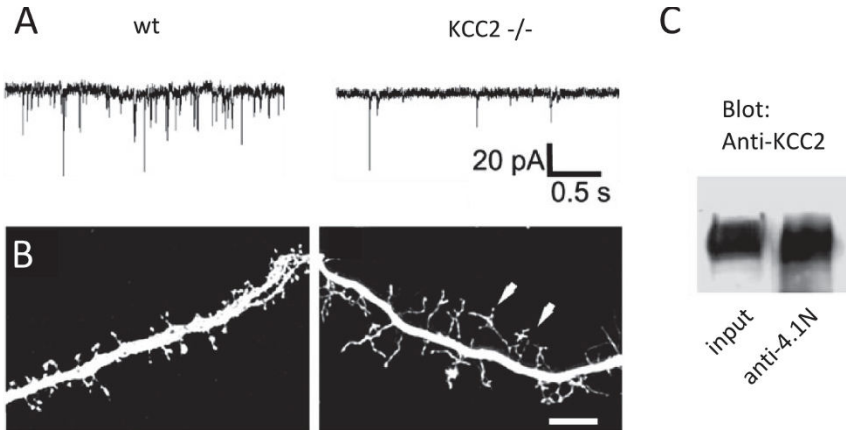

Figure 15 Genetic ablation of KCC2 impairs maturation of glutamatergic synapses
(A). KCC2 genetic ablation decreases the frequency of miniature EPSCs in immature hippocampal neurons. (B) This is associated with an altered spinogenesis (scale, 4µm). (C) This effect relies on KCC2-4.1N interaction, that is revealed by co-immunoprecipitation. Adapted from Li et al., 2007.

The authors then screened different excitatory synaptic-related proteins to look for an interaction with KCC2. It appeared that KCC2 interacts with the **actin-linked protein 4.1N** but neither with the GluA1 or GluA4 subunit of the AMPAR, the AMPAR interacting protein GRIP, the scaffolding protein PSD95 or the Ca^{2+} Calmodulin-dependent Kinase II (Figure 15C). Hence, overexpression of the interacting 4.1N FERM domain mimicked the spine maturation deficit

in wild type neurons. Moreover, this phenotype was specific to the **interaction between KCC2 and 4.1N**: overexpression in KCC2$^{-/-}$ neurons of KCC3 which lacks a 4.1N interaction did not rescue the normal spinogenesis (Li et al., 2007). In this context, it is striking that KCC2 upregulation temporally parallels spinogenesis and excitatory synaptic maturation. This study has demonstrated for the first time a non-canonical, transport-independent role of KCC2 in neurons.

b) 4.1 proteins: a structural link between transporters and actin cytoskeleton

Although surprising, involvement of **transporters in cytoskeleton organization** is not a novel idea and has been described in other cell types. Ion transporters as well as other transmembrane proteins are thought to act as anchors for cortical cytoskeleton. This was firstly described in erythrocytes in which the $Cl^-/HCO3^-$ anion exchanger AE3 interacts with the red blood cell specific 4.1R and ankyrin to dock the spectrin-actin network (Mohandas et al., 1992; Morgans and Kopito, 1993). Since then, **4.1 proteins** have been shown to interact with numerous membrane-spanning proteins such as the GluA1 subunit of AMPAR (Lin et al., 2009; Shen et al., 2000b), mGluR1 (Lu et al., 2004), KCC2 (Li et al., 2007), kainate receptors (Copits and Swanson, 2013) and others (for a complete list, see Baines et al., 2014).

In vertebrates, the 4.1 protein family comprises four members: 4.1R, 4.1N, 4.1B, 4.1G. Several protein domains have been described for 4.1R and are likely to be shared within the other members of the 4.1 family. A FERM domain (Four.one, Ezrin, Radixin, Moesin) underlies binding with transmembrane proteins and a SAB domain promotes the Spectrin-Actin binding. Different hypotheses about the function of these interactions have been proposed:

- Anchoring of actin-spectrin cortical network;
- Trafficking and aggregation of transmembrane proteins;
- Maintenance of higher-order complexes;
- Cross-talk between actin-dynamic and transmembrane protein function.

Interestingly, 4.1 interactions have been suggested to serve a crosstalk between transport function and cytoskeleton dynamics in a context of volume and osmotic regulation (Cantiello et al., 1993). At the time it was not clear whether actin acts as a direct osmosensor through a volume-dependent stretching of the cytoskeleton network or if it was an indirect effect

through activation of proteins controlling actin polymerization and depolymerization. For instance, small GTPase RhoA and RhoA-associated kinase ROCK proteins, which control actin dynamics (see introduction II.3.c), have been shown to regulate the sodium proton exchanger NHE1, FERM-interacting proteins and to be activated by osmotic changes (Denker and Barber, 2002). More recently, the osmosensor WNK2 has been shown to activate RhoA, Rac1 and the downstream pathway (Moniz et al., 2008). Hence, **KCC2 interaction with 4.1N** could affect actin cytoskeleton directly by acting as a **membrane anchor** and/or indirectly through **regulation of actin dynamics**.

c) Investigating the role of KCC2 in dendritic spines using genetic manipulations

Using different genetic tools, researchers have further investigated the involvement of KCC2 on excitatory transmission. In 2008, Riekki and collaborators used the same KCC2-deficient mouse model ($KCC2^{hyp/null}$) as used in Li et al. 2007. In this mouse, KCC2 expression is reduced to 15% of control and the reversal potential of GABAA response is depolarized by 20mV compared to wild type mice (Riekki et al., 2008). Nonetheless, the frequency but not the amplitude of miniature GABAAR-mediated currents was diminished. Whereas the unexpected lack of change in amplitude might be explained by the recording methods – whole cell patch clamp with fixed chloride concentration – the reason for the decrease in frequency remains unclear (but see (Smith et al., 2014)). On the other hand, neither the amplitude nor the frequency of mEPSCs were affected in the KCC2 hypomorphe mouse as observed by Li et al. 2007. Only a mild effect on field EPSC fatigue (i.e. a progressive decrease in the strength of excitatory transmission) upon repetitive stimulation was observed. The authors hypothesized this effect was due to a lack of extracellular potassium buffering by KCC2 upon repetitive neuronal stimulation. Finally, they observed no modification of synaptic plasticity upon partial KCC2 depletion suggesting KCC2 may not be directly involved in excitatory transmission. Other contradictory results arose from *in utero* overexpression of KCC2 mutants (Fiumelli et al., 2013). In agreement with the observations made by Li et al. 2007, overexpression of a non-functional form of KCC2 led to an increase of dendritic spines density. Surprisingly, the overexpression of KCC2-CTD also induced an increase in spine density, contrary to what was reported by Li et al. 2007.

The development of RNA interference to knock down KCC2 in adult animals has permitted to study the effect of KCC2 suppression independently of compensatory developmental effects. The same year, 3 independent teams, including ours, used shRNA approach to acutely suppress KCC2 (see Materials and Methods). The first study showed that KCC2 has a neuroprotective effect since KCC2 suppression in mature hippocampal neurons in culture induced a decrease in cell survival after NMDA application or oxidative stress-like protocol (Pellegrino et al., 2011). This change in neuronal fate was dependent on KCC2 function since it was reproduced by application of DIAO, a KCC2 antagonist. Two putative mechanisms were discussed: a decrease in inhibitory synaptic efficacy upon KCC2 suppression could favor Ca^{2+} influx through VDCC and NMDAR as described above (Akerman and Cline, 2006) increasing cell death; or a lack of KCC2 could induce a defect in cell volume regulation upon activity-dependent cell-swelling.

Another study performed by Wei and colleagues represents a small detour from neurons to tumors but yet greatly contributes to deciphering KCC2 ion transport-independent functions (Wei et al., 2011). They observed KCC2 was surprisingly expressed in non-neuronal tumor cells wherein it promoted cell migration by an ion transport-independent mechanism. In these cells, suppression of KCC2 by RNA interference led to an increase in actin stress fibers. This last observation is interesting in regard of the aforementioned link between 4.1N and actin dynamics regulation. In addition, overexpression of KCC2 in early embryos as well as in a heterologous system has been shown to decrease actin polymerization and thereby influence neuronal development (Horn et al., 2010).

Non canonical function of KCC2 is not only critical for maturation and spinogenesis (Li et al., 2007) but also for basal excitatory activity (Gauvain et al., 2011). Suppression of KCC2 in mature hippocampal neurons in culture leads to a decrease in spontaneous excitatory transmission (Figure 16A). This effect correlates with a reduced aggregation of GluA1-containing AMPA receptor in dendritic spines (Figure 16B). This phenotype was mimicked by an overexpression of KCC2-CTD acting as a dominant negative for KCC2-protein interactions but not by the KCC2 antagonist VU0240551. The decrease in GluA1 clustering was explained by an increase in its membrane diffusion, as revealed by quantum-dot-based single-particle tracking (Figure 16C). Since this increase in diffusion was not observed for non-actin anchored

proteins, we concluded that this effect reflected an ion-transport independent membrane anchoring of actin cytoskeleton by KCC2.

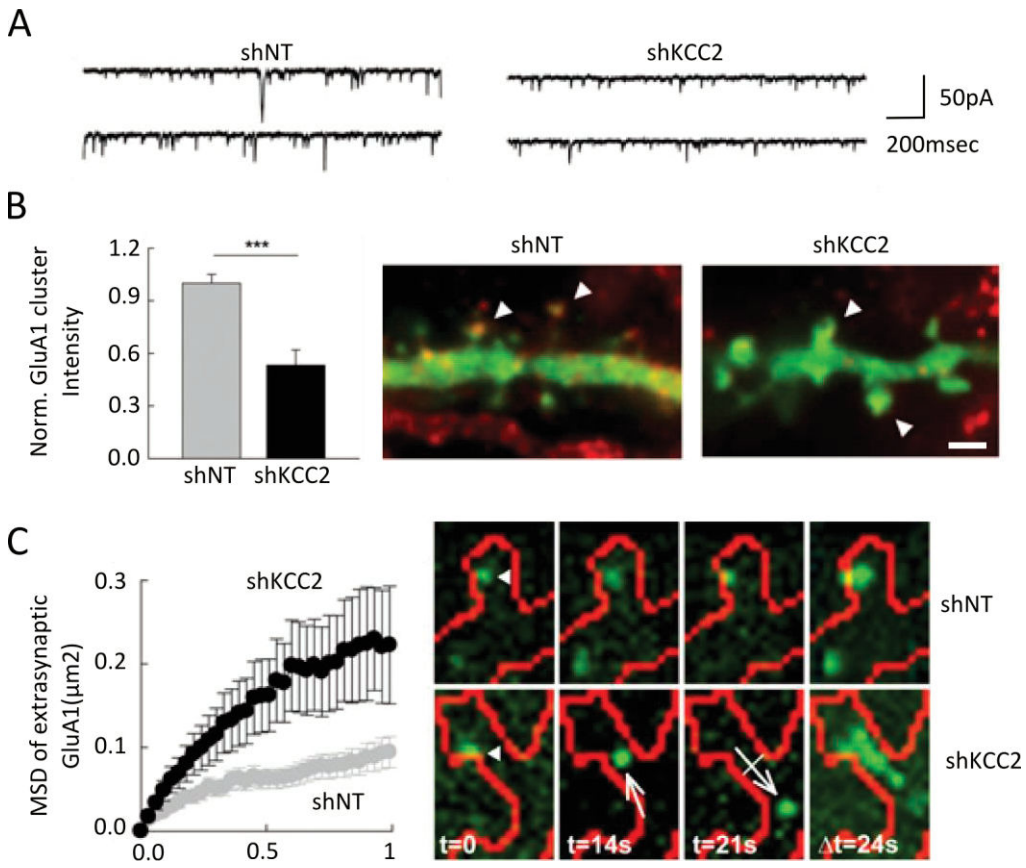

Figure 16 KCC2 influences AMPAR aggregation and lateral diffusion in dendritic spines
(A) Compared to control condition (shNT), KCC2 suppression (shKCC2) in mature hippocampal neurons decreases basal glutamatergic transmission (i.e. decreased mEPSCs amplitude). (B) This decrease correlates with smaller aggregates of GluA1-containing AMPARs within spines (scale, 1µm). (C) KCC2 contributes to GluA1-containing AMPARs confinement within spines. KCC2 knock down increases surface area explored (MSD: mean square displacement) and lateral diffusion of GluA1-subunits (Green: quantum dot-based single particle trajectories, Red: outline of dendrite). Adapted from Gauvain et al., 2011.

Intriguingly, the decrease in excitatory transmission upon KCC2 suppression was not observed in a mouse model in which KCC2 was specifically deleted from cerebellar Purkinje cells (Seja et al., 2012). This discrepancy may arise from compensatory effects due to long term suppression of KCC2 or more interestingly, can be explained by a specific role of KCC2 in GluA1 trafficking. Indeed, AMPAR in mature Purkinje cells lack the GluA1 subunit (Douyard et al., 2007). Conversely, 4.1N that interacts with KCC2 has been shown to be necessary for GluA1 but not GluA2 subunit activity-dependent trafficking (Lin et al., 2009). Exocytosis of GluA1-containing AMPAR is thought to be one of the main mechanisms underlying long term potentiation of excitatory synapses.

During my thesis, I therefore asked whether acute suppression of KCC2 might affect LTP of excitatory synapses. The next chapter of this manuscript will review the mechanisms supporting glutamatergic LTP.

II. LONG TERM POTENTIATION OF GLUTAMATERGIC SYNAPSES.

Plasticity in the CNS is thought to represent the neuronal substrate of learning (Whitlock et al., 2006) and allows adaptation to external (Espinosa and Stryker, 2012) or internal (Turrigiano, 2008) constraints. The purpose of this short introduction on plasticity is to introduce the heterogeneity of neuronal plasticity before focusing on the well characterized LTP of the Schaffer collateral (SC) to CA1 pyramidal cell synapse. Except when otherwise specified LTP or LTD will refer to plasticity of glutamatergic synapses.

Since the discovery of LTP at the perforant path synapse to dentate gyrus granule cells by Bliss & Lomo (Bliss and Lomo, 1973), many forms of plasticity have been described at many different synapses (For reviews Huganir and Nicoll, 2013; Kessels and Malinow, 2009; Kullmann and Lamsa, 2007; Kullmann et al., 2012; Luscher et al., 2011). Nevertheless, one common feature of all these forms of plasticity is a change in synaptic strength. Schematically, this phenomenon arises either from changes in neurotransmitter release probability at the **presynaptic level** (Weisskopf and Nicoll, 1995) or from modifications in the **postsynaptic** conductances. Although the relative importance of this two loci of expression is still debated (Lisman, 2009; Malinow and Tsien, 1990; Perkel and Nicoll, 1993), this simplistic view of synaptic plasticity has been successfully used as a theoretical background to explain both short lasting- and long lasting-plasticity leading either to a potentiation or a depression of synaptic transmission.

In addition to the locus of expression, a wide range of induction mechanisms have also been described and depend on species, synapse localization, experimental paradigms, age etc. As an example of this heterogeneity, induction of plasticity may involve other cellular partners than the pre- and the postsynaptic neurons and is referred as **heterosynaptic plasticity**. One of the first example of heterosynaptic plasticity and the underlying molecular mechanisms have been described by the laboratory of Eric Kandel in the sensory system of *Aplysia* (Antonov et al., 2003). Since then, heterosynaptic plasticity has been observed in many synaptic models with the requirement of additional neuromodulators release, inhibitory transmission or astrocytes (Chevaleyre and Castillo, 2003; Dittman and Regehr, 1997; Hartell, 2001; Ishikawa et al., 2013; Panatier et al., 2006; Rose et al., 2009).

Homosynaptic LTP can be induced by **different experimental paradigms** each one involving different molecular pathways (Albensi et al., 2007; Reymann and Frey, 2007). High frequency stimulation (HFS) protocol also referred as tetanus stimulation is commonly used to induce potentiation of hippocampal synapses. Although, this protocol is effective in inducing LTP at other synapses, it is also clear that it relies on a non-natural pattern of stimulation (Reymann and Frey, 2007). Pairing depolarization of the postsynaptic neuron with presynaptic stimulation at lower frequency or shorter high frequency stimulation delivered at frequencies relevant to hippocampal activity such as called theta-burst stimulation, have been shown to induce LTP in hippocampus. More recently, spike-timing dependent plasticity (STDP) has been proposed as a physiological way to induce plasticity within a network with sparse but temporally organized neuronal activity (Debanne and Poo, 2010).

In parallel to the discovery of paradigms to induce long term plasticity, development of pharmacological inhibitors and genetic tools has allowed to specify some underlying **molecular determinants**. For instance, homosynaptic plasticity with a presynaptic locus of expression often involves **retrograde messengers** such as endocannabinoids or nitric oxide that are produced in the postsynaptic elements and act in the presynaptic bouton (for review Duguid and Sjöström, 2006). Postsynaptic mechanisms leading to increased postsynaptic conductance have been extensively studied, particularly in the context of the classical SC to CA1 pyramidal cell synapse. It is now widely accepted that, at this synapse, Ca^{2+} influx through NMDAR leads to activation of Ca^{2+}/Calmoduline Kinase II (CaMKII) and protein Kinase A (PKA). Activation of these kinases ultimately leads to an increase in the conductance and the number of phosphorylated AMPARs at the postsynaptic density (PSD), as well as remodeling of dendritic spines that host the excitatory synapses (Figure 17).

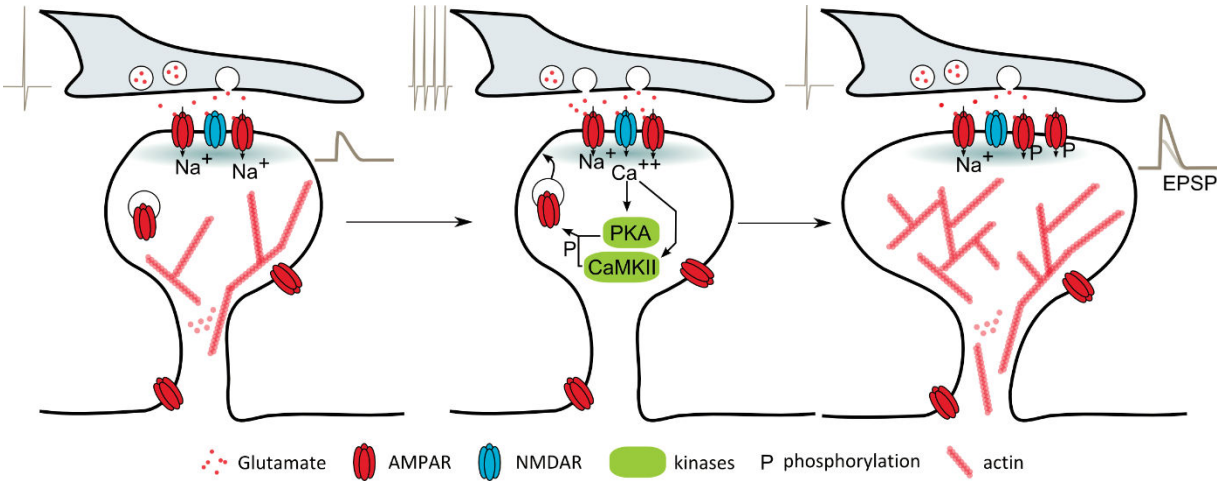

Figure 17 The classical postsynaptic mechanism of LTP induction and expression
(Center) Induction of LTP: high frequency stimulation of presynaptic terminal leads to Ca^{2+} influx through NMDARs. Ca^{2+}-dependent CaMKII and PKA activation leads to phoshphorylation of AMPARs and triggers their membrane insertion. (Right) Expression of LTP: newly inserted AMPARs contribute to increase the postsynaptic response to glutamate release. Addition of new AMPARs is accompanied by an increase in spine volume and actin spine-content.

After a brief presentation of the glutamatergic synapse, I will then present the proposed molecular pathways leading to functional plasticity by addition of new AMPAR and to structural plasticity through remodeling of actin-enriched dendritic spines housing the excitatory synapses

1. Glutamatergic receptors and associated proteins at the postsynaptic density

Fast excitatory synaptic transmission is mediated by glutamate release from the presynaptic element onto the postsynaptic neuron expressing glutamate-gated channels (iGluRs). iGluRs have been identified according to their affinity to specific natural (kainate) or synthetic (AMPA and NMDA) agonists. Hence, glutamate can bind to the well characterized AMPA, NMDA and kainate receptors. Glutamate release can also activate G-protein mediated signaling cascade through metabotropic receptor (mGluRs) activation. The different genes encoding for the different types of mGluRs and iGluRs have been now identified and the biophysical properties of the proteins are well characterized. For the purpose of this thesis, I will not further describe the properties of mGluRs and kainate receptors but readers could refer to (Bellone and Mameli, 2012; Lerma, 2006; Willard and Koochekpour, 2013) for complementary information.

a) AMPA receptor subunit composition

AMPARs are tetramers composed of two identical dimers. These dimers are formed by combinations of different subunits, **GluA1, GluA2, GluA3 and GluA4** encoded by four different genes, *GRIA1-4.* Messenger RNAs encoding for these subunits undergo important posttranscriptional modifications that confer specific biophysical properties and constrain subunit assemblage (for review, Greger and Esteban, 2007). Notably, GluA2 containing AMPAR are Ca^{2+} impermeable due to the introduction of a positively-charged arginine in the GluR2 pore loop (Arg586) by RNA editing at the Q/R site (Cull-Candy et al., 2006). In addition to impeding Ca^{2+} permeability, this Q/R site editing also precludes formation of homo-tetrameric GluA2 containing AMPARs (Cull-Candy et al., 2006). Moreover GluA2 mRNA is alternatively spliced leading to two variants: GluA2 and GluA2L which possess a longer carboxy terminal domain (CTD). Similarly, GluA4 is reported to exist in two spliced variants including one with a short CTD and is referred as GluA4S.

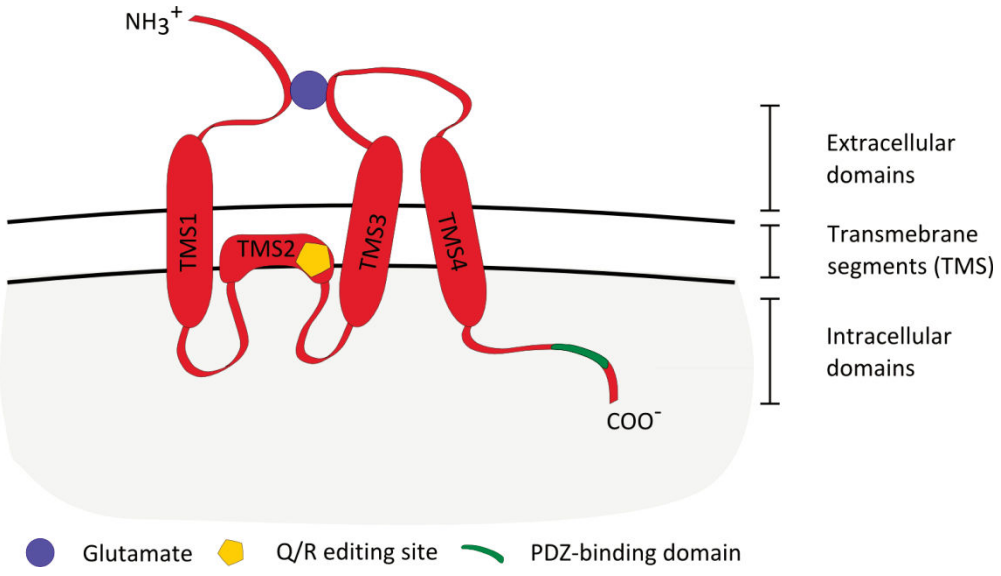

Figure 18 General structure of AMPAR subunit.
AMPAR subunits are composed of 4 transmembrane segments. The glutamate binding site is formed by the amino-terminal domain and the extracellular loop between TMS3 and TMS4. GluA2 mRNA undergoes a Q/R editing impeding the AMPAR Ca^{2+} permeability. The carboxy-terminal domain contains a PDZ-binding domain important for AMPAR synaptic clustering and its length differs between subunits: carboxy-terminal domain of GluA1, GluA2L and GluA4 is longer than the one of the GluA2, GluA3 and GluA4S subunits.

All four AMPAR subunits adopt the same **secondary structure** with an extracellular N-terminal domain, 3 hydrophobic membrane-spanning segments (TMS1, TMS3, TMS4) with an additional hydrophobic loop that forms the pore between TMS1 and TMS2 (Figure 18). The glutamate binding site is formed by the amino-terminal domain and the extracellular loop

between TMS3 and TMS4. GluA2, GluA3 and GluA4S have a short cytosolic CTD. On the contrary, GluA1, GluA4 and GluA2L subunit have a long cytosolic carboxy tail that hosts various regulatory phosphorylation sites and domains to interact with cytosolic proteins. It is commonly admitted that long-tailed subunits allow for activity-dependent regulation of AMPAR trafficking (Anggono and Huganir, 2012) whereas short-tailed subunit containing AMPAR appear to be constitutively expressed at the membrane (but see Granger et al., 2013; Lu et al., 2009).

Hence, it is accepted that **GluA2/GluA3 containing AMPA** receptors constitutively recycle in and out the synapse while **GluA1-containing AMPARs** are delivered in an activity-dependent manner (Hayashi et al., 2000; Kopec et al., 2006; Plant et al., 2006; Shi et al., 1999). These receptors have been suggested to lack the GluA2-subunit by experiment using activity-dependent delivery of exogenous tagged-GluA1 subunit (Hayashi et al., 2000) or more recently using the particular electrophysiological signature of the receptor (see below) (Plant et al., 2006). As suggested above, **GluA2-lacking AMPA receptors** are Ca^{2+} permeable and could therefore contribute to Ca^{2+} induced plasticity (Isaac et al., 2007). While it is not clear whether hippocampal principal cells express a sufficient amount of GluA1 homomers (Wenthold et al., 1996), interneurons in hippocampus (Isaac et al., 2007; Kullmann and Lamsa, 2007; Lamsa et al., 2007; Le Roux et al., 2013) or neurons in other brain regions (Isaac et al., 2007; Li et al., 2011; Maroteaux and Mameli, 2012) do express Ca^{2+} permeable AMPA receptors that contributes to LTP. In addition to their particular Ca^{2+} permeability, GluA2-lacking AMPARs exhibit an inward rectification at depolarized potentials due to endogenous polyamine block. Hence, Ca^{2+} influx through AMPAR and subsequent synaptic plasticity is only possible when the membrane is hyperpolarized conferring to the neuron an “anti-hebbian” plasticity mechanism (Lamsa et al., 2007; Le Roux et al., 2013). Additional information of activity-dependent exocytosis on GluA1-containing AMPARs will be provided in introduction II.2.

While it is widely accepted that **GluA4-containing** AMPARs decrease with neuronal maturation (Akaneya, 2007; Lohmann and Kessels, 2014; Zhu et al., 2000), the **relative proportion of GluA1/GluA2-containing versus GluA2/GluA3-containing AMPARs** remains uncertain. Kessels and colleagues estimated that GluA1/2- and GluA2/3-containing AMPAR are expressed in similar amounts in mature hippocampal neurons. This observation is however hardly compatible with the 80% and 15 % decrease in synaptic transmission in GluA1- and

GluA3–lacking mice respectively (Lu et al., 2009). One proposed explanation is that the lack of activity-dependent exocytosis of GluA1- but not GluA3-containing AMPAR could explain the overall effect observed in knock-out mice (Lohmann and Kessels, 2014). Recently, the group of Roger Nicoll has proposed that activity-dependent synaptic addition of AMPARs may not be subunit-specific but instead relies on availability of AMPARs (Granger et al., 2013). These observations highlight the complexity and the different compensatory mechanisms taking place to regulate synaptic activity. However, they are yet not sufficient to refute the current dogma regarding the basal expression of GluA2/3 containing AMPAR and the activity-dependent delivery of GluA1-containing AMPARs. Moreover, GluA1 requirement has been shown to be crucial for *in vivo* synaptic plasticity-based learning in amygdala (Humeau et al., 2007; Rumpel et al., 2005), hippocampus (Whitlock et al., 2006) or in barrel cortex (Takahashi et al., 2003). In addition to the subunit composition, AMPARs trafficking and function also dependent on auxillary subunits as well as on interactions with scaffolding proteins.

b) MAGUK, TARP and AMPAR-interacting proteins

Differences in AMPAR trafficking are due to differential interactions between AMPAR subunits and proteins tethered to or composing the postsynaptic density. First evidence of this regulation arose from studies using point-mutations as well as ablations of AMPAR containing the PDZ-interacting domain.

PDZ domain-containing proteins interact with the long CTD of AMPAR subunits as well as with NMDAR. For instance, **PSD-95**, the major scaffolding protein of the PSD, directly interacts with NMDAR via its PDZ domain (Kornau et al., 1995). Several PDZ domain-containing proteins have been identified within the PSD and are collectively named as membrane-associated guanylate kinase proteins or **MAGUK proteins**. This family contains the PSD-95 homologous proteins: PSD-93, SAP102 and SAP97. Although interaction between PSD-95 or SAP97 and NMDARs was the first one to be described, the role of MAGUK protein in NMDAR trafficking is less clear (Jeyifous et al., 2009) than for AMPAR synaptic targeting (for reviews Xu, 2011; Zheng et al., 2011). The relationship between MAGUK proteins and AMPAR-mediated synaptic plasticity is complex, depends on the neuronal maturation and is hard to predict due to overlapping functions (for review Huganir and Nicoll, 2013). For instance, while increase in PSD-95 and PSD-93 expression leads to an increase in AMPA-mediated synaptic transmission, double

genetic ablations of both PSD-95 and SAP-102 enhances LTP expression. The precise role of MAGUKs in AMPAR trafficking remains also elusive. SAP-97 binds the GluA1 subunit but also links the PKA anchoring molecule AKAP79 (Colledge et al., 2000) and could therefore favor GluA1-Ser845 phosphorylation by PKA that favors GluA1-containing AMPAR exocytosis (Colledge et al., 2000; Lee et al., 2003).

A second class of proteins has been shown to influence AMPAR activity and trafficking (Wyszynski et al., 1999; Ziff, 2007). Five transmembrane AMPAR regulatory proteins (**TARPs**) have been identified so far, **stargazin** protein being the best characterized one (Bats et al., 2007; Chen et al., 2000; Kessels et al., 2009; Opazo et al., 2010). It has been proposed that the PDZ-binding domain of TARPs is responsible for the synaptic clustering of AMPAR through MAGUK protein binding (Huganir and Nicoll, 2013). The TARP-unrelated proteins **cornichon-2 and cornichon-3** also act as auxiliary subunits of AMPARs and influence GluA1-containing AMPAR trafficking or gating (Herring et al., 2013; Shi et al., 2010).

In addition, GluA2- and GluA3-CTD can link Glutamate Receptor Interacting Proteins **(GRIP1 and GRIP2)** (Dong et al., 1997, 1999) and Protein Interacting with C-Kinase 1 **(PICK1)** (Xia et al., 1999) which all possess a PDZ domain. These AMPARs also interacts with N-ethylmaleimide-sensitive factor **(NSF)** (Lüscher et al., 1999; Lüthi et al., 1999; Nishimune et al., 1998). Schematically, following a protocol leading to LTD, dissociation of the complexes GluA2-GRIP1/2, GluA2-NSF and the interaction with PICK1 favor GluA2-containing AMPARs internalization (Lin and Huganir, 2007; Rocca et al., 2013; Steinberg et al., 2006; Terashima et al., 2008). The AMPAR endocytosis is clathrin-mediated and GluA2-CTD interacts with the aforementioned KCC2-interacting **AP-2** adaptor protein (Lee et al., 2002) (Figure 19).

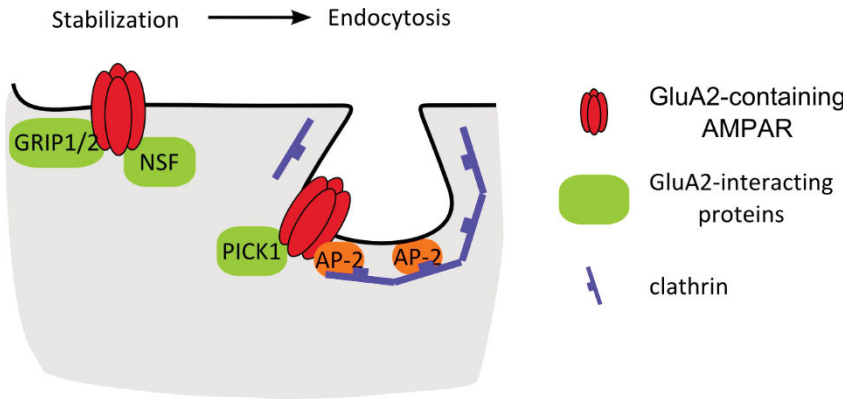

Figure 19 Endocytosis of GluA2-containing AMPARs
GluA2-containing AMPARs are stabilized by their association with GRIP1/2 and NSF. Dissociation of these complexes and interactions with PICK1 and the clathrin adaptator AP-2 favor clathrin-dependent endocytosis of the receptor.

Interestingly AMPAR share other intracellular partners with KCC2. GluA1 interacts with the actin-binding **protein 4.1N** described in introduction I.5.b). This interaction is enhanced by PKC phosphorylation of GluA1 on residues Ser816 and Ser818 and is necessary for GluA1-containing AMPAR exocytosis (Lin et al., 2009). Besides the role of subunit composition and interacting proteins, AMPAR trafficking underpinning excitatory plasticity is dependent of NMDAR activation.

c) NMDA receptor subunit composition

NMDAR are Ca^{2+} permeable and are critical to most forms of LTP. However the binding of glutamate alone is not sufficient to trigger Ca^{2+} influx. First, NMDAR activation requires the presence of a glutamate coagonist. Glycine has first been identified as a natural coagonist (Johnson and Ascher, 1987) and later on, glial-release of D-Serine has been suggested to overcome the low concentration of ambient glycine in the forebrain (Panatier et al., 2006). In addition to coagonist requirement, NMDARs exhibit a voltage-sensitive block by extracellular Mg^{2+} (Nowak et al., 1984). NMDAR is therefore qualified as a **detector of coincidence** since Ca^{2+} influx occurs only when presynaptic glutamate release is concomitant with postsynaptic depolarization.

NMDAR are tetramers composed of **two GluN1 subunits and two GluN2 subunits**. There are eight splicing variants of the GluN1-encoding gene *GRIN1* and GluN2A-D subunits are encoded by 4 genes *GRIN2A*, *GRIN2B*, *GRIN2C* and *GRIN2D* (Cull-Candy et al., 2001). The GluN2 composition of NMDAR is **regionally and developmentally regulated** and confers them with specific biophysical properties. In hippocampal principal cells, GluN2A- and GluN2B-containing NMDARs are predominant. GluN2A expression increases with age while GluN2B expression remains only in the hippocampus in adult rodent (Monyer et al., 1994) (Figure 20). GluN2C-containing NMDARs are restricted to cerebellum while GluN2D is sparsely expressed during development but not in the adult CNS (Monyer et al., 1994).

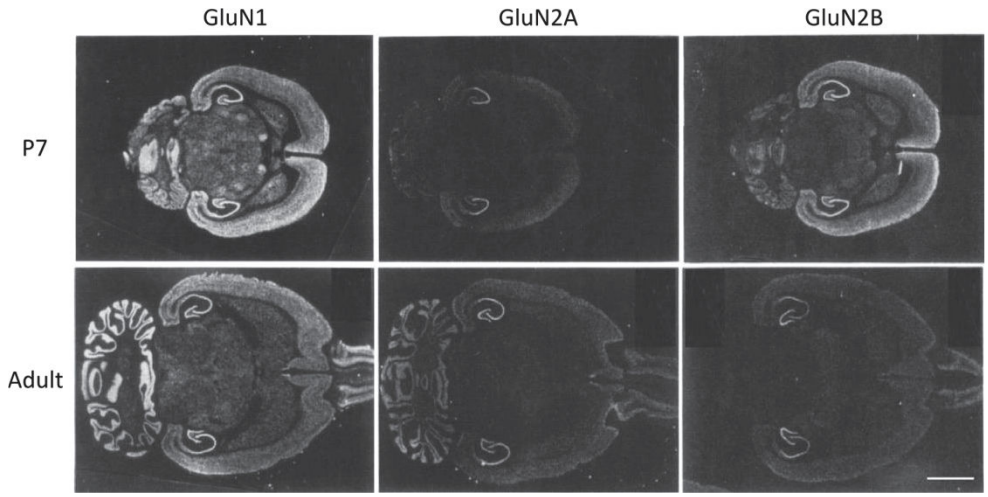

Figure 20 Subunit-specific regional and developmental regulation of NMDARs.
NMDARs are tetramers typically composed of two GluN1 and two GluN2 subunits. Expression of multiple variants of the GluN2 subunit is both developmentally and regionally regulated. Here an example of the developmental increase and decrease of GluN2A and GluN2B mRNA expression, respectively (Scale, 3.4mm). It is thought that GluN2B expression favors LTP. Adapted from Monyer et al., 1994.

Little is known about the characteristics of the GluN1 splice variants except that exon 5 influence the pH sensitivity and Zn^{2+} blockade (Cull-Candy et al., 2001; Traynelis et al., 1995). The decrease in GluN2B- to GluN2A-containing synapses ratio over development has functional implications (Foster et al., 2010). GluN2B-containing NMDARs show a higher affinity for glutamate, slower deactivation and desensitization kinetics and an higher affinity for CaMKII (for review Lohmann and Kessels, 2014), leading to overall larger Ca^{2+} transients. Hence, **GluN2B subunit is thought to promote LTP** in young neurons (Barria and Malinow, 2005; Foster et al., 2010) and therefore represents a way to modulate neuronal plasticity (Kopec et al., 2006; Lee et al., 2010b; Yashiro and Philpot, 2008).

Recently, Roberto Malinow has published a series of papers (Kessels et al., 2013; Nabavi et al., 2013) suggesting that tenuous Ca^{2+} influx through NMDAR could not be a requirement for LTD as previously thought (Cummings et al., 1996; Lisman, 1989). Instead, they suggested that involvement of NMDAR in the induction of LTD was metabotropic i.e. relying on direct modulation of downstream protein activity. Although these results have not been replicated (Babiec et al., 2014), it is possible that this putative metabotropic effect reflects a NMDAR conformation-dependent interaction with CaMKII that I will describe in the next section.

d) Ca^{2+}/Calmodulin Kinase II: another moonlighting protein ?

Both postsynaptic-dependent LTP and LTD are tightly regulated by **phosphorylation** and **dephosphorylation** of AMPAR and other synaptic proteins. Briefly, activation of the Ser/Thr kinases **PKA, PKC and CaMKII** are usually involved in LTP induction (see introduction II.2) while dephosphorylation events by protein phosphatases **PP1, PP2A or PP2B** (calcineurin) leads to LTD (Malenka and Bear, 2004). PP2B is the only phosphatase eliciting a modulation by Ca^{2+}/calmodulin (Baumgärtel and Mansuy, 2012).

CaMKII is a circular holoenzyme composed of twelve subunits, mainly CaMKIIα-CaMKIIβ (Figure 21A). CaMKIIγ and CaMKIIδ subunits are less abundant in the brain. Each CaMKIIα and CaMKIIβ is composed of a kinase domain, an **autoinhibitory** domain and a domain of interaction. Interestingly, CaMKIIβ subunit also hosts an actin-binding domain. Under basal conditions, the CaMKII catalytic core is masked by its own autoinhibitory domain. The binding of Ca^{2+}/Calmodulin complex upon a rise of intracellular Ca^{2+} leads to the unmasking of the catalytic domain. Once activated, the enzyme is **autophosphorylated on Thr286** and Thr287 residues of the CaMKIIα and the CaMKIIβ, respectively. This autophosphorylation within the autoinhibitory domain allows the CaMKII activity to persist longer after the calcium concentration falls to baseline levels (for reviews Lisman et al., 2012; Okamoto et al., 2009). A recent imaging-based study has evaluated that CaMKII activation decays within a couple of minutes after LTP induction (Lee and Yasuda, 2009; Lee et al., 2009).

Moreover, upon LTP induction, **CaMKII is translocated toward the activated PSD** in a Ca^{2+}/Calmodulin-dependent manner but that interestingly does not require CaMKII kinase activity (Shen et al., 2000a). On the contrary, its activity-dependent translocation preferentially **toward the GluN2B subunit** of the NMDAR is regulated by Thr286 phosphorylation and promotes CaMKII activity (Bayer et al., 2001) (Figure 21B). One hypothesis for the CaMKII translocation relies on its interaction with the actin spine cytoskeleton. Electron and light microscopy shows that CaMKIIβ but not CaMKIIα is able to bundle and stabilize actin microfilaments (Okamoto et al., 2007; Sanabria et al., 2009). Addition of new CaMKII and translocation toward the PSD could participate in actin cytoskeleton stabilization and remodeling necessary for plasticity (see introduction II.3.c).

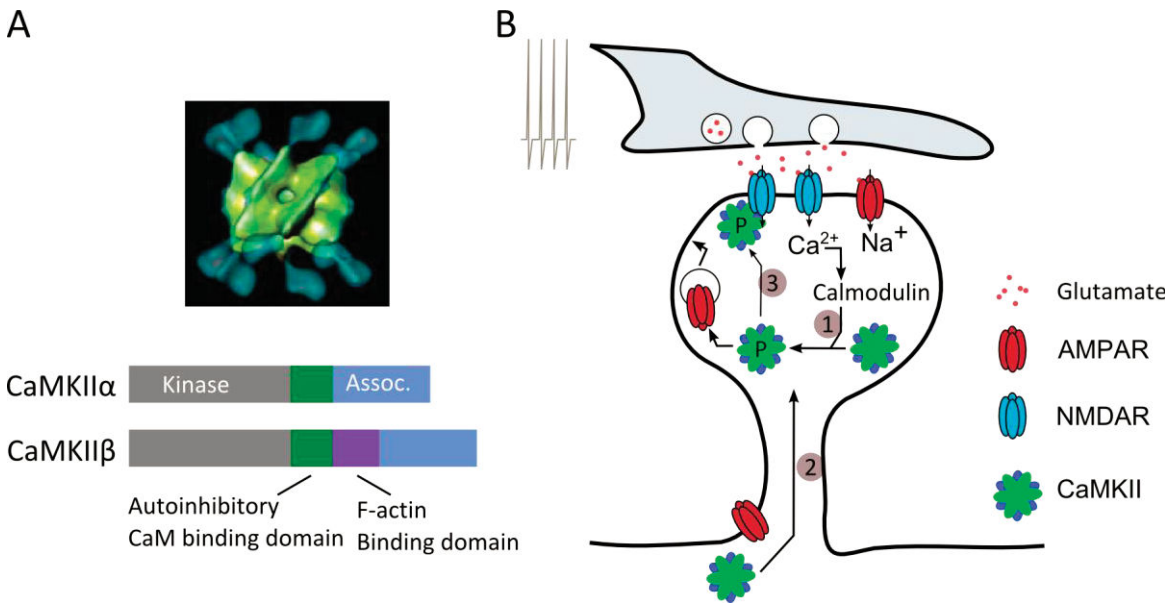

Figure 21 Structure and synaptic translocation of Ca^{2+}/Calmodulin Kinase II
(A) Top: 3D reconstruction of CaMKII structure. Bottom: CaMKII is composed of twelve subunits, mainly CaMKIIα-CaMKIIß. Auto-inhibition of the kinase domain is relieved upon binding of Ca^{2+}/Calmodulin. Adapted from Okamoto et al., 2009. (B) 1. NMDAR-dependent activation of Ca^{2+}/Calmodulin induces CaMKII autophosphorylation. 2. During LTP induction, CaMKII is translocated into the activated spine independently of its phosphorylation state. 3. Within the spine, translocation toward NMDARs is dependent of CaMKII phosphorylation and is thought to favor CaMKII activity.

Hence, CaMKII is a multifunctional protein that gates activity-driven change in synaptic strength through its kinase activity and regulates actin cytoskeleton through both its kinase activity and structural role.

2. Post synaptic potentiation of excitatory synapses

As previously mentioned, changes in the efficacy of excitatory synapse efficacy relies on changes in neurotransmitter release probability or changes in the postsynaptic receptors. Despite on-going debates on the locus of LTP expression at the Schaeffer collateral to CA1 synapses, it is admitted that this form of LTP is primarily driven by post-translational modification of postsynaptic AMPARs. Non-stationary fluctuation analysis of EPSCs shows that phosphorylation of Ser831 by either PKC or CaMKII (Barria et al., 1997; Mammen et al., 1997) increases the unitary conductance of AMPARs (Derkach et al., 1999; Kristensen et al., 2011). Similarly, imaging and electrophysiology experiments have demonstrated that phosphorylation of the GluA1-CTD by PKA at Ser845 (Man et al., 2007; Roche et al., 1996) and by CaMKII and PKC at Ser816, Ser818 and Ser831 (Boehm et al., 2006; Lin et al., 2009; Roche et al., 1996) lead to an increase in the number of synaptic receptors. Altogether, these

phosphorylations sustain the increase in excitatory transmission underlying long term potentiation.

a) Addition of GluA1-containing AMPAR sustains LTP

On the way to the 2000s, the first physiological evidence for GluA1-containing AMPA receptor insertion arose from Roberto Malinow's group. Using expression of recombinant GluA1-tagged with GFP, they showed that tetanic stimulation (Shi et al., 1999) or overexpression of the constitutively active CaMKII (Hayashi et al., 2000) leads to the synaptic aggregation of GluA1-GFP containing AMPA receptors. In the same study, Hayashi and coworkers showed that mutation of Thr887 within the PDZ-binding domain, into an alanine hindered insertion of new AMPARs. On the contrary, the mutation of Ser831 that influence unitary conductance of the channel, did not impair this mechanism (Hayashi et al., 2000).

The importance of GluA1-containing AMPARs in LTP expression and learning was further confirmed using mice carrying a complete genetic ablation of *GRIA1*. These mice show altered LTP expression in acute slices as well as impairment in some but not all hippocampal-dependent spatial memory tasks (Reisel et al., 2002). Similarly, overexpressing the GluA1-CTD in amygdala neurons precluded both LTP and fear conditioning memory (Rumpel et al., 2005). Overexpression of the long GluA1-CTD is nowadays widely used to block activity-dependent addition AMPARs.

CaMKII- and PKA-dependent synaptic recruitment of GluA1-containing AMPARs seems the most parsimonious and widely accepted mechanism of LTP expression (but see Granger et al., 2013). This scenario assumes the availability of both AMPARs and synaptic slots to receive additional AMPARs (Figure 22).

b) Local endosomal reserve pool

Membrane AMPARs undergo continuous recycling through clathrin-dependent endocytosis, transfer to recycling endosome and activity-dependent or constitutive exocytosis. The molecular determinants of these **recycling endosomes** in the regulation of the membrane pool of AMPAR are still under investigation (for review Hirling, 2009). In 2004, two groups

observed that insertion of new AMPAR was dependent on the endosomal, small GTPases Rab8 (Gerges et al., 2004) and Rab11 (Park et al., 2004). It appears that myosin Vb can bind Rab11 and translocate endosomes with GluA1-containing AMPAR into spines. This translocation allows exocytosis of new AMPARs and growth of dendritic spines (Wang et al., 2008).

Different markers of endosomes have then been used to demonstrate the importance of this subcellular compartment. In C. Elegans, Rab6.2- and retromer-containing endosomes are crucial to maintain synaptic transmission (Zhang et al., 2012). In mouse, retromer-associated endosomes contain and regulate trafficking of beta-adrenergic receptors and glutamate-gated channels (Choy et al., 2014). Similarly, endosomes containing the vesicular pH regulating transporter NHE6 are recruited into spines upon LTP-triggering stimuli (Deane et al., 2013). Finally, the endosomal sorting protein nexin-27 is a PDZ-domain containing protein enriched in dendrites and spines. It interacts with the GTPase Ras (see introduction II.3.c) in a Ca^{2+}/Calmodulin-dependent manner (Loo et al., 2014). This interaction drives homomeric GluA1-containing AMPAR exocytosis and its impairment prevents LTP (Loo et al., 2014; Zhu et al., 2002).

c) Equilibrium of AMPAR endocytosis/exocytosis in long term plasticity

Activity-dependent exocytosis of AMPAR is at the origin of LTP. Using total internal reflection fluorescence (TIRF) imaging of AMPAR in postsynaptic like structures, Tanaka & Hirano showed that LTP leads to addition of GluA1- and removal of GluA2-containing AMPARs, followed by a delayed addition of GluA2-containing AMPARs (Tanaka and Hirano, 2012). These *in vitro,* imaging results corroborate electrophysiological measurements of the transient insertion of GluA2-lacking AMPARs in slices (Plant et al., 2006). This two-step mechanism is proposed to drive and maintain the increase in synaptic transmission and highlights the differential regulation in exocytosis and endocytosis of AMPAR.

Activity-dependent AMPAR endocytosis is mainly involved in LTD and therefore is beyond the scope of this thesis. However, I will briefly evoke some of the activity-dependent mechanisms of AMPAR endocytosis for comparison with the mechanisms underlying LTP. As previously mentioned, **endocytosis of GluA2-containing AMPARs** is under the control of PICK1 (Rocca et al., 2013). In a model of glycine-induced LTP, transient insertion of GluA2-lacking AMPAR has

been proposed to be due to an increase in PICK1 (Jaafari et al., 2012). The stabilizing interaction between GluA2 and GRIP1 is in part dependent on a protein called thorase. Suppression of this protein greatly impacts long term depression relying on GluA2-containing AMPAR internalization (Zhang et al., 2011). Other proteins have been shown to influence AMPA receptor endocytosis. The microtubule associated protein 1B (MAP1B) implicated in the Rac1 pathway (see introduction II.3.c) is necessary for GluA2 endocytosis-mediated LTD (Benoist et al., 2013). GluA1-containaing AMPARs also undergo regulated endocytosis. Thus, the local translation of the activity-regulated cytoskeleton-associated protein (Arc/Erg3.1) has been shown to promote its endocytosis (Chowdhury et al., 2006).

On the other hand, **exocytosis of AMPAR is a SNARE-dependent mechanism**. Soluble N-ethylmaleimide-sensitive-factor Attachment protein Receptors (SNAREs) are a superfamilly of proteins implicated in exocytosis. Originally, they were divided in v-(vesicular-) SNARE and t-(target-) SNARE depending respectively on their membrane localization. A second biochemical classification has been proposed with the R-SNAREs (equivalent to v-SNAREs) that are arginine enriched in and the Q-SNAREs (equivalent to t-SNAREs) that are glutamine enriched. Association of the v-SNARE and t-SNARE complex is tethered by a protein called complexin with help of the calcium-sensitive protein, synaptotagmin. The group of Robert Malenka has investigated the SNARE dependency of activity-dependent insertion of AMPAR. They showed that it relies on complexin- but not synaptotagmin-1 dependent mechanisms (Ahmad et al., 2012). In addition, they observed that the activity-dependent exocytosis but not constitutive recycling of AMPARs was dependent of the t/Q-SNAREs syntaxin-3 and SNAP-47 (Jurado et al., 2013).

The development of a pH sensitive GFP, called **SuperEcliptic Phluorin** (SEP) (Miesenböck et al., 1998), made it possible to specifically visualize the membrane pool of AMPARs: coupled to the extracellular NTD of AMPAR, SEP is fluorescent when AMPARs are facing neutral, extracellular medium while SEP is quenched when AMPARs lie in acidic, exocytotic vesicles. Thereby, it made it possible to follow AMPAR subunit specific trafficking (Ashby et al., 2004; Kopec et al., 2006; Lin et al., 2009). By combining GluA1-SEP recombinant protein and TIRF imaging Lin and collaborators were able to identify **single spontaneous exocytosis** events. They showed that GluA1 phosphorylation of Ser816 and Ser818 by protein kinase C increases its interaction with 4.1N. This enhanced binding facilitates the insertion of GluA1- but not

GluA2-containing AMPARs. They finally observed that lentivirus-mediated **suppression of 4.1N impairs LTP** in acute hippocampal slice. Similarly, using the same GluA1-SEP construct but two-photon microscopy, Kopec and colleagues showed that a chemically induced form of LTP leads to the delivery of GluA1- but not GluA2-containaing AMPARs (Kopec et al., 2006). Identical results were obtained using two-photon glutamate uncaging-evoked LTP while monitoring GluA1-SEP fluorescence recovery after photobleaching (FRAP) (Makino and Malinow, 2009; Patterson et al., 2010).

A recent study from the group of Richard Huganir has, however, highlighted some limitation in the use of GluA2-SEP to monitor its internalization (Rathje et al., 2013). Quenching of residual fluorescence originating from intracellular pools of receptors occurs upon NMDA application due a NMDA-dependent decrease in intracellular pH. The origin of this transient quenching is unknown but can be misinterpreted as a GluA2-SEP internalization. Nevertheless, It seems still valid to use GluA1-SEP to monitor insertion or diffusion of GluA1-containing AMPA receptor (Kopec et al., 2006; Lin et al., 2009; Makino and Malinow, 2009, 2011).

Despite all these advanced microscopy techniques, the **exact location of AMPAR exocytosis** remains unclear due to apparently conflicting results (for a review addressing this point Henley et al., 2011).

Nevertheless, exocytosis seems unlikely to occur directly at the PSD due to steric hindrance. Therefore, newly exocytosed-AMPARs likely need to travel toward the synapse. To my knowledge, no directional diffusion from the locus of the exocytosis to the PSD has ever been described**. Lateral diffusion of transmembrane receptor** is therefore only governed by free diffusion in a crowded environment, with trapping events when the receptor binds to an anchoring protein like PSD-95. The development of quantum-dot based single particle tracking has allowed to follow the diffusive behavior of receptors (Choquet and Triller, 2013). Protocols triggering LTP leads to a stabilization of AMPAR at activated synapses (Petrini et al., 2009; Tardin et al., 2003). Petrini and collaborators additionally showed that the recycling pathway maintains a pool of mobile AMPAR required for LTP (Petrini et al., 2009). As previously mentioned, the exact locus of exocytosis is not known yet. However, a theoretical model based on experimental data shows that the distance between the site of exocytosis and the synapse negatively influences the strengthening of synapses. This is due to the absence of directional diffusion toward the synapse. On the other hand, basal number of AMPARs at the

PSD is solely governed by the number of AMPAR, the affinity between AMPAR and scaffolding proteins and the size of the PSD but not by the location of exocytosis (Czöndör et al., 2012).

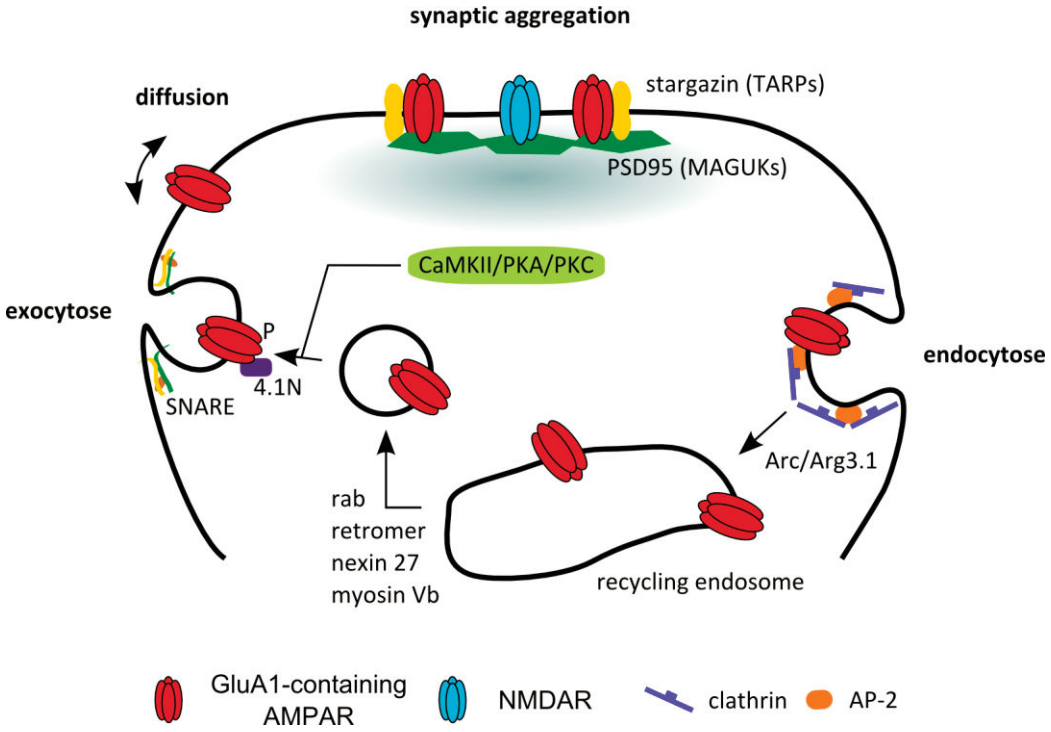

Figure 22 Trafficking of GluA1-containing AMPARs
Functional long term potentiation relies on exocytosis of GluA1-containing AMPARs stocked in recycling endosomes. Several effectors are implicated in the endosomal trafficking of AMPARs. Exocytosis is favored by phosphorylation of the GluA1 subunit and interactions with the actin-linked protein 4.1N. AMPARs reach postsynaptic density by lateral diffusion where they are stabilized by MAGUKs and TARPs. The intracellular pool of AMPARs is replenished through endocytosis.

In summary, regulation of AMPARs trafficking allows addition and stabilization of new AMPARs within the postsynaptic density and underlies LTP expression (Figure 22). In addition, **LTP is accompanied by an increase in volume of dendritic spine** that hosts the PSD. Both spine swelling and AMPAR trafficking relies on **remodeling of actin-cystokeleton**. Hence, the next section will explore the actin-dependent interplay between structural and functional plasticity.

3. Structural plasticity: dendritic spine and actin remodeling

a) Phenomenology of dendritic spine shape and motility

Dendritic spines that host excitatory synapses are actin-rich protrusions emerging from dendritic shafts. They are composed of a bulbous head housing all the postsynaptic machinery connected to the shaft through a thin spine neck acting as a chemical and electrical diffusion barrier (Bloodgood and Sabatini, 2005; Majewska et al., 2000; Takasaki and Sabatini, 2014; Tønnesen et al., 2014; Yuste, 2013). Dendritic spines are usually classified into three types: **thin, mushroom and stubby** (Figure 23). Thin spines are stable filopodia-like structures with a thin and long neck and small spine head. They are usually thought to represent immature or silent synapses (Matsuzaki et al., 2001). Mushroom-type spines possess a larger spine head while stubby spines are devoid of a neck (but see Tønnesen et al., 2014). The position and the **organization of the PSD** within the spine are variable, from simple, round PSD to multiple PSDs facing distinct release sites from a presynaptic terminal (Hering and Sheng, 2001; Jones and Powell, 1969). Overall, the size of the spine head and of the PSD directly correlate with synaptic strength (Cane et al., 2014).

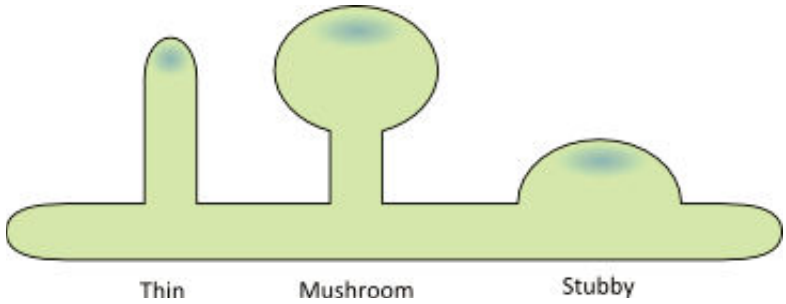

Figure 23 Classification of dendritic spines
Typically, dendritic spines are classified into three types according to the size of the spine head hosting the glutamatergic PSD (blue) and the length of spine neck connecting the dendritic shaft.

Dendritic spines are dynamic structures that change in shape and number as a function of development and activity. **During development**, spines with a mushroom-type structure gradually substitute for filopodia and thin-type spines (Ziv and Smith, 1996). *In vitro,* changes in spine number are associated with **homeostatic plasticity** (Papa and Segal, 1996) as well as LTP (Engert and Bonhoeffer, 1999). **Spine head swelling associated with LTP** has been described soon after discovery of functional LTP (Van Harreveld and Fifkova, 1975) and observed in hippocampal cultures of dissociated neurons (Gu et al., 2010) and organotypic slices (Bosch et al., 2014; Matsuzaki et al., 2001; Steiner et al., 2008). However, direct evidence

are still scarce for LTP-induced changes in spine volume in hippocampus *in vivo* (Gu et al., 2014). In other brain regions, learning paradigms or drugs of abuse lead to an increase in the number and size of spines *in vivo* (e.g. Holtmaat et al., 2005; Muñoz-Cuevas et al., 2013). **Long-term *in vivo* imaging** further revealed heterogeneity in spine stability with highly mobile spines and stably maintained dendritic spines (Holtmaat et al., 2005) which are thought to be associated with long-term memories (Hofer and Bonhoeffer, 2010; Yang et al., 2009).

Recently, development of two-photon glutamate uncaging has made possible to study **structural changes at a single dendritic spine scale** (Figure 24). Glutamate-uncaging in a non-spiny region of a dendritic shaft leads to *de novo* spine growth in a NMDAR- and PKA- but not CaMKII- or TrkB-dependent manner (Kwon and Sabatini, 2011) and spontaneously-formed spines becomes rapidly functional with a presynaptic apposition (Zito et al., 2009). Long term structural changes correlating with functional plasticity may also be elicited by glutamate-uncaging onto preexisting spines (Bosch and Hayashi, 2012; Harvey and Svoboda, 2007).

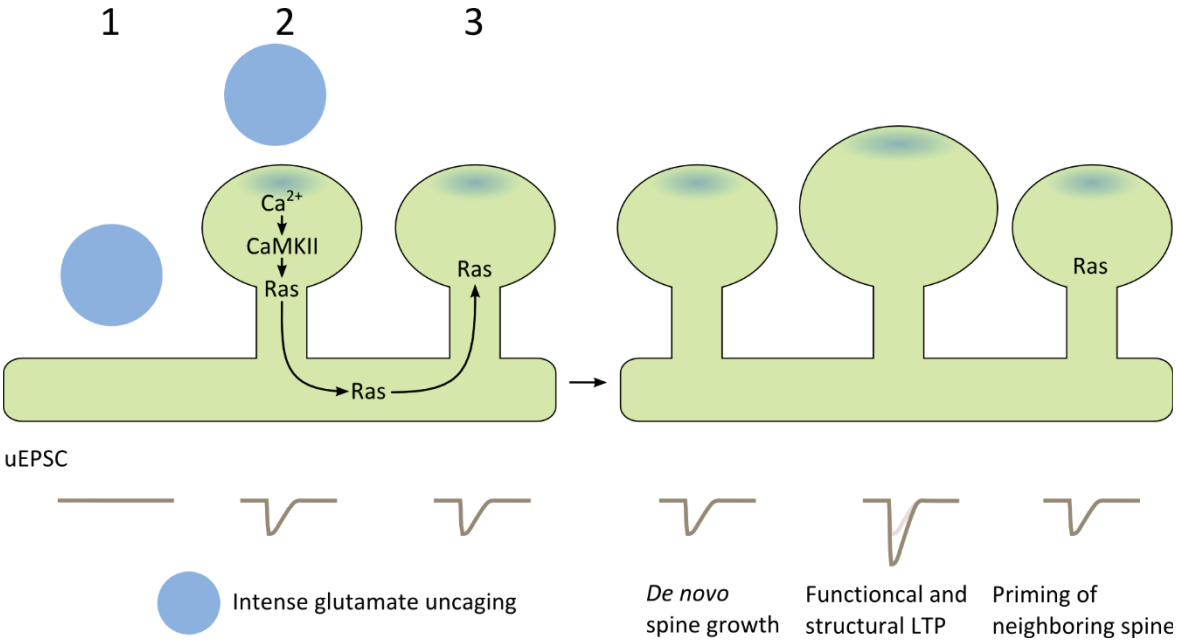

Figure 24 Structural changes using focal uncaging of glutamate
1. Focal MNI-glutamate uncaging on unspiny region of dendritic shafts leads to de novo spine growth associated with appearance of uncaging-induced excitatory postsynaptic current (uEPSC). Adapted from Kwon and Sabataini 2011. 2. Single spine functional and structural plasticity can be induced using focal uncaging of MNI-glutamate. 3. Spreading of Ras, but not Ca^{2+} or CaMKII is thought to lower the threshold of LTP induction at neighboring spines. Adapted from Harvey et al., 2008.

Both **functional and structural LTP are restricted to the stimulated spine** (Bosch et al., 2014; Harvey and Svoboda, 2007; Matsuzaki et al., 2001; Steiner et al., 2008) but have been shown to lower the threshold of LTP induction at neighboring synapses (Harvey et al., 2008). Since

the increases in intracellular Ca^{2+} and activated CaMKII are restricted to the spine compartment (Harvey et al., 2008; Lee and Yasuda, 2009; Lee et al., 2009; Lisman et al., 2012), they cannot account for the priming of LTP at neighboring synapses. However, the **small G protein Ras**, a downstream effector of CaMKII, does diffuse to nearby synapses and may be responsible for local-regulation of LTP threshold (Harvey et al., 2008).

I previously mentioned this small G protein as a regulator of GluA1-containing AMPAR exocytosis (Zhu et al., 2002). Ras is a GTPase enzyme (i.e. binding of GTP activates its kinase activity) at the crossroad of several molecular pathways. Within dendritic spines, Ras is involved in actin-cytoskeleton regulation. **Spine actin cytoskeleton** is involved in AMPAR exocytosis (Gu et al., 2010; Kopec et al., 2007), clustering (Allison et al., 1998) and PSD maintenance (Allison et al., 1998; Kuriu et al., 2006), spinogenesis (Haeckel et al., 2008; Hotulainen et al., 2009) and structural plasticity (Bosch et al., 2014; Gu et al., 2010; Okamoto et al., 2009, 2004). Conversely, increase in spine volume precedes GluA1-containing AMPAR membrane insertion (Kopec et al., 2006) but its maintenance requires exocytosis (Park et al., 2006; Yang et al., 2008) suggesting a strong interdependency between functional and structural plasticity through actin regulation. Hence, it is crucial to understand the underlying mechanism governing activity-induced actin-cytoskeleton remodeling.

b) Measuring actin in a submicron compartment

Actin microfilament (F-actin) is a key component of the eukaryote cellular cytoskeleton. F-actin is the primary cytoskeleton of dendritic spines (Korobova and Svitkina, 2010) although transient microtubules have been shown to invade spines and might play a role in synaptic plasticity (for review Dent et al., 2011). A dynamic equilibrium exists between F-actin and G-(globular-) actin, the monomeric form of actin. This equilibrium is controlled by different types of enzymes. Nucleation as well as branching of F-actin is promoted by the **Arp2/3 complex**. Polymerization of actin at the barbed end - plus end - is under the control of **profilin** that binds G-actin and allows the exchange of ADP for ATP. Depolymerization of F-actin at the pointed end – minus end - is promoted by the severing protein **cofilin** (Mizuno, 2013). Other actin-associated proteins have been also described. Among them **cortactin** promotes Arp2/3 complex recruitment and **capping proteins** block F-actin polymerization at the barbed end (Figure 25).

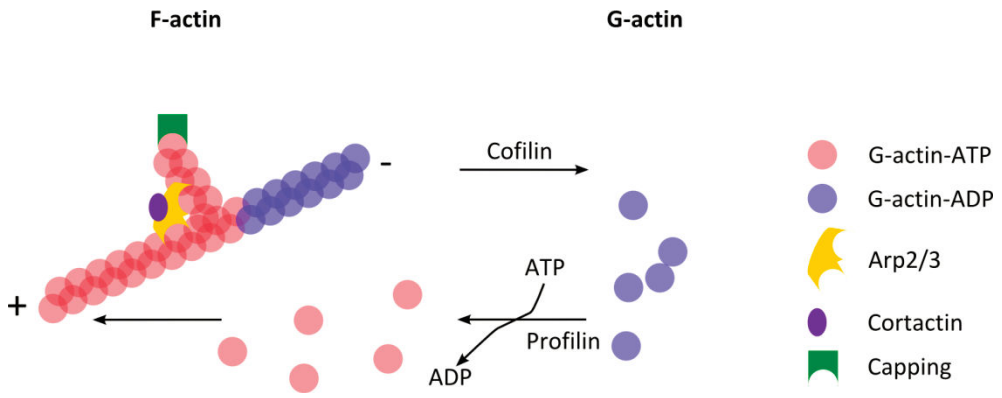

Figure 25 Dynamics of actin microfilaments
Addition of ATP-bound G-actin at the + end of filamentous actin is promoted by the protein profilin which binds G-actin and allows the exchange of ATP for ADP. Arp2/3 complex promotes the nucleation and the branching of F-actin. Capping of F-actin + end or the severing protein cofilin promotes depolymerization of actin microfilaments.

Different methods exist to alter and to visualize the F-actin cytoskeleton. The **pharmacological agents** latrunculin A and cytochalasin D both lead to depolymerization of F-actin. On the contrary, jasplakinolide stabilizes filamentous actin. Phalloidin, a F-actin stabilizing toxin is now widely used coupled to a fluorochrome to visualize F-actin, mostly in fixed tissue. Different optogenetic approaches have also been developed to **measure actin dynamic in living cells**. FRAP of recombinant actin- (Koskinen and Hotulainen, 2014; Koskinen et al., 2012) or lifeAct- (a small actin binding peptide, Riedl et al., 2008; Rocca et al., 2013), tagged with a fluorophore allows such measurements. Local activation of a photoactivable-GFP coupled to actin subunit reveal the presence of a highly diffusible pool of G-actin with a diffusion time constant of 30 μm^2/sec and of a second pool of F-actin with a longer time constant (Frost et al., 2010; Honkura et al., 2008). To overcome the simultaneous visualization of both G-actin and F-actin, Förster Resonant Energy Transfer-(FRET-) based measurement can be performed in neurons coexpressing actin-tagged with either CFP or YFP (Okamoto et al., 2004). More recently, super resolution techniques have been applied to measurements of actin dynamics and structure within dendritic spines (Frost et al., 2010; Izeddin et al., 2011; Tatavarty et al., 2009; Urban et al., 2011).

Altogether, these experiments reveal that F-actin does not show a preferred orientation (Tatavarty et al., 2009). Instead, the **dynamics of actin polymerization varies within spine** with a dynamic pool at the tip of the spine head and a more stable pool at the base of the spine head. A third, dynamic “enlargement” pool is transiently observed upon an increase in activity and is dependent of CaMKII activity (Honkura et al., 2008).

c) Activity-dependent regulation of actin cytoskeleton

What are the molecular determinants of the activity-dependent remodeling and increase in F-actin? Surprisingly, little is known about the polymerizing factor that could be activated upon LTP protocol. The number of profilin-containing synapses is increased upon KCl treatment (Neuhoff et al., 2005) in an NMDA-dependent manner (Ackermann and Matus, 2003). Conditional genetic ablation of Arp2/3 leads to a decrease in the number of spines and in the magnitude of LTP but not LTD (Kim et al., 2013).

The involvement of CaMKII in activity-dependent remodeling of F-actin may reflect its role in F-actin bundling and stabilization that is lost when CaMKII is translocated to the GluN2B subunit of the synaptic NMDARs (Okamoto et al., 2009, 2007). Nevertheless, CaMKII has also the capacity to modulate actin dynamics through indirect **inhibition of the actin-severing cofilin** (Mizuno, 2013). Importantly, both LTP *in vivo* (Fukazawa et al., 2003) and exploratory behavior (Fedulov et al., 2007) induce an NMDAR-dependent inhibition of cofilin leading to an increase in dendritic spines F-actin content in hippocampus. Conversely, cofilin activity is required for extinction of conditioned aversive memory (Wang et al., 2013).

Cofilin is inhibited by phosphorylation at the residue Ser3 by LIM kinase (LIMK). Several pathways and shortcuts link CaMKII to LIMK but all of them converge to activate LIMK either by **PAK** (p21-activated kinase) or **ROCK** (RhoA-specific kinase) (for review Calabrese et al., 2006; Okamoto et al., 2009) (Figure 26):

- **CaMKII** activation lead to phosphorylation of the guanine-nucleotide-exchange factor (GEF) **kalirin-7**. Kalrin-7 GEF activity leads to the activation of the GTPase **Rac1** that activates **PAK**. Hence, kalirin-7 has been reported to be required for both GluA1 trafficking and spine enlargement (Xie et al., 2007);
- **Tiam1**, another GEF, activated directly by **CaMKII** or indirectly through the activation of the GTPase **Ras** also leads to the activation of **Rac1.** Tiam1 is involved in MAP1B signaling leading to endocytosis of AMPARs (Benoist et al., 2013)**;**
- The indirect, **CaMKII-**dependent activation of the GEF **Beta-PIX** (Beta-PAK interacting exchange factor), together with its binding partner **GIT1** (G protein-coupled receptor kinase-interacting protein1) leads to the activation of both **Rac1** and **PAK.** This pathway has been so far mainly involved in spinogenesis (Saneyoshi et al., 2008) and the regulation of GABAergic transmission (Smith et al., 2014) ;

- **ROCK** is phosphorylated by the GTPase **RhoA,** indirectly activated by **CaMKII** through the GEF protein **Icf** together with **spinophilin** recruitment.

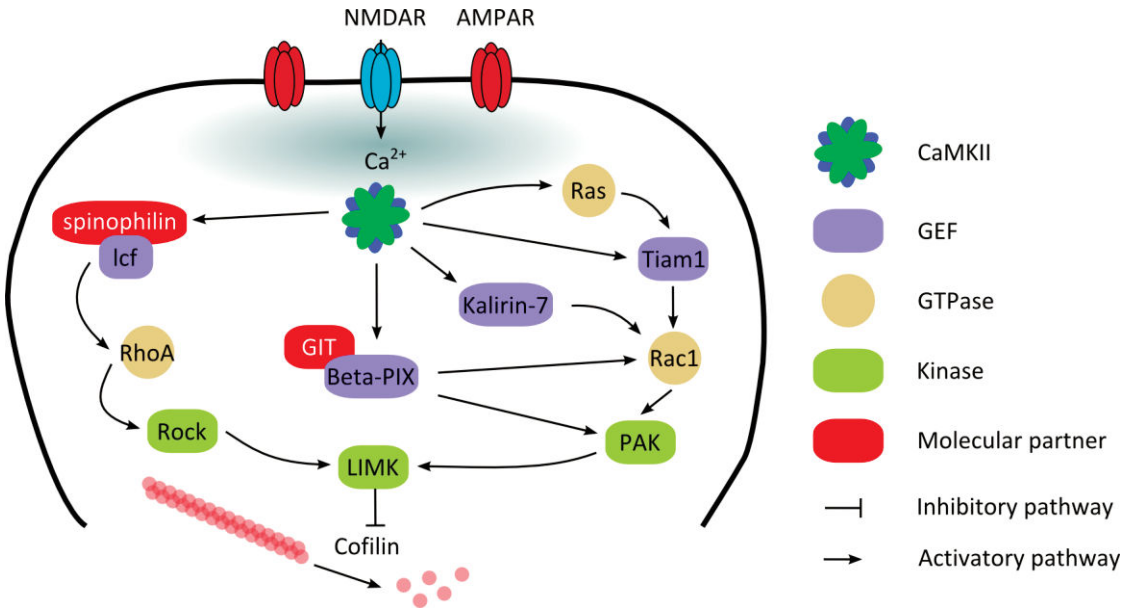

Figure 26 Actin remodeling during LTP: CaMKII-dependent pathways
CaMKII activation leads to an overall inhibition of cofilin and thereby promotes actin polymerization. Several molecular pathways are activated by CaMKII but all of them converge to activate LIMK that in turn inhibits cofilin. GEFs are guanine-nucleotide-exchange factors that active GTPases by promoting the replacement of GDP by GTP. GTPases are GTP-dependent kinases.

An elegant and exhaustive study has recently investigated the **temporal dynamics of activation** and the requirement of all the aforementioned proteins during LTP (Bosch et al. 2014). The authors monitored each actor using expression of a recombinant tagged protein and then evaluated the impact of its inhibition while using spine volume changes as a proxy to LTP. Surprisingly, cofilin is massively transported into the activated spine and at first actively helps the remodeling of actin cytoskeleton. Then, it seems that a high concentration of **cofilin stabilizes F-actin** as described in vitro (Andrianantoandro and Pollard, 2006).

These observations are somewhat difficult to reconcile with the molecular cascades stimulated upon CaMKII activation and leading to LIMK activation, cofilin inhibition and putative actin polymerization (Figure 26). Nevertheless, other studies have suggested that cofilin activity is necessary for both LTP-associated increase in spine volume and GluA1 trafficking (Gu et al., 2010). In line with this observation, it is also interesting to note that genetic ablation of LIMK has little effect on basal excitatory transmission and leads to an unpredicted increase in LTP amplitude (Meng et al., 2002). Conditional knock-out of cofilin

(Rust et al., 2010) as well as latrunculin A-mediated disruption of actin cytoskeleton (Krucker et al., 2000) both lead to an alteration of the late but not early phase of LTP. Ouyang and colleagues proposed in 2005 that transient decrease in actin polymerization might be necessary for translocation of proteins, such as the CaMKII, inside the spine (Ouyang et al., 2005).

In conclusion, tight activity-dependent regulation of the actin cytoskeleton is crucial for both structural and functional LTP. Actin polymerization is necessary for the maintenance of dendritic spine swelling upon LTP. Nevertheless, actin depolymerization through activated cofilin seems as well mandatory for the first step of LTP and both activity-driven exocytosis of AMPARs.

MATERIALS AND METHODS

MATERIALS & METHODS

Detailed materials and methods may be found in the manuscript included in this thesis. They include details on the DNA and lentiviral constructs used to alter KCC2 function and expression or to monitor structural and functional long-term potentiation. During my PhD, dissociated hippocampal neuron cultures were mostly prepared from embryonic day 19 sprague Dawley rat pups. These neurons were then used for both electrophysiological recordings and live- or fixed-imaging. In this material and methods section, I would like to discuss more specifically the methodological rationales for the techniques used during my PhD.

I. HOW TO MEASURE KCC2 ION-TRANSPORT ACTIVITY?

KCC2 transport stoichiometry renders this carrier electroneutral. Hence, its transport function cannot be directly measured using electrophysiological recordings. The techniques used to overcome this limitation are based on measurements of potassium or potassium-substitute transport and direct or indirect intracellular chloride concentration. For an exhaustive and comprehensive review on these techniques, please refer to the review of Medina and coworkers after which this section was entitled (Medina et al., 2014).

1. Direct measurement of KCC2 activity using potassium or potassium substitutes

KCC2 transports various cation species. Classical approaches to measure KCC2 and other CCC function has involved assays of chloride dependent transports of **radioactive $^{40}K^+$** or more frequently, **$^{86}Rb^+$** (Gamba, 2005; Mount et al., 1998; Payne, 1997). Within the same group of the periodic table, below Rb^+, lies cesium which is commonly used in whole cell patch-clamp recordings as substitute for potassium to increase membrane resistance and space-clamp. In addition to blocking K^+ channels, **Cs^+** greatly reduces KCC2 transport activity and could then influence the readout of experiments involving KCC2 function (Payne, 1997).

To avoid the use of radio-elements in neuronal systems, several groups have used NH_4^+-based assays as NH_4^+ is also transported by KCC2. **Extracellular NH_4^+ application** leads to biphasic changes in intracellular pH: a KCC2-independent alkalinisation due to the entrance of NH_3, followed by a KCC2-dependent acidification. The first phase reflects the permeability of cytoplasmic membrane to the alkyl NH_3 while the second relies on KCC2-mediated import of

NH_4^+. The pH-sensitive dye BCECF is commonly used to monitor intracellular pH. The slope of the second acidification phase upon NH_4^+ application may then be used to "extrapolate" KCC2 activity (Chorin et al., 2011; Hershfinkel et al., 2009). This approach however has serious limitations, as it involves reverse chloride transport through KCC2 and induces uncontrolled and sometimes dramatic changes in intracellular pH.

During my PhD, I used NH_4^+ collapse transmembrane pH gradients in order to reveal the intracellular pool of GluA1-SEP. Under basal conditions, this intracellular-pool lies in acidic exocytosis vesicles leading to a quenching of the SEP. Hence, NH_4^+ application allowed me to visualize and to quantify the intracellular pool. As reported using BCECF-dye, prolonged application of NH_4^+ (>3min) leads to a reversible acidification leading to a re-quenching of GluA1-SEP. Interestingly, the slope of this quenching was dependent on the presence or absence of KCC2, as described for BCECF-based pH measurements (Figure 27). If applied for too long (>5min) however, NH_4^+ leads to neuronal swelling and death.

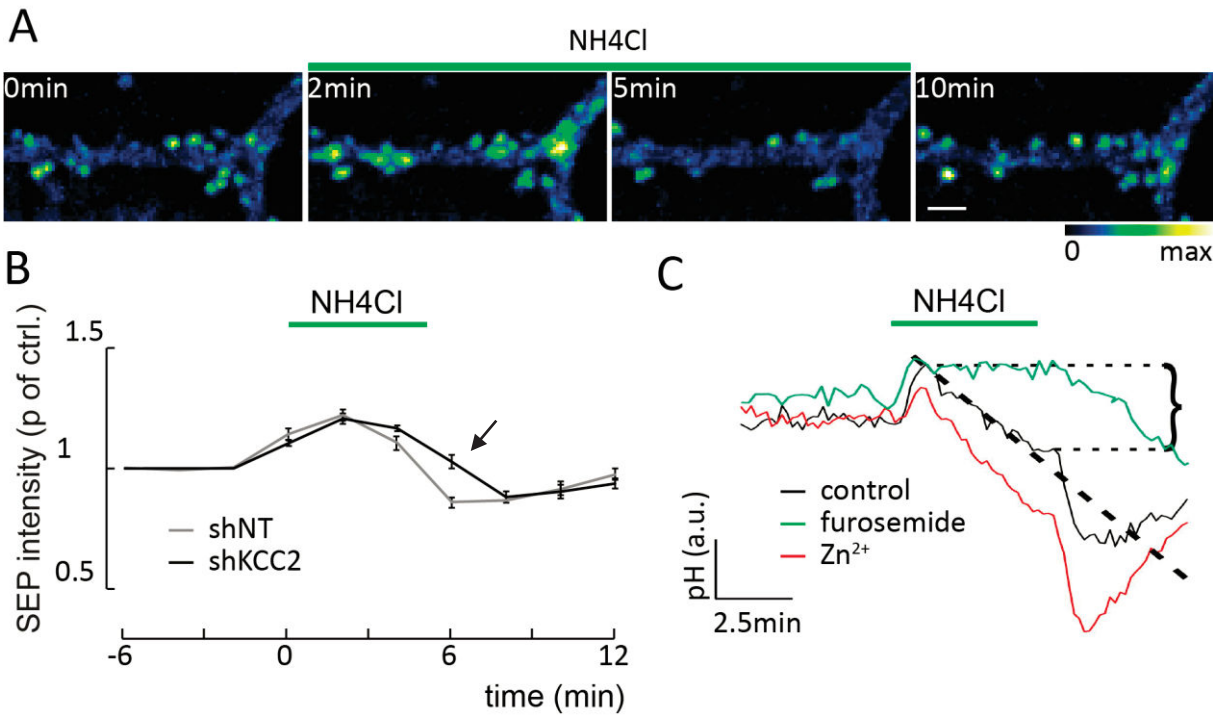

Figure 27 NH_4^+ application leads to biphasic intracellular pH changes
(A) NH_4Cl application collapses transmembrane pH gradient and thereby reveals the intracellular pool of GluA1-SEP containing AMPARs (pseudocolors). If applied for too long, NH4Cl application leads to a reversible acidification leading to a re-quenching of GluA1-SEP fluorescence (Scale, 2µm). (B) Quantification of the effect of NH_4Cl application on GluA1-SEP fluorescence. The suppression of KCC2 (shKCC2) leads to a modification of the acidification kinetics (arrow). (C) NH_4Cl application in combination with intracellular pH measurement is used to evaluate KCC2 transport. The slope of the reversible acidification upon NH_4Cl application is decreased by KCC2 inhibition (furosemide) and increased upon Zn^{2+}-dependent upregulation of KCC2 function. A,B Unpublished data. C, adapted from Saadi et al., 2012.

2. Electrophysiology-based indirect measurement of KCC2 function

All electrophysiological readouts of intracellular chloride concentration are based on the permeability of GlyRs or GABAARs to chloride (see introduction). Intracellular chloride concentration or KCC2-mediated chloride extrusion capacity of the cell may then be extrapolated from the reversal potential of GABAAR-mediated currents (E_{GABA}). The more hyperpolarized E_{GABA}, the lower intracellular chloride concentration, the more KCC2 is active.

Some recordings are less invasive in terms of intracellular dialysis than others. **Intracellular recordings** lead to minimal dialysis but may alter input resistance. They have particularly been used to measure E_{GABA} and the role of perturbed chloride homeostasis in epilepsy (Cohen et al., 2002; Huberfeld et al., 2007). Addition of gramicidin that makes cation-selective pores in the membrane, allows an electrical access to the intracellular compartment using a patch pipette, with little or no modification of intracellular chloride concentration. This technique is referred to as **gramicidin-perforated patch clamp** and has been occasionally used in the laboratory but abandoned due to its low success rate in our hands. Nevertheless, several groups use this technique routinely to assess E_{GABA} and thereby KCC2 function (e.g. Akerman and Cline, 2006; Lee et al., 2011; Woodin et al., 2003). **Single GABAA channel recordings** represent the only fully non-invasive electrophysiological technique to assess E_{GABA}. Cell-attached recording are performed with a patch pipette containing a cocktail of channel blockers and a low concentration of GABA (1 to 5µM) to transiently activate GABAAR without desensitization (Tyzio et al., 2006). However, the size of the detected currents requires a really low level of noise, making this technique difficult to use.

Somewhat surprisingly, changes in E_{GABA} can be directly observed in **whole-cell recording** while chloride concentration is clamped by the intrapipette chloride concentration (Hewitt et al., 2009). A more robust approach to assess chloride extrusion capacity while using the versatility of whole-cell patch-clamp consists in measuring the **somato-dendritic gradient of E_{GABA}**. GABAergic currents are elicited using local puff of GABA or uncaging of caged-GABA at the level of the soma and in distal dendrites (Kelsch et al., 2001; Khirug et al., 2005; Li et al., 2007). The difference between somatic and dendritic E_{GABA} is thought to represent the extrusion capacity of chloride coming from the patch-pipette. Variations in series resistance and dendrites diameter add variability to measurement but in our hands, this technique is

highly reliable with a clear effect of KCC2 inhibition or suppression (Chamma et al., 2013; Gauvain et al., 2011).

In the laboratory, I used Rubi-GABA (15µM, Ascent Scientific) uncaging using a 405nm laser pulse (5ms, 10 effective mW) delivered through a single-path photolysis head (Prairie technologies). I-V relationships of GABA-evoked currents were obtained by measuring currents elicited by somatic or dendritic (100µm from soma) Rubi-GABA uncaging while applying voltage steps to the neuron. As an additional materials and methods tip for readers and future lab members, use of a multimodal fiber to prime the alignment with the monomodal fiber is unnecessary. On the fiber alignment module, little screws are used to secure the correct alignment and should be tighten at the very last moment and all three together. To troubleshoot alignment process, one may refer to the videos provided with the alignment module but also to an online youtube video called “coupling a laser into a single mode fiber” https://www.youtube.com/watch?v=kQvhbJbDG0M) which describes the “walking the beam” technique. Once the laser is coupled to the optic fiber (i.e. less than 40% power loss), the final path toward the objective needs to be adjusted in x and y until the laser beam forms a vertical column as revealed using fluoresceine-containing solution in the recording chamber.

3. Chloride imaging using organic or genetically-encoded dyes.

Recent developments in optogenetic and microscopy allow imaging of neurons morphology and activity both at a fine structure- and large number-scale but most importantly in a non invasive manner (Deisseroth and Schnitzer, 2013). Different dyes have been developed to measure intracellular chloride concentration but some limitations remain. One common limitation to all these dyes appears when used to monitor inhibitory currents. Changes in intracellular chloride concentration due to synaptic GABAergic currents are small. Therefore, chloride sensors require an astonishing sensitivity since only the subfraction of dye located at the vicinity of the innerside of the membrane will carry changes in fluorescence. Nevertheless, as basal chloride concentration is set by KCC2 activity (Doyon et al., 2011), it is definitely worthwhile to developing chloride sensors to assess KCC2 function.

MQAE is an organic dye that can be loaded inside the cell by bath application. It has a good sensitivity and selectivity to chloride. MQAE is excited using UV light (350nm) and emission is collected at 460nm. Using typical fluorescence intensity measurements, single fluorochrome-based sensors do not allow ratiometric measurement. Recently, two-photon excitation at 760nm combined with FLIM (Fluorescence lifetime imaging microscopy) has made it possible to circumvent this issue since FLIM-based measurements are independent of dye concentration (Doyon et al., 2011).

Two different approaches based on different **genetically-encoded sensors** have been used. Both approaches suffer from parasitic pH sensitivity and low chloride sensitivity, although these may be overcome. The yellow fluorescent protein (YFP) is sensitive to chloride and has been engineered to serve as a chloride sensor. First, YFP has been coupled to the chloride insensitive cyan fluorescent protein to allow ratiometric measurement (Kuner and Augustine, 2000). Then the sensitivity of the **clomeleon sensor** has been gradually improved (Grimley et al., 2013; Markova et al., 2008) and a transgenic mouse strain encoding clomeleon has been generated (Berglund et al., 2006). Clomeleon and the derived Cl-Sensor are able to reveal changes in chloride concentration due to KCC2 or CCC alteration (Chamma et al., 2013; Glykys et al., 2009). To bypass the issue of pH sensitivity, a GFP-based chloride sensor has been developed and improved in terms of expression and is called **ClopHensor and ClopHensorN**. It uses a modified E^2GFP with an overall higher pH sensitivity but fluorescence emission is pH-insensitive when excited at 458nm (Arosio et al., 2010; Raimondo et al., 2013). Hence, these sensors allow simultaneous chloride and pH monitoring.

I did not have the opportunity to use imaging techniques to measure chloride concentrations but I participated in a study using Cl-sensor in COS-cells to validate the function of recombinant KCC2-tagged with an extracellular Flag (Chamma et al., 2012). The original article is provided in the additional publications at the end of this thesis.

II. How to acutely suppress KCC2 function?

I will not discuss here the different *Slc12a5* genetically-modified mouse strains since we never used them in the laboratory. However, most if not all of them have been described in the introduction of this thesis.

KCC2 function was first described as sensitive to the loop diuretic furosemide. However furosemide also inhibits NKCC1. Hence, one of the controls when using furosemide (100µM) consists in the addition of bumetanide, a specific inhibitor of NKCC1 (10µM). Recently, a KCC2-specific inhibitor, VU0240551, has been identified (Delpire et al., 2009). During my PhD, I used this antagonist at a concentration of 10µM to inhibit the function of KCC2 (IC_{50}=560nM with <20% NKCC1 inhibition at 50µM).

To suppress KCC2 expression, I used a short hairpin RNA (shRNA) approach to knock-down KCC2 expression (shKCC2). This shKCC2 has been tested by Gregory Gauvain, a PhD student in the laboratory and its sequence is: ACGAGGTCATCGTGAATAAATCTTCCTG-TCAATTTATTCACGATGACCTCGT (Gauvain et al., 2011). I used this sequence to develop a **lentiviral-based approach to massively suppress KCC2s *in vitro* or *in vivo* using hippocampal stereotaxic injection**. Following the work of Gregory Gauvain, I also developed **a shRNA-proof recombinant KCC2** that has silent mutations in the nucleotide region targeted by the shRNA. The modified sequence can be found in the material and methods of my research article. Other teams have developed their KCC2-specific shRNA using different sequences. Two of them have been shown to efficiently decrease KCC2 expression by targeting different regions in the KCC2 mRNA sequence: between ribonucleotides 1405 and 1423 or between ribonucleotides 2715 and 2735 (Pellegrino et al., 2011).

III. How to induce LTP in dissociated hippocampal cultured neurons?

Different methods exist and all aim to increase synaptic transmission efficacy. None is better than the other but some of them are more convenient to answer molecular and cellular biology-based question. Paired-recording can be used to induce LTP in one of the recorded cells (Fiumelli et al., 2005; Woodin et al., 2003) but this technique does not allow large-scale screening of the molecular determinants underlying the studied mechanism.

Tetraethylamonium (TEA), a potassium channel blocker has been used to induce LTP (Gu et al., 2010; Stewart et al., 2005) but leads to an increase in the frequency rather than amplitude of mEPSCs suggesting a pre-synaptic locus of expression although it is associated with addition of AMPAR in postsynapse (Gu et al., 2010). The most widely used chemical LTP (cLTP) paradigm is based on **200µM glycine application** for 10min that promotes NMDAR opening

together with strychnine to prevent direct glycine receptor activation (Fortin et al., 2010; Lu et al., 2001; Sharma et al., 2006). However in my hands, this protocol failed to lead to a robust and reliable increase in amplitude of mESPCs (ctl: 20.1+/-1.4pA vs. cLTP: 23.6+/-1.2pA, n=18 & 19 neurons, p=0.11, t-test). An alternative cLTP paradigm involves co-application of **50µM forskolin, 0.1µM rolipram and 20µM bicuculline in the absence of magnesium** (Kopec et al., 2006). To promote LTP, this protocol combines an increase in synaptic activity due to adenylate cyclase activation (forskolin) and phosphodiesterase in inhibition (rolipram), an increase in neuronal excitability due to decreased inhibitory transmission (bicuculline) and enhanced NMDAR activation (0 Mg^{2+}). I showed that after 16min application, this protocol leads to a robust increase in mEPSC amplitude (Chevy et al., submitted). I therefore used this protocol to induce cLTP in cultured neurons.

IV. From diffraction-limited confocal imaging to super-resolution STED microscopy: quantitative and qualitative measurement of fluorescent signals.

1. Confocal imaging and reconstruction of dendritic spines

Increased spine volume and membrane insertion of GluA1-SEP-containing AMPAR are often used as a proxy for LTP. Following the cLTP protocol, these parameters were monitored using spinning-disc confocal microscopy that allows fast imaging and reduced bleaching of fluorochrome (more information on the used set-up are gathered in the manuscript). While GluA1-SEP fluorescence was analyzed in 2D –maximal fluorescent intensity z-projection – dendritic spine volume was measured in 3D using Neuronstudio software (Dumitriu et al., 2011). **Neuronstudio** is an easy to use software that permits semi-automatic detection and reconstruction of dendritic arborization and spines. Automatic detection and classification (thin, mushroom, stubby) is also possible but less convenient when tracking of the same set of spines overtime is desired. Few parameters need to be provided: voxel dimension, minimal and maximal expected sizes of spines and shaft diameter. The reconstruction is then based on local threshold calculation. Unfortunately, only the diameter of the sphere contained in the spine head is provided as an output while the exact 3D volume is only graphically computed. Additionally, it is impossible to automatize 4D (x,y,z,t) spine volume measurements.

Nevertheless, coordinates of the reconstructed dendritic spines can be extracted and used in ImageJ to measure fluorescence originating from GluA1-SEP for instance.

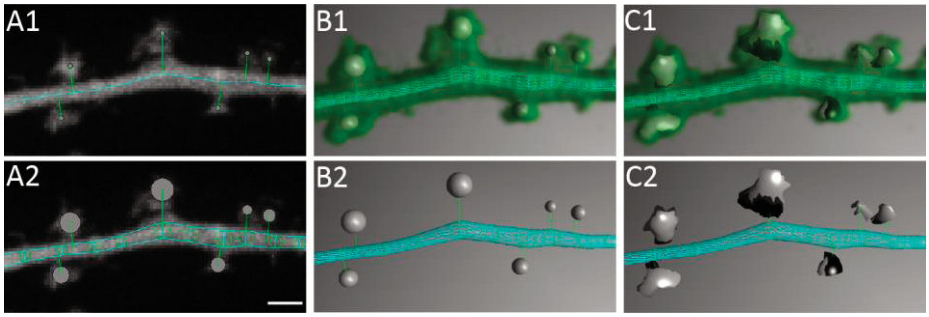

Figure 28 Dendritic shaft and spine 3D-reconstruction using neuronstudio
(A1-2) wire-frame model superimposed on the maximal fluorescence projection of a confocal image of a pyramidal cell dendrite expressing GFP. (B-C) 3D rendering of the wire-frame model superimposed (B1, C1) or not (B2, C2) on the confocal stack. Although neuronstudio can compute the 3D morphology of the dendritic spines (C), only the diameter of the spine-containing sphere (A2, B1) and the neck length (A1-2) can be extracted. Scale 2µm.

Other approaches are used to measure spine volume. **Imaris** is a commercially-available software specifically developed for biological imaging. It allows fast 3D and 4D data visualization and it includes a module for dendrite and spine reconstruction in 4D (filamentracer). However, simple 3D reconstruction requires many adjustments of different parameters that are not always directly related to biology. In my opinion, in its 7.4 version, Imaris is not yet convenient to use for quantitative spine reconstruction on a daily basis.

A more commonly used technique to measure spine area is based on integrated fluorescence intensity measurement ($mean_{spine}$ x $area_{ROI}$), or **photometry** (Bosch et al., 2014; Harvey and Svoboda, 2007; Patterson et al., 2010). Photometry depends on the quantity of fluorophore. Since concentration of dye is unlikely to change, photometry indicates the volume of image fluorophore. Fluorescence intensity is corrected for background ($mean_{bg}$) and for bleaching using shaft fluorescent measurement ($mean_{shaft}$). Hence, calculated spine size in pixels ($area_{spine}$) follows the equation:

$$area_{spine} = \frac{\left(mean_{spine} - mean_{bg)}\right) \times area_{ROI}}{mean_{shaft} - mean_{bg}}$$

Nevertheless, all these techniques to analyze dendritic spines are limited by diffraction that constrains microscope resolution.

2. Breaking the diffraction limit: deconvolution and STED microscopy

In optical microscopy, light diffraction limits the discrimination of two objects if they are closer than a typical distance that can be calculated using the Abbe's equation. The maximal resolution of a microscope (D) is a function of the wavelength (λ) and the numerical aperture (NA) of the objective and follows the Abbe's equation:

$$D = \frac{\lambda}{2NA}$$

Due to diffraction, a sub-resolution object does not appear as a point-like image but as a point-spread function (PSF). **Confocal light-scanning microscope** (CLSM) approaches the theoretical diffraction-limit resolution using a pinhole that blocks light originating from out-of-focus points. The observed signal is then a combination of the PSFs of the excitation and the emission light passing through the pinhole. **Spinning-disc confocal microscope** is made of a rotating, multi-pinhole disc that increases the speed of acquisition and therefore reduces photobleaching of the sample. Increase in resolution of **two-photon laser-scanning microscope** (2PLSM) is based on the same principle: the observed PSF is the resultant of the combination of the PSF from the two, low energy photons required to excite the fluorochrome. 2PLSM outperforms CLSM in that 1) it limits photobleaching of the sample above and below the focal point and 2) the absence of pinhole allows collecting more emitted photons originating from the focal point, even scattered ones. However, CLSM have a slighter better resolution than 2PLSM due to the use of lower wavelength photons for excitation (see Abbe's equation).

Resolution can be further improved using mathematical **deconvolution** that gets rid of the remaining out-of-focus information based on the knowledge of a theoretical or measured PSF. Deconvolution algorithms were first applied to widefield fluorescence microscopy but are also effective in improving resolution of a confocal microscope. This is particularly relevant when observing submicron structures such as dendritic spines the size of which often approaches the resolution of optical microscopes. Although the quantification of dendritic spine volume performed in the following research article (Chevy et al., submitted) were not performed on deconvolved images, Figure 29 represents the same dataset of images on which a blind-deconvolution algorithm was applied.

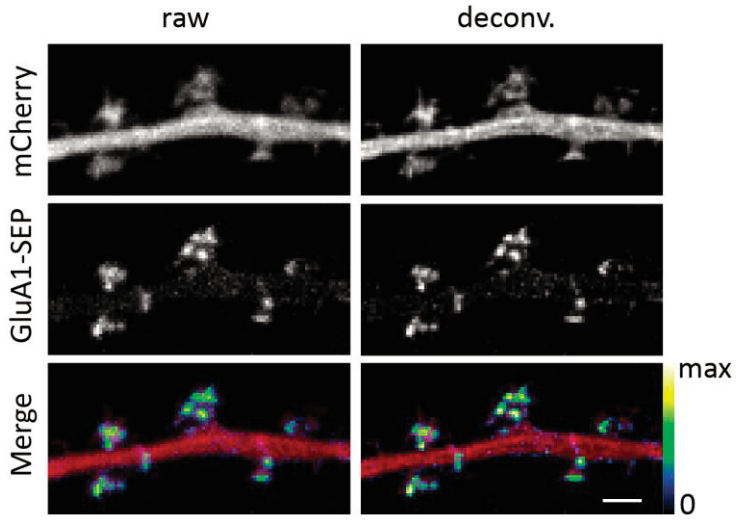

Figure 29 Deconvolution of dendritic spines confocal images
Spinning disc confocal fluorescence micrographs of hippocampal neurons expressing mCherry (red) and GluA1-SEP (pseudocolors). Blind-deconvolution algorithm (Huygens software) increases both the contrast and the resolution of the original images (scale, 2µm).

Recently, different super resolution techniques have been developed to improve the optical resolution beyond the diffraction limit. These breakthroughs in optical microscopy have been rewarded by the Nobel Prize in chemistry this year. **Stimulated Emission Depletion (STED) microscopy** is the only purely optical microscope yielding super resolution. STED microscopes are more and more routinely used in Neuroscience in particular for observing dendritic spines (Nägerl and Bonhoeffer, 2010; Nägerl et al., 2008; Tønnesen et al., 2014; Urban et al., 2011).

This technique relies on a classical laser-scanning microscope that takes advantage of particular physical properties of the fluorescence process and of optics. Fluorescence excitation occurs by photon-based excitation of an electron that jumps from a resting state to an excited state. Relaxation of this electron to its ground state is accompanied by emission of a photon. STED aims at interrupting this process. Indeed, it is possible to force the relaxation of the excited electron using a second type of laser. This laser is referred to as a **depletion laser**. This forced-relaxation leads to emission of a lower energy photon and can therefore be ignored using appropriate emission filters. In addition, while emission of photons from a laser source or a fluorochrome is constrained in size by light diffraction, the “non-emission” of a photon is not. Using **destructive interference**, it is possible to create a laser beam with a donut shape, i.e. with a minimum of light energy in the center of the beam. Hence, fluorochromes can be “switched-off” or deactivated everywhere but in the center by applying this destructive

interference to the depletion laser beam. The resolution of such microscope is no longer limited by diffraction but instead by the size of the destructive interference. Several improvements have been made to increase resolution (**Gated-STED**) access to **3D STED** effect, or to use STED microscopy with continuous wavelength (**CW-STED**) (with pulsed-laser, the emission laser and the depletion laser need to be synchronized and delayed with a femto-second precision) (Vicidomini et al., 2011).

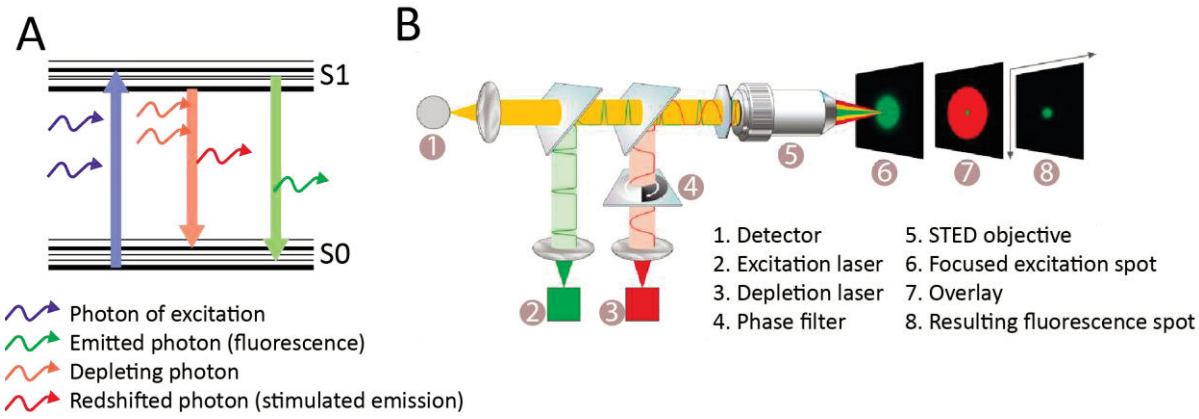

Figure 30 STED microscopy
(A) Jablonski diagram illustrating the mechanism of fluorescence and stimulated emission of photons. In the latter, the emitted photon is redshifted and can be ignored. (B) Diagram of a STED microscope with pulsed-lasers for excitation and depletion (Adapted from Leica microsystem website).

During my PhD, I used a commercial-version of a non-gated CW-STED microscope (Leica) with the help of David Geny. In combination with deconvolution, it allowed me to reveal actin bundles and to adress the effect of KCC2 suppression on the actin cytoskeleton within individual dendritic spines. For quantification, Marie Goutierre and I developed imageJ and Matlab routines to compute some spine head and spine neck characteristics as well as actin aggregation within spine heads (Chevy et al., submitted). Unfortunately, due to a certain lack of expertise and limitations of the CW-STED microscope, it has been impossible to perform three dimensional imaging of dendritic spines. Indeed, contrary to two-photon-based STED microscopy, CW-STED microscopy is less suitable for 3D imaging due to photobleaching. However the use of high-frequency resonant scanner is supposed to reduce photobleaching and in combination with time-gated detection of emitted photon, it should be possible to achieve 3D imaging with CW-STED microscope (Moneron et al., 2010).

RESULTS

RESULTS

I. PREFACE

My PhD project aimed at investigating the role of KCC2 in glutamatergic long term potentiation. KCC2 is a potassium/chloride cotransporter that lowers the intracellular concentration of chloride. Thereby, KCC2 allows the hyperpolarizing influx of chloride through GABAARs mediating inhibitory GABAergic transmission. Suppression of KCC2 and subsequent decrease in GABAergic transmission efficacy have been involved in many neurological disorders. Nevertheless, KCC2 has recently been involved in glutamatergic transmission as well. Thus, the rational of the study presented below is based on two observations. First, KCC2 suppression leads to a decrease in basal glutamatergic transmission. This effect relies on an ion-transport independent function of KCC2. Second, KCC2 has been shown to co-immunoprecipitate with the protein 4.1N that interacts with both actin and the GluA1-subunit of the AMPARs. This interaction has been shown to be a requirement for AMPARs membrane insertion. Recently, KCC2 has also been shown to interact with Beta-PIX, a GEF protein involved in long term plasticity of excitatory synapses. Hence, KCC2 interaction with 4.1N and Beta-PIX represent two putative ways by which KCC2 may be involved in glutamatergic transmission. Using a chemical LTP protocol, I therefore studied the impact of KCC2 suppression on LTP. I observed that:

- LTP is totally compromised upon KCC2 suppression;
- This can be explained by an inhibition of activity-driven AMPAR membrane insertion downstream of NMDAR and CaMKII activation;
- This effect is associated with cofilin inhibition and enhanced mobilization of F-actin in spines;
- LTP is rescued by preventing cofilin inhibition upon KCC2 suppression.

At the beginning of my PhD, my original hypothesis was slightly different. Our idea was that KCC2 down-regulation could participate in the initial increase in spine volume through a regulation of ion and water transport. In the introduction, I mentioned that in addition to salt transport, KCC2 also transports water. A previous study from the laboratory showed that genetic or pharmacological suppression of KCC2 function both lead to an increase in spine

volume which we hypothesized was due to a decrease in water export leading to dendritic spine swelling. Our hypothesis was therefore that local down-regulation of KCC2 upon LTP induction may underlie the initial increase in spine volume associated with LTP. Actin cytoskeleton remodeling and exocytosis would be then necessary for the maintenance of this osmotic-dependent spine swelling. To test this hypothesis, I acutely applied the specific KCC2 antagonist VU0240551 to block KCC2 function and monitored dendritic spine volume using spinning-disc confocal microscopy and 3D-reconstruction using Neuronstudio (See Materials and Methods). However, acute inhibition of KCC2 did not lead to a detectable increase in spine volume unlike chronic application (Figure 31). I then asked whether the increase in spine volume induced by KCC2 suppression might occlude the LTP-associated increase in spine volume. As I was testing this hypothesis, I observed that KCC2 suppression was not only occluding the increase in spine volume but also the LTP of synaptic efficacy. This observation sets the ground to the main study of my thesis.

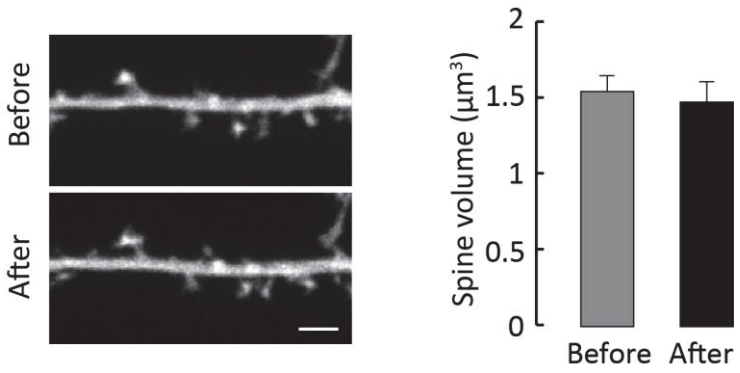

Figure 31 Acute inhibition of KCC2 does not modify spine volume
Left: Spinning disc confocal fluorescence micrographs of dendritic sections of neurons expressing mCherry before and after 30min exposure to 10µM VU0240551 (Scale, 2µm). Right: Summary graph of the effect of VU0240551 on average spine volume (n=8, p=0.72 paired t-test)

II. KCC2 GATES ACTIVITY-DRIVEN AMPA RECEPTOR TRAFFIC THROUGH COFILIN PHOSPHORYLATION

Quentin Chevy[1,2,3], Martin Heubl[1,2,3], Marie Goutierre[1,2,3], Imane Moutkine[1,2,3], Emmanuel Eugène[1,2,3], Sabine Lévi[1,2,3], Jean Christophe Poncer[1,2,3,4]

[1] INSERM, UMR_S 839, F-75005, Paris, France

[2] Sorbonne Universités, UPMC Univ Paris 06, UMR_S 839, F-75005, Paris, France

[3] Institut du Fer a Moulin, F-75005, Paris France

[4] Correspondence to J.C. Poncer, jean-christophe.poncer@inserm.fr

Running title: KCC2 gates LTP expression at hippocampal synapses

Acknowledgements

This work was supported by the Human Frontier Science Program (research grant, to JCP), INSERM, Ville de Paris (Biomedical and Health Research Program, to JCP), the Fédération pour la Recherche sur le Cerveau (to JCP), Fondation pour la Recherche Médicale (to JCP) and PICPEN (Center for Psychiatry & Neuroscience, Paris). QC was the recipient of a doctoral fellowship from Université Pierre & Marie Curie. We thank Ingrid Chamma for the quantitative analysis of phalloidin staining data, Theano Irinopoulou for support with spinning disc and confocal imaging, David Geny at PICPEN for assistance with STED microscopy, Alain Prochiantz for helpful discussions, and Eric J. Schwartz, Manuel Mameli, David diGregorio and Richard Miles for constructive comments on the manuscript.

Author contributions

Q.C. and J.C.P. designed the research. Q.C. performed all electrophysiological and imaging experiments and analyzed the data. M.H. performed all biochemical assays under supervision of SL. M.G., I.M. and E.E. contributed new reagents and analytical tools. Q.C. and J.C.P prepared the figures and wrote the paper.

Conflict of interest

The authors declare no conflict of interest.

1. Abstract

Expression of the neuronal K/Cl transporter KCC2 is tightly regulated throughout development and by both normal and pathological neuronal activity. Changes in KCC2 expression have often been associated with altered chloride homeostasis and GABA signaling. However, recent evidence supports a role of KCC2 in the development and function of glutamatergic synapses through mechanisms that remain poorly understood. Here we show that suppressing KCC2 expression in hippocampal neurons precludes long term potentiation of glutamatergic synapses specifically by preventing activity-driven membrane delivery of AMPA receptors. This effect is independent of KCC2 transporter function and can be accounted for by an increased LIMK-dependent cofilin phosphorylation and actin polymerization in dendritic spines. Our results demonstrate KCC2 plays a critical role in the regulation of spine actin cytoskeleton and suggest KCC2 membrane expression may act as a metaplastic switch to gate long term plasticity at excitatory synapses in cortical neurons.

2. Introduction

Fast synaptic inhibition in the brain relies on activation of chloride permeant GABAA and glycine receptor channels. Hence chloride homeostasis is critical to maintain the efficacy and even the polarity of signals mediated by these receptors. In most mature neurons, transmembrane Cl gradients are primarily established by the opposing actions of the electroneutral ion transporters NKCC1 and KCC2, resulting in a net efflux of chloride ions (Blaesse et al., 2009; Chamma et al., 2012). Upregulation of KCC2 expression during neuronal maturation is associated with a progressive hyperpolarizing shift in the reversal potential of GABAA receptor-mediated currents (Rivera et al., 1999). KCC2 may also be rapidly down-regulated by neuronal activity through post-translational modifications (Blaesse et al., 2009; Chamma et al., 2013; Medina et al., 2014). These involve phosphorylation and dephosphorylation of specific residues of its carboxy-terminal domain and mostly affect the membrane stability rather than the intrinsic ion transport function of KCC2 (Chamma et al., 2012; Chamma et al., 2013; Kahle et al., 2013; Lee et al., 2011; Medina et al., 2014; Watanabe et al., 2009). Down-regulation of KCC2 at the transcriptional level is also induced by neuronal activity e.g. (Rivera et al., 2004) and in a variety of neurological and psychiatric disorders including epilepsy (Loscher et al., 2013; Miles et al., 2012), chronic pain (Coull et al., 2003), spasticity after spinal cord injury (Boulenguez et al., 2010) and possibly autism spectrum

disorders (Tyzio et al., 2014). Since most of these conditions are associated with partial disinhibition, high expectations are put on diuretic drugs and other therapeutic strategies that may act to compensate for the loss of KCC2 expression and thereby restore neuronal chloride homeostasis and synaptic inhibition (Gagnon et al., 2013; Kahle et al., 2008; Loscher et al., 2013).

KCC2 however is not specifically enriched near GABAergic synapses but instead shows a diffuse distribution throughout the somato-dendritic plasma membrane, with large clusters in dendritic spines in the vicinity of the excitatory postsynaptic density (Chamma et al., 2013; Gauvain et al., 2011; Gulyas et al., 2001). This distribution suggests possible interactions of KCC2 also with glutamatergic signaling (Chamma et al., 2012). Precocious expression of recombinant KCC2 in embryonic cortical neurons leads to exuberant spinogenesis and excitatory synapse density (Fiumelli et al., 2013). Conversely, genetic ablation of KCC2 precludes both spine morphogenesis and excitatory synapse formation (Li et al., 2007). Chronic KCC2 suppression in mature neurons on the other hand does not compromise spine maintenance but reduces the confinement of several transmembrane protein including AMPA receptors (AMPARs) within dendritic spines (Gauvain et al., 2011). Interestingly, these effects are all independent of ion transport and instead seem to involve KCC2 interactions with intracellular partners. KCC2 has been shown to be engaged in variety of protein interactions that may impact its aggregation and function in dendritic spines (reviewed in (Medina et al., 2014)). These comprise synaptic proteins such as the GluK2 subunit of kainate receptors (Mahadevan et al., 2014) and its interacting protein Neto2 (Ivakine et al., 2013) which may act to enhance KCC2 membrane stability. KCC2 also interacts with actin-related proteins, such as the spectrin/actin binding protein 4.1N (Li et al., 2007) and the guanine nucleotide exchange factor betaPIX (Medina et al., 2014), which may influence KCC2 anchoring to spine cytoskeleton (Chamma et al., 2013) and actin polymerization (Saneyoshi et al., 2008), respectively. Although such interactions are predicted to influence spine actin cytoskeleton, direct experimental evidence to support this prediction is still missing.

Dendritic spines exhibit various forms of activity-driven plasticity leading to coordinated modulation of both their anatomical structure and synaptic function that likely represents the cellular substrate of learning and memory (Bosch and Hayashi, 2012). Thus, long term potentiation (LTP) of excitatory synapses involves both a synaptic translocation of several

proteins including AMPARs (Hayashi et al., 2000; Makino and Malinow, 2009; Malinow and Malenka, 2002; Park et al., 2006)as well as a persistent increase in spine volume (Engert and Bonhoeffer, 1999; Harvey and Svoboda, 2007; Kopec et al., 2006). The two processes are mechanistically correlated (Kopec et al., 2007) and rely on rapid remodeling of actin cytoskeleton within dendritic spines. This remodeling may be both permissive for activity-driven AMPA receptor membrane insertion (Gu et al., 2010) and lateral diffusion (Rust et al., 2010) and structurally required for spine head enlargement (Okamoto et al., 2004). Here, we therefore tested whether the reciprocal interaction between KCC2 and spine actin cytoskeleton may impact structural and synaptic LTP at excitatory synapses in mature hippocampal neurons. Our results show that KCC2 is strictly required for LTP expression at these synapses. Suppressing KCC2 expression or protein interactions with its carboxy-terminal domain prevents both activity-driven membrane insertion of AMPARs and increase in spine volume. This effect is independent of KCC2 ion transport and instead reflects remodeling of F-actin in dendritic spines due to LIMK-dependent inhibition of cofilin. Our results reveal that KCC2 plays a critical role at mature cortical excitatory synapses where it not only controls synaptic efficacy (Gauvain et al., 2011) but also gates the expression of long term plasticity. We predict that activity- and pathology-induced changes in KCC2 expression may have a complex impact on neuronal network activity through concomitant alterations of both GABAergic and glutamatergic signaling.

3. Results

a) Suppressing KCC2 expression but not function precludes cLTP in hippocampal neurons

We examined the impact of suppressing KCC2 expression on long term potentiation in primary hippocampal neurons. A classical, chemical LTP (cLTP) paradigm consisting in a 16-minute application of rolipram/forskolin/bicuculline in the absence of external Mg (Kopec et al., 2006; Otmakhov et al., 2004) was used to induce a persistent (>80 min) potentiation of synaptic efficacy at excitatory inputs onto hippocampal neurons (Figures 1A and 1B). This potentiation was detected as a 30% increase in mEPSC amplitude as compared to neurons exposed to vehicle only (26.8±1.6 vs. 20.6±1.6 pA, p=0.01) with no significant change in their mean frequency (34.7±5.5 vs. 29.6±5.6 Hz, n=19 and 16 cells, respectively, p=0.48), suggesting its locus of expression was primarily postsynaptic (Kopec et al., 2006; Otmakhov et al., 2004).

Suppressing KCC2 expression for 7-10 days by RNA interference (Gauvain et al., 2011) completely abolished cLTP in mature hippocampal neurons (Figures 1A-C). Thus, mEPSC amplitude was not significantly different after a cLTP paradigm as compared to control (19.2±0.6 vs. 18.4±0.5 pA, n=13 cells each, p=0.34). In contrast, expression of a non-target shRNA sequence did not affect cLTP expression (24.1±1.0 vs. 20.2±0.8 pA, n=12 and 13 cells, respectively, p=0.006). This effect of KCC2 suppression was independent of the loss of ion transport function since chronic application of the specific antagonist VU0240551 (Delpire et al., 2009; Gauvain et al., 2011) (6 µM; Figure S3D) had no effect on cLTP expression (30.0±2.6 vs. 23.0±1.7 pA, n=12 cells each, p<0.05; Figure 1C). In contrast, specifically preventing KCC2 interactions with intracellular partners, using overexpression of a dominant negative peptide (KCC2-CTD (Gauvain et al., 2011; Li et al., 2007; Puskarjov et al., 2014)), completely abolished cLTP (20.2±1.0 vs. 21.3±0.9 pA, n=11 and 18 cells, respectively, p=0.44).

LTP at hippocampal synapses is associated with a concomitant and persistent increase in spine volume e.g. (Engert and Bonhoeffer, 1999; Harvey and Svoboda, 2007; Kopec et al., 2006; Kopec et al., 2007). We monitored spine volume in cLTP experiments using time-lapse, spinning-disc confocal imaging of mCherry-expressing neurons (Figures 1D-F). In neurons expressing mCherry only, cLTP was associated with a significant increase in spine volume that persisted >30 minutes after induction (to +27.8±3.0 % of control at 30 minutes post induction, n=143 spines from 7 cells, p<0.05; Figure 1D). Similarly, neurons expressing non-target shRNA showed a 33.4±8.9 % increase in spine volume 30 minutes after cLTP induction. In contrast, no significant change in spine volume was detected in neurons expressing KCC2-directed shRNA (-9.5±4.7 % of control, n=9 cells, p=0.1; Figures 1D-F), similar to shNT-expressing neurons exposed to vehicle only (DMSO 0.2 %, -12.6±3.7 % of control, n=6 cells, p=0.06; Figure 1E). Again, this effect did not involve KCC2 function since a 72-hour exposure to the specific antagonist VU0240551 did not prevent cLTP-induced increase in spine volume (to +19.7±5.1 % of control, n=576 spines from 20 cells, p<0.005 Figure 1D) to a similar extent as in neurons exposed to vehicle only (n=20 and 15 cells, respectively, p=0.6). Our results show that KCC2 is strictly required for both synaptic and structural LTP at hippocampal excitatory synapses, through a mechanism likely requiring intracellular protein interactions but independent of ion transport.

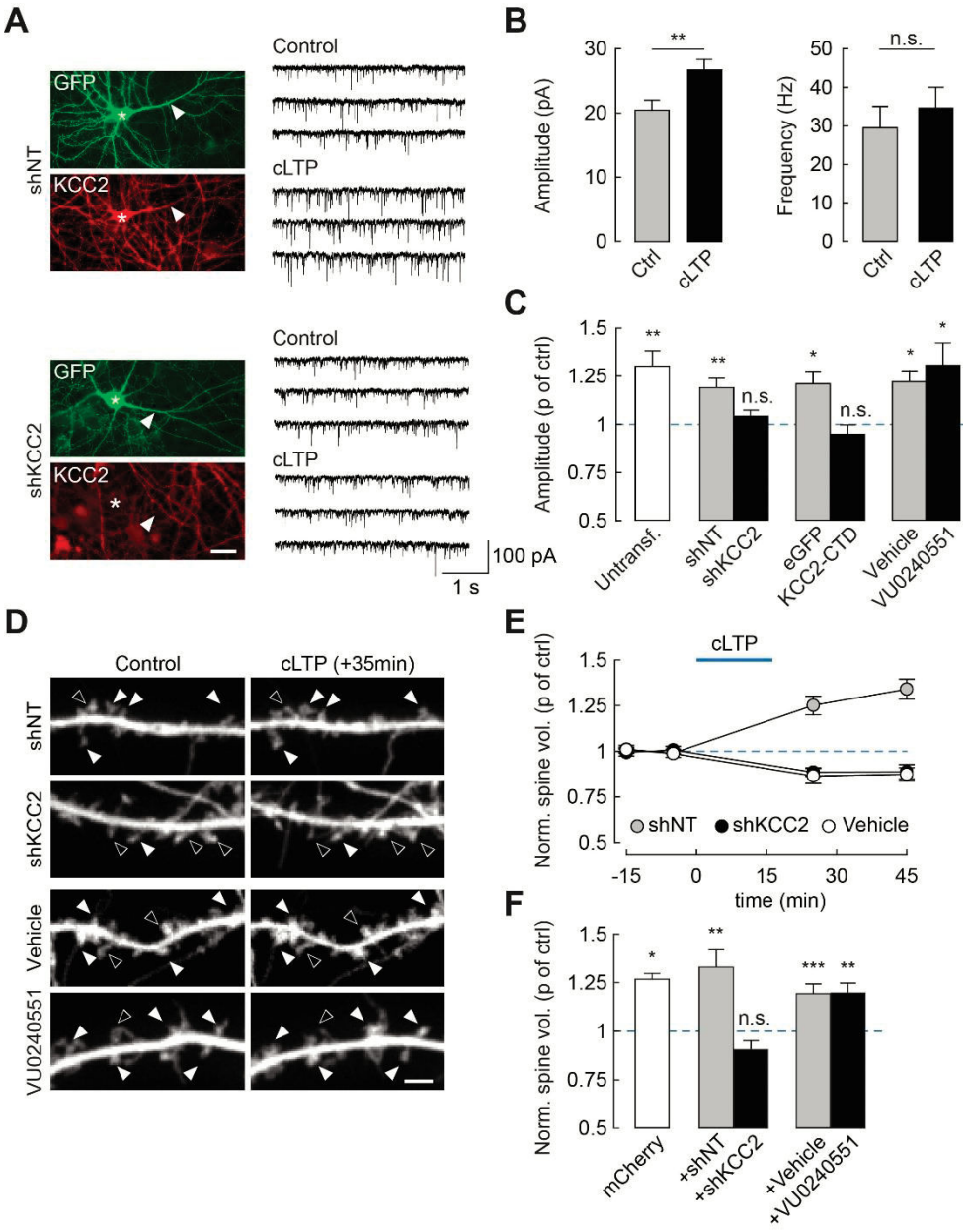

Figure 1. KCC2 suppression precludes cLTP expression through an ion transport independent mechanism. (**a**) Left, wide-field fluorescence micrographs showing GFP fluorescence and KCC2 immunolabeling in hippocampal neurons transfected with non-target (shNT, top) or KCC2-specific (shKCC2, bottom) shRNA. Stars and arrows indicate the soma and primary dendrite of transfected cells, respectively. Scale, 20 µm. Right, 12 s recordings of mEPSCs from neurons either after cLTP protocol (see Methods, 'cLTP') or vehicle application only (DMSO 0.6 µl/ml, 'Control'). (**b**) Summary data from 16 (Ctrl) and 19 (cLTP) untransfected neurons showing cLTP specifically increases mEPSC amplitude ($p<0.01$) but not frequency ($p=0.5$). (**c**) Summary data showing change in mEPSC amplitude (proportion of control) upon cLTP in untransfected neurons ($p<0.01$), or neurons expressing either non-target ($p<0.01$) or KCC2-specific shRNA ($p=0.2$), eGFP alone ($p<0.05$) or eGFP with KCC2 carboxy-terminal domain (KCC2-CTD, $p=0.4$), and neurons exposed to the KCC2 antagonist VU0240551 (6 µM, $p<0.05$) or vehicle only (DMSO, $p<0.05$). n=11 to 18 in each condition. (**d**) Spinning disc confocal fluorescence micrographs of dendritic sections of neurons expressing mCherry and either shNT or shKCC2, or exposed for 72 hours to VU0240551 or vehicle only. Images represent maximal projections of confocal stacks acquired 15 minutes before and 35 minutes after cLTP induction. Filled arrowheads show spines that increased in volume during cLTP whereas empty arrowheads show spines that decreased in volume or remained unchanged. Scale, 2 µm. (**e**) Time course of changes in spine volume upon cLTP in neurons expressing shNT (n=11), shKCC2 (n=9) and neurons expressing mCherry only and exposed for 16 minutes to vehicle only (vehicle, n=6). (**f**) Summary graph of average spine volume (normalized to control before cLTP induction) measured 30 minutes after cLTP induction in neurons expressing mCherry alone (n=7), or together with shNT (n=11), shKCC2 (n=9), or after 72 hour exposure to VU0240551 (n=14) or vehicle only (n=20). * $p<0.05$, ** $p<0.01$, *** $p<0.005$, n.s. non-significant difference.

b) KCC2 is required for activity-driven GluA1 exocytosis

efect in cLTP upon suppression of KCC2 expression may reflect alterations in either induction or expression mechanisms, or both. Our cLTP paradigm has been suggested to primarily rely on NMDAR activation (Kopec et al., 2006; Otmakhov et al., 2004). Reduced recruitment of synaptic NMDARs upon KCC2 suppression may then prevent cLTP induction. We previously showed that suppressing KCC2 expression or interaction with cytoskeleton increased GluA1-containing AMPAR diffusion and decreased their aggregation in dendritic spines, thereby reducing the efficacy of excitatory synapses (Gauvain et al., 2011). We tested whether KCC2 suppression may similarly suppress NMDAR function in hippocampal neurons by measuring NMDA/AMPA ratios of postsynaptic currents evoked by single photon uncaging of MNI-glutamate onto hippocampal neurons. We evoked u-(uncaging-evoked)PSCs that were similar in amplitude and kinetics to mEPSCs when recorded at -60mV (see Methods, Figure S1A). We then compared the AMPAR- and NMDAR-mediated components of u-PSCs (Maroteaux and Mameli, 2012) in neurons expressing non-target or KCC2-specific shRNAs (Figures S1B and S1C). Consistent with our previous observations (Gauvain et al., 2011), AMPAR-mediated u-PSCs were decreased in amplitude in neurons with suppressed KCC2 expression (21.9±2.1 vs. 28.8±1.9 pA, n=13 cells each, $p<0.05$). In contrast, the amplitude of NMDAR-mediated u-PSCs was not significantly affected (36.0±6.0 vs. 30.2±4.2, $p=0.7$), so that NMDA/AMPA ratio increased, rather than decreased, upon KCC2 suppression (1.7±0.2 vs. 1.0±0.1, $p<0.05$; Figure S1C). Consistent with this observation, synaptic aggregation of the GluN1 subunit was not significantly different in neurons expressing KCC2-specific as compared with non-target shRNA (-2.3±6.4 %, n=22 and 24 cells, respectively, $p=0.8$; Figures S1D and S1E). We conclude that a defect in NMDAR activation is unlikely to account for the lack of cLTP upon KCC2 suppression.

LTP in hippocampal pyramidal neurons relies in part on activity-driven membrane insertion of AMPARs e.g.(Collingridge et al., 2004; Huganir and Nicoll, 2013; Malinow and Malenka, 2002; Poncer, 2003). We therefore asked whether activity-driven AMPAR exocytosis might be compromised in the absence of KCC2. We used super-ecliptic pHluorin (SEP)-tagged GluA1 to specifically monitor the membrane-inserted pool of GluA1-containing AMPARs (Ashby et al., 2006; Kopec et al., 2006; Lin et al., 2009; Makino and Malinow, 2011) (Figures 2A and S2). Application of a pH 5.5 external solution led to complete quenching of SEP-GluA1 (to 12.7±3.1 % of control, n=11 cells, $p<0.001$), whereas a collapse of transmembrane proton gradients by

ammonium increased SEP-GluA1 fluorescence (to 125.0±13.3 % of control, n=26 cells, p<0.001), likely revealing intracellular receptor pools (Figure S2). SEP-GluA1 fluorescence was rapidly and persistently increased upon cLTP induction in hippocampal neurons, indicating membrane insertion of new SEP-GluA1-containing AMPARs (+23.0±5.1 % of control after 35 min., n=19 cells, p<0.001; Figures 2B, 2C and S2). This effect was not observed upon application of vehicle only (DMSO, -2.1±3.7 % of control, n=5 cells, p=0.3) and was specific to SEP-GluA1 but not SEP-GluA2-containing receptors (+2.3±3.2 % of control, n=18 cells, p=0.33).

Using this assay, we then examined how SEP-GluA1 traffic may be affected by altering KCC2 expression or function. Chronic suppression of KCC2 expression by RNA interference prevented cLTP-induced membrane insertion of SEP-GluA1 containing receptors (+3.2±1.7 % of control, n=21 cells, p=0.44; Figures 2B and 2C). This effect was specific to KCC2 suppression as it could be rescued by overexpressing an shRNA-proof recombinant KCC2 (+17.4±4.5 % of control, n=20 cells, p<0.001; Figures S3 and 2C). However, it was not mimicked by blocking KCC2 function using the specific antagonist VU0240551 (Figures 2B and 2C), again suggesting KCC2 expression, but not function, is required for cLTP-induced AMPAR membrane traffic. Importantly, whereas SEP-GluA1 steady-state fluorescence was reduced in neurons expressing KCC2-specific as compared to non-target shRNA as described (Gauvain et al., 2011) (-24.8±9.5 %, n=28 and 23 cells, respectively, p<0.01), it was increased to a similar extent upon application of NH_4Cl (+20.6±2.2 %, n=28 cells, p<0.001 and +22.1±4.0 %, n=23 cells, p<0.001, respectively; Figure 2D). These results suggest that altered GluA1 membrane insertion in the absence of KCC2 does not reflect a loss of intracellular GluA1, but rather a specific disruption of its activity-driven exocytosis.

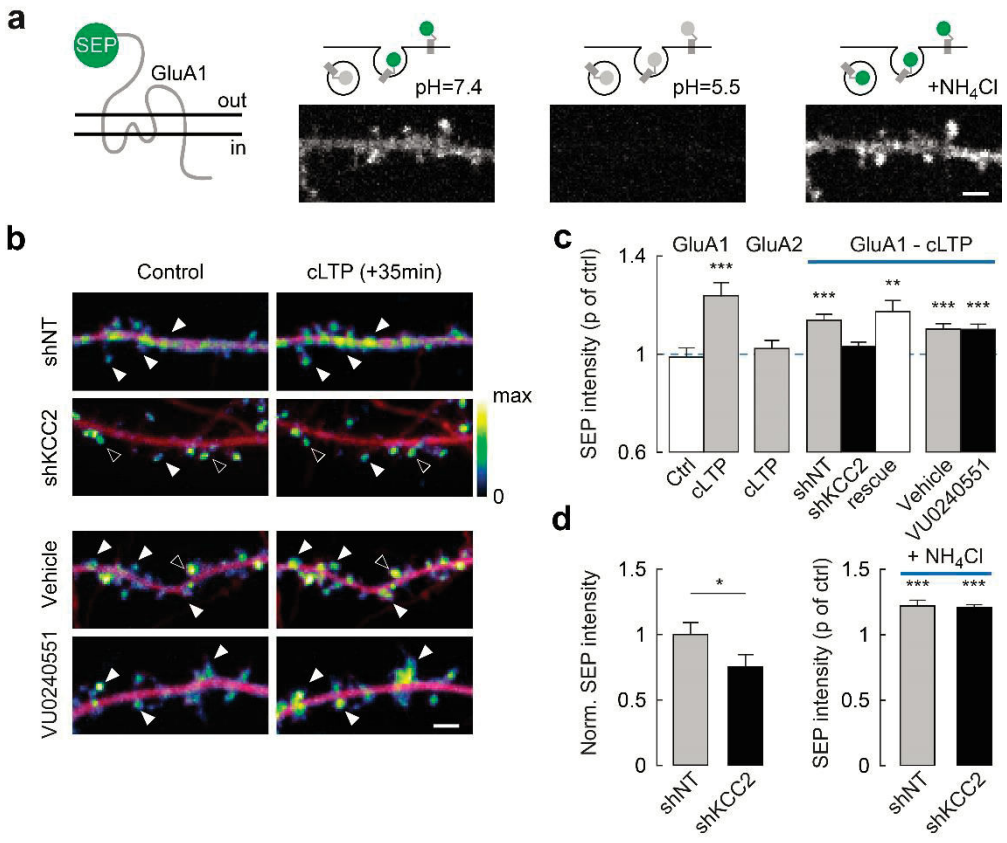

Figure 2. Lack of activity-driven, membrane insertion of AMPARs in neurons lacking KCC2. (**a**) Spinning disc confocal fluorescence micrographs of hippocampal neurons expressing SEP-GluA1. SEP fluorescence was detected in neurons imaged at pH 7.4 but was near-completely quenched at pH 5.5. Upon collapse of pH gradients using 50 mM NH_4Cl at pH 7.4, additional fluorescence was detected reflecting an intracellular pool of SEP-GluA1. Scale, 2 µm. (**b**) Overlay of mCherry (red) and SEP (pseudocolors) fluorescence micrographs of dendritic sections of neurons before (Control) and 35 minutes after cLTP induction. Filled arrowheads show cLTP-induced SEP fluorescence spots whereas empty arrowheads show spines with unchanged SEP fluorescence. KCC2 suppression by RNA interference but not blockade by the antagonist VU0240551 (6 µM) abolished cLTP-induced increase in SEP fluorescence. Scale, 2 µm. (**c**) SEP fluorescence 35 minutes after cLTP induction normalized to control in neurons expressing SEP-GluA1 or SEP-GluA2 and either non-target (shNT) or KCC2-directed (shKCC2) shRNA, KCC2 shRNA together with shRNA-proof recombinant KCC2 (rescue) or neurons exposed to KCC2 antagonist VU0240551 (6 µM) or vehicle only. ** p<0.01; *** p<0.005. n=18 to 29 neurons in each condition. (**d**) Left, SEP fluorescence before cLTP induction in neurons expressing SEP-GluA1 and either non-target (n=47) or KCC2-directed (n=56) shRNA, normalized to the mean SEP fluorescence in shNT-expressing neurons. * p<0.05. Right, Change in SEP fluorescence (p of control) upon 5 minutes perfusion of NH_4Cl solution (pH 7.4) to reveal intracellular SEP-GluA1 pool (shNT, n=23; shKCC2, n=28). *** p<0.005.

During LTP in hippocampal neurons, aCaMKII activation induces membrane insertion of GluA1-containing AMPARs (Esteban et al., 2003; Hayashi et al., 2000) which requires PKA phosphorylation of GluA1 Ser845 (Esteban et al., 2003). A defect in either aCaMKII activation or GluA1 phosphorylation on Ser845 in neurons lacking KCC2 may then preclude activity-dependent AMPAR traffic. In order to bypass aCaMKII activation, we over-expressed a constitutively active aCaMKII to directly promote GluA1 exocytosis. The catalytic domain of aCaMKII (CaMKII1-290 (Esteban et al., 2003; Hayashi et al., 2000; Poncer et al., 2002)) fused

to mCherry was expressed under a doxycycline-inducible promoter to allow for a precise control over the timing of its expression (Figure 3A). We first verified that mCherry-CaMKII1-290 transgene expression was strictly restricted to neurons exposed to doxycycline, as shown by the lack of mCherry expression in neurons transfected with this construct for 8-10 days (Figure 3B).

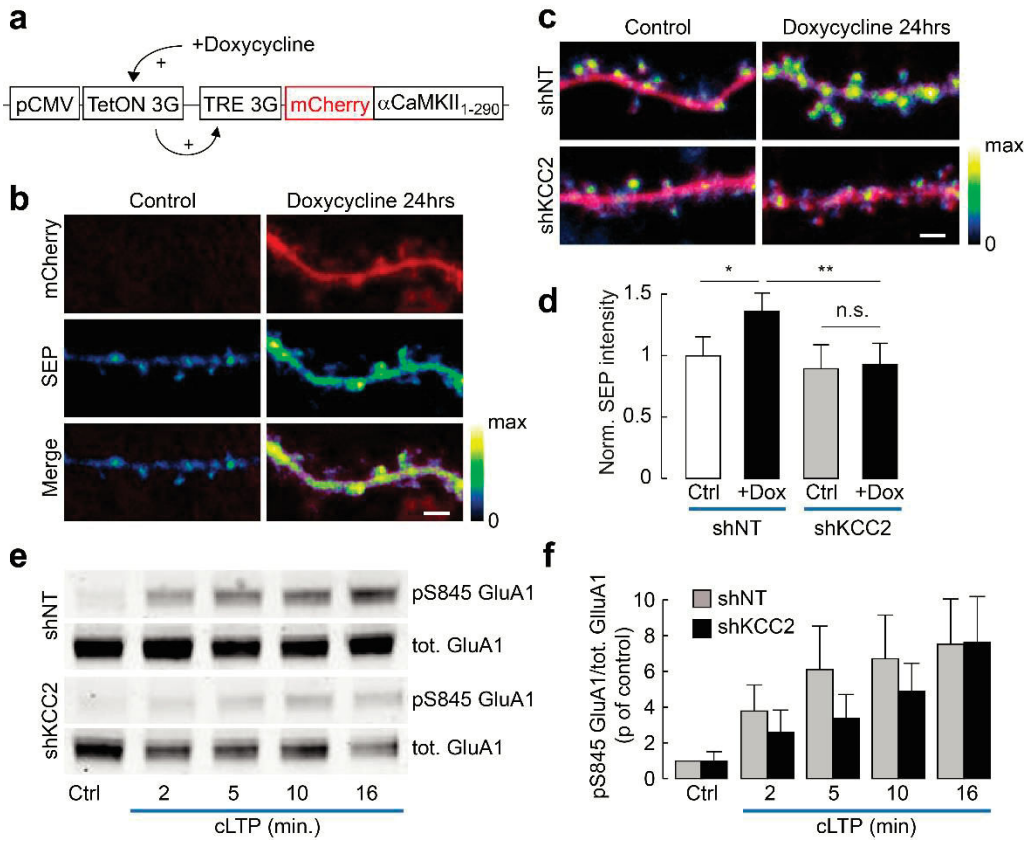

Figure 3. Defect in activity-dependent GluA1 membrane delivery downstream αCaMKII activation and GluA1 S845 phosphorylation. (**a**) Schematic representation of construct used for doxycycline-inducible, truncated (constitutively-active) αCaMKII expression in hippocampal neurons. (**b**) Confocal fluorescence micrographs of mCherry (red) and SEP-GluA1 (pseudocolors) in dendritic sections of neurons expressing mCherry, SEP-GluA1 and inducible truncated αCaMKII, in the absence (Control) or after 24-hour exposure to 2µg/ml doxycycline. No mCherry expression was detected in the absence of doxycycline. Scale, 2 µm. (**c**) Overlay of confocal fluorescence micrographs of mCherry and SEP-GluA1 in neurons expressing mCherry, SEP-GluA1 and inducible truncated αCaMKII and either non-target (shNT) or KCC2-directed (shKCC2) shRNA, in the absence or 24-hour presence of doxycycline. Scale, 2 µm. (**d**) Quantification of SEP-fluorescence in neurons not exposed to doxycycline (Ctrl) or exposed to doxycycline for 24 hours (+Dox), normalized to the mean SEP-fluorescence in the absence of doxycycline (shNT: Ctrl, n=105; +Dox, n=121 shKCC2: Ctrl, n=84; +Dox, n=90). * p<0.05, ** p<0.01; n.s., non-significant. (**e**) Representative immunoblots of total or Ser845-phosphorylated GluA1 and Tuj1 from hippocampal cultures infected with lentiviruses expressing either non-target (shNT) or KCC2-directed (shKCC2) shRNA, before (Ctrl) or at different times of cLTP induction. (**f**) Quantification from 3 independent experiments of pS845/total GluA1 ratios from immunoblots as in (d), normalized to that in shNT-expressing neurons before cLTP induction. No significant difference in GluA1 S845 phosphorylation was observed between shNT and shKCC2-expressing neurons, either in control or upon cLTP induction.

Doxycycline-induced overexpression of $CaMKII_{1-290}$ for 24 hours led to a significant increase in SEP-GluA1 fluorescence in neurons expressing non-target shRNA (+28.3±8.8 % of control,

n=105 and 121 cells, respectively, p=0.006; Fig. 3B). However, this effect was abolished in neurons in which KCC2 expression was suppressed (+9.3±12.1 % of control, n=84 and 90 cells, respectively, p=0.8; Fig. 3C). In contrast, in cultures transduced with shRNA-expressing lentiviruses (Fig. E4), we observed no difference in GluA1 Ser845 phosphorylation in neurons expressing KCC2-specific as compared to non-target shRNA, either at rest (+1.7±4.5 %, n=3 experiments, p=0.9) or upon cLTP (+758±131% *vs.* +687±246 % of control, respectively, p=1.0; Fig. 3D-E). These results demonstrate that KCC2 is required for activity-dependent GluA1 membrane delivery in hippocampal neurons and acts through mechanisms downstream of αCaMKII activation and pKA-dependent GluA1 phosphorylation on Ser845.

c) Altered spine actin polymerization upon KCC2 suppression

How may KCC2 gate activity-driven AMPAR membrane insertion? KCC2 has been shown to interact with spine cytoskeleton through the FERM-domain protein 4.1N (Li et al., 2007) and GluA1 binding to 4.1N is required for its activity-dependent membrane insertion (Lin et al., 2009). We therefore tested whether the loss of KCC2 may affect 4.1N expression in hippocampal neurons. However, suppressing KCC2 or over-expressing KCC2-CTD had no apparent effect on 4.1N expression as detected by immunofluorescence, either globally (97.2±3.4 and 104.3±5.3% of control intensity, p=0.7 and 0.6, respectively) or specifically in dendritic spines (97.7±4.0 and 110.7±5.2% of control, n=37 (41 control) and 43 (54 control) cells, p=0.6 and 0.1, respectively; Figure S5). Therefore altered 4.1N expression and/or clustering seems unlikely to be responsible for the defect in GluA1 membrane traffic upon KCC2 suppression.

Both activity-driven AMPAR trafficking and spine enlargement rely on remodeling of actin cytoskeleton. Whereas transient actin depolymerization by cofilin may be permissive for AMPAR membrane insertion (Bosch et al., 2014; Gu et al., 2010), delayed increase in F-actin spine content may be required for spine enlargement (Okamoto et al., 2004). We previously reported increased lateral diffusion of several transmembrane actin-binding proteins in dendritic spines upon KCC2 suppression (Gauvain et al., 2011), suggestive of submembrane cytoskeleton alterations. In order to examine the subspine spatial distribution of actin, we used super-resolution STED microscopy of the synthetic, actin-binding peptide Lifeact-Venus (Riedl et al., 2008; Urban et al., 2011).

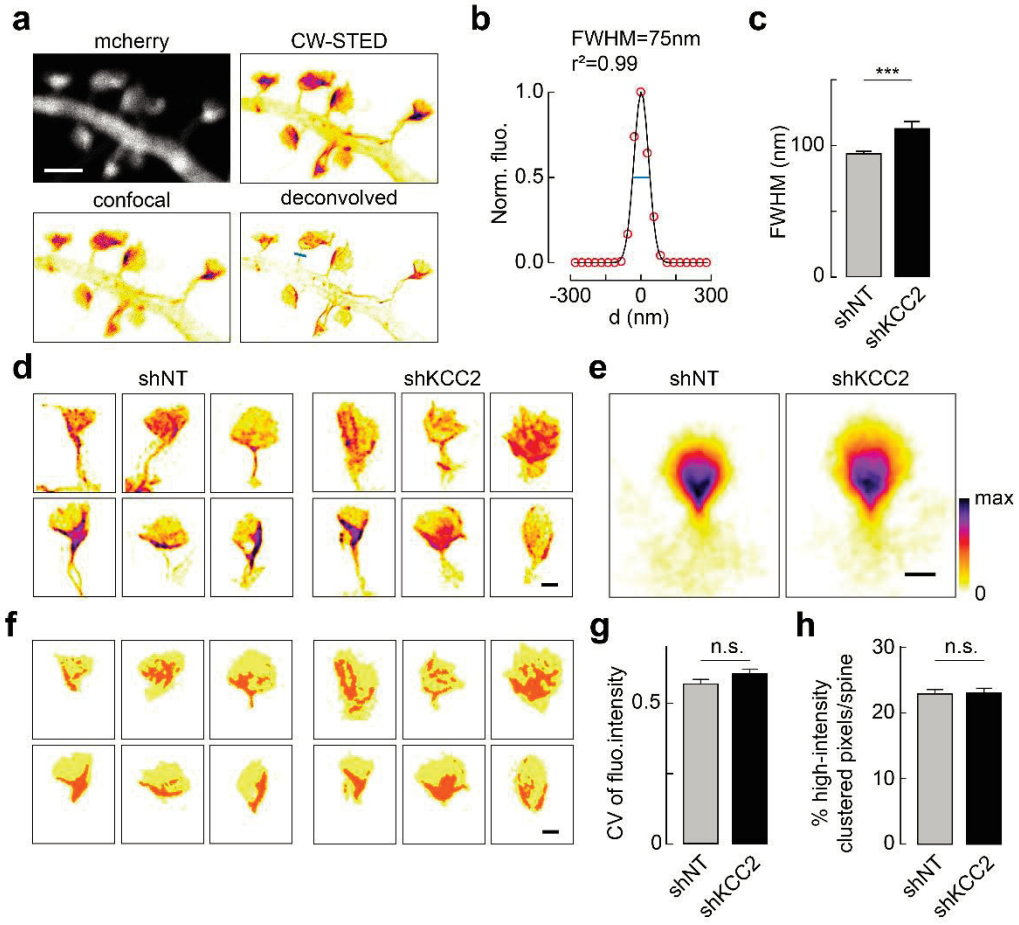

Figure 5. Subspine distribution of F-actin is unchanged upon KCC2 suppression. (**a**) Representative fluorescence micrographs of a dendritic section of a neuron expressing mCherry and Lifeact-Venus (pseudocolors), imaged in confocal (left) and CW-STED microscopy with or without deconvolution (right). (**b**) Gaussian fit of the pixel intensity profile across spine neck following the blue line shown in (a). (**c**) Summary graph showing FWHM of Gaussian fit of Lifeact-Venus signals across spine necks of neurons expressing non-target or KCC2-directed shRNA (n=128 and 60 spines from 19 and 18 neurons, respectively). **p<0.01. (**d**) Representative, pseudocolored fluorescence STED micrographs of 6 individual spines from 12 different neurons expressing either non-target or KCC2-directed shRNA. Scale, 500 nm. (**e**) Pseudocolored averages of 149 and 85 individual spine images from 19 and 20 neurons, respectively, as in (d), aligned as described in Experimental procedures to show the mean distribution of Lifeact-Venus fluorescence within spine heads. Scale, 500 nm. (**f**) Schematic representation of spine heads (yellow) isolated from the micrographs shown in (d) with high-intensity clustered pixels (orange), as derived from spatial autocorrelation analysis using Moran's index (see Experimental procedures for details). (**g-h**) Summary graphs of the mean coefficient of variation (CV) of Lifeact-Venus fluorescence (g) and the mean percentage of high-intensity clustered pixels (h) in spine heads of neurons expressing non-target or KCC2-directed shRNA (same dataset as in (e)). n.s., non-significant difference.

Using this approach we were able to resolve individual actin bundles within spine necks and heads (Figure 4A). The full width at half maximum (FWHM) of Lifeact-labeled spine necks in neurons transfected with non-target shRNA was 93.7±1.9 nm, (n=128 spines from 19 neurons, Figure 4B), consistent with previous data in hippocampal pyramidal neurons (Urban et al., 2011). In neurons with suppressed KCC2 expression, however, the FWHM of Lifeact-labeled spine necks was significantly increased by 20.3 % (112.8±5.6 nm, n= 60 spines from 18 neurons, p=0.001; Figure 4C), suggesting increased F-actin content in spine necks. We next

asked whether suppression of KCC2 may lead to a redistribution of F-actin within spines or a global increase in F-actin content. Lifeact-Venus fluorescence was heterogeneously distributed within individual spines with some spines showing intense, calyx-shaped bundles and others more widely distributed signal (Figures 4D and 4E). Overall, however, we could not detect a significant difference in the coefficient of variation of Lifeact-Venus fluorescence between neurons expressing non-target or KCC2-directed shRNA (0.57±0.02 vs. 0.60±0.02, n=149 and 85 spines, from 19 and 20 neurons, respectively, p=0.13; Figures 4E-G). In order to compare the spatial distribution of F-actin within spines, we performed spatial autocorrelation analysis of LifeAct-Venus signal using Moran's index (Moran, 1948) (see Materials and Methods; Figure 4F). Again, we found no significant difference in the proportion of high-intensity clustered pixels (Moran's index p-value<0.05) between neurons expressing non-target or KCC2-directed shRNA (23.0±0.3 vs. 23.1±0.4 %, same dataset as above, p=1.0; Figures 4F-H). These results show that suppression of KCC2 does not cause a substantial subspine redistribution of F-actin but instead may result in a net increase in F-actin accumulation within dendritic spines.

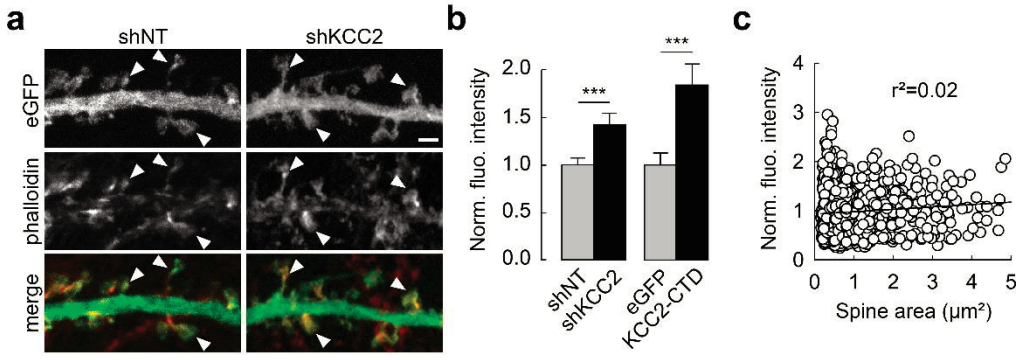

Figure 4. Enhanced F-actin content in dendritic spines upon KCC2 suppression. (**a**) Maximal projections of 20-25 confocal fluorescence micrographs of representative dendritic sections of hippocampal neurons expressing either non-target (shNT) or KCC2-directed (shKCC2) shRNA, after GFP (green) and Alexa546-phalloidin (red) staining. Arrowheads indicate dendritic spines. Scale, 1 µm. (**b**) Normalized fluorescence intensity of phalloïdin staining in dendritic spines from neurons expressing either shNT (1022 spines from 36 cells), shKCC2 (861 spines, from 29 cells), EGFP (538 spines from 15 cells) or KCC2-CTD (591 spines from 18 cells) from 2 independent experiments. *** p<0.005. (**c**) Normalized fluorescence intensity of phalloïdin staining in dendritic spines from shNT-expressing neurons plotted against spine area. No significant correlation was observed between these variables (linear regression r^2=0.02; p>0.05 Spearman rank order correlation test).

Consistent with this conclusion, phalloidin staining to reveal F-actin in dendritic spines showed a 40% increase of fluorescence in neurons with suppressed KCC2 expression (1.42±0.12 of control, n=29 and 36 cells, respectively, p<0.005; Figures 5A and 5B). This effect was even

more pronounced in neurons expressing KCC2-CTD (1.84±0.22 of control, n=18 and 15 cells, respectively, p<0.001) and was likely independent on changes in spine volume since no significant correlation was detected between phalloidin staining and spine size (Figure 5C). Thus, suppressing KCC2 expression or precluding its interaction with intracellular partners results in increased F-actin content in dendritic spines.

d) Reduced cofilin activity accounts for the lack of activity-driven GluA1 traffic and LTP upon KCC2 suppression

We next asked whether increased actin polymerization upon KCC2 suppression may be responsible for the defect in LTP expression in hippocampal neurons. Although LTP expression ultimately involves increased actin polymerization (Okamoto et al., 2004), a transient depolymerization is required for activity-driven AMPAR membrane traffic and spine enlargement (Gu et al., 2010; Ouyang et al., 2005) This was shown to reflect a transient activation (i.e. dephosphorylation) of the actin-severing enzyme cofilin upon LTP induction. We therefore compared cofilin phosphorylation in neurons expressing non-target or KCC2-specific shRNA and observed a nearly 2-fold increase in phospho-cofilin/total cofilin ratio upon KCC2 suppression under basal conditions (+85.8±14.3 %, n=3 independent experiments, p<0.02; Figures 6A and 6B). However, the lack of KCC2 did not prevent cLTP-induced decrease in cofilin phosphorylation (-79.7±9.4 % of control after 16 minutes of cLTP induction, p<0.001), to a similar extent as in neurons expressing non-target shRNA (p=0.4).

These results suggest KCC2 suppression may enhance actin polymerization in spines through increased cofilin phosphorylation without preventing LTP-induced cofilin activation. This predicts that enhanced cofilin phosphorylation at the time of cLTP induction may occlude activity-driven AMPAR membrane insertion (Gu et al., 2010). Inhibiting steady-state cofilin phosphorylation in neurons lacking KCC2 may then be sufficient to rescue LTP expression. We tested this hypothesis by monitoring cLTP-induced SEP-GluA1 exocytosis in neurons pre-treated with LIMK inhibitors. A peptide containing the first 16-amino-acid sequence of cofilin (Ser3) fused to penetratin for cell internalization was first used to inhibit endogenous LIMK activity (Gu et al., 2010). A 4-hour application of Ser3 peptide had no effect on cLTP-induced SEP-GluA1 membrane insertion in neurons transfected with non-target shRNA (+11.2±1.8 vs. +9.6±1.9 % of control, n=13 and 17 cells, respectively, p=0.6; Figures 6C and 6D) but rescued

it in neurons with suppressed KCC2 expression (+8.6±1.4 vs. -1.6±2.0 % of control, n=24 and 21 cells, respectively, p<0.001). Similar rescue was obtained in experiments using the recently developed LIMK inhibitor LIMKi (Ross-Macdonald et al., 2008) (+15.7±2.9 % of control, n=20 cells, p<0.001; Figures 6C and 6D).

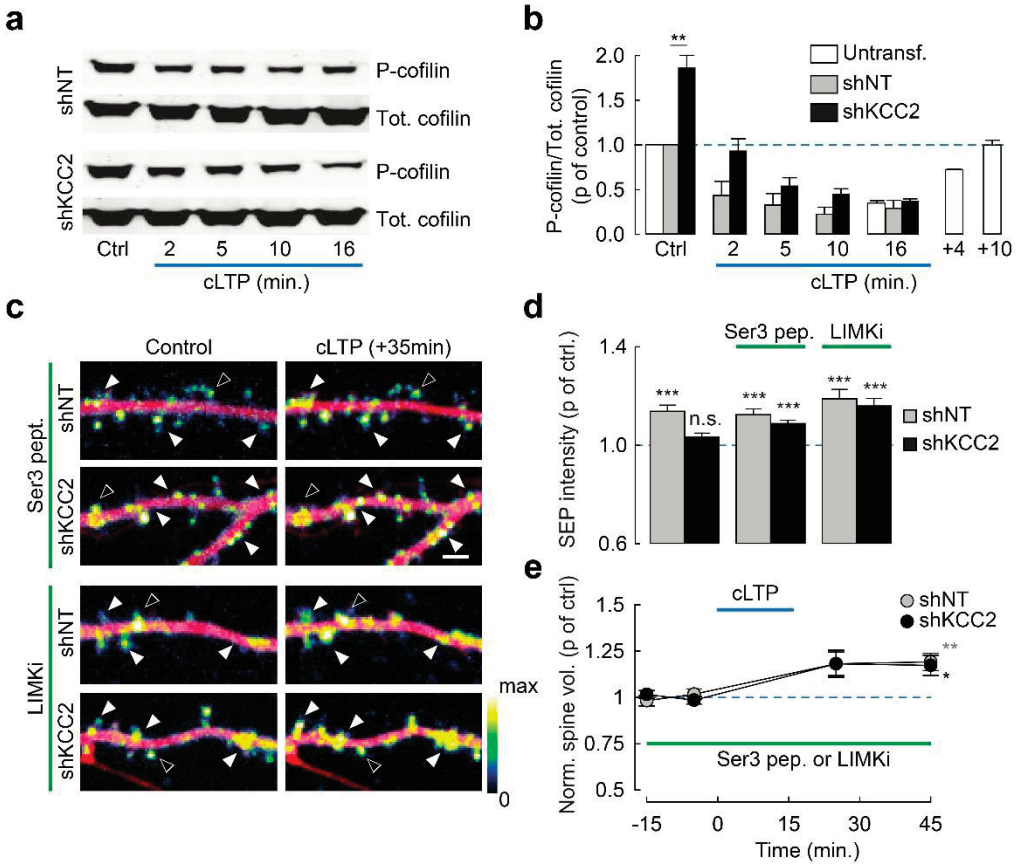

Figure 6. Preventing cofilin hyper-phosphorylation rescues activity-driven GluA1 membrane insertion and cLTP expression in neurons lacking KCC2. (**a**) Representative immunoblots of total (Tot.) or Ser3-phosphorylated (P-) cofilin from hippocampal cultures transduced with lentiviruses expressing either non-target (shNT) or KCC2-directed (shKCC2) shRNA, before (Ctrl) or at different times of cLTP induction. (**b**) Quantification from 3 independent experiments of pSer3/total cofilin ratios from immunoblots as in (a), normalized to that in shNT-expressing neurons before cLTP induction. Note the 2-fold increase in pSer3/total cofilin ratio in shKCC2-expressing neurons before cLTP induction. ** p<0.01. White bars represent data from untransfected neurons, showing a transient, ≈75% decrease in pSer3/total cofilin ratio during cLTP induction with complete recovery within 10 min. (**c**) Overlay of mCherry (red) and SEP (pseudocolors) spinning-disc fluorescence micrographs of dendritic sections of shNT or shKCC2-expressing neurons before (Control) and 35 minutes after cLTP induction. Neuron cultures were exposed for 4 hours to either cofilin N-ter hexadeca-peptide fused to penetratin (Ser3 pep., 20 µg/ml) or the LIMK inhibitor LIMKi (10 µM). Filled arrowheads show cLTP-induced SEP fluorescence spots whereas empty arrowheads show spines with unchanged or reduced SEP fluorescence. Scale, 2 µm. (**d**) Summary graph of SEP fluorescence as in (c) measured 35 minutes after cLTP induction and normalized to control, in neurons expressing SEP-GluA1 and either shNT or shKCC2 exposed to Ser3 peptide or LIMKi. *** p<0.005. n=7 to 24 neurons from the same cultures in each condition. (**e**) Summary graph of average spine volume (normalized to control before cLTP induction) measured 30 minutes after cLTP induction in neurons expressing mCherry together with either shNT (n=9 cells) or shKCC2 (n=21 cells), after 4 hour exposure to LIMK inhibitors (either Ser 3 peptide or LIMKi). * p<0.05, ** p<0.01.

Since activity-induced GluA1 traffic gates spine enlargement during LTP (Kopec et al., 2007), we then asked whether rescuing activity-driven AMPAR insertion by inhibiting LIMK upon

KCC2 suppression may be sufficient to also restore structural LTP. After 4-hour application of either LIMKi or Ser3 peptide, cLTP led to a similar increase in spine volume in neurons expressing KCC2-specific shRNA (+17.3±5.5 % of control, n=355 spines from 21 cells) and neurons expressing non-target shRNA (+19.2±4.7 % of control, n=208 spines from 9 cells, p=0.8; Figure 6E). Together, these data suggest that loss of KCC2 expression affects actin dynamics through enhanced cofilin phosphorylation and thereby precludes both synaptic and structural LTP expression.

Discussion

Our results reveal an unexpected role of the potassium/chloride cotransporter KCC2 in the regulation of glutamatergic signaling in hippocampal neurons. We show that KCC2 membrane expression, but not function, is strictly required for activity-driven AMPAR membrane insertion and thereby gates the expression of long term potentiation at glutamatergic synapses. This effect involves interaction of KCC2 with intracellular partners through its carboxy-terminal domain, resulting in enhanced cofilin phosphorylation and F-actin mobilization in dendritic spines. Thus, preventing cofilin hyper-phosphorylation upon KCC2 suppression rescues normal, activity-driven AMPAR membrane insertion as well as structural long term potentiation. KCC2-mediated control of actin polymerization in dendritic spines may then represent a new modality of metaplasticity at hippocampal glutamatergic synapses.

LTP of excitatory synapses involves a cascade of biochemical events (Poncer, 2003), each of which could in principle be perturbed by suppressing KCC2 expression. Our results however suggest synaptic and structural LTP were primarily compromised due to altered actin dynamics. Thus, NMDAR function and aggregation in dendritic spines were unaffected by KCC2 suppression, and direct activation of CaMKII failed to induce AMPAR membrane insertion, suggesting LTP was not compromised due to a defect in induction mechanisms. In addition, cLTP-induced GluA1 Ser845 phosphorylation was unaffected in neurons lacking KCC2, suggesting only the very last steps of activity-driven AMPAR traffic were hindered. Using phalloidin staining, we showed that suppressing KCC2 expression or overexpressing its C-terminal domain increases F-actin content in dendritic spines (Figure 5). This may reflect

increased aggregation of F-actin bundles within spines or increased actin polymerization. KCC2 interaction with the spectrin/actin binding protein 4.1N (Li et al., 2007) suggests KCC2-4.1N may be part of a complex acting to anchor submembrane actin cytoskeleton to the plasma membrane. A similar role has been ascribed to other ion transport proteins in a variety of cell types (Baines et al., 2014). Accordingly, we previously observed that suppressing KCC2 increased membrane diffusion of GluA1-containing AMPARs and NCAM180 (Gauvain et al., 2011), both of which are known to interact with actin. Conversely, suppressing 4.1N expression increased membrane diffusion of KCC2 near excitatory synapses (Chamma et al., 2013). However, we could not detect changes in 4.1N expression in spines upon KCC2 suppression, suggesting KCC2 is not strictly required for 4.1N aggregation in spines. In addition, STED imaging of LifeAct reveals an increased F-actin content in spine necks with no significant difference in the distribution of F-actin clusters within spines (Figure 4). Although more subtle changes in F-actin interactions with plasma membrane may occur upon KCC2 suppression, our observations are consistent with increased actin polymerization rather than a major reorganization of F-actin cytoskeleton within dendritic spines.

Consistent with this conclusion, we observed a reduction in active cofilin in neurons lacking KCC2 (Figure 6). Cofilin plays a major role in actin signaling in dendritic spines (Bosch and Hayashi, 2012; Cingolani and Goda, 2008). Its active, dephosphorylated form promotes actin depolymerization. Our results show a near-complete recovery of AMPAR traffic and structural LTP by LIMK inhibitors. This strongly suggests LIMK is hyperactivated in the absence of KCC2, resulting in enhanced actin polymerization. Importantly, we observed a two-fold increase in cofilin phosphorylation upon suppression of KCC2 expression at rest. However, phosphorylation could still be reduced in an activity-dependent manner during cLTP (Figure 6), suggesting steady-state but not activity-driven regulation of cofilin activity was specifically affected by the lack of KCC2 expression. How KCC2 influences LIMK activity remains to be explored. Among the numerous molecular interactions KCC2 may be engaged in, a recent report suggests KCC2 may directly interact with the guanine-nucleotide exchange factor betaPIX (Medina et al., 2014) involved in Rac1 activation (Saneyoshi et al., 2008), which in turn activates LIMK through activation of Pak1 (Figure S6). Although the exact modalities of KCC2 interaction with betaPIX remain to be fully characterized, we propose it may somehow hinder

betaPIX function. Since F-actin content in dendritic spines is similarly increased in neurons lacking KCC2 or over-expressing its C-terminal domain, it seems unlikely that KCC2 may solely compete with betaPIX binding to other proteins. Instead, since membrane-inserted KCC2 usually surrounds but is excluded from the PSD (Chamma et al., 2013; Gulyas et al., 2001) it may then act to trap betaPIX at distance from PSD partners (Park et al., 2003), thereby spatially restricting betaPIX-driven Rac1/Pak1 activation.

How may reduced cofilin activity prevent activity-driven AMPAR exocytosis and spine enlargement? Although LTP is associated with F-actin accumulation in dendritic spines (Bosch and Hayashi, 2012), a transient increase in both cofilin activity (Gu et al., 2010) (see also Figure 6B) and density of actin barbed ends has been reported during cLTP induction (Gu et al., 2010). Preventing cofilin activation by dephosphorylation or stabilizing F-actin pharmacologically compromised AMPAR membrane insertion during cLTP (Gu et al., 2010). Therefore transient, cofilin-mediated, actin depolymerization may represent a permissive step for activity-driven AMPAR membrane insertion. The underlying mechanisms remain unclear but may involve hindering of vesicle fusion to plasma membrane by cortical actin cytoskeleton, as described in some non-neuronal cells (Gasman et al., 1999), or cytoskeleton entrapping of secretory vesicles preventing their traffic towards the plasma membrane. Suppressing KCC2 expression also abolished cLTP-induced spine enlargement. This effect is unlikely to be due to the increase in spine volume induced by the loss of KCC2 function (Gauvain et al., 2011) since the KCC2 antagonist VU0241550 produced the same increase in volume as KCC2 suppression (Gauvain et al., 2011) but did not prevent cLTP-induced spine enlargement (Figure 1F). In neurons lacking KCC2, inhibiting LIMK with a pharmacological antagonist or dominant negative peptide rescued both activity-driven AMPAR insertion and spine enlargement (Figures 6D and 6E). This suggests the two processes may either be linked together or both independently linked to actin dynamics. Although not sufficient on its own, synaptic translocation of GluA1-containing AMPARs is permissive to activity-induced spine enlargement during cLTP (Kopec et al., 2007). However, GluA1 synaptic translocation in the absence of actin polymerization fails to induce spine enlargement (Kopec et al., 2007). These observations suggest spine enlargement during LTP requires both activity-driven GluA1 translocation and actin polymerization. Therefore, LIMK-dependent cofilin inactivation in neurons lacking KCC2 is likely to prevent spine

enlargement during cLTP primarily by hindering GluA1 traffic. Since spine enlargement during cLTP was suggested to precede GluA1 membrane insertion by several minutes (Kopec et al., 2007), our result support the idea that enhanced actin polymerization upon KCC2 suppression may hinder GluA1 intracellular translocation towards the plasma membrane rather than its actual membrane insertion.

KCC2 membrane expression and stability are tightly regulated by neuronal activity (Chamma et al., 2012; Kahle et al., 2013). In particular, Ca2+ influx through postsynaptic NMDARs rapidly reduces KCC2 function at least in part through calcium-dependent Ser940 dephosphorylation (Chamma et al., 2013; Lee et al., 2011) and calpain-mediated cleavage (Chamma et al., 2013; Puskarjov et al., 2012), leading to reduced membrane stability of the transporter. Phosphorylation of Tyr903 and Tyr1087 by Src-family tyrosine kinases on the other hand was suggested to enhance (Wake et al., 2007; Watanabe et al., 2009) or reduce (Lee et al., 2010) KCC2 membrane stability through as yet not fully elucidated mechanisms. Activation of muscarinic acetylcholine receptors, known to stimulate tyrosine phosphorylation, enhances KCC2 tyrosine phosphorylation while promoting its endocytosis and degradation (Lee et al., 2010). Thus, both Ca2+ influx and tyrosine kinase activation may rapidly affect the membrane pool of KCC2. Our results predict this may in turn influence the ability of excitatory synapses to undergo LTP. This raises the possibility that activity-dependent regulation of KCC2 membrane stability may not only tune GABA signaling to ongoing neuronal activity (Fiumelli et al., 2005; Woodin et al., 2003), but also act as a metaplastic switch at glutamatergic synapses. In this context, it is interesting to note that NMDA (Huang et al., 1992) receptor activation prior to induction were shown to suppress LTP at hippocampal synapses. Although the underlying mechanisms were not fully identified, they may involve recruitment of protein phosphatase 1 (Kato et al., 1999), which mediates KCC2 membrane destabilization (Lee et al., 2011), consistent with a contribution of activity-dependent KCC2 internalization in gating LTP expression at excitatory synapses. More experiments are clearly needed to fully explore how chronic suppression or activity-driven down-regulation of KCC2 membrane stability may affect plasticity rules at glutamatergic synapses. However, manipulations that prevent activity-driven AMPAR membrane traffic were usually associated with partial (Lin et al., 2009) or complete (Boehm et al., 2006) impairment of physiologically-induced LTP in slice preparations.

In addition to activity-induced changes at the post-translational level, KCC2 expression is also down-regulated in a variety of pathological conditions. These include neurological disorders such as epilepsy (Jin et al., 2005; Miles et al., 2012; Pallud et al., 2014; Rivera et al., 2004), spasticity after spinal cord injury (Boulenguez et al., 2010), neuropathic pain (Coull et al., 2003), stroke (Jaenisch et al., 2010) as well as psychiatric disorders such as schizophrenia (Hyde et al., 2011) and autism (Tyzio et al., 2014). These conditions are associated with increased neuronal activity that are often assumed to reflect reduced GABAergic signaling due to altered chloride extrusion. Therefore, agents acting to compensate for the loss of KCC2 function represent promising therapeutic options. KCC2 enhancers for instance, may be effective in reducing neuropathic pain in animal models (Gagnon et al., 2013). Conversely, blockers of the NKCC1 chloride importer such as bumetanide effectively suppress interictal discharges in human epileptic cortex in vitro (Pallud et al., 2014). These strategies however are predicted not to compensate altered glutamatergic signaling induced by KCC2 suppression. Although the net impact of a reduced excitatory synaptic function (Gauvain et al., 2011) and long term plasticity (this study) on network activity is somewhat difficult to predict, rhythmogenesis and mnesic performances are likely to be affected. In this respect, therapeutic strategies acting to restore KCC2 expression (Bos et al., 2013) rather than function (Gagnon et al., 2013) may be more effective in fully compensating the effects of its suppression in neurological and psychiatric disorders.

4. Materials and Methods

DNA and lentiviral constructs

Rat Slc12a5 specific and non-target shRNA sequences (Gauvain et al, 2011) were inserted in a pGeneClip hMGFP vector (Promega). The pEGFP-N1 vector used in some experiments was from Clontech. The GluA1-SEP construct in pCI vector from the Malinow lab (Kopec et al, 2006) was obtained from Addgene. Rat KCC2-CTD (aa 637-1116) was cloned into the pEGFP-IRES vector as described (Gauvain et al, 2011). LifeAct Venus construct was obtained by replacing GFP by Venus sequence from a pCMV LifeAct-GFP2 construct (Ibidi). Homer-dsRed plasmid was a gift from D. Choquet. mCherry-tCaMKII was obtained by replacing GFP by mCherry from

GFP-tCaMKII plasmid from the Malinow lab. mCherry-tCaMKII was then cloned into a pCMV-Tet3G-TRE vector to allow for doxycycline-induced expression (TET-ON system).

Cell culture and transfection

Hippocampal neurons were prepared as described (Gauvain et al, 2011) from embryonic day 19 Sprague Dawley rat pups. After dissociation, cells were plated on polyornithine-coated glass coverslips at a density of $3.4.10^4$ cells/cm^{-2} and maintained in a CO_2 incubator set at 37°C in a culture medium composed of Neurobasal supplemented with B27 (Invitrogen), 2 mM glutamine and penicillin/streptomycin. After 2 weeks, neurons were transfected using transfectin (BioRad) according to manufacturer's instructions (with 1 µg DNA for 3 µl transfectin per well). Neurons were then used for biological assays within 10-12 days. In some experiments shown in Fig. 6, neurons were exposed to LIMK inhibitors. Ser 3 peptide were synthetized by Proteogenix and contained the 16 N-terminal amino-acid sequence of cofilin (MASGVAVSDGVIKVFN) fused after 3 glycine residues to the penetratin sequence (RQIKIWFQNRRMKWKK), as described (Gu et al, 2010). Ser3 peptide (20 $\mu g.ml^{-1}$) or LIMKi (10 µM in DMSO, Millipore) were applied onto neuron cultures for 4 hours prior to experiments.

Electrophysiology

Neurons were recorded at 31°C under superfusion with a solution containing (in mM) 125 NaCl, 20 D-glucose, 10 HEPES, 4 $MgCl_2$, 2 KCl, 1 $CaCl_2$ (pH = 7.4). For miniature excitatory postsynaptic currents (mEPSCs) recordings, neurons were recorded in whole cell configuration with borosilicate glass micropipettes filled with a solution containing (in mM) 110 CsMeSO4, 20 CsCl, 10 HEPES, 10 EGTA, 4 MgATP and 0.4 Na3GTP (pH = 7.4). Cells were held at -70mV and mEPSCs were isolated by adding TTX (1 µM) and bicuculline methochloride (20 µM) to the extracellular solution. Currents were recorded with a Multiclamp 700B amplifier (Molecular Devices), filtered at 2 kHz and digitized at 20 kHz. Access and input resistance were regularly monitored with -5 mV voltage steps. mEPSCs were detected and analyzed offline using Detectivent software.

Chemical LTP (cLTP) was induced as described (Kopec et al, 2006) by switching extracellular solution for 16 minutes to a nominally Mg-free solution containing (in mM) 125 NaCl, 20 D-glucose, 10 HEPES, 2 KCl, 5 $CaCl_2$ (pH=7.4) supplemented with (in µM) 50 forskolin, 0.1

rolipram and 20 bicuculline. Forskolin and rolipram stock solutions were prepared in anhydrous DMSO, leading to a final DMSO concentration of 0.2 %. Hence control experiments involved a 16-minute application of a solution containing an equivalent DMSO concentration.

For glutamate uncaging experiments, 200 µM MNI-Glutamate (Tocris) was uncaged using a 0.5 ms 405 nm laser pulse (Omicron Deepstar; PhotonLines) delivered through a single-path photolysis head (Prairie Technologies). Position along dendrites and laser pulse intensity (from 1 to 10 effective mW) was finely adjusted to best mimic the kinetics and amplitude of mEPSCs. Peak amplitude of AMPAR-mediated currents was measured at -60 mV, whereas NMDAR-mediated current amplitude was measured at +40 mV, over a 5 ms window set 50 ms after laser pulse triggering. For GABA uncaging (Fig. E3), neurons were whole-cell patch-clamped using a K-gluconate based internal solution containing 28 mM Cl^-, as described(Chamma et al, 2013). Rubi-GABA (15 µM, Ascent Scientific) was added to the extracellular solution containing 2 mM kynurenate (Sigma), 1 µM TTX (Latoxan) and 3 µM CGP52432 (Tocris biosciences). I-V relationships of GABA-evoked currents were obtained by measuring currents elicited by 5 ms somatic or dendritic (100 µm from soma) uncaging of Rubi-GABA while applying voltage steps to the neuron (ranging from -75 mV to -25 mV). Voltages were corrected for liquid junction potential (-14.1 mV) and voltage drop across the series resistance of the pipette.

Immunocytochemistry, fluorescence image acquisition and quantitative analysis

Cultures were fixed in 4% paraformaldehyde and permeabilized with 0.2 % Triton X100 in PBS. KCC2 immunostaining was performed using rat KCC2 antibody (1:400, Sigma Aldrich) and Cy3-coupled goat anti-rabbit (1:400). NR1 (1:100, Millipore) and 4.1N (1:500, BD Biosciences) immunostainings were performed after methanol fixation and permeabilization (10 minutes at -20°C) and revealed respectively with FITC-coupled goat anti-mouse (1:400) and Cy3-coupled donkey anti-mouse antibodies (1:400). GFP immunostainings were performed using GFP (1:1000, Chemicon) and Alexa488-coupled goat anti-chicken secondary antibodies (1:400). All secondary antibodies were from Jackson Labs. Alexa456-coupled phalloidin (1:250, Invitrogen) was sometimes added, in the absence of serum, in order to stain F-actin.

Neurons were then imaged on a Leica DM6000 upright microscope using 40x (1.25 N.A., for KCC2 immunofluorescence) or 100x (1.40 N.A., for all other experiments) objectives. Images were acquired with a 12-bit cooled CCD camera (Micromax or Coolsnap fx, Roper Scientific) operated with MetaMorph (Molecular Devices). For quantification, cultures were stained

simultaneously and images were acquired using same exposure time. Mean fluorescence intensity was then quantified using ImageJ, blind to the experimental conditions. For 4.1N and phalloidin immunofluorescence, regions of interests (ROIs) were semi-automatically drawn around shaft and spines based on thresholded GFP signal. For NR1 immunofluorescence, ROIs were based on Homer-dsRed or PSD95 fluorescence. Normalization was performed for each culture by dividing mean fluorescence intensity from each cell by the average of the mean fluorescence intensity of all cells of the control group.

GluA-SEP fluorescence and spine tracking

Neurons expressing GluA1/2-SEP and mCherry were maintained at 37°C in a thermostated chamber and superfused with ACSF pre-heated at 37°C. Time-lapse confocal images of neurons were acquired using an inverted spinning-disc microscope (Leica DMI4000, Yokogawa CS20 spinning Nipkow disk, 100x/1.4 N.A. objective). At every time point, neurons were successively illuminated by 491nm / 561nm light from an Ar/Kr laser. Emitted light was collected using corresponding emission filters (525-39 and 607-36 nm) and a cooled EM-CCD camera (512x512, 16 µm pixel size). Importantly, laser intensity, time of illumination and acquisition parameters of the camera remained identical to allow comparison between experiments and bleach correction (Fig. E2). An X,Y,Z motorized platform (Märzhäuser) was used to perform acquisition from multiple neurons and z-stack (6 µm stack, 0.2 µm steps).

Confocal stacks were analyzed with Neuronstudio (Dumitriu et al, 2011), blind to experimental conditions, to quantify changes in spine head volume overtime using the mCherry channel. Only spines that could be accurately followed over the entire experiments were measured. Spine volumes from each cell were then averaged to test statistical significance. SEP fluorescence was measured on registered maximal projection in z of confocal stacks. ROIs were automatically drawn around the entire dendrites using thresholded mCherry signal and mean SEP fluorescence intensity was calculated. For experiments shown in Fig. 2, spine coordinates obtained with Neuronstudio were transferred to imageJ for measuring SEP fluorescence within spines. Fluorescence intensity values were then background-subtracted and bleach-corrected. Normalization of SEP intensity was performed for each cell by dividing the mean fluorescence intensity by the average of fluorescence intensities of the 3 time points before cLTP induction.

In experiments shown in Fig. 3, αCaMKII$_{1\text{-}290}$ expression was induced by 24h-application of doxycycline (2 µg/ml). Neurons were then maintained in ACSF in a thermostated chamber for acquisition using an upright confocal microscope (Leica TCS SP5, 40x/0.8 N.A., water immersion objective). GluA1-SEP and mCherry were successively excited by 488nm (Ar laser) and 561nm (HeNe laser) and emitted fluorescence was filtered by 500-600nm and 570-700nm (Leica AOBS). Pinhole was set as fully open (600 µm, 10 µm thickness) to collect fluorescence originating from the entire dendritic section. Laser power and scanning parameters were maintained identical to allow quantitative measurements and comparison of SEP fluorescence between conditions. All mCherry positive neurons were imaged and GluA1-SEP negative neurons were discarded during analysis process.

STED microscopy

Neurons expressing LifeAct-Venus and mCherry were fixed and mounted in mowiol. The STED microscope consisted in an inverted Leica TCS SP5 STED CW microscope with a 100x/1.4 N.A. objective, 488nm Ar laser, 594 HeNe laser and 561nm 10mW DPSS laser for depletion, non-resonant galvanometer mirror (used at 400Hz, 1024x1024, 28.7nm pixel size), Leica AOBS for emission filters and GaAsP hybrid detectors (HyD^{TM}). Focus onto dendritic spines was performed using mCherry signal and a single confocal slice was acquired for each dendritic section. Diffraction limited- and STED-resolution images of LifeAct-Venus were successively acquired. STED images were then deconvolved using special Leica CW-STED plugin of Huygens (SVI) and recommended parameters from Huygens. A custom plugin on ImageJ was used to delimit individual spines and measure the full width at half maximum (FWHM) of Lifeact-labeled spine necks based on a Gaussian fit (accuracy of the fit was evaluated both by eye and by r^2 measurement, blind to experimental conditions). Several spine head parameters were also computed: mean and variance of LifeAct-Venus fluorescence intensity and geometric center of the spine. Spine heads were then realigned using a line originating from the attachment point of the spine neck to the head (manually determined) and passing through the geometric center.

For spatial autocorrelation analysis of Lifeact-Venus signal (Fig. 5), data from isolated spine heads were first normalized. The degree of clustering in each dataset was assessed using Moran's index analysis(Moran, 1948). This index ranges values from -1 (complete dispersion) to 1 (complete clustering), with 0 representing random distribution. For each pixel i, local

Moran's index (I_i) was computed as: $I_i = z_i . \sum_j W_{i,j} . z_j$, where z_i is the value of the pixel i and W represents the matrix of neighboring weights. Equal weights were attributed to all pixels within a 2-pixel distance from pixel i, all other weights being set to 0. In order to compute a statistical significance threshold for I, a bootstrap analysis was performed for each spine head. Data were resampled randomly 1000 times and local Moran's indexes were computed for each pixel in the random distributions. For each pixel, Moran's index was compared to the 1000 values derived from bootstrap analysis to compute a local p-value. Statistical significance of positive spatial autocorrelation was considered for pixels with p-values below 0.05. The proportion of high-intensity clustered pixels per spine was then computed as the proportion of pixels with significant autocorrelation index and intensity above the mean, and was used for statistical comparison between experimental groups.

Western blots

Hippocampal cultures were infected at 15-17 DIV using lentiviral vectors expressing shRNAs and eGFP using 500ng/ml of purified virus (375-440 $ng.ml^{-1}$ p24 titer, as detected by Elisa). One week later, cultures were processed for cLTP (see below) or exposed to vehicle only (DMSO 0.2 %) for 2-16 min. Immediately after cLTP induction, cultures were washed twice in ice-cold PBS and lysed in lysis buffer (25 mM Tris-HCl, pH 7.4, 250 mM NaCl, 50 mM NaF, 5 mM PPi, 5 mM EDTA, 5 mM EGTA, 1 mM sodium orthovanadate, 1% Triton-X, and protease inhibitor mixture (Roche)). After centrifugation at 14.000g for 15 min., supernatants were mixed with Laemmli sample buffer and boiled at 95°C for 5 min. Samples were subjected to standard SDS-PAGE and transferred to nitrocellulose membranes. Blots were probed with primary antibodies against cofilin (Abcam), cofilin phospho-Ser3 (Abcam), GluA1 (Millipore), GluA1 phospho-Ser845 (Millipore), KCC2 (Millipore) Tuj1 (R&D Systems), and detected with fluorescent secondary antibodies (DyLight 800) using Odyssey infrared imaging system (LI-COR Bioscience). For quantification, all data were normalized to internal Tuj1 control signals.

Biochemical assays were repeated at least 3 times on independent cultures and data were compared using Student's t-test, after testing normality and equal variance of the data with SigmaPlot 12.5 (SPSS). In all other experiments, data were compared using non-parametric paired (Wilcoxon) or unpaired (Mann-Whitney) tests. Differences were considered significant for p-values below 0.05.

5. References

Ashby, M.C., Maier, S.R., Nishimune, A., and Henley, J.M. (2006). Lateral diffusion drives constitutive exchange of AMPA receptors at dendritic spines and is regulated by spine morphology. The Journal of neuroscience : the official journal of the Society for Neuroscience 26, 7046-7055.

Baines, A.J., Lu, H.C., and Bennett, P.M. (2014). The Protein 4.1 family: hub proteins in animals for organizing membrane proteins. Biochimica et biophysica acta 1838, 605-619.

Blaesse, P., Airaksinen, M.S., Rivera, C., and Kaila, K. (2009). Cation-chloride cotransporters and neuronal function. Neuron 61, 820-838.

Boehm, J., Kang, M.G., Johnson, R.C., Esteban, J., Huganir, R.L., and Malinow, R. (2006). Synaptic incorporation of AMPA receptors during LTP is controlled by a PKC phosphorylation site on GluR1. Neuron 51, 213-225.

Bos, R., Sadlaoud, K., Boulenguez, P., Buttigieg, D., Liabeuf, S., Brocard, C., Haase, G., Bras, H., and Vinay, L. (2013). Activation of 5-HT2A receptors upregulates the function of the neuronal K-Cl cotransporter KCC2. Proceedings of the National Academy of Sciences of the United States of America 110, 348-353.

Bosch, M., Castro, J., Saneyoshi, T., Matsuno, H., Sur, M., and Hayashi, Y. (2014). Structural and molecular remodeling of dendritic spine substructures during long-term potentiation. Neuron 82, 444-459.

Bosch, M., and Hayashi, Y. (2012). Structural plasticity of dendritic spines. Current opinion in neurobiology 22, 383-388.

Boulenguez, P., Liabeuf, S., Bos, R., Bras, H., Jean-Xavier, C., Brocard, C., Stil, A., Darbon, P., Cattaert, D., Delpire, E., et al. (2010). Down-regulation of the potassium-chloride cotransporter KCC2 contributes to spasticity after spinal cord injury. Nature medicine 16, 302-307.

Chamma, I., Chevy, Q., Poncer, J.C., and Levi, S. (2012). Role of the neuronal K-Cl co-transporter KCC2 in inhibitory and excitatory neurotransmission. Frontiers in cellular neuroscience 6, 5.

Chamma, I., Heubl, M., Chevy, Q., Renner, M., Moutkine, I., Eugene, E., Poncer, J.C., and Levi, S. (2013). Activity-dependent regulation of the K/Cl transporter KCC2 membrane diffusion, clustering, and function in hippocampal neurons. The Journal of neuroscience : the official journal of the Society for Neuroscience 33, 15488-15503.

Cingolani, L.A., and Goda, Y. (2008). Actin in action: the interplay between the actin cytoskeleton and synaptic efficacy. Nature reviews Neuroscience 9, 344-356.

Collingridge, G.L., Isaac, J.T., and Wang, Y.T. (2004). Receptor trafficking and synaptic plasticity. Nature reviews Neuroscience 5, 952-962.

Coull, J.A., Boudreau, D., Bachand, K., Prescott, S.A., Nault, F., Sik, A., De Koninck, P., and De Koninck, Y. (2003). Trans-synaptic shift in anion gradient in spinal lamina I neurons as a mechanism of neuropathic pain. Nature 424, 938-942.

Delpire, E., Days, E., Lewis, L.M., Mi, D., Kim, K., Lindsley, C.W., and Weaver, C.D. (2009). Small-molecule screen identifies inhibitors of the neuronal K-Cl cotransporter KCC2. Proceedings of the National Academy of Sciences of the United States of America 106, 5383-5388.

Dumitriu, D., Rodriguez, A., and Morrison, J.H. (2011). High-throughput, detailed, cell-specific neuroanatomy of dendritic spines using microinjection and confocal microscopy. Nature protocols 6, 1391-1411.

Engert, F., and Bonhoeffer, T. (1999). Dendritic spine changes associated with hippocampal long-term synaptic plasticity. Nature 399, 66-70.

Esteban, J.A., Shi, S.H., Wilson, C., Nuriya, M., Huganir, R.L., and Malinow, R. (2003). PKA phosphorylation of AMPA receptor subunits controls synaptic trafficking underlying plasticity. Nature neuroscience 6, 136-143.

Fiumelli, H., Briner, A., Puskarjov, M., Blaesse, P., Belem, B.J., Dayer, A.G., Kaila, K., Martin, J.L., and Vutskits, L. (2013). An ion transport-independent role for the cation-chloride cotransporter KCC2 in dendritic spinogenesis in vivo. Cerebral cortex (New York, NY : 1991) 23, 378-388.

Fiumelli, H., Cancedda, L., and Poo, M.M. (2005). Modulation of GABAergic transmission by activity via postsynaptic Ca2+-dependent regulation of KCC2 function. Neuron 48, 773-786.

Gagnon, M., Bergeron, M.J., Lavertu, G., Castonguay, A., Tripathy, S., Bonin, R.P., Perez-Sanchez, J., Boudreau, D., Wang, B., Dumas, L., et al. (2013). Chloride extrusion enhancers as novel therapeutics for neurological diseases. Nature medicine 19, 1524-1528.

Gasman, S., Chasserot-Golaz, S., Popoff, M.R., Aunis, D., and Bader, M.F. (1999). Involvement of Rho GTPases in calcium-regulated exocytosis from adrenal chromaffin cells. Journal of cell science 112 (Pt 24), 4763-4771.

Gauvain, G., Chamma, I., Chevy, Q., Cabezas, C., Irinopoulou, T., Bodrug, N., Carnaud, M., Levi, S., and Poncer, J.C. (2011). The neuronal K-Cl cotransporter KCC2 influences postsynaptic AMPA receptor content and lateral diffusion in dendritic spines. Proceedings of the National Academy of Sciences of the United States of America 108, 15474-15479.

Gu, J., Lee, C.W., Fan, Y., Komlos, D., Tang, X., Sun, C., Yu, K., Hartzell, H.C., Chen, G., Bamburg, J.R., and Zheng, J.Q. (2010). ADF/cofilin-mediated actin dynamics regulate AMPA receptor trafficking during synaptic plasticity. Nature neuroscience 13, 1208-1215.

Gulyas, A.I., Sik, A., Payne, J.A., Kaila, K., and Freund, T.F. (2001). The KCl cotransporter, KCC2, is highly expressed in the vicinity of excitatory synapses in the rat hippocampus. The European journal of neuroscience 13, 2205-2217.

Harvey, C.D., and Svoboda, K. (2007). Locally dynamic synaptic learning rules in pyramidal neuron dendrites. Nature 450, 1195-1200.

Hayashi, Y., Shi, S.H., Esteban, J.A., Piccini, A., Poncer, J.C., and Malinow, R. (2000). Driving AMPA receptors into synapses by LTP and CaMKII: requirement for GluR1 and PDZ domain interaction. Science 287, 2262-2267.

Huang, Y.Y., Colino, A., Selig, D.K., and Malenka, R.C. (1992). The influence of prior synaptic activity on the induction of long-term potentiation. Science 255, 730-733.

Huganir, R.L., and Nicoll, R.A. (2013). AMPARs and synaptic plasticity: the last 25 years. Neuron 80, 704-717.

Hyde, T.M., Lipska, B.K., Ali, T., Mathew, S.V., Law, A.J., Metitiri, O.E., Straub, R.E., Ye, T., Colantuoni, C., Herman, M.M., et al. (2011). Expression of GABA signaling molecules KCC2, NKCC1, and GAD1 in cortical development and schizophrenia. The Journal of neuroscience : the official journal of the Society for Neuroscience 31, 11088-11095.

Ivakine, E.A., Acton, B.A., Mahadevan, V., Ormond, J., Tang, M., Pressey, J.C., Huang, M.Y., Ng, D., Delpire, E., Salter, M.W., et al. (2013). Neto2 is a KCC2 interacting protein required for neuronal Cl- regulation in hippocampal neurons. Proceedings of the National Academy of Sciences of the United States of America 110, 3561-3566.

Jaenisch, N., Witte, O.W., and Frahm, C. (2010). Downregulation of potassium chloride cotransporter KCC2 after transient focal cerebral ischemia. Stroke; a journal of cerebral circulation 41, e151-159.

Jin, X., Huguenard, J.R., and Prince, D.A. (2005). Impaired Cl- extrusion in layer V pyramidal neurons of chronically injured epileptogenic neocortex. Journal of neurophysiology 93, 2117-2126.

Kahle, K.T., Deeb, T.Z., Puskarjov, M., Silayeva, L., Liang, B., Kaila, K., and Moss, S.J. (2013). Modulation of neuronal activity by phosphorylation of the K-Cl cotransporter KCC2. Trends in neurosciences 36, 726-737.

Kahle, K.T., Staley, K.J., Nahed, B.V., Gamba, G., Hebert, S.C., Lifton, R.P., and Mount, D.B. (2008). Roles of the cation-chloride cotransporters in neurological disease. Nature clinical practice Neurology 4, 490-503.

Kato, K., Li, S.T., and Zorumski, C.F. (1999). Modulation of long-term potentiation induction in the hippocampus by N-methyl-D-aspartate-mediated presynaptic inhibition. Neuroscience 92, 1261-1272.

Kopec, C.D., Li, B., Wei, W., Boehm, J., and Malinow, R. (2006). Glutamate receptor exocytosis and spine enlargement during chemically induced long-term potentiation. The Journal of neuroscience : the official journal of the Society for Neuroscience 26, 2000-2009.

Kopec, C.D., Real, E., Kessels, H.W., and Malinow, R. (2007). GluR1 links structural and functional plasticity at excitatory synapses. The Journal of neuroscience : the official journal of the Society for Neuroscience 27, 13706-13718.

Lee, H.H., Deeb, T.Z., Walker, J.A., Davies, P.A., and Moss, S.J. (2011). NMDA receptor activity downregulates KCC2 resulting in depolarizing GABA(A) receptor-mediated currents. Nature neuroscience doi:10.1038/nn.2806.

Lee, H.H., Jurd, R., and Moss, S.J. (2010). Tyrosine phosphorylation regulates the membrane trafficking of the potassium chloride co-transporter KCC2. Mol Cell Neurosci.

Li, H., Khirug, S., Cai, C., Ludwig, A., Blaesse, P., Kolikova, J., Afzalov, R., Coleman, S.K., Lauri, S., Airaksinen, M.S., et al. (2007). KCC2 interacts with the dendritic cytoskeleton to promote spine development. Neuron 56, 1019-1033.

Lin, D.T., Makino, Y., Sharma, K., Hayashi, T., Neve, R., Takamiya, K., and Huganir, R.L. (2009). Regulation of AMPA receptor extrasynaptic insertion by 4.1N, phosphorylation and palmitoylation. Nature neuroscience 12, 879-887.

Loscher, W., Puskarjov, M., and Kaila, K. (2013). Cation-chloride cotransporters NKCC1 and KCC2 as potential targets for novel antiepileptic and antiepileptogenic treatments. Neuropharmacology 69, 62-74.

Mahadevan, V., Pressey, J.C., Acton, B.A., Uvarov, P., Huang, M.Y., Chevrier, J., Puchalski, A., Li, C.M., Ivakine, E.A., Airaksinen, M.S., et al. (2014). Kainate Receptors Coexist in a Functional Complex with KCC2 and Regulate Chloride Homeostasis in Hippocampal Neurons. Cell reports 7, 1762-1770.

Makino, H., and Malinow, R. (2009). AMPA receptor incorporation into synapses during LTP: the role of lateral movement and exocytosis. Neuron 64, 381-390.

Makino, H., and Malinow, R. (2011). Compartmentalized versus global synaptic plasticity on dendrites controlled by experience. Neuron 72, 1001-1011.

Malinow, R., and Malenka, R.C. (2002). AMPA receptor trafficking and synaptic plasticity. Annual review of neuroscience 25, 103-126.

Maroteaux, M., and Mameli, M. (2012). Cocaine evokes projection-specific synaptic plasticity of lateral habenula neurons. The Journal of neuroscience : the official journal of the Society for Neuroscience 32, 12641-12646.

Medina, I., Friedel, P., Rivera, C., Kahle, K.T., Kourdougli, N., Uvarov, P., and Pellegrino, C. (2014). Current view on the functional regulation of the neuronal K(+)-Cl(-) cotransporter KCC2. Frontiers in cellular neuroscience 8, 27.

Miles, R., Blaesse, P., Huberfeld, G., Wittner, L., and Kaila, K. (2012). Chloride homeostasis and GABA signaling in temporal lobe epilepsy. In Jasper's Basic Mechanisms of the Epilepsies, J.L. Noebels, M. Avoli, M.A. Rogawski, R.W. Olsen, and A.V. Delgado-Escueta, eds. (Bethesda MD: Michael A Rogawski, Antonio V Delgado-Escueta, Jeffrey L Noebels, Massimo Avoli and Richard W Olsen.).

Moran, P.A. (1948). The interpretation of statistical maps. Journal of the Royal Statistical Society Series B (Methodological) 10, 243-251.

Okamoto, K., Nagai, T., Miyawaki, A., and Hayashi, Y. (2004). Rapid and persistent modulation of actin dynamics regulates postsynaptic reorganization underlying bidirectional plasticity. Nature neuroscience 7, 1104-1112.

Otmakhov, N., Tao-Cheng, J.H., Carpenter, S., Asrican, B., Dosemeci, A., Reese, T.S., and Lisman, J. (2004). Persistent accumulation of calcium/calmodulin-dependent protein kinase II in dendritic spines after induction of NMDA receptor-dependent chemical long-term potentiation. The Journal of neuroscience : the official journal of the Society for Neuroscience 24, 9324-9331.

Ouyang, Y., Wong, M., Capani, F., Rensing, N., Lee, C.S., Liu, Q., Neusch, C., Martone, M.E., Wu, J.Y., Yamada, K., et al. (2005). Transient decrease in F-actin may be necessary for translocation of proteins into dendritic spines. The European journal of neuroscience 22, 2995-3005.

Pallud, J., Le Van Quyen, M., Bielle, F., Pellegrino, C., Varlet, P., Labussiere, M., Cresto, N., Dieme, M.J., Baulac, M., Duyckaerts, C., et al. (2014). Cortical GABAergic excitation contributes to epileptic activities around human glioma. Science translational medicine 6, 244ra289.

Park, E., Na, M., Choi, J., Kim, S., Lee, J.R., Yoon, J., Park, D., Sheng, M., and Kim, E. (2003). The Shank family of postsynaptic density proteins interacts with and promotes synaptic accumulation of the beta PIX guanine nucleotide exchange factor for Rac1 and Cdc42. The Journal of biological chemistry 278, 19220-19229.

Park, M., Salgado, J.M., Ostroff, L., Helton, T.D., Robinson, C.G., Harris, K.M., and Ehlers, M.D. (2006). Plasticity-induced growth of dendritic spines by exocytic trafficking from recycling endosomes. Neuron 52, 817-830.

Poncer, J.C. (2003). Hippocampal long term potentiation: silent synapses and beyond. Journal of physiology, Paris 97, 415-422.

Poncer, J.C., Esteban, J.A., and Malinow, R. (2002). Multiple mechanisms for the potentiation of AMPA receptor-mediated transmission by alpha-Ca2+/calmodulin-dependent protein kinase II. The Journal of neuroscience : the official journal of the Society for Neuroscience 22, 4406-4411.

Puskarjov, M., Ahmad, F., Kaila, K., and Blaesse, P. (2012). Activity-dependent cleavage of the K-Cl cotransporter KCC2 mediated by calcium-activated protease calpain. The Journal of neuroscience : the official journal of the Society for Neuroscience 32, 11356-11364.

Puskarjov, M., Seja, P., Heron, S.E., Williams, T.C., Ahmad, F., Iona, X., Oliver, K.L., Grinton, B.E., Vutskits, L., Scheffer, I.E., et al. (2014). A variant of KCC2 from patients with febrile seizures impairs neuronal Cl- extrusion and dendritic spine formation. EMBO reports 15, 723-729.

Riedl, J., Crevenna, A.H., Kessenbrock, K., Yu, J.H., Neukirchen, D., Bista, M., Bradke, F., Jenne, D., Holak, T.A., Werb, Z., et al. (2008). Lifeact: a versatile marker to visualize F-actin. Nature methods 5, 605-607.

Rivera, C., Voipio, J., Payne, J.A., Ruusuvuori, E., Lahtinen, H., Lamsa, K., Pirvola, U., Saarma, M., and Kaila, K. (1999). The K+/Cl- co-transporter KCC2 renders GABA hyperpolarizing during neuronal maturation. Nature 397, 251-255.

Rivera, C., Voipio, J., Thomas-Crusells, J., Li, H., Emri, Z., Sipila, S., Payne, J.A., Minichiello, L., Saarma, M., and Kaila, K. (2004). Mechanism of activity-dependent downregulation of the neuron-specific K-Cl cotransporter KCC2. The Journal of neuroscience : the official journal of the Society for Neuroscience 24, 4683-4691.

Ross-Macdonald, P., de Silva, H., Guo, Q., Xiao, H., Hung, C.Y., Penhallow, B., Markwalder, J., He, L., Attar, R.M., Lin, T.A., et al. (2008). Identification of a nonkinase target mediating cytotoxicity of novel kinase inhibitors. Molecular cancer therapeutics 7, 3490-3498.

Rust, M.B., Gurniak, C.B., Renner, M., Vara, H., Morando, L., Gorlich, A., Sassoe-Pognetto, M., Banchaabouchi, M.A., Giustetto, M., Triller, A., et al. (2010). Learning, AMPA receptor mobility and synaptic plasticity depend on n-cofilin-mediated actin dynamics. Embo J 29, 1889-1902.

Saneyoshi, T., Wayman, G., Fortin, D., Davare, M., Hoshi, N., Nozaki, N., Natsume, T., and Soderling, T.R. (2008). Activity-dependent synaptogenesis: regulation by a CaM-kinase kinase/CaM-kinase I/betaPIX signaling complex. Neuron 57, 94-107.

Tyzio, R., Nardou, R., Ferrari, D.C., Tsintsadze, T., Shahrokhi, A., Eftekhari, S., Khalilov, I., Tsintsadze, V., Brouchoud, C., Chazal, G., et al. (2014). Oxytocin-mediated GABA inhibition during delivery attenuates autism pathogenesis in rodent offspring. Science 343, 675-679.

Urban, N.T., Willig, K.I., Hell, S.W., and Nagerl, U.V. (2011). STED nanoscopy of actin dynamics in synapses deep inside living brain slices. Biophysical journal 101, 1277-1284.

Wake, H., Watanabe, M., Moorhouse, A.J., Kanematsu, T., Horibe, S., Matsukawa, N., Asai, K., Ojika, K., Hirata, M., and Nabekura, J. (2007). Early changes in KCC2 phosphorylation in response to neuronal stress result in functional downregulation. The Journal of neuroscience : the official journal of the Society for Neuroscience 27, 1642-1650.

Watanabe, M., Wake, H., Moorhouse, A.J., and Nabekura, J. (2009). Clustering of neuronal K+-Cl- cotransporters in lipid rafts by tyrosine phosphorylation. The Journal of biological chemistry 284, 27980-27988.

Woodin, M.A., Ganguly, K., and Poo, M.M. (2003). Coincident pre- and postsynaptic activity modifies GABAergic synapses by postsynaptic changes in Cl- transporter activity. Neuron 39, 807-820.

6. Supplementary Figures

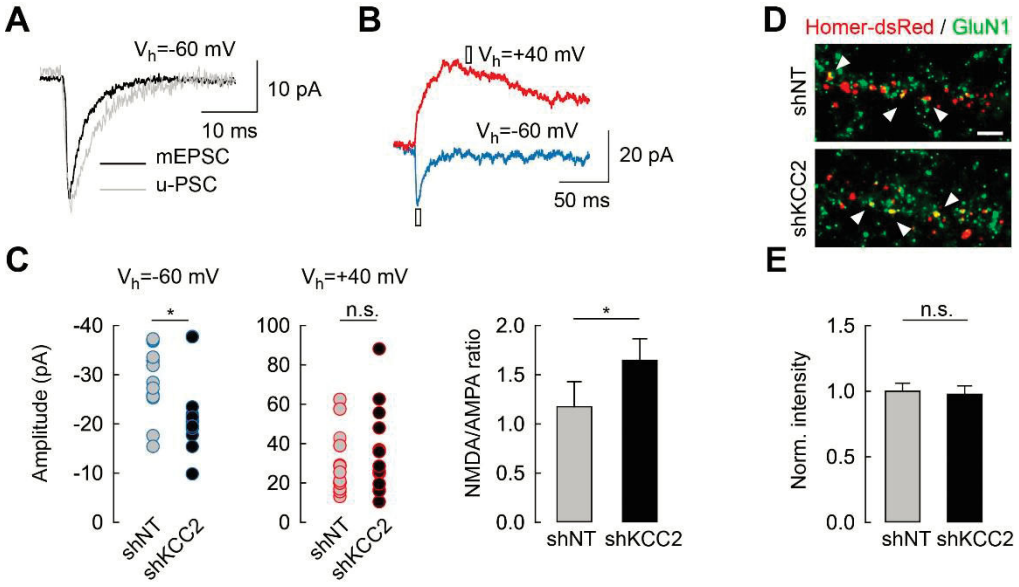

Figure S1. KCC2 suppression does not affect NMDA-receptor mediated transmission or postsynaptic clustering. *(a) Average of 50 mEPSCs (black trace) superimposed with average of 20 u-PSCs (grey trace) evoked in a hippocampal neuron by uncaging MNI-glutamate on primary dendrite with a 0.5 ms 405 nm laser pulse. Note that the amplitude and kinetics of u-PSCs and mEPSCs are quite similar. (b) Average of 21 u-PSCs recorded at a holding potential of -60 (blue) and +40 (red) mV. Open boxes show the positions at which peak currents were measured at each holding potential. (c) Left, summary graphs showing amplitudes of u-PSCs recorded at either -60 (blue-edged circles) or +40 mV (red-edged circles), in neurons expressing either non-target (grey-filled circles) or KCC2-directed shRNA (black-filled circles). n=13 cells. * p<0.05, n.s., non-significant difference. Right, summary graph of NMDA/AMPA ratios from the same neurons as in left panels. * p<0.05. (d) Wide-field fluorescent micrographs of representative dendritic sections of neurons expressing shNT or shKCC2 and Homer-dsRed (Red), immunostained for GluN1 subunit. Arrowheads show co-localized Homer/GluN1 positive clusters. Scale, 2 µm. (e) Summary graph of GluN1 immunofluorescence within Homer-dsRed-positive clusters from neurons expressing shNT (grey, n=34 cells) or shKCC2 (black, n=22 cells).*

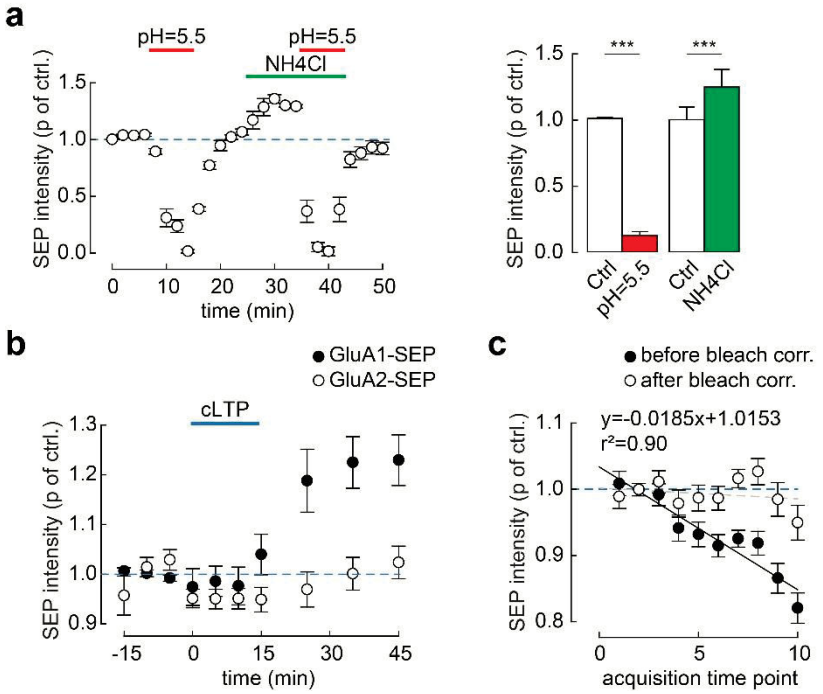

Figure S2, related to Figure 2. Probing AMPAR membrane-insertion using SEP-GluA1. *(**A**) Left, SEP-fluorescence (normalized to the first 4 min.) measured in the dendrite of SEP-GluA1 expressing neurons (n=3), is plotted over time. Application of a pH 5.5 external solution resulted in near-complete and reversible quenching of SEP fluorescence. Subsequent application of a 50 mM NH_4Cl-containing solution to collapse transmembrane pH gradients increased SEP fluorescence by about 25%, revealing the intracellular SEP-GluA1 pool. Further reduction of extracellular pH to 5.5 again led to complete and reversible quenching of SEP fluorescence. Right, Summary graph of mean SEP fluorescence (normalized to control, white) at pH 5.5 (n=11, red) and upon NH_4Cl application (n=26 cells, green). *** p<0.005. (**B**) Compared behavior of SEP-GluA1 (filled symbols, n=19 cells) and SEP-GluA2 (open symbols, n=18 cells) upon cLTP. Note the slight, reversible drop in SEP fluorescence upon cLTP induction, as previously reported (Rathje et al (2013) PNAS 110: 14426-14431). (**C**) Graph showing how bleach correction was performed in all experiments using SEP imaging. Filled symbols represent the mean normalized SEP fluorescence measured from 8 cells in 10 consecutive trials. Linear regression was used to correct the data for the bleach of SEP fluorescence (open symbols).*

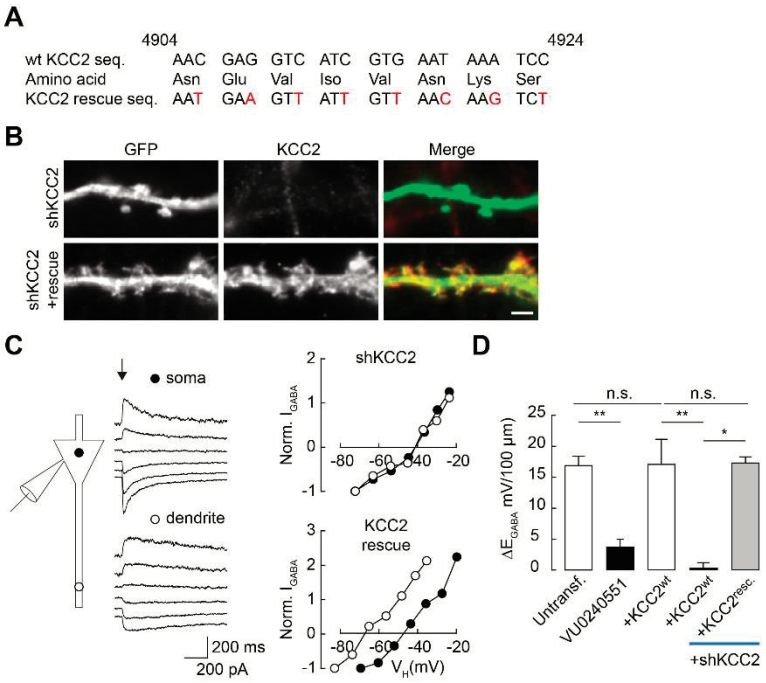

Figure S3, related to Figures 1 and 2. shRNA-proof recombinant KCC2 restores KCC2 expression and function. *(a) Nucleotide and amino-acid sequences of WT (wt KCC2) and shRNA-proof, recombinant KCC2 (KCC2 rescue) used in experiments shown in Fig. 2, restricted to the target sequence of the KCC2-specific shRNA used in our experiments. (b) Wide-field fluorescence micrographs showing GFP fluorescence (green) and KCC2 immunolabeling (red) in hippocampal neurons transfected with KCC2-specific (shKCC2) shRNA, in the absence (top) or presence of shRNA-proof recombinant KCC2. Scale, 2 µm. (c) (Left) Currents evoked at voltage steps ranging from −85 to −25 mV by local photolysis of RuBi-GABA, either on the soma or distal dendrite of a somatically whole-cell patch-clamped neuron. (Right) Representative, normalized current/voltage relations derived from recordings as shown in left panel, from neurons expressing KCC2-specific shRNA either alone (top) or together with shRNA-proof recombinant KCC2 (bottom). Note the leftward shift in current/voltage relations of dendritic vs. somatic GABA currents in the presence but not absence of recombinant KCC2 expression. (d) Summary data showing a similar somato-dendritic EGABA gradient (EGABA) in untransfected neurons (Untransf., n=6) and neurons expressing WT recombinant KCC2 (+KCC2wt, n=5). In neurons expressing KCC2-directed shRNA, this gradient was near-completely abolished when recombinant WT KCC2 was co-expressed (n=5) but could be rescued by expression of shRNA-proof KCC2 (n=3 cells). Similar collapse of EGABA was observed upon application of KCC2 specific antagonist 6µM VU0240551 (n=4). * p<0.05, ** p<0.01. n.s. non-significant difference.*

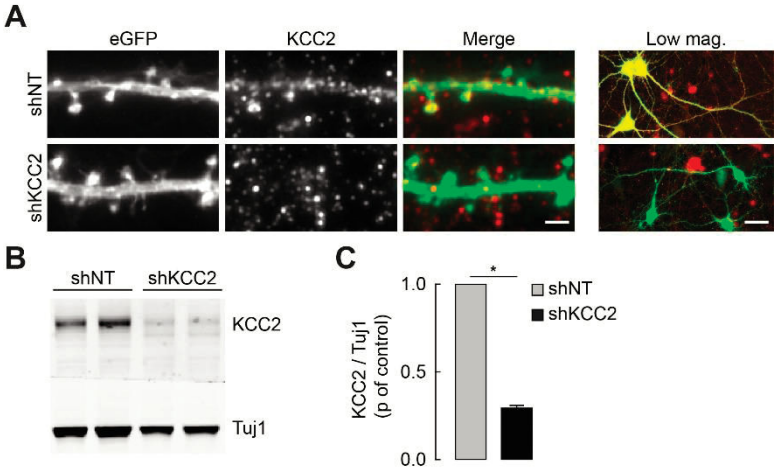

Figure S4, related to Figure 3 and 6. KCC2 knock-down using lentivirus-mediated RNA intereference. *(**A**) Wide-field fluorescence micrographs showing GFP fluorescence (green) and KCC2 immunolabeling (red) in hippocampal neurons transduced with lentiviruses eGFP and expressing either non-target (shNT) or KCC2-specific (shKCC2) shRNA sequences. Scale, left: 2 µm, right: 20 µm. (**B**) Representative immunoblot of KCC2 and Tuj1 from 24 DIV hippocampal cultures, one week after infection with the same lentiviruses as above. (**C**) Quantification from 4 independent experiments of KCC2 immunoreactivity, normalized by Tuj1 immunoreactivity, showing a >70 % reduction in KCC2 protein expression. * p<0.05.*

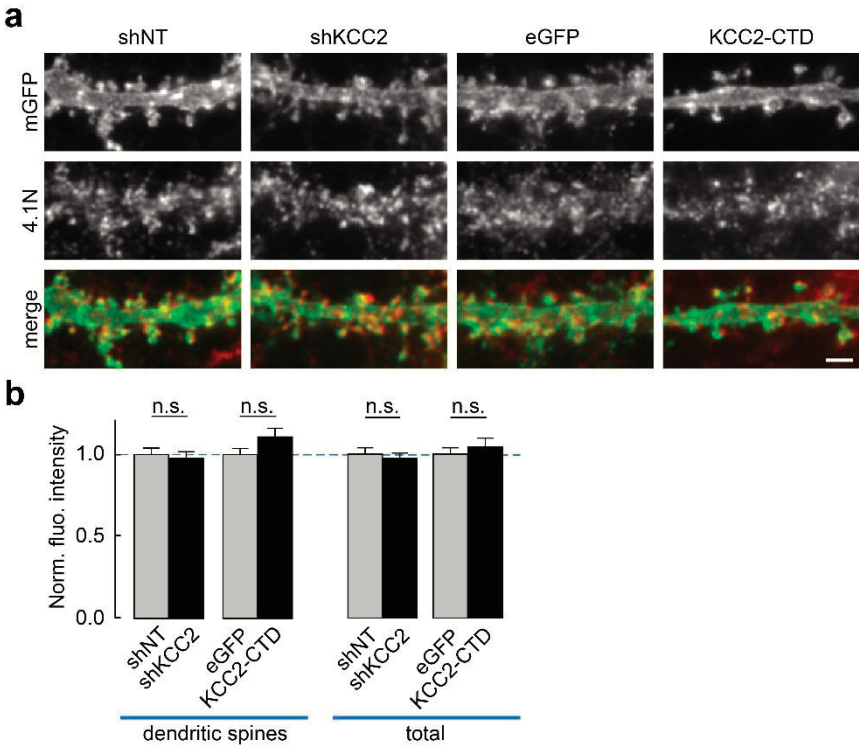

Figure S5. KCC2 suppression does not affect 4.1N expression in dendritic spines or shafts. *(**A**) Wide-field fluorescent micrographs of representative dendritic sections of neurons expressing plasma-membrane GFP and either non-target (shNT, n=41) or KCC2-directed shRNA (shKCC2, n=37), eGFP alone (eGFP, n=54) or eGFP together with KCC2-CTD (KCC2-CTD, n=43). Neurons were immunostained for GFP (green) and 4.1N (red). Scale, 2 µm. (**B**) Quantification of immunostainings as in (a) showing 4.1N mean immunofluorescence intensity per pixel either from dendritic spines only (left) or from entire dendritic sections (right), normalized to internal controls (grey bars) for each experimental condition (black bars). n.s., non-significant difference.*

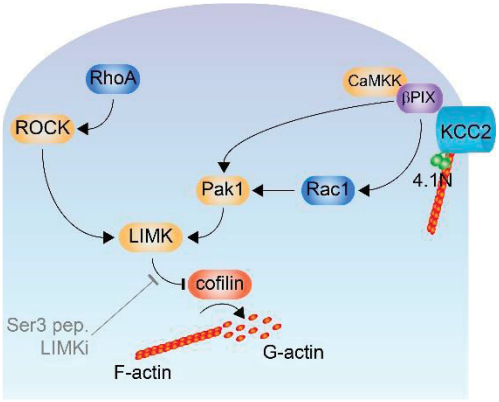

Figure S6. Signaling pathways involved in the regulation of actin depolymerization. *Cofilin plays a central role in regulating actin dynamics as it catalyzes depolymerization of F-actin into G-actin. Cofilin activity is inhibited by phosphorylation of its Ser3 residue by LIMK. Several signaling cascades converge to activate LIMK in neurons. These include the RhoA/ROCK as well as the Rac1/Pak1 pathways. βPIX, a guanine nucleotide exchange factor (GEF) involved in Rac1 activation has been shown to interact with KCC2 (Medina et al, (2014) Frontiers in cellular neuroscience 8: 27). We propose this interaction may hinder recruitment of βPIX and consequently activation of Rac1 at rest. Disrupting this interaction may then favor Rac1/Pak1 activation, increase LIMK activity and thereby inactivate cofilin through Ser3 phosphorylation, resulting in enhanced actin polymerization. The LIMK inhibitor LIMKi as well as the dominant negative peptide Ser 3 pept. (grey) both favor actin polymerization by antagonizing LIMK-mediated cofilin phosphorylation. In this scheme, kinases are shown in orange, Rho GTPases in blue, and GEF in purple. Adapted from Cingolani LA, Goda Y (2008) Nature reviews Neuroscience* ***9:*** *344-356*

DISCUSSION

DISCUSSION

During my PhD, I revealed an unexpected role of KCC2 on long term potentiation of glutamatergic synapses. Both structural and functional LTP are hindered upon KCC2 knock-down. KCC2 suppression seems to affect the very last steps leading to exocytosis of new GluA1-containing AMPARs, downstream of the activation of NMDARs and CaMKII. KCC2 suppression is associated with an enhanced mobilization of F-actin in spines that reflects an inhibition of the actin-severing protein cofilin. Although I did not demonstrate the molecular link between KCC2 suppression and a decrease in cofilin activity, I was able to rescue both structural and functional LTP upon KCC2 suppression by preventing cofilin inhibition. Hence we concluded that KCC2 suppression alters F-actin polymerization dynamics and thereby precludes structural and functional LTP. These observations raise several questions in particular regarding 1) the underlying mechanisms involved; 2) the consequence of the activity-dependent regulation of KCC2 on LTP and 3) the overall impact of pathological KCC2 suppression on neuronal activity.

I. HOW DOES KCC2 INFLUENCE GLUTAMATERGIC TRANSMISSION AND PLASTICITY

Knock-down of KCC2 in mature hippocampal neurons leads to a decreased basal glutamatergic transmission (Gauvain et al., 2011) as well as a suppression of LTP (Chevy et al., submitted). These observations seem to rely on the same KCC2-mediated ion-transport independent mechanism since they cannot be mimicked by pharmacological inhibition of KCC2. On the contrary, overexpression of the carboxy-terminal domain of KCC2 prevents glutamatergic LTP expression and mimics the decrease in basal glutamatergic transmission upon KCC2 suppression. Through its carboxy-terminal domain, KCC2 interacts with many intracellular partners (see introduction I.1.b). Among them, the actin-linked protein 4.1N and the protein Beta-PIX involved in actin dynamic regulation are candidates to link KCC2 to glutamatergic synapse function.

1. 4.1N-KCC2 interaction: cytoskeleton anchoring and AMPARs traffic

The **4.1N-KCC2 interaction** has been first demonstrated in the context of altered spinogenesis upon KCC2 genetic ablation (Li et al., 2007). 4.1N belongs to a family of proteins that interacts through their FERM domain with numerous transmembrane proteins including the GluA1-subunit of the AMPARs (Lin et al., 2009; Shen et al., 2000b). The SAB domain of 4.1 proteins allows interaction with spectrin and actin. Among the different proposed functions of these interactions (see introduction I.5.b), two are particularly relevant in the context of activity-dependent regulation of dendritic spines and AMPARs trafficking: 4.1 proteins family is implicated in the **trafficking of transmembrane proteins** and in the **anchoring of actin cortical network**.

- In neurons, 4.1N protein has been shown to be crucial for GluA1- but not GluA2-containing **AMPARs exocytosis** and LTP (Lin et al., 2009). Here we report alterations upon knock-down of KCC2 similar to the one observed upon 4.1N suppression. However, I could not demonstrate a causal effect of KCC2 suppression on 4.1N that could explain the hindrance in LTP. Nevertheless measurement of 4.1N immunostaining might be not sufficient to prove this causal link. Hence, further investigations of 4.1N-GluA1 interactions using biochemical assays or 4.1N subspine localization using superresolution microscopy upon KCC2 suppression could help to identify the exact underlying mechanism.
- No direct effect of 4.1N alteration on **actin cytoskeleton** has been demonstrated so far in neurons. However, indirect evidence suggests an altered anchoring of actin cytoskeleton upon KCC2 suppression. Knock-down of KCC2 in mature hippocampal neurons leads to an increased diffusion of actin-linked proteins such as the GluA1-subunit or NCAM-180 (Gauvain et al., 2011). On the contrary, diffusion of NCAM-120, a phospholipid-bound isoform of NCAM, is not affected by KCC2 suppression. These observations led us to conclude that KCC2 acts as a membrane anchor for cortical actin cytoskeleton potentially through 4.1N mutual interactions (Gauvain et al., 2011). Nevertheless, not all the transmembrane proteins are affected by KCC2 suppression. Indeed, aggregation of GluN1 subunit of the NMDAR (Chevy et al., submitted) is not decreased by KCC2 knock-down. This suggests that involvement of KCC2 in glutamatergic synaptic transmission cannot be restricted to its interaction with the protein 4.1N.

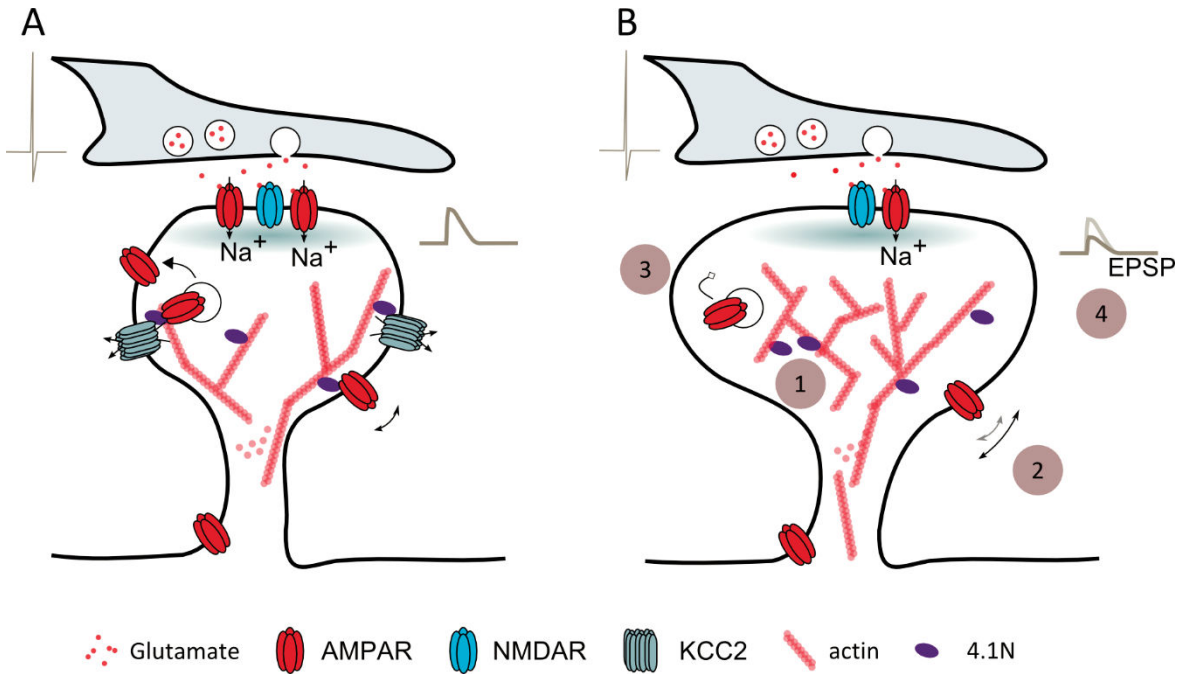

Figure 32 KCC2-4.1N interaction in AMPAR traffic
Diagram of a dendritic spine in presence (A) or absence (B) of KCC2. KCC2-4.1N interaction might participate in cortical actin membrane anchoring. KCC2 Suppression may then alter this anchoring (1). Thereby, actin and 4.1N-dependent traffic of GluA1-containing AMPARs could be affected. Thus, we observed that GluA1-containg AMPAR diffusion (2) and activity-dependent exocytosis (3) are altered upon KCC2 suppression leading to decreased glutamatergic transmission (4) and plasticity (not represented).

2. Beta-PIX-KCC2 interaction: cytoskeleton dynamics… and AMPARs traffic

A newly described interaction of KCC2 and Beta-PIX could explain the enhanced mobilization of F-actin within the dendritic spine (Medina et al., 2014). Beta-PIX is a guanine-nucleotide-exchange factor which is indirectly activated by CaMKII. Beta-PIX GEF protein targets the GTPase Rac1 and the p21-activated kinase PAK. Then, PAK phosphorylates the LIM kinase leading to the inactivation of the actin-severing protein cofilin. In summary, CaMKII-mediated activation of Beta-PIX leads to inhibition of cofilin and thereby favors actin polymerization. This pathway, together with others pathways linking CaMKII and LIMK activation (see Introduction II.3.c), is thought to participate in the maintenance of structural plasticity. Although no direct link between AMPAR trafficking and Beta-Pix function has yet been demonstrated, dynamic of spine actin cytoskeleton is crucial for activity-driven AMPARs delivery (Gu et al., 2010; Kopec et al., 2006; Rust et al., 2010). How **KCC2 modulates Beta-PIX function** and how an **increase in F-actin content affects LTP** remain to be elucidated.

- We have shown that KCC2 suppression leads to an increase in both F-actin content in spine heads and the width of actin bundles within spine necks. This increase in actin polymerization correlates with an increase in inactivated cofilin. Increase in Beta-PIX activity upon KCC2 suppression might be at the origin of the decrease in cofilin severing activity. **Two isoforms of Beta-PIX** have been described: unlike the Beta2-isoform, the Beta1-isoform contains a PDZ-binding domain (for review Kiraly et al., 2010). The two isoforms share several domains important to both their function and their localization. In particular, they both contain a RhoGEF domain underpinning their function as well as a Sh3 domain (SRC homology domain 3) which is conserved in several proteins involved in signaling pathways regulating cytoskeleton. This domain is thought to increase the specificity of the binding to the targeted molecules. Thus, Beta-PIX SH3 domain binds to PAK (Mott et al., 2005) and mutations in this domain induce a mislocalization of PAK in heterologous cells (Manser et al., 1998). Reciprocally, phosphorylation of the Thr526 residue of Beta-PIX by PAK enhances its GEF activity and its membrane localization (Shin et al., 2002). Phosphorylation of Beta-PIX Ser516 residue has been also described to increase its GEF activity and to participate in Ca^{2+} dependent activation (Saneyoshi et al., 2008).

Several observations suggest a tight **regulation of Beta-PIX localization**. Beta-PIX contains a PH domain (Pleckstrin homology domain) known to bind membrane phospholipids (Wang and Shaw, 1995). Hence, this domain could participate in the membrane anchoring of Beta-PIX. More intriguingly, Beta-PIX function does not rely on its activation (e.g. phosphorylation, post-translational modification) but instead involves its synaptic recruitment by GIT1 (Zhang et al., 2003). Within the PSD, GIT1 is part of a complex including PDZ-containing proteins such as the aforementioned GRIP protein (Ko et al., 2003) (see introduction II.1.a). Recruitment of Beta-PIX by GIT1 is necessary for spinogenesis (Saneyoshi et al., 2008; Zhang et al., 2003). Similarly, PDZ-domain dependent interaction with the PSD scaffolding protein Shank3 promotes Beta1-PIX synaptic localization (Park et al., 2003). Finally, deletion of the Beta-PIX ortholog in Drosophila or disruption of GIT1 macrocomplex in mouse both alter AMPAR synaptic content (Ko et al., 2003; Parnas et al., 2001).

All the aforementioned interacting partners of Beta-PIX participate in its synaptic localization and favor its GEF activity and subsequent activation of PAK. Although the exact modalities of KCC2 interaction with Beta-PIX remain to be fully characterized, we propose that KCC2 may

hinder Beta-PIX function. Membrane-inserted KCC2 usually surrounds but is excluded from the PSD (Chamma et al., 2013; Gulyás et al., 2001) where Beta-PIX is active. Hence, KCC2 may then act to sequestrate Beta-PIX at distance from PSD partners, thereby spatially restricting Beta-PIX-driven PAK activation. This hypothesis might explain why both KCC2 suppression and overexpression of KCC2-CTD induce a similar increase in F-actin content within dendritic spines. Both manipulations of KCC2 expression or interaction may then lead to an enhancement of the amount of Beta-PIX protein available for GIT1 recruitment.

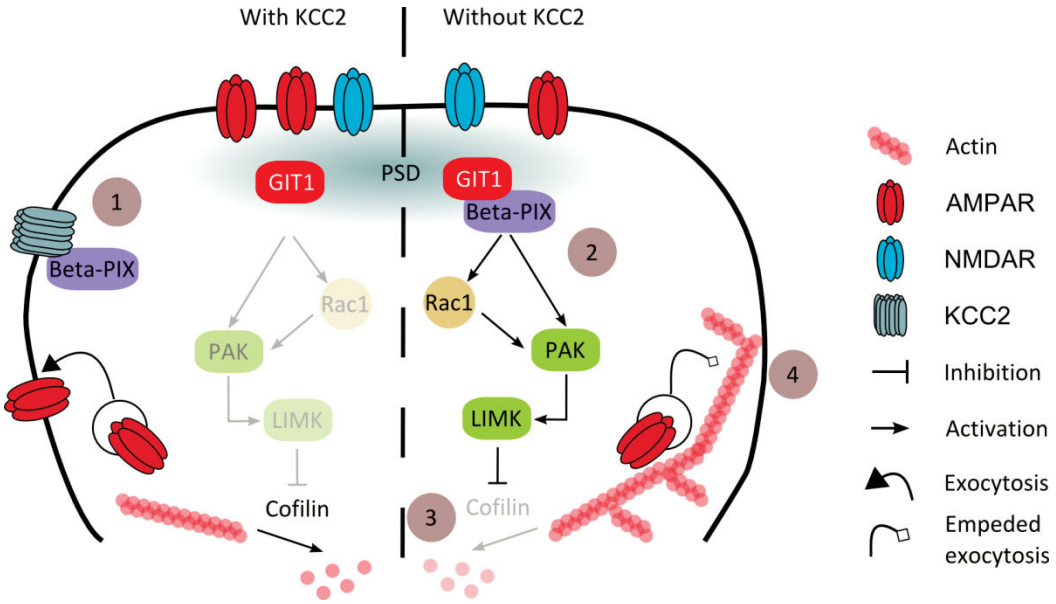

Figure 33 KCC2 sequestrates Beta-PIX away from PSD
In our model, KCC2 traps Beta-PIX away from the PSD (1). KCC2 suppression leads to the recruitment of Beta-PIX by GIT1 within the PSD (2). Beta-PIX signaling pathway ultimately leads to the inhibition of cofilin and an increase in F-actin (3). This increase in F-actin might hinder the activity-dependent exocytosis of AMPARs (4).

- Upon KCC2 suppression, an increase in GIT1-mediated recruitment of Beta-PIX may ultimately lead to an increase in actin polymerization. How this might prevent functional and structural LTP is still unclear. LTP is generally associated with increased F-actin content in dendritic spines (Okamoto et al., 2004). The underlying pathways involve CaMKII and lead to an inhibition of cofilin activity through LIMK activation. However, a transient activation of cofilin has also been observed upon LTP protocol (Gu et al., 2010) but the underlying mechanism is not known yet. Nevertheless, cofilin activity during LTP seems to undergo a two-step modulation. First, a transient activation of cofilin that might enable remodeling of actin cytoskeleton and release of molecular effectors previously trapped by the actin cytoskeleton. Furthermore, hindering of vesicle trafficking or fusion to plasma membrane by cortical actin

cytoskeleton has been described in non-neuronal cells (Gasman et al., 1999). Second, delayed inactivation of cofilin by the RhoA/Rac1 pathways may then increase actin polymerization necessary for the maintenance of spine swelling.

Although we did not test cofilin activity over time after LTP induction, we observed that KCC2 suppression does not prevent the transient dephosphorylation of cofilin (Chevy et al., submitted). Instead, we found that basal level of cofilin phosphorylation was strongly increased upon KCC2 suppression. The basal level of activated cofilin at the time of LTP induction therefore seems to be as well critical for LTP expression. Incubation of a peptide promoting the inactive form of cofilin prevents activity-driven AMPAR exocytosis and spine enlargement (Gu et al., 2010). Using the reverse strategy or LIMK inhibition, we aimed to normalize cofilin activity upon KCC2 suppression. Thus, using a peptide promoting the active form of cofilin or an inhibitor of LIMK, we were able to rescue both cLTP-induced AMPARs exocytosis and the increase in spine volume upon knock down of KCC2. In order to better identify the pathway linking KCC2 membrane expression to cofilin activity, we are planning to measure the activity of Rac1 and of RhoA. Our prediction is that the activity of Beta-PIX-dependent Rac1 will be increased upon KCC2 suppression unlike the Beta-PIX-independent RhoA activity. Then, we could try to rescue the LTP upon KCC2 suppression by inhibiting the Rac1 as we did while inhibiting the LIMK (Chevy et al., submitted).

II. KCC2: Down-regulated by Neuronal Activity but Necessary for Activity-Dependent Glutamatergic Plasticity

KCC2 membrane expression is astonishingly labile. While its developmental upregulation takes days to complete, KCC2 can be endocytosed within minutes upon increase in neuronal or synaptic activity. Firing of the postsynaptic cell, increasing neuronal excitability or glutamate application all leads to a rapid depolarizing shift of the reversal potential GABAAR-mediated currents *in vitro* (Chamma et al., 2013; Fiumelli et al., 2005; Lee et al., 2011). This shift is mediated by a Ca^{2+}-dependent internalization of KCC2. Different mechanisms have been involved in this effect. Among them, Ca^{2+} influx through NMDARs leads to a calcium-dependent Ser940 dephosphorylation putatively mediated by PP1 (Chamma et al., 2013; Lee

et al., 2011). This dephosphorylation favors calpain cleavage of KCC2-CTD leading to KCC2 internalization and degradation. In this context, how LTP protocols affect KCC2 membrane stability might be a crucial point to elucidate. Furthermore, if KCC2 is down-regulated by LTP-like protocols, how can we reconciliate this observation with its requirement for LTP expression?

In this section, I would like to try answering these questions. However, since the spatio-temporal dynamics of the regulation of KCC2, cofilin or others molecules involved in LTP is not fully established, I will be only able to speculate on the different mechanisms that could explain this apparent paradox.

1. KCC2 as a metaplastic switch of glutamatergic transmission.

In the discussion of the main article of this thesis, we proposed that KCC2 might act as a metaplastic switch at glutamatergic synapses. Metaplasticity refers to the mechanisms modulating synaptic plasticity i.e. the plasticity of synaptic plasticity (Abraham and Bear, 1996). As a previously mentioned example of metaplasticity, the switch from GluN2B- to GluN2A-containing NMDAR is thought to increase the threshold of LTP induction in mature neurons and thereby to modify the plasticity rule (Lee et al., 2010b; Yashiro and Philpot, 2008). Here, the presence of KCC2 would favor LTP expression while its absence would do the opposite. Thus, one could predict that LTP expression would be occluded if preceded by activity-dependent KCC2 internalization. Interestingly, NMDA receptor activation prior to induction suppresses LTP at hippocampal synapses in a PP1-dependent manner (Huang et al., 1992). It therefore seems possible that NMDAR/PP1-mediated KCC2 down-regulation may play a role in this occlusion.

2. KCC2 as a direct actor of glutamatergic plasticity?

A more audacious hypothesis is that activity-dependent regulation of KCC2 might be directly involved in glutamatergic plasticity. From what we already know about the link between KCC2 and glutamatergic transmission/actin cytoskeleton, two putative scenarios can be proposed. Before describing them, I should mention that they both rely on the assumption that KCC2 membrane localization may be regulated by plasticity-inducing protocols. In the absence of

direct experimental evidence for the latter, I will also speculate on the effect of these protocols on KCC2 membrane expression.

- The most conservative, yet hypothetical scenario is that upon LTP protocol, KCC2 may be down-regulated (Fiumelli and Woodin, 2007; Lee et al., 2011). This down-regulation might be necessary for the synaptic recruitment of Beta-PIX by GIT1 and the subsequent inhibition of cofilin necessary for the structural LTP, as described above. To test active participation of KCC2 in LTP, we should first verify the premise hypothesis, i.e. that KCC2 is down-regulated upon LTP protocol. Since dephosphorylation of Ser940 has been shown to be required for KCC2 activity-dependent down-regulation (Chamma et al., 2013), we could then use a recombinant KCC2 in which Ser940 has been replaced with an aspartate to mimic its phosphorylation. The membrane localization of this KCC2 S940D has been shown to be insensitive to an increase in neuronal activity (Chamma et al., 2013). Hence, our prediction would be that expression of this KCC2 S940D will hinder LTP due to the lack of KCC2 down-regulation and subsequent release of extrasynaptically trapped Beta-PIX. However, this hypothesis does not solve the paradoxical requirement of KCC2 for LTP.

- The second hypothesis is that KCC2 might be actually down-regulated during LTD but not LTP protocols. This scenario is supported by different observations: KCC2 membrane expression is down- and up-regulated by PP1 and PKC respectively (Bos et al., 2013; Lee et al., 2011). PKC activation is generally associated with LTP and has been shown to promote GluA1-containing AMPAR membrane delivery. Conversely, PP1 activation is likely to induce LTD. Thus, PP1-dependent down-regulation of KCC2 membrane expression upon LTD would prevent activity-driven AMPAR insertion. In parallel, AMPARs endocytosis would be promoted in particular through PICK1 recruitment as described in the introduction. Testing this hypothesis would allow to answer two questions: does KCC2 suppression only affect GluA1-containing AMPARs traffic? Is KCC2 down-regulation implicated in LTD expression? During my PhD, we attempted to test GluA2-containing AMPARs trafficking upon KCC2 suppression using intrapipette infusion of a small peptide that competes with GluA2-NSF interaction. This peptide has been shown to induce an internalization of GluA2-containing AMPAR and thereby leads to a rundown of the glutamatergic transmission (Lüscher et al., 1999; Lüthi et al., 1999; Nishimune et al., 1998). Our hypothesis was that KCC2 may affect only GluA1-containing

AMPARs through interactions with 4.1N. Unfortunately, assessment of the effect of this peptide in cultured neurons appeared to be more difficult than expected. Nevertheless, the lack of change in 4.1N immunostaining as well as the recent observation of the Beta-PIX-KCC2 interaction have led us to reconsider this hypothesis. Using the KCC2 S940D mutant in combination with a LTD protocol, one could test the second hypothesis regarding a possible involvement of KCC2 in LTD. Then, the prediction would be that in the absence of PP1-dependent internalization of KCC2 S940D, LTD would be occluded. This last scenario has the benefit to reconciliate both PP1-dependent KCC2 down-regulation and KCC2-dependent LTP.

III. Wrap Up of KCC2 functions at Glutamatergic and GABAergic synapses

KCC2-mediated chloride extrusion is crucial for the appearance and maintenance of a **hyperpolarizing GABAergic signaling**. In my opinion, the controversies regarding the role of cation chloride cotransport in GABAergic transmission arise solely from the difficulties in assessing CCCs function. The tight, activity-dependent regulation of KCC2 expression and function might then allow KCC2 to underlie forms of plasticity of GABA signaling. Alterations of chloride homeostasis have been implicated in many neurological disorders. Hence, drugs targeting CCCs are developed and used to compensate for these defects. However, it remains unclear whether KCC2 down-regulation is a cause or a consequence of pathological conditions such as epilepsy. In the laboratory, we are currently investigating this question using lentiviral-based suppression of KCC2 in the hippocampus *in vivo* and testing how it affects hippocampal rhythmogenesis.

With the recent discovery of a **non-canonical function of KCC2**, we need to re-evaluate the overall impact of KCC2 suppression on synaptic activity and neuronal function. The ion-transport independent function of KCC2 has been first described for the control of glutamatergic synaptic transmission. Thus, genetic ablation of KCC2 alters spinogenesis while its suppression in mature hippocampal neurons leads to a decrease in glutamatergic transmission. During my thesis, I showed that KCC2 suppression prevents the expression of LTP at glutamatergic synapse. Both structural and functional LTP were hindered by KCC2 suppression. This occlusion is likely to be due to an increase in the F-actin cytoskeleton.

Interestingly, this increase in F-actin cytoskeleton was already described in non-neuronal cell (Wei et al., 2011) and precocious expression of KCC2 leads to a decrease in F-actin content (Horn et al., 2010). Different mechanisms have been proposed to underlie this non-canonical function of KCC2 at glutamatergic synapse. First, its interaction with the 4.1N protein suggests that KCC2 could serve as a membrane anchor for cortical cytoskeleton. Thus, disruption of this interaction would lead to increased diffusion of both GluA1-subunit AMPARs and KCC2 (Chamma et al., 2013; Gauvain et al., 2011). The newly described interaction between KCC2 and Beta-PIX allows us to propose new hypotheses. First, this interaction could explain why KCC2 suppression leads to increased actin polymerization through inhibition of the actin-severing protein cofilin. Second, cofilin is implicated in LTP and therefore could explain why KCC2 suppression hinders this form of plasticity. Third, Beta-PIX interaction with KCC2 or the lack of AMPARs exocytosis upon KCC2 suppression may account for the 4.1N-dependent spinogenesis defect observed upon genetic-ablation of KCC2. Beta-PIX has been indeed involved in spinogenesis and its mislocalization leads to increase in filopodia-like dendritic spines. Moreover, this particular type of spine is thought to host glutamatergic synapses that lack AMPARs (i.e. silent synapses). Hence, it might be interesting to re-evaluate or complete the mechanisms leading to the hindrance of spinogenesis in KCC2 knock-out mice.

The non-canonical function of KCC2 may not be restricted to the glutamatergic synapse. Recently, a disruption of the GIT1/Beta-PIX complex has been shown to induce a decrease of GABAARs aggregation (Smith et al., 2014). Therefore, suppression of KCC2 might not only affect GABAergic transmission through changes in chloride homeostasis but could also modify the clustering of GABAARs similarly to what we have observed at glutamatergic synapses. This KCC2-Beta-PIX interaction might then explain the decrease in the frequency of miniature inhibitory events observed in KCC2 hypomorphic mice (Riekki et al., 2008) that is also observed upon knock-down of Beta-PIX or GIT1.

Ultimately, KCC2 suppression leads to a decrease in inhibitory efficacy through altered chloride homeostasis and/or decrease in GABAergic aggregation and to a decrease in glutamatergic transmission through decrease in spinogenesis, AMPARs aggregation and activity-dependent exocytosis of AMPARs. These paralleled mechanisms might reflect a homeostatic regulation of decrease in either excitation or inhibition through KCC2 down-regulation. Although the exact mechanisms of this non-canonical mechanism remain largely

to be explored, both the ion-transport dependent and ion-transport independent needs to be taken into account while assessing the impact of KCC2 suppression onto neuronal activity and particularly during neurological conditions. Interestingly, recently reported human mutants of KCC2 observed in epileptic patients induce a decrease in GABAergic transmission efficacy and affect spine morphology (Kahle et al., 2014; Puskarjov et al., 2014a). Hence KCC2 suppression in neurological conditions might not only affect the GABAergic transmission efficacy but also the glutamatergic plasticity leading to potential learning deficits that still need to be explored. Then, development of new therapeutical strategy that only focus on chloride homeostasis regulation may not be sufficient to overcome the deficits induced by a decrease in KCC2 expression.

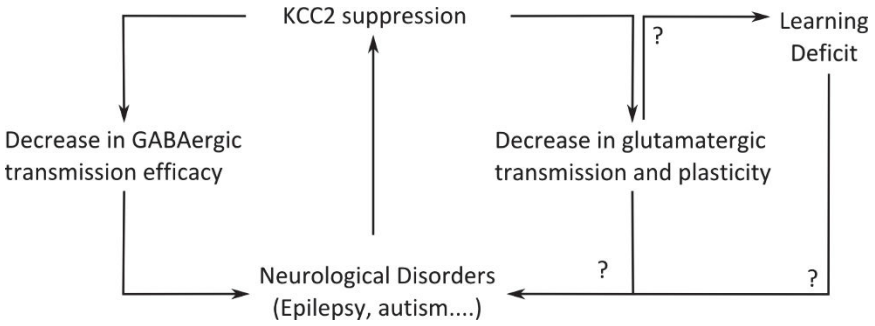

Figure 34 KCC2 suppression impacts both GABAergic and glutamatergic transmission
KCC2 suppression is observed in many neurological disorders. KCC2 suppression leads to decreased GABAergic transmission efficacy that may contribute to neurological conditions. KCC2 suppression also impacts the plasticity of glutamatergic transmission. The overall impact of KCC2 suppression on glutamatergic plasticity-dependent learning and pathologies remains to be explored.

ADDITIONAL

PUBLICATIONS

ADDITIONAL PUBLICATIONS

I. THE NEURONAL K-CL COTRANSPORTER KCC2 INFLUENCES POSTSYNAPTIC AMPA RECEPTOR CONTENT AND LATERAL DIFFUSION IN DENDRITIC SPINES

Although KCC2 has been mainly involved in the maintenance of GABAergic transmission polarity, its aggregation within dendritic spines hosting glutamatergic synapses raises questions on its potential role in excitatory transmission. KCC2 genetic ablation leads to a decreased spinogenesis through an ion-independent transport function of KCC2, possibly involving the interaction between KCC2 and the actin-linked protein 4.1N (Li et al., 2007). However, little was known on the role of KCC2 in excitatory transmission. In this study, we suppressed KCC2 in mature neurons using RNA interference and showed that:

- KCC2 is not required for spine maintenance after spinogenesis;
- KCC2 suppression in mature neurons leads to decreased glutamatergic transmission efficacy through reduced postsynaptic aggregation of GluA1-containing AMPARs;
- Disruption of KCC2 interactions with intracellular partners but not inhibition of KCC2 transport mimics the effect of KCC2 suppression on excitatory transmission, suggesting an ion-transport independent function of KCC2;
- Nevertheless, I showed that KCC2 transport affects dendritic spine volume possibly due to the involvement of KCC2 in osmotic regulation;
- Finally, we suggest that KCC2 acts as a membrane anchor for cortical actin cytoskeleton and thereby influences the diffusion and aggregation of AMPARs in spines.

In conclusion, we proposed that KCC2 suppression, as observed in several neurological conditions, might not only affect GABAergic transmission but also glutamatergic synaptic efficacy.

The neuronal K-Cl cotransporter KCC2 influences postsynaptic AMPA receptor content and lateral diffusion in dendritic spines

Grégory Gauvain[a,b,c], Ingrid Chamma[a,b,c,1], Quentin Chevy[a,b,c,1], Carolina Cabezas[a,b,c], Theano Irinopoulou[a,b,c], Natalia Bodrug[a,b,c], Michèle Carnaud[a,b,c], Sabine Lévi[a,b,c,2], and Jean Christophe Poncer[a,b,c,2]

[a]Institut National de la Santé et de la Recherche Médicale, Unité Mixte de Recherche-S 839, F75005 Paris, France; [b]Université Pierre et Marie Curie, F75005 Paris, France; and [c]Institut du Fer à Moulin, F75005 Paris, France

Edited* by Roger A. Nicoll, University of California, San Francisco, CA, and approved August 9, 2011 (received for review May 25, 2011)

The K-Cl cotransporter KCC2 plays an essential role in neuronal chloride homeostasis, and thereby influences the efficacy and polarity of GABA signaling. Although KCC2 is expressed throughout the somatodendritic membrane, it is remarkably enriched in dendritic spines, which host most glutamatergic synapses in cortical neurons. KCC2 has been shown to influence spine morphogenesis and functional maturation in developing neurons, but its function in mature dendritic spines remains unknown. Here, we report that suppressing KCC2 expression decreases the efficacy of excitatory synapses in mature hippocampal neurons. This effect correlates with a reduced postsynaptic aggregation of GluR1-containing AMPA receptors and is mimicked by a dominant negative mutant of KCC2 interaction with cytoskeleton but not by pharmacological suppression of KCC2 function. Single-particle tracking experiments reveal that suppressing KCC2 increases lateral diffusion of the mobile fraction of AMPA receptor subunit GluR1 in spines but not in adjacent dendritic shafts. Increased diffusion was also observed for transmembrane but not membrane-anchored recombinant neuronal cell adhesion molecules. We suggest that KCC2, likely through interactions with the actin cytoskeleton, hinders transmembrane protein diffusion, and thereby contributes to their confinement within dendritic spines.

The neuronal K-Cl cotransporter KCC2 transports chloride using the electrochemical gradient of K^+ ions (1). In mature neurons, this action maintains a low intraneuronal chloride concentration that ensures a hyperpolarizing effect of GABA at chloride-permeable $GABA_A$ receptors. KCC2 expression, activity, and membrane traffic are tightly regulated by neuronal activity, particularly through the phosphorylation of its carboxyl-terminal domain (CTD) (2–4). Activation of postsynaptic glutamate receptors, for instance, reduces KCC2 activity through dephosphorylation and endocytosis within minutes (3, 5). KCC2 expression is also suppressed in pathological conditions associated with enhanced neuronal activity (6), leading to a rise in intraneuronal chloride and an alteration of GABA function (7–9). KCC2 therefore appears to mediate a functional cross-talk between synaptic excitation and inhibition in neurons.

Although KCC2 function primarily influences the efficacy of GABAergic signaling, its presence in dendritic spines (10) raises the question of its role in spine morphogenesis and function. Genetic ablation of KCC2 in mice compromises spine maturation and excitatory synapse formation in immature hippocampal neurons (11). This effect appears to be independent of KCC2 function but, instead, involves KCC2 interaction with the neuronal FERM-domain protein 4.1N (12). However, KCC2 expression is up-regulated during postnatal development and is maximal in mature neurons (13), after spine formation, where its role in the maintenance and function of dendritic spines remains unknown. Here, we show that suppression of KCC2 after spine morphogenesis reduces postsynaptic glutamate receptor content and relieves a constraint to the lateral diffusion and aggregation of these receptors and other transmembrane proteins within dendritic spines. This effect likely involves KCC2 interaction with submembrane actin cytoskeleton through its CTD but not its ion transport function. Thus, suppression of KCC2 in mature neurons influences synaptic efficacy at glutamatergic synapses independent of GABAergic function.

Results

Suppression of KCC2 Expression in Mature Hippocampal Neurons. KCC2 is expressed throughout the somatodendritic membrane of cortical neurons but also in dendritic spines (10). In mature [>28 days in vitro (DIV)] hippocampal neurons, anti-KCC2 immunostaining revealed numerous KCC2-immunopositive clusters within both spine heads and spine necks (Fig. 1 *A* and *E*). The intensity of KCC2 cluster immunostaining was 76% higher in dendritic spines than on dendritic shafts ($P < 0.001$), suggesting that KCC2 primarily aggregates in dendritic spines. We evaluated the role of KCC2 in dendritic spine maintenance and function using RNAi. In cultured hippocampal neurons, excitatory synapses are formed from 5 to 7 DIV, whereas mature synapses onto dendritic spines appear from 8 to 10 DIV (14). Neurons were thus transfected at 14 DIV with plasmids expressing GFP and either nontarget shRNA or shRNA against KCC2 and were processed 10 d later. The efficacy and specificity of RNAi on KCC2 expression were established at the protein level (Fig. 1 *C–E*) by comparing KCC2 and MAP2 immunoreactivity in neurons expressing either construct. We selected one of four shRNA sequences leading to maximal reduction of KCC2 immunoreactivity ($-86.4 \pm 4.1\%$ of control; $P < 0.005$). Overexpression of this sequence had no significant effect on MAP2 immunoreactivity ($P = 0.2$).

KCC2 suppression in mature neurons had no significant effect on the mean density ($P = 0.1$) or length ($P = 0.2$) of dendritic spines but caused a 30% increase in spine head diameter ($P < 0.001$) and an increase in the proportion of mushroom-type spines (Fig. 1 *F* and *G* and Table S1). This effect contrasts with the genetic ablation of KCC2, which prevents dendritic spine morphogenesis in immature neurons, leading to predominant long filopodia-like protrusions (11). We asked whether this discrepancy was related to the mode or the timing of KCC2 suppression. In hippocampal neurons transfected at 4 DIV, before spine formation, suppression of KCC2 resulted in a 12% increase in spine length ($P < 0.005$) and a modest but significant reduction in spine head diameter ($P < 0.05$; Fig. S1). The overall spine density was unchanged ($P = 0.9$), but the proportion of filopodia-like protrusions was increased in neurons expressing shRNA against KCC2 ($P < 0.02$; Table S1). Therefore, suppression of KCC2 expression has opposite effects on spine morphology in mature vs.

Author contributions: S.L. and J.C.P. designed research; G.G., I.C., Q.C., C.C., N.B., S.L., and J.C.P. performed research; M.C. contributed new reagents/analytic tools; G.G., I.C., Q.C., T.I., S.L., and J.C.P. analyzed data; and S.L. and J.C.P. wrote the paper.

The authors declare no conflict of interest.

*This Direct Submission article had a prearranged editor.

[1]I.C. and Q.C. contributed equally to this work.

[2]To whom correspondence may be addressed. E-mail: sabine.levi@inserm.fr or jean-christophe.poncer@inserm.fr.

This article contains supporting information online at www.pnas.org/lookup/suppl/doi:10.1073/pnas.1107893108/-/DCSupplemental.

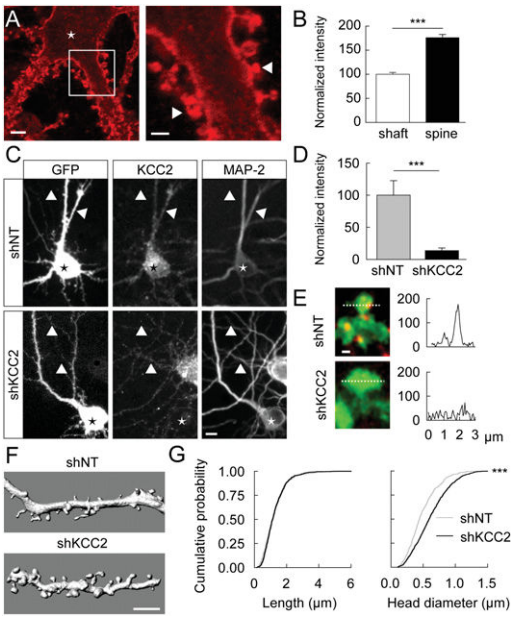

Fig. 1. Suppression of KCC2 expression in mature hippocampal neurons. (*A*) Confocal section of a 28-DIV hippocampal neuron immunostained for KCC2. (*Left*) asterisk shows the soma. (*Right*) Enlarged boxed region shows intense immunoreactivity in spines (arrowheads). (Scale bar: *Left*, 5 μm; *Right*, 2 μm.) (*B*) Normalized fluorescence intensity per cluster of KCC2 staining in dendritic shaft vs. spines in 30 cells from three independent cultures (***$P < 0.001$). (*C*) Effect of KCC2 silencing on protein expression in neurons at 24 DIV. Arrows and stars show dendrites and somata of transfected neurons, respectively. (Scale bar: 5 μm.) (*D*) Normalized fluorescence intensity per pixel of KCC2 staining in neurons expressing shNT ($n = 10$) or shKCC2 ($n = 7$) ($P < 0.005$). shKCC2, shRNA against KCC2; shNT, nontarget shRNA. (*E*) (*Left*) Confocal images of dendritic spines in neurons expressing shNT or shKCC2 showing GFP (green) and KCC2 (red) immunostaining. (*Right*) Line scans (from white dotted lines) of KCC2 immunofluorescence. The vertical axis shows raw KCC2 fluorescence intensity. (Scale bar: 0.5 μm.) (*F*) 3D reconstructions from tertiary dendrites of neurons expressing shNT or shKCC2 and GFP. (Scale bar: 5 μm.) (*G*) Quantification of spine length and head diameter from neurons expressing shNT or shKCC2.

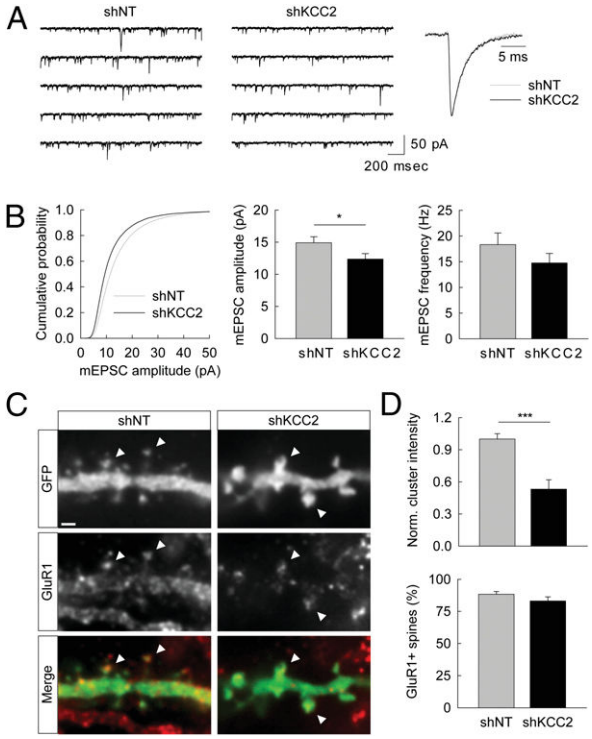

Fig. 2. Decreased quantal size and GluR1 postsynaptic clustering upon suppression of KCC2. (*A*) (*Left*) Ten-second recordings of mEPSCs in neurons expressing nontarget shRNA or shRNA against KCC2. (*Right*) Scaled averages of 150 mEPSCs from the same recordings revealed no change in onset or decay kinetics. (*B*) Summary graphs of mEPSC amplitude distributions (*Left*), mean amplitude, and frequency (*Right*) in neurons expressing shNT ($n = 27$) or shKCC2 ($n = 23$) from five experiments. Suppression of KCC2 expression reduced the amplitude of mEPSCs by ~17% ($P < 0.001$ on distributions and $P < 0.05$ on means) without affecting their frequency ($P = 0.2$). (*C*) Representative sections of dendrites with GFP and GluR1 immunostaining. Arrowheads indicate dendritic spines. KCC2 suppression induces a reduction in GluR1 clusters in dendritic spines. (Scale bar: 1 μm.) (*D*) (*Upper*) Normalized fluorescence intensity per cluster of GluR1 staining (shNT, $n = 55$; shKCC2, $n = 44$) from three experiments (***$P < 0.005$). (*Lower*) Quantification of the proportion of spines bearing GluR1-immunopositive clusters from the same samples ($P = 0.2$).

immature hippocampal neurons and KCC2 is not required for the anatomical maintenance of mature dendritic spines.

Reduced Quantal Size and GluR1 Accumulation in Dendritic Spines After KCC2 Suppression. Dendritic spine morphology has been correlated with synaptic function, particularly with postsynaptic density (PSD) size (15), postsynaptic receptor content (16), and lateral diffusion (17). Therefore, increased spine head volume upon KCC2 suppression might be expected to correlate with an increased number of postsynaptic receptors and synaptic strength (18). We tested this hypothesis by recording miniature excitatory postsynaptic currents (mEPSCs) from hippocampal neurons expressing nontarget or KCC2-specific shRNAs (Fig. 2 *A* and *B*). Surprisingly, mEPSC amplitude was not increased but rather reduced in neurons expressing shRNA against KCC2 compared with nontarget shRNA (12.4 ± 0.9 pA vs. 14.9 ± 0.9 pA; $P < 0.05$). Suppression of KCC2, on the other hand, had no significant effect on mEPSC frequency (14.8 ± 1.9 Hz vs. 18.3 ± 2.3 Hz; $P = 0.2$), suggesting that the mean number of functional synapses was unaffected (Fig. 2*B*).

Spine enlargement may increase PSD size, and thus reduce the probability of postsynaptic receptor activation by released glutamate (19). However, we detected no difference in the onset kinetics of mEPSCs in neurons expressing KCC2-specific vs. nontarget shRNA (0.97 ± 0.03 ms vs. 0.95 ± 0.03 ms; $P = 0.8$; Fig. 2*A*). We thus asked whether suppressing KCC2 affected postsynaptic receptor density, by comparing GluR1 expression in neurons expressing shRNA against KCC2 compared with nontarget shRNA (Fig. 2 *C* and *D*). GluR1 immunostaining showed marked punctae primarily on dendritic spines and, to some extent, on dendritic shafts (Fig. 2*C*). The relative intensity of GluR1 clusters within dendritic spines was significantly reduced in neurons expressing KCC2-specific shRNA (−46.9 ± 8.7%; $P < 0.005$; Fig. 2*D*). In contrast, the proportion of dendritic spines bearing GluR1 clusters was unaffected (83.1 ± 3.2% vs. 88.4 ± 2.1%, respectively; $P = 0.2$), consistent with the lack of effect of KCC2 suppression on mEPSC frequency. These results suggest that the reduction in EPSC quantal size induced by KCC2 suppression reflects a reduced density of postsynaptic AMPA receptors at excitatory synapses.

Preventing Molecular Interactions of KCC2 with Intracellular Partners Mimics KCC2 Suppression. KCC2 suppression may increase chloride concentration (20) and thereby reduce GABAergic signaling. This may subsequently lead to scaling of excitatory synapses through homeostatic plasticity (21). We tested this hypothesis using chronic application of the KCC2-specific antagonist VU0240551 (22). Treatment of 21 DIV neurons with 6 μM VU0240551 in DMSO for longer than 72 h induced a significant increase in spine head volume compared with treatment with DMSO alone ($P < 0.001$; Table S1). However, no significant change was observed in the mean amplitude (18.7 ± 1.1 pA vs. 16.8 ± 0.8 pA; $P = 0.2$), frequency (30.1 ± 3.1 Hz vs. 31.3 ± 3.0 Hz; $P = 1.0$), or onset kinetics (1.03 ± 0.02 ms vs. 1.07 ± 0.02 ms;

$P = 0.2$) of mEPSCs (Fig. 3 *A* and *B*). Consistent with these observations, VU0240551 did not induce detectable changes in GluR1 cluster immunofluorescence in dendritic spines (+7.3 ± 8.9% of control; $P = 0.2$) or in the proportion of GluR1-immunopositive spines (84.1 ± 1.0% vs. 82.6 ± 1.2%; $P = 0.7$; Fig. 3 *C* and *D*). Therefore, decreased excitatory synapse efficacy upon suppression of KCC2 expression does not result from the loss of KCC2 function and subsequent reduction of GABA signaling.

The C-terminal domain of KCC2 interacts with the 4.1N protein (11), a neuronal FERM-domain protein (12) that binds both actin and the GluR1 subunit of AMPA receptors (23). Because stabilization of synaptic AMPA receptors depends critically on the actin cytoskeleton (24), direct or indirect interaction between AMPA receptors, actin, and KCC2 may influence the maintenance of synaptic AMPA receptors. We therefore aimed at preventing KCC2-4.1N interaction without affecting KCC2 function by overexpressing the KCC2-CTD (11). We first verified that overexpressing KCC2-CTD did not affect KCC2 function by comparing the gradient in reversal potential of GABA currents (E_{GABA}) induced at the soma vs. distal dendrites using local photolysis of caged GABA (11). In our conditions, the E_{GABA} evoked by photolysis of RuBi-GABA (Ascent Scientific) onto the soma of hippocampal neurons was −51.3 ± 1.6 mV ($n = 25$; Fig. 4*A*), close to the equilibrium potential for Cl^- (−52.3 mV). In neurons expressing GFP only, we measured a gradient of 7.3 ± 1.6 mV per 100 μM between somatic and dendritic E_{GABA} (Fig. 4 *A* and *B*). This gradient was not significantly different in neurons overexpressing KCC2-CTD (7.2 ± 2.3 mV per 100 μM; $P = 0.6$). In contrast, it was strongly reduced in neurons expressing shRNA against KCC2 vs. nontarget shRNA (1.7 ± 1.1 mV vs. 6.6 ± 1.5 mV per 100 μM; $P < 0.05$) and in cells exposed to the KCC2 antagonist VU0240551 vs. DMSO alone (2.5 ± 0.5 mV vs. 6.4 ± 0.7 mV per 100 μM; $P < 0.005$). Therefore, overexpressing KCC2-CTD in hippocampal neurons does not affect their apparent chloride extrusion capacity, suggesting that KCC2 transport is functional.

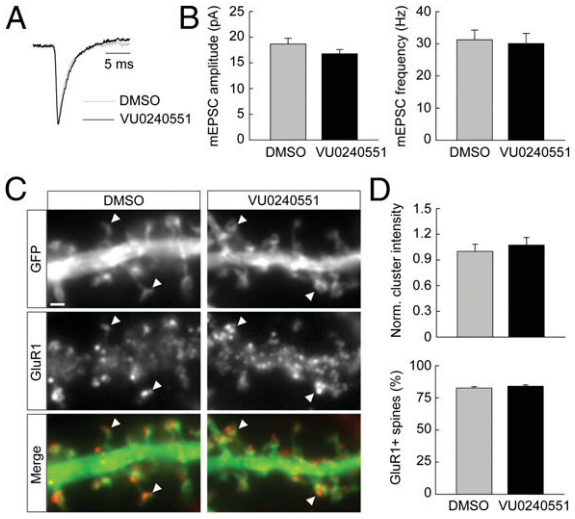

Fig. 3. Effect of KCC2 suppression is independent of KCC2 function. (*A*) Scaled averages of 100 mEPSCs from neurons treated for >72 h with either 6 μM VU0240551 in DMSO or DMSO alone. (*B*) Summary graphs of mEPSC amplitude (*Left*) and frequency (*Right*) in neurons treated with DMSO ($n = 23$) or VU0240551 ($n = 24$) from four experiments. KCC2 antagonist did not significantly affect mEPSC amplitude ($P = 0.2$) or frequency ($P = 0.8$). (*C*) GFP and GluR1 immunostaining of hippocampal neurons treated with either DMSO or VU0240551. Arrowheads indicate dendritic spines. (Scale bar: 1 μm.) (*D*) (*Upper*) Normalized fluorescence intensity per cluster of GluR1 staining in neurons treated with either DMSO ($n = 44$ cells) or VU0240551 ($n = 40$ cells) from three experiments ($P = 0.2$). (*Lower*) Quantification of the proportion of spines bearing GluR1-immunopositive clusters from the same samples ($P = 0.7$).

Overexpression of KCC2-CTD did not cause any significant change in the morphology of dendritic spines (Table S1) but decreased mEPSC amplitude to a similar extent as did suppression of KCC2 expression by RNAi (10.6 ± 0.3 pA vs. 13.1 ± 0.9 pA; $P < 0.05$; Fig. 4 *C* and D). The effect of KCC2-CTD was not associated with significant changes in mEPSC frequency (15.8 ± 1.6 Hz vs. 14.3 ± 3.0 Hz; $P = 0.2$) or rise time (0.88 ± 0.04 ms vs. 0.93 ± 0.0.3 ms; $P = 0.1$). Accordingly, GluR1 immunostaining showed reduced cluster intensity in the dendritic spines of neurons expressing KCC2-CTD vs. GFP only (−22.3 ± 8.1%; $P < 0.005$), whereas the proportion of GluR1-immunopositive spines was unaffected (90.1 ± 1.6% vs. 85.7 ± 3.1%; $P = 0.4$; Fig. 4 *E* and *F*). Therefore, suppressing KCC2 expression or interfering with KCC2 interaction with cytoplasmic partners without affecting its transport function reduces the strength of excitatory synapses. This effect likely reflects reduced aggregation of GluR1-containing AMPA receptors in dendritic spines.

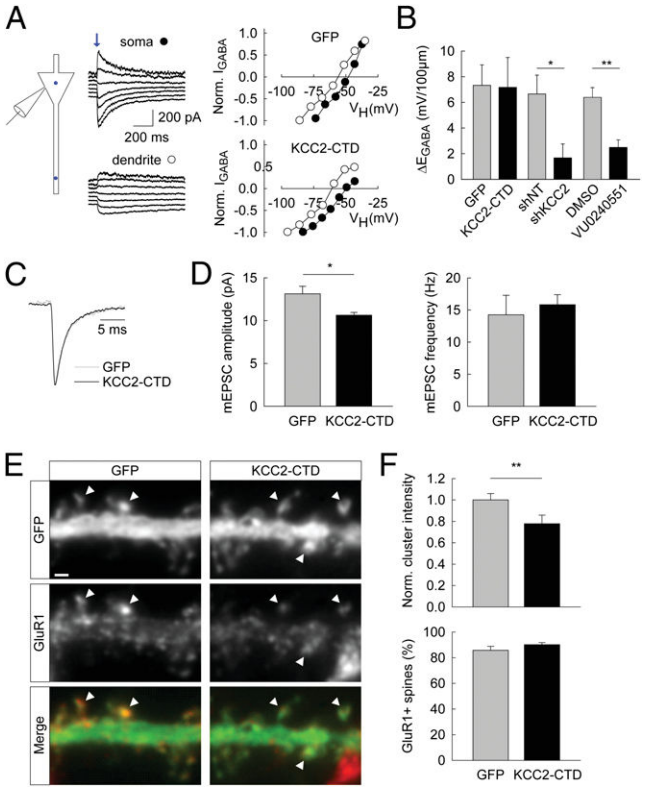

Fig. 4. Overexpression of KCC2-CTD mimics the effects of KCC2 suppression. (*A*) (*Left*) Currents evoked by local photolysis of RuBi-GABA on the soma or distal dendrite of somatically whole-cell patch-clamped neurons. (*Right*) Representative currents at voltage steps ranging from −95 to −35 mV, with corresponding normalized current/voltage relations. Note the leftward shift in current/voltage relations of dendritic vs. somatic GABA currents. (*B*) Summary data showing a similar shift in neurons expressing GFP vs. KCC2-CTD ($P = 0.6$) but not in neurons expressing KCC2-specific vs. nontarget shRNA (*$P < 0.05$) or in neurons treated with VU0240551 (6 μM) vs. DMSO alone (**$P < 0.005$). $n = 10$–12 cells for each condition. (*C*) Scaled averages of 100 mEPSCs recorded from neurons expressing either GFP or KCC2-CTD and GFP. (*D*) Mean mEPSC amplitude (*Left*) and frequency (*Right*) charts. Overexpression of KCC2-CTD significantly reduced mEPSC amplitude by ∼19% (*$P < 0.05$) but not frequency ($P = 0.2$). $n = 22$ KCC2-CTD cells and 20 GFP cells. (*E*) Representative sections of dendrites with GFP and GluR1 immunostaining. Arrowheads show dendritic spines. (Scale bar: 1 μm.) (*F*) Normalized fluorescence intensity per cluster of GluR1 staining (*Upper*, **$P < 0.005$) and proportion of GluR1-immunopositive spines (*Lower*, $P = 0.4$) in neurons expressing GFP ($n = 28$) or KCC2-CTD and GFP ($n = 30$) in two independent experiments.

Increased Lateral Diffusion of GluR1 Subunit in Dendritic Spines upon KCC2 Suppression. Synaptic AMPA receptor content is influenced by interactions with anchoring proteins, exocytosis, endocytosis, and lateral receptor diffusion in the plasma membrane (25, 26). KCC2 might then contribute to diffusional constraints for AMPA receptors in dendritic spines by interacting with 4.1N and actin cytoskeleton (17). We tested this hypothesis by monitoring AMPA receptor lateral diffusion with quantum dot (QD)-based single-particle tracking (27). Neurons were cotransfected with vectors expressing recombinant GluR1 GFP-tagged at its extracellular N terminus and either nontarget or KCC2-specific shRNA constructs. QD-bound recombinant GluR1 displayed heterogeneous diffusion behaviors in dendritic spines and shafts, as do native AMPA receptors (28). In dendritic spines, some receptors located in spine heads diffused slowly, exploring only a restricted membrane area (e.g., gray trajectory in Fig. 5*B*). Others, although confined to the spine head, diffused more rapidly over a larger membrane area (gray trajectory in Fig. 5*C*). These distinct behaviors may reflect differential synaptic anchoring or trapping of receptors in endocytic zones (28, 29). We therefore distinguished slowly ($D \leq 1.5 \times 10^{-2} \cdot \mu m^2 \cdot s^{-1}$] and rapidly ($D > 1.5 \times 10^{-2} \cdot \mu m^2 \cdot s^{-1}$) diffusing receptors, where D represents the diffusion coefficient. Consistent with the preferential synaptic anchoring of GluR1 in dendritic spines (29), the proportion of slow QDs was larger in spines than on dendritic shafts (46.5 vs. 34.3%; $n = 43$ and $n = 137$ QDs, respectively).

KCC2 extinction did not affect the exploratory behavior or confinement of slow receptors in spines (Fig. 5 *A* and *C*). Their mean diffusion coefficient and confinement domain were not significantly different in neurons expressing KCC2-specific vs. nontarget shRNA ($D = 0.82 \pm 0.01 \times 10^{-2} \cdot \mu m^2 \cdot s^{-1}$ vs. $0.85 \pm 0.07 \times 10^{-2} \cdot \mu m^2 \cdot s^{-1}$, $P = 0.6$; $L = 97 \pm 6$ nm vs. 111 ± 7 nm, $P = 0.1$), where L represents the confinement domain. In contrast, rapid QD-bound GluR1 in dendritic spines exhibited a twofold increase in diffusion coefficient and a 1.7-fold increase in confinement domain in neurons expressing KCC2-specific vs. nontarget shRNA ($D = 12.05 \pm 2.45 \times 10^{-2} \cdot \mu m^2 \cdot s^{-1}$ vs. $5.99 \pm 1.40 \times 10^{-2} \cdot \mu m^2 \cdot s^{-1}$, $P < 0.05$; $L = 611 \pm 13$ nm vs. 366 ± 5 nm, respectively, $P < 0.05$; Fig. 5 *D* and *E*). This effect was also reflected by the steeper slope of mean square displacement functions derived from trajectories in either condition (Fig. 5*C*). Thus, KCC2 apparently constrains, directly or indirectly, lateral movements of rapid GluR1-containing AMPA receptors in dendritic spines. This effect seems to be independent of changes in spine head diameter, because control experiments showed that lateral diffusion of GluR1 was unrelated to spine size (Fig. S2). In contrast to its effect on GluR1 diffusion in spines, KCC2 suppression did not significantly alter diffusion on dendritic shafts. Thus, the mean diffusion coefficient and confinement domain of both slow and rapid QD-bound GluR1 were not significantly different in neurons expressing KCC2-specific vs. nontarget shRNA (Fig. S3). We conclude that KCC2 constrains GluR1 lateral diffusion specifically in dendritic spines but not on dendritic shafts. This constraint primarily affects rapidly diffusing GluR1, suggesting that distinct molecular interactions restrict diffusion of slow GluR1-containing AMPA receptors.

KCC2 Constrains Lateral Diffusion of Transmembrane but Not Membrane-Anchored Neuronal Cell Adhesion Molecule in Dendritic Spines. KCC2 molecules are densely clustered in dendritic spines (ref. 10 and our observations) and bind actin cytoskeleton through direct 4.1N interaction (11). They might then constrain lateral diffusion of membrane proteins in dendritic spines by specific cytoskeletal interactions or by nonspecific molecular crowding. To discriminate between these possibilities, we examined the lateral diffusion of two distinct isoforms of the neuronal cell adhesion molecule (NCAM). NCAM 180 is a transmembrane isoform with a short intracellular domain that interacts with the actin cytoskeleton through β1-spectrin, whereas NCAM 120 lacks an intracellular domain and is membrane-anchored by a GPI (30) (Fig. 6*A*). We transfected neurons with chicken NCAM 180 or NCAM 120 together with nontarget or KCC2-specific shRNA. Consistent with their distinct membrane interactions, NCAM 180 explored a smaller area than NCAM 120 in dendritic spines (Fig. 6 *B* and *C*) and its diffusion in dendritic spines was 3.2-fold slower than that of NCAM 120 (Fig. 6*D*). In neurons in which KCC2 expression was suppressed by RNAi, membrane diffusion of NCAM 180 (black trajectory in Fig. 6*B*) but not NCAM 120 (black trajectory in Fig. 6*C*) was increased by almost twofold compared with neurons expressing nontarget shRNA ($D = 6.62 \pm 0.46 \times 10^{-2} \cdot \mu m^2 \cdot s^{-1}$ vs. $3.81 \pm 0.32 \times 10^{-2} \cdot \mu m^2 \cdot s^{-1}$; $P < 0.001$; Fig. 6*D*) and their confinement domain was increased by 1.5-fold ($L = 440 \pm 39$ nm vs. 299 ± 18 nm; $P < 0.003$). Because the 180 isoform is the predominant NCAM in dendritic spines (31), we also examined endogenous NCAM in spines and observed a similar increase in lateral diffusion on suppression of KCC2 (Fig. S4). In contrast, NCAM 120 diffusion was not significantly affected in these conditions ($D = 15.05 \pm 1.78 \times 10^{-2} \cdot \mu m^2 \cdot s^{-1}$ vs. $12.18 \pm 1.32 \times 10^{-2} \cdot \mu m^2 \cdot s^{-1}$, respectively; $P = 0.2$; Fig. 6*D*). These results show that KCC2 suppression specifically facilitates lateral diffusion of transmembrane but not membrane-anchored NCAM in dendritic spines. We conclude that KCC2 constrains protein diffusion in dendritic spines, likely via interactions with submembrane proteins and cytoskeleton rather than by nonspecific molecular crowding.

Discussion

Our results show that suppressing KCC2 expression in mature neurons, after spine formation, does not compromise spine maintenance but reduces the efficacy of excitatory synapses. This

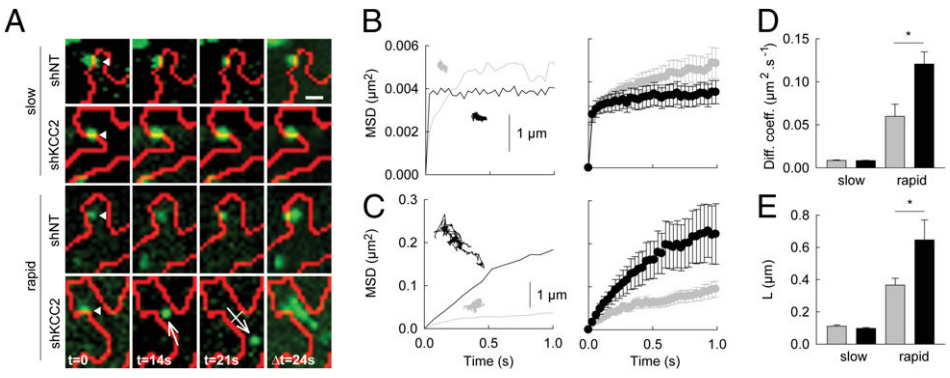

Fig. 5. KCC2 suppression increases the lateral diffusion of GluR1 in dendritic spines. (*A*) Image sequences (24 s) of slow (*Upper rows*) and rapid (*Lower rows*) QD-labeled GluR1s in dendritic spines of neurons expressing either shNT or shKCC2. QD images (green) are overlaid with outlined spine membrane (red). Surface exploration of QDs (green) is visualized on maximum intensity projections. (Scale bar: 1 μm.) Arrowheads show QDs in spine heads, arrows show QD in spine neck, and the crossed arrow shows QD in dendritic shaft. (*B* and *C*) (*Left*) Time-averaged mean square displacement (MSD) functions of slow (*B*) and rapid (*C*) GluR1 shown in *A*. GluR1 diffusion in neurons transfected with shNT (gray) or shKCC2 (black) is shown. (*Insets*) Reconstructed trajectories of slow (shNT, 479 frames; shKCC2, 633 frames) and rapid (shNT, 427 frames; shKCC2, 266 frames) QDs. (*Right*) Mean MSD functions from 20 (shNT, slow), 17 (shKCC2, slow), 24 (shNT, rapid), and 15 (shKCC2, rapid) spine trajectories. Diffusion coefficients (*D*) and confinement domains (*E*) for slow vs. rapid GluR1 in neurons expressing shNT (gray) or shKCC2 (black). KCC2 extinction increases the diffusion coefficient and confinement domain of rapid (*$P < 0.05$ for both parameters) but not slow ($P = 0.6$ and $P = 0.1$, respectively) GluR1 in spines.

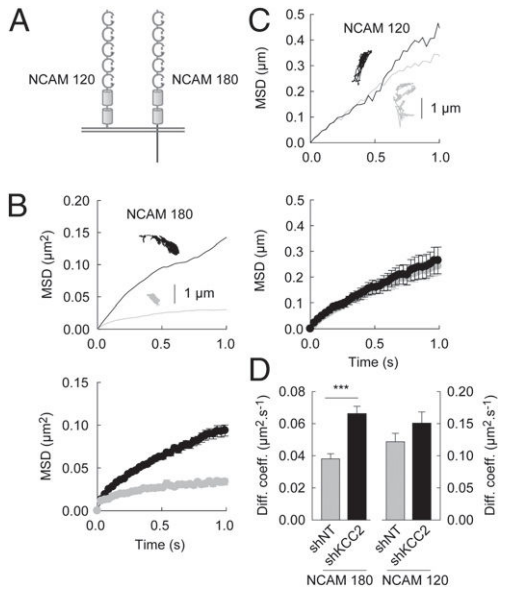

Fig. 6. KCC2 suppression increases the lateral diffusion of transmembrane but not membrane-bound NCAM in dendritic spines. (*A*) Schematic structure of NCAM 120 and NCAM 180. (*B* and *C*) (*Upper*) Representative reconstructed trajectories (*Insets*) and time-averaged mean square displacement (MSD) functions for recombinant NCAM 180 (*B*: shNT, 725 frames; shKCC2, 692 frames) and NCAM 120 (*C*: shNT, 248 frames; shKCC2, 307 frames) in dendritic spines of neurons expressing shNT (gray) or shKCC2 (black). (Scale bar: 1 μm.) (*Lower*) Mean MSD functions from 51 (shNT, NCAM 180), 66 (shKCC2, NCAM 180), 37 (shNT, NCAM 120), and 65 (shKCC2, NCAM 120) spine trajectories. (*D*) Diffusion coefficients (Diff. coeff.) of NCAM 180 (*Left*) and NCAM 120 (*Right*) show increased diffusion of NCAM 180 (***$P < 0.001$) but not NCAM 120 ($P = 0.2$) in neurons expressing shKCC2 (black) compared with shNT (gray). Data are from three and two independent cultures, respectively.

effect is independent of KCC2 function but reflects an alteration of AMPA receptor aggregation in dendritic spines.

In rat cortical neurons, KCC2 expression is very low at birth and increases steadily during the first 2 wk of postnatal development, inducing hyperpolarization of E_{GABA} (13) with a timing strikingly paralleling that of spinogenesis (32). Several arguments suggest that KCC2 may differentially affect spine morphogenesis and excitatory synaptic function in neonate vs. mature neurons. Genetic ablation of KCC2 prevented spine maturation, leading to filopodia-like protrusions in immature neurons (11), whereas no evidence for compromised spine maturation was detected on chronic suppression of KCC2 after spine formation (Fig. 1), suggesting that KCC2 is required for the formation but not the maintenance of dendritic spines in hippocampal neurons. Accordingly, mEPSC frequency was reduced in $KCC2^{-/-}$ neurons, but suppression of KCC2 in mature neurons did not affect mEPSC frequency or the proportion of spines bearing GluR1 clusters. Therefore, the number of functional synapses seems to be unaffected by KCC2 suppression in mature neurons. However, we observed a remarkable increase in spine head volume, which was mimicked by pharmacological suppression of KCC2 function. This increase may reflect the loss of ion transport function by KCC2. K-Cl cotransport is known to be crucial for volume regulation in many cell types (33). KCCs mediate transmembrane transport of K^+ and Cl^- ions, and thereby function as solute efflux pathways (34). Because KCC2 is the only transporter that extrudes Cl^- under isotonic conditions in neurons, its loss of function may then prevent osmotic regulation in dendritic spines, particularly upon cation influx through postsynaptic glutamate receptors. Although this hypothesis deserves further testing, our results predict that modulation of KCC2 function (35, 36) or trafficking (5) by synaptic activity might contribute to activity-dependent remodeling of spine volume.

Suppression of KCC2 led to reduced aggregation of postsynaptic AMPA receptors and reduced quantal size at excitatory synapses. This effect was not a consequence of the increase in spine volume because it was also observed upon overexpression of the KCC2-CTD (which did not induce increased spine volume) but not on pharmacological blockade of KCC2 function. The number and stability of synaptic AMPA receptors are controlled by several mechanisms, including (*i*) membrane insertion and removal through endo- and exocytosis (25), (*ii*) anchoring to submembrane scaffolding proteins (37–39), and (*iii*) lateral diffusion in plasma membrane (40). Our results suggest that KCC2 interferes with GluR1 accumulation at synapses mostly through the latter mechanism. First, KCC2 suppression did not reduce lateral diffusion of GluR1 on dendritic shafts, suggesting that GluR1 was not massively trapped and endocytosed throughout the extrasynaptic membrane (29). Second, KCC2 suppression had no detectable effect on lateral diffusion of slow ($D \leq 1.5 \times 10^{-2} \cdot \mu m^2 \cdot s^{-1}$) recombinant GluR1 in dendritic spines. Slowly moving receptors probably form part of the synaptic receptor pool strongly anchored to subsynaptic scaffold (17, 28, 29) and, to a lesser extent, the pool of receptors immobilized in endocytic zones (29). In contrast, rapid receptors may be part of either a synaptic pool loosely interacting with the scaffold or an extrasynaptic pool located in the vicinity of the PSD and rapidly exchanging with synaptic receptors (28, 41). We suggest that by specifically constraining the lateral diffusion of rapidly moving receptors in dendritic spines, KCC2 may contribute to maintain the exchange pool of receptors within spines, and thus influence the size of the synaptically anchored pool. In fact, reduced synaptic efficacy attributable to increased AMPA receptor mobility at the spine surface was recently demonstrated at hippocampal synapses and was associated with a redistribution of AMPA receptors (AMPARs) between the PSD and perisynaptic membrane (19). In addition, a reduction in synaptic receptor content is observed following impaired filling of the recycling (extrasynaptic) receptor pool by displacement of endocytic zones from the vicinity of the PSD without affecting the diffusion of slow synaptic receptors (29).

How might KCC2 constrain lateral diffusion of AMPARs? Suppression of KCC2 expression may influence GluR1 lateral diffusion as a consequence of the morphological changes in dendritic spines. Larger spine heads may have reduced steric constraints to lateral diffusion of membrane proteins. However, this seems unlikely because spines with large heads were shown to have slower membrane kinetics than spines with small heads (42). In addition, the KCC2 antagonist VU0240551 increased spine head diameter without affecting GluR1 clustering. Finally, increased diffusion after KCC2 suppression was limited to transmembrane spine proteins (GluR1 and NCAM 180) but did not affect GPI-anchored NCAM. This observation suggests that KCC2 may specifically alter the diffusion of proteins interacting with submembrane protein partners. Several ion transport proteins have been shown to play a critical role in anchoring the actin cytoskeleton to plasma membrane in a variety of cell types. In fibroblasts, the Na^+/H^+ exchanger NHE1 anchors actin filaments to control cytoskeleton organization and cell shape independent of its ion transport function (43). In erythrocytes, the anion exchanger AE1 docks actin to plasma membrane through direct interaction with linker proteins of the ankyrin and 4.1 families (44). These linker proteins contain an aminoterminal FERM domain that binds transmembrane proteins, such as ion transport proteins, and a CTD that binds actin or actin-associated proteins (45). In particular, the neuronal 4.1N protein binds both GluR1 (23) and KCC2 (11). We suggest that KCC2 hinders transmembrane protein diffusion through a mechanism involving its interaction with 4.1N and actin cytoskeleton. Indeed, preventing KCC2 interactions with intracellular partners by overexpressing its CTD mimicked the effects of KCC2 suppression on GluR1 clustering and synaptic efficacy. This constraint to lateral diffusion also affects other transmembrane proteins interacting with 4.1N and/or the actin cytoskeleton, such as NCAM. KCC2 may then contribute to the membrane anchoring of a complex involving actin, 4.1N, and possibly other partners. The organization of such

a complex remains to be determined, as well as the role of the direct 4.1N-GluR1 interaction, which has recently been shown to be necessary for the extrasynaptic insertion of AMPA receptors (46).

In addition to being developmentally regulated (13), KCC2 expression is suppressed in mature neurons in several pathological conditions, including epilepsy (9) and neuropathic pain (8). Suppression of KCC2 in these conditions has been suggested to induce a depolarizing shift in E_{GABA} that might reduce the efficacy or even shift the polarity of GABAergic transmission and increase neuronal excitability (9). Our results reveal that KCC2 suppression in mature neurons may act in a homeostatic manner to reduce simultaneously the efficacy of excitatory inputs onto neurons with reduced KCC2 expression. Finally, KCC2 function has been shown to be modulated in physiological conditions both by intrinsic (47) and synaptic (36) activity. Such modulation mostly involves phosphorylation of the KCC2-CTD, which may act directly to affect ion transport function (48) or decrease KCC2 membrane stability (3, 5). Therefore, a rapid increase in PKC and Src-kinase activities associated with long-term plasticity (49, 50) may rapidly and locally modulate KCC2 function and membrane aggregation. Our results predict that this may have an impact on both spine volume through modulation of ion transport and synaptic efficacy through increased lateral diffusion of AMPA receptor in dendritic spines.

Materials and Methods

Hippocampal neurons were prepared from embryo day 19 Sprague–Dawley rat pups. Cells were plated on polyornithine-coated glass coverslips at a density of 2.5×10^4 cells·cm^{-2} and cultured at 37 °C in a CO_2 incubator in Neurobasal medium supplemented with B27 (Invitrogen), 2 mM glutamine, and penicillin/streptomycin. After 4 or 14 DIV, neurons were transfected using Lipofectamine 2000 (Invitrogen) according to the manufacturer's instructions (DNA/lipofectamine ratio of 1 μg/3 μL per well). Neurons were used for biological assays within 10–12 d. Additional details are available in *SI Materials and Methods*.

ACKNOWLEDGMENTS. We thank J. Nabekura for rat KCC2-IRES-GFP construct; J. A. Esteban for GluR1-GFP; R. Miles, J. A. Esteban, C. Bernard, and E. Petrini for critical reading of an earlier version of the manuscript; R. M. Mège for chicken NCAM constructs and antibodies; and M. Dahan for sharing single particle tracking analysis software. This work was supported by the Institut National de la Santé et de la Recherche Médicale (Avenir program grant to J.C.P.), research grants (to J.C.P.) from the City of Paris, Federation pour la Recherche sur le Cerveau, Fyssen Foundation, and Fondation pour la Recherche Medicale. G.G. was the recipient of fellowships from the Neuropole-Ile de France and the Fondation pour la Recherche Medicale.

1. Payne JA, Rivera C, Voipio J, Kaila K (2003) Cation-chloride co-transporters in neuronal communication, development and trauma. *Trends Neurosci* 26:199–206.
2. Blaesse P, Airaksinen MS, Rivera C, Kaila K (2009) Cation-chloride cotransporters and neuronal function. *Neuron* 61:820–838.
3. Lee HH, Deeb TZ, Walker JA, Davies PA, Moss SJ (2011) NMDA receptor activity downregulates KCC2 resulting in depolarizing GABAA receptor-mediated currents. *Nat Neurosci* 14:736–743.
4. Rivera C, et al. (2004) Mechanism of activity-dependent downregulation of the neuron-specific K-Cl cotransporter KCC2. *J Neurosci* 24:4683–4691.
5. Lee HH, Jurd R, Moss SJ (2010) Tyrosine phosphorylation regulates the membrane trafficking of the potassium chloride co-transporter KCC2. *Mol Cell Neurosci* 45:173–179.
6. Kahle KT, et al. (2008) Roles of the cation-chloride cotransporters in neurological disease. *Nat Clin Pract Neurol* 4:490–503.
7. Boulenguez P, et al. (2010) Down-regulation of the potassium-chloride cotransporter KCC2 contributes to spasticity after spinal cord injury. *Nat Med* 16:302–307.
8. Coull JA, et al. (2003) Trans-synaptic shift in anion gradient in spinal lamina I neurons as a mechanism of neuropathic pain. *Nature* 424:938–942.
9. Huberfeld G, et al. (2007) Perturbed chloride homeostasis and GABAergic signaling in human temporal lobe epilepsy. *J Neurosci* 27:9866–9873.
10. Gulyás AI, Sík A, Payne JA, Kaila K, Freund TF (2001) The KCl cotransporter, KCC2, is highly expressed in the vicinity of excitatory synapses in the rat hippocampus. *Eur J Neurosci* 13:2205–2217.
11. Li H, et al. (2007) KCC2 interacts with the dendritic cytoskeleton to promote spine development. *Neuron* 56:1019–1033.
12. Walensky LD, et al. (1999) A novel neuron-enriched homolog of the erythrocyte membrane cytoskeletal protein 4.1. *J Neurosci* 19:6457–6467.
13. Rivera C, et al. (1999) The K+/Cl– co-transporter KCC2 renders GABA hyperpolarizing during neuronal maturation. *Nature* 397:251–255.
14. Grabrucker A, Vaida B, Bockmann J, Boeckers TM (2009) Synaptogenesis of hippocampal neurons in primary cell culture. *Cell Tissue Res* 338:333–341.
15. Harris KM, Jensen FE, Tsao B (1992) Three-dimensional structure of dendritic spines and synapses in rat hippocampus (CA1) at postnatal day 15 and adult ages: Implications for the maturation of synaptic physiology and long-term potentiation. *J Neurosci* 12:2685–2705.
16. Nusser Z, et al. (1998) Cell type and pathway dependence of synaptic AMPA receptor number and variability in the hippocampus. *Neuron* 21:545–559.
17. Ashby MC, Maier SR, Nishimune A, Henley JM (2006) Lateral diffusion drives constitutive exchange of AMPA receptors at dendritic spines and is regulated by spine morphology. *J Neurosci* 26:7046–7055.
18. Kopec C, Malinow R (2006) Neuroscience. Matters of size. *Science* 314:1554–1555.
19. Arendt KL, et al. (2010) PIP3 controls synaptic function by maintaining AMPA receptor clustering at the postsynaptic membrane. *Nat Neurosci* 13:36–44.
20. Pellegrino C, et al. (2011) Knocking down of the KCC2 in rat hippocampal neurons increases intracellular chloride concentration and compromises neuronal survival. *J Physiol* 589:2475–2496.
21. Turrigiano GG, Leslie KR, Desai NS, Rutherford LC, Nelson SB (1998) Activity-dependent scaling of quantal amplitude in neocortical neurons. *Nature* 391:892–896.
22. Delpire E, et al. (2009) Small-molecule screen identifies inhibitors of the neuronal K-Cl cotransporter KCC2. *Proc Natl Acad Sci USA* 106:5383–5388.
23. Shen L, Liang F, Walensky LD, Huganir RL (2000) Regulation of AMPA receptor GluR1 subunit surface expression by a 4. 1N-linked actin cytoskeletal association. *J Neurosci* 20:7932–7940.
24. Rust MB, et al. (2010) Learning, AMPA receptor mobility and synaptic plasticity depend on n-cofilin-mediated actin dynamics. *EMBO J* 29:1889–1902.
25. Greger IH, Esteban JA (2007) AMPA receptor biogenesis and trafficking. *Curr Opin Neurobiol* 17:289–297.
26. Newpher TM, Ehlers MD (2009) Spine microdomains for postsynaptic signaling and plasticity. *Trends Cell Biol* 19:218–227.
27. Bannai H, Lévi S, Schweizer C, Dahan M, Triller A (2006) Imaging the lateral diffusion of membrane molecules with quantum dots. *Nat Protoc* 1:2628–2634.
28. Tardin C, Cognet L, Bats C, Lounis B, Choquet D (2003) Direct imaging of lateral movements of AMPA receptors inside synapses. *EMBO J* 22:4656–4665.
29. Petrini EM, et al. (2009) Endocytic trafficking and recycling maintain a pool of mobile surface AMPA receptors required for synaptic potentiation. *Neuron* 63:92–105.
30. Büttner B, Horstkorte R (2010) Intracelluar ligands of NCAM. *Adv Exp Med Biol* 663: 55–66.
31. Fux CM, Krug M, Dityatev A, Schuster T, Schachner M (2003) NCAM180 and glutamate receptor subtypes in potentiated spine synapses: An immunogold electron microscopic study. *Mol Cell Neurosci* 24:939–950.
32. Yuste R, Bonhoeffer T (2004) Genesis of dendritic spines: Insights from ultrastructural and imaging studies. *Nat Rev Neurosci* 5:24–34.
33. Lauf PK, et al. (1992) Erythrocyte K-Cl cotransport: Properties and regulation. *Am J Physiol* 263(Pt 1):C917–C932.
34. Gamba G (2005) Molecular physiology and pathophysiology of electroneutral cation-chloride cotransporters. *Physiol Rev* 85:423–493.
35. Wake H, et al. (2007) Early changes in KCC2 phosphorylation in response to neuronal stress result in functional downregulation. *J Neurosci* 27:1642–1650.
36. Woodin MA, Ganguly K, Poo MM (2003) Coincident pre- and postsynaptic activity modifies GABAergic synapses by postsynaptic changes in Cl- transporter activity. *Neuron* 39:807–820.
37. Elias GM, et al. (2006) Synapse-specific and developmentally regulated targeting of AMPA receptors by a family of MAGUK scaffolding proteins. *Neuron* 52:307–320.
38. Kim CH, Lisman JE (1999) A role of actin filament in synaptic transmission and long-term potentiation. *J Neurosci* 19:4314–4324.
39. Matsuzaki M, Honkura N, Ellis-Davies GC, Kasai H (2004) Structural basis of long-term potentiation in single dendritic spines. *Nature* 429:761–766.
40. Triller A, Choquet D (2005) Surface trafficking of receptors between synaptic and extrasynaptic membranes: And yet they do move! *Trends Neurosci* 28:133–139.
41. Heine M, et al. (2008) Surface mobility of postsynaptic AMPARs tunes synaptic transmission. *Science* 320:201–205.
42. Hugel S, et al. (2009) Dendritic spine morphology determines membrane-associated protein exchange between dendritic shafts and spine heads. *Cereb Cortex* 19:697–702.
43. Denker SP, Huang DC, Orlowski J, Furthmayr H, Barber DL (2000) Direct binding of the Na–H exchanger NHE1 to ERM proteins regulates the cortical cytoskeleton and cell shape independently of H(+) translocation. *Mol Cell* 6:1425–1436.
44. Jöns T, Drenckhahn D (1992) Identification of the binding interface involved in linkage of cytoskeletal protein 4.1 to the erythrocyte anion exchanger. *EMBO J* 11:2863–2867.
45. Baines AJ, Bennett PM, Carter EW, Terracciano C (2009) Protein 4.1 and the control of ion channels. *Blood Cells Mol Dis* 42:211–215.
46. Lin DT, et al. (2009) Regulation of AMPA receptor extrasynaptic insertion by 4.1N, phosphorylation and palmitoylation. *Nat Neurosci* 12:879–887.
47. Fiumelli H, Cancedda L, Poo MM (2005) Modulation of GABAergic transmission by activity via postsynaptic Ca2+-dependent regulation of KCC2 function. *Neuron* 48:773–786.
48. Lee HH, et al. (2007) Direct protein kinase C-dependent phosphorylation regulates the cell surface stability and activity of the potassium chloride cotransporter KCC2. *J Biol Chem* 282:29777–29784.
49. Klann E, Chen SJ, Sweatt JD (1993) Mechanism of protein kinase C activation during the induction and maintenance of long-term potentiation probed using a selective peptide substrate. *Proc Natl Acad Sci USA* 90:8337–8341.
50. Lu YM, Roder JC, Davidow J, Salter MW (1998) Src activation in the induction of long-term potentiation in CA1 hippocampal neurons. *Science* 279:1363–1367.

Supporting Information

Gauvain et al. 10.1073/pnas.1107893108

SI Materials and Methods

DNA Constructs. shRNA sequences against rat *Slc12a5* mRNA and nontarget shRNA sequences were obtained from SABiosciences (Qiagen). The rat *Slc12a5* shRNA sequence was ACGAGGTCATCGTGAATAAATCTTCCTGTCAATTTATTCACGATGACCTCGT, and the rat nontarget shRNA sequence was CCTGCTTGTTGGCATCTATTTCTTCCTGTCAAAATAGATGCCAACAAGCAGG. Small hairpin sequences were inserted in a pGeneClip hMGFP vector (Promega). The pEGFP-N1 vector used in some experiments was from Clontech. The pEGFP-GluR1 construct was a gift from Jose Esteban (Universidad Autonoma de Madrid, Madrid, Spain). Chicken NCAM180 and NCAM120 constructs were provided by René Marc Mège (Institut National de la Santé et de la Recherche Médicale, Paris, France). Rat KCC2-CTD (amino acids 637–1116) was cloned into the pEGFP-IRES vector between XbaI and EcoRV restriction sites for bicistronic expression of KCC2-CTD and EGFP. The CTD was generated using a PCR assay with appropriate oligonucleotides from rat pEGFP-IRES-KCC2 full-length (GenBank accession no. U55816) construct (a gift from Junichi Nabekura, Kyushu University, Fukuoka, Japan).

Electrophysiological Recordings. Neurons were superfused with a solution containing 125 mM NaCl, 20 mM D-glucose, 10 mM Hepes, 4 mM $MgCl_2$, 2 mM KCl, and 1 mM $CaCl_2$ (pH 7.4) in a recording chamber (BadController V; Luigs & Neumann) maintained at 31 °C and mounted on an upright microscope (BX51WI; Olympus). mEPSCs were recorded in whole-cell mode at −60 or −70 mV (Fig. 3) with an internal solution containing 110 mM $CsMeSO_4$, 20 mM CsCl, 10 mM Hepes, 10 mM EGTA, 4 mM MgATP, and 0.4 mM Na_3GTP (pH = 7.4) in the presence of TTX (1 μM; Latoxan) and bicuculline methochloride (20 μM). Currents were recorded with an Axopatch 200B amplifier (Molecular Devices), filtered at 2 kHz, and digitized at 20 kHz. Access and input resistance were monitored with −5-mV voltage steps. mEPSCs were detected and analyzed offline using Detectivent software (kindly provided by N. Ankri, Institut National de la Santé et de la Recherche Médicale, Marseille, France).

GABA Uncaging. In some experiments (Fig. 4*A*), photolysis of caged GABA was used to elicit GABA currents at somatic or dendritic locations. RuBi-GABA (15 μM; Ascent Scientific) was added to the extracellular solution, together with 2 mM kynurenic acid (Sigma–Aldrich), 3 μM CGP52432 (Tocris Bioscience), and 1 μM TTX. RuBi-GABA was photolyzed using a digital modulated diode laser beam at 405 nm (Omicron Deepstar; Photon Lines) delivered through a single-path photolysis head (Prairie Technologies). The laser beam diameter was set to a diameter of 3–5 μm and was directed onto the soma or distal dendrites of the recorded neuron. Photolysis was induced by a pulse lasting 5 ms at 30 mW (soma) or 10 ms at 60 mW. GABA currents were recorded in whole-cell mode with a potassium gluconate-based intracellular solution containing 18 mM Cl^- and 20 μM Alexa 594. Cells were held at a potential of −60 mV, and 3.5-s voltage steps ranging from −60 to 0 mV were applied to the cell >5 min after break-in. Laser pulses were delivered at 2.2 s after the onset of the voltage step to allow for stabilization of the current. Voltages were corrected for liquid junction potential (−14.0 mV) and voltage drop across the series resistance of the pipette (usually 6–15 mΩ).

Western Blots. HEK293 cells were cultured in DMEM supplemented with 4 mM L-glutamine, 10% (vol/vol) FBS, and penicillin/streptomycin. They were transfected with pEGFP-IRES-KCC2 constructs (either full-length or CTD) or pEGFP alone using Lipofectamine 2000 (Invitrogen) according to the manufacturer's instructions. After 48 h, cells were washed rapidly with cold PBS buffer and then lysed in cold radioimmunoprecipitation assay buffer (Sigma–Aldrich) supplemented with a protease inhibitor mix (cOmplete; Roche Applied Sciences). Lysates were clarified by centrifugation at 20,000 × g for 10 min at 4 °C. Protein concentration was determined using the micro BCA Protein Assay Reagent Kit (Pierce). Cell extracts were denatured in NuPAGE lithium dodecyl sulfate sample buffer (Invitrogen), resolved on NuPAGE BisTris gels (Invitrogen), and then transferred onto a nitrocellulose membrane (Amersham) for 90 min at 400 mA per gel in 25 mM Tris (pH 8.3), 200 mM glycine, and 20% (vol/vol) ethanol. Membranes were blocked in 5% (wt/vol) nonfat milk in PBS and incubated with rabbit anti-KCC2 antibody raised against the most distal part of the CTD of the protein (1/500) overnight. Bound antibodies were detected using IRdye800CW-coupled anti-rabbit secondary antibody (1/10,000; Rockland Immunochemicals). Blots were then visualized and imaged using the Odyssey Imaging System (Li-COR Biosciences). As expected, a double band around 140 kDa was detected for protein extracts from cells transfected with full-length KCC2, whereas a band at about 55–60 kDa was observed for protein extracts from cells transfected with KCC2-CTD. This shows that KCC2-CTD is reliably expressed and stable in mammalian cells.

Confocal Microscopy and Spine Detection. To study the impact of KCC2 extinction on dendritic spines (Fig. 1), GFP-labeled dendritic segments of 72.0 ± 5.0 μm in length were imaged on a Leica SP2 confocal microscope using a 100× 1.40-N.A. objective with an electron zoom with a magnification of 5× and an Ar/Kr laser set at an excitation wavelength of 488 nm. Typically, stacks of 15–30 sections were acquired at a pixel resolution of 512 × 512 with a *z*-step of 0.242 μm. All confocal stacks included ~1 μm above and below the identified dendritic segment. Confocal stacks were analyzed with NeuronStudio (1, 2) (http://www.mssm.edu/cnic) to examine global and local morphometric characteristics of dendrites and spines, such as dendritic spine densities, shape (stubby, mushroom, thin, and filopodes), and head volume. A total of 15–30 dendritic segments were analyzed per condition from three independent cultures. Each segment was visually inspected, and appropriate corrections were made with the NeuronStudio interface.

Immunocytochemistry, Fluorescence Image Acquisition, and Quantitative Analysis. The efficiency of KCC2 shRNA for KCC2 extinction (Fig. 1) was determined by quantifying triple immunostaining for KCC2, GFP, and MAP2. Coverslips were processed for immunocytochemistry with rabbit polyclonal antibody raised against residues 932–1,043 of rat KCC2 (Sigma–Aldrich), mouse monoclonal antibody against MAP2 (Millipore), and chicken polyclonal antibody against GFP (Millipore). MAP2 and KCC2 immunostaining was then compared quantitatively. Neuronal GluR1 was quantified by immunostaining with rabbit-anti GluR1 and chicken anti-GFP antibodies (both from Millipore).

Neurons were then imaged using an objective with a magnification of 40× (1.40 N.A. for KCC2 immunofluorescence) or 100× (1.40 N.A. for GluR1 immunofluorescence) on a Leica DM6000 upright microscope with a 12-bit cooled CCD camera

(Micromax; Roper Scientific) run with MetaMorph software (Molecular Devices). Sets of neurons compared for quantification were stained simultaneously. Image exposure time was determined on bright cells transfected with nontarget shRNA to avoid pixel saturation. All images from a given culture were then acquired with the same exposure time. For each image, a region of interest was chosen based on the GFP image from one to two dendrites of moderate diameter. KCC2 and MAP2 images were background-subtracted, and the fluorescence intensity per pixel was measured in the regions of interest on KCC2 and MAP2 images using ImageJ (National Institutes of Health). GluR1 cluster intensity was quantified from GluR1 and cytoplasmic GFP costaining experiments using MetaMorph. For each image, several regions of interest were chosen from one or two dendrites of moderate diameter. For quantification, GluR1 clusters were selected; their coalescence was avoided by means of a user-defined intensity threshold, and mean fluorescence intensity per cluster was measured in the regions of interest. Normalization was performed for each culture by dividing fluorescence intensity from each cell by the mean fluorescence intensity of all cells of the control group.

Single-Molecule Imaging and Analysis. For single particle tracking (SPT) of GluR1, neurons cotransfected with GFP-GluR1 and either nontarget shRNA or shRNA against KCC2 were incubated for 5 min at 37 °C with a rabbit antibody against GFP (20–40 ng/mL; Roche Applied Sciences). For SPT of chicken NCAM, neurons expressing chicken NCAM with either nontarget shRNA or shRNA against KCC2 were incubated for 5 min at 37 °C with a rabbit antibody against chicken NCAM (a gift from R. M. Mège, INSERM, Paris, France). Cells were then washed and incubated for 5 min at 37 °C with a biotinylated Fab antibody (goat anti-rabbit, 0.5 μg/mL; Jackson ImmunoResearch). Coverslips were then washed and incubated for 1 min at 37 °C with streptavidin-coated, ZnS-encapsulated, CdSe Qdot nanocrystals (605-nm emission, 0.5 nM; Invitrogen) in borate buffer (50 mM) supplemented with sucrose (200 mM). Coverslips were transferred to a temperature-controlled open chamber (Luigs & Neumann) mounted on an inverted microscope (IX71; Olympus) equipped with an objective with a magnification of 60× (N.A. = 1.42). GFP and QDs were detected using an X-Cite 120PC lamp (EXFO) with appropriate filters (excitation: HQ470/40 and D455/70, dichroic: Q495LP and 500DCXR, and emission: HQ525/50 and HQ605/20; GFP and rhodamin filters from Chroma Technology and QD filters from Omega Optical). Real-time movies of 800 images were acquired at 33 Hz with an EM-CCD camera (Imagem; Hamamatsu Photonics) using MetaVue software (Molecular Devices). Cells were imaged within 30 min following primary antibody incubation. For each SPT experiment, QD dynamics were measured from two to three independent cultures.

Single molecules were tracked with custom software (3) using Matlab (MathWorks). The center of fluorescent spots was determined by Gaussian fitting with a spatial resolution of ~10 nm. Single QDs were identified by their blinking property (4). For each QD, we calculated the mean square displacement (MSD), diffusion coefficient, confinement area, transition between compartments and dwell time within a compartment. MSD vs. time plots (5) were constructed for each trajectory according to the formula:

$$MSD(n\tau) = \frac{1}{N-n}\sum_{i=1}^{N-n}\Big[(x((i+n)\tau) - x(i\tau))^2 + (y((i+n)\tau) - y(i\tau))^2\Big]$$

where τ is the frame acquisition time, N is the total number of frames, $x(t)$ and $y(t)$ represent the position coordinates of a QD at time t, and n and i are positive integers with n determining the time increment. For simple 2D Brownian mobility, the MSD, as a function of time, is linear with a slope of $4D$, where D is the diffusion constant. If the MSD as a function of time tends to a constant value, the diffusion is confined in a domain of size L. The diffusion coefficient is determined by a fit on the first four points of the MSD as a function of time with MSD $(n\tau) = 4Dn\tau +$ b, where b is a constant reflecting the spot localization accuracy. The area in which diffusion is confined can be estimated by fitting the MSD as a function of time with the following formula:

$$MSD(n\tau) = \frac{L^2}{3}\left(1 - \exp\left(-\frac{12Dn\tau}{L^2}\right)\right) + 4\mathrm{Dmac}\, n\tau$$

where L^2 is the confined area in which diffusion is restricted and Dmac is the diffusion coefficient on a long time scale (6). In some experiments, spine and shaft trajectories were separately analyzed. Spine and shaft membrane was distinguished by performing a manual threshold on cytoplasmic GFP fluorescence and overlaying outlined regions onto QD image sequences (Fig. 5*A*). This permitted identification of spine vs. shaft portions of QD trajectories (e.g., Fig. 5 B and C) and estimates of spine size (Fig. S2).

Data are presented as mean ± SEM. Means were compared using the nonparametric, Mann–Whitney rank sum test unless otherwise stated. Correlations were statistically assessed using the Spearman rank order correlation test. Both tests were performed using SigmaStat software (SPSS). Cumulative distributions were compared using the Kolmogorov–Smirnov test under StatView (SAS). Differences were considered significant for P values above 5%.

1. Rodriguez A, Ehlenberger DB, Dickstein DL, Hof PR, Wearne SL (2008) Automated three-dimensional detection and shape classification of dendritic spines from fluorescence microscopy images. *PLoS One* 3:e1997.
2. Wearne SL, et al. (2005) New techniques for imaging, digitization and analysis of three-dimensional neural morphology on multiple scales. *Neuroscience* 136:661–680.
3. Bonneau S, Dahan M, Cohen LD (2005) Single quantum dot tracking based on perceptual grouping using minimal paths in a spatiotemporal volume. *IEEE Trans Image Process* 14:1384–1395.
4. Alivisatos AP, Gu W, Larabell C (2005) Quantum dots as cellular probes. *Annu Rev Biomed Eng* 7:55–76.
5. Saxton MJ, Jacobson K (1997) Single-particle tracking: Applications to membrane dynamics. *Annu Rev Biophys Biomol Struct* 26:373–399.
6. Kusumi A, Sako Y, Yamamoto M (1993) Confined lateral diffusion of membrane receptors as studied by single particle tracking (nanovid microscopy). Effects of calcium-induced differentiation in cultured epithelial cells. *Biophys J* 65:2021–2040.

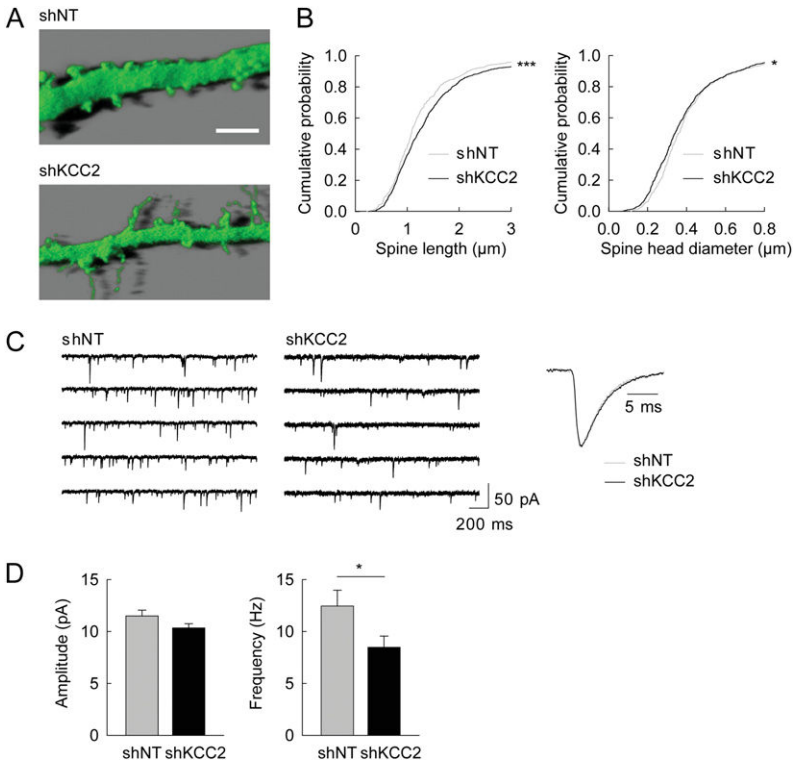

Fig. S1. KCC2 suppression in immature hippocampal neurons prevents spine maturation. Neurons were transfected with nontarget or KCC2-specific shRNA constructs at 4 DIV and imaged at 14 DIV. shKCC2, shRNA against KCC2; shNT, nontarget shRNA. (*A*) 3D reconstructions of tertiary dendritic sections from neurons expressing either shNT or shKCC2 from confocal images of GFP immunostaining. Note the presence of long and sometimes bifurcated protrusions on dendrites from neurons expressing shKCC2. (Scale bar: 5 μm.) (*B*) Cumulative histograms of spine length and head diameter distributions from neurons expressing either shNT or shKCC2. Suppressing KCC2 induced a significant increase in spine length (***$P < 0.005$) and a small but significant reduction in spine head diameter (*$P < 0.05$; Table S1). Data were obtained from 467 (shNT) and 554 (shKCC2) spines, from 28 and 26 neurons, respectively, in three independent experiments. (*C*) Ten-second continuous recordings of mEPSCs from neurons expressing either shNT or shKCC2 shRNA. (*Inset*) One hundred fifty mEPSCs were superimposed and normalized to their peak amplitude to compare their onset and decay kinetics. (*D*) Summary graphs of mean mEPSC amplitude and frequency in neurons expressing either shNT ($n = 10$ cells) or shKCC2 ($n = 10$ cells). Suppressing KCC2 expression reduced mEPSC frequency by about 32% ($P < 0.05$) without significantly affecting mEPSC amplitude (*$P = 0.1$).

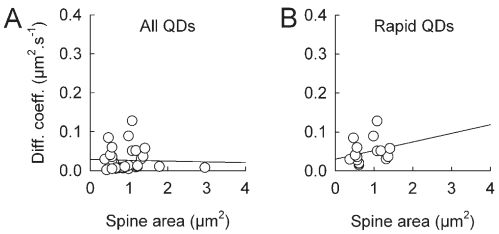

Fig. S2. GluR1 lateral diffusion is independent of spine size. Hippocampal neurons were transfected at 14 DIV with nontarget shRNA and GFP-tagged recombinant GluR1 and processed for SPT at 21 DIV. (*A*) Plotting diffusion coefficients of all QD-bound recombinant GluR1 in dendritic spines against spine area shows no significant correlation between spine size and GluR1 diffusion ($r = 0.07$; Spearman rank order correlation test, $P = 0.7$; $n = 35$). Diff. coeff., diffusion coefficient. (*B*) Same relation plotted only for rapid ($D > 0.015$ $\mu m^2 \cdot s^{-1}$) QD-bound GluR1 in dendritic spines. Again, GluR1 diffusion was not significantly correlated with spine area ($r = 0.18$, $P = 0.5$; $n = 16$).

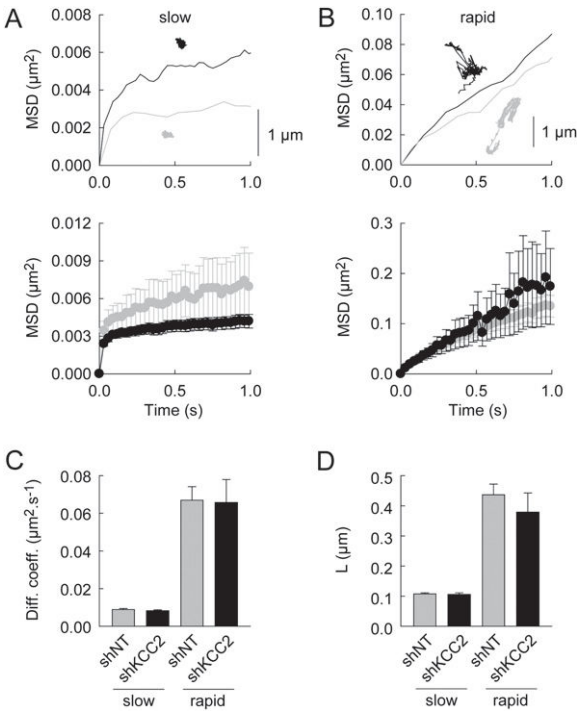

Fig. S3. KCC2 suppression does not affect the lateral diffusion of GluR1 on dendritic shafts. (*A* and *B*) (*Upper*) Time-averaged MSD functions for slow (*A*; $D \leq 1.5 \times 10^{-2} \cdot \mu m^2 \cdot s^{-1}$) and rapid (*B*; $D > 0.015 \cdot \mu m^2 \cdot s^{-1}$) QD-labeled GluR1 located on dendritic shafts. Diffusion was compared in neurons expressing nontarget shRNA (shNT, gray) or shRNA against KCC2 (shKCC2, black). (*A* and *B*, *Insets*) Reconstructed trajectories of corresponding slow (shNT, 583 frames; shKCC2, 591 frames) and rapid (shNT, 553 frames; shKCC2, 330 frames) QDs. (Scale bar: 1 μm.) (*Lower*) Mean MSD functions from 47 (shNT, slow), 30 (shKCC2, slow), 90 (shNT, rapid), and 37 (shKCC2, rapid) shaft trajectories. Diffusion coefficients (Diff. coeff.; *C*) and confinement domains (*L*; *D*) for slow (*Left*) and rapid (*Right*) QD-labeled GluR1 in neurons expressing shNT (gray) or shKCC2 (black). KCC2 suppression had no significant effect on lateral diffusion of GluR1 in dendritic shafts ($P > 0.4$).

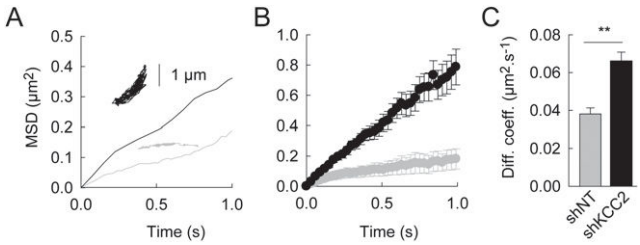

Fig. S4. KCC2 suppression enhances lateral diffusion of endogenous NCAM in dendritic spines. Hippocampal neurons were transfected at 14 DIV with either KCC2-specific shRNA (shKCC2) or nontarget shRNA (shNT) and processed for SPT at 21 DIV with an anti-NCAM antibody. (*A*) Time-averaged MSD functions for QD-labeled NCAM in dendritic spines of neurons expressing shNT (gray) or shKCC2 (black) constructs. (*Insets*) Reconstructed trajectories of corresponding QDs (shNT, 221 frames; shKCC2, 352 frames). (Scale bar: 1 μm.) (*B*) Mean MSD functions from 11 (shNT) and 21 (shKCC2) spine trajectories. (*C*) Diffusion coefficients (Diff. coeff.) of QD-bound NCAM show increased diffusion (**$P < 0.01$) in neurons expressing shKCC2 (black) compared with shNT (gray).

Table S1. Anatomical characteristics of dendritic spines in hippocampal neurons on suppression of KCC2 expression or function

Experimental condition	Density, per 10 μm	Length, μm	Head diameter, μm	Spine subtype proportions				No. spines/ experiments
				Filopode	Thin	Stubby	Mushroom	
Mature neurons (14 + 10 DIV)								
shNT	5.9 ± 0.7	1.26 ± 0.03	0.47 ± 0.01	0.09 ± 0.01	0.37 ± 0.02	0.26 ± 0.03	0.27 ± 0.03	647/3
shKCC2	7.2 ± 0.6	1.27 ± 0.02	0.61 ± 0.01	0.08 ± 0.01	0.26 ± 0.02	0.24 ± 0.02	0.42 ± 0.01	811/3
P value	0.1	0.2	<0.001	0.6	<0.005	0.4	<0.001	
DMSO	10.5 ± 1.6	1.56 ± 0.03	0.49 ± 0.01	n.d.	n.d.	n.d.	n.d.	794/3
VU0240551	12.8 ± 0.12	1.43 ± 0.02	0.55 ± 0.01	n.d.	n.d.	n.d.	n.d.	1615/3
P value	0.2	<0.005	<0.001					
GFP	11.0 ± 1.1	1.40 ± 0.02	0.55 ± 0.01	n.d.	n.d.	n.d.	n.d.	741/3
KCC2-CTD	9.3 ± 1.0	1.47 ± 0.02	0.55 ± 0.01	n.d.	n.d.	n.d.	n.d.	925/3
P value	0.3	0.3	0.7					
Immature neurons (4 + 10 DIV)								
shNT	3.0 ± 0.3	1.32 ± 0.05	0.41 ± 0.01	0.26 ± 0.03	0.36 ± 0.03	0.22 ± 0.03	0.16 ± 0.02	367/3
shKCC2	3.1 ± 0.3	1.48 ± 0.04	0.39 ± 0.01	0.39 ± 0.03	0.32 ± 0.03	0.17 ± 0.02	0.12 ± 0.02	881/3
P value	0.9	<0.005	<0.05	<0.05	0.4	0.2	0.2	

Mean values of spine density, length, head diameter, and proportions of spine subtypes were obtained in four experimental paradigms. The number of spines that were analyzed and the number of independent experiments are shown for each experimental condition. Mature and immature neurons were transfected at 14 and 4 DIV, respectively, and processed 10 d later. In DMSO vs. VU0240551 experiments, neurons were transfected with GFP at 14 DIV and treated with drugs for >72 h. *P* values are provided for Mann–Whitney rank sum tests to compare mean values obtained in control vs. test conditions. n.d., not determined.

II. Activity-dependent regulation of the K/Cl transporter KCC2 membrane diffusion, clustering, and function in hippocampal neurons

KCC2 membrane expression is tightly regulated by neuronal activity and its suppression might lead to decreased inhibitory transmission efficacy. Nevertheless, KCC2 is also highly enriched at the vicinity of glutamatergic synapses and KCC2 function has been shown to be modulated by NMDAR activation. Several KCC2 residues can be phosphorylated and influence KCC2 membrane trafficking at different levels. In this study, we aimed at investigating the membrane expression and lateral diffusion of KCC2 in basal conditions or upon increased neuronal activity. Using electrophysiological recordings of E_{GABA}, I correlated the modifications in KCC2 membrane expression and lateral diffusion with KCC2-dependent neuronal chloride extrusion capacity. Overall, our results showed that:

- KCC2 is slowed down in the vicinity of both excitatory and inhibitory synapses;
- The interactions between KCC2 and its intracellular partners, the actin- and KCC2-interacting protein 4.1N and the actin cytoskeleton participate to confine KCC2 near excitatory, but not inhibitory synapses;
- Increased neuronal activity leads to an NMDA-dependent dephosphorylation of Ser940 KCC2 residue and subsequent calpain-dependent cleavage internalization of KCC2;
- Hindrance of Ser940 dephosphorylation or calpain activity rescues both the function and diffusion of KCC2 upon increased neuronal activity.

In conclusion, we proposed that lateral diffusion might be a molecular mechanism to rapidly regulate KCC2 membrane expression and function.

Cellular/Molecular

Activity-Dependent Regulation of the K/Cl Transporter KCC2 Membrane Diffusion, Clustering, and Function in Hippocampal Neurons

Ingrid Chamma,[1,2,3] Martin Heubl,[1,2,3] Quentin Chevy,[1,2,3] Marianne Renner,[4] Imane Moutkine,[1,2,3] Emmanuel Eugène,[1,2,3] Jean Christophe Poncer,[1,2,3] and Sabine Lévi[1,2,3]

[1]Institut National de la Santé et de la Recherche Médicale (INSERM), Unité Mixte de Recherche en Santé 839, F-75005 Paris, France, [2]Université Pierre et Marie Curie, F-75005 Paris, France, [3]Institut du Fer a Moulin, F-75005 Paris, France, and [4]Institut de Biologie de l'Ecole Normale Supérieure, INSERM, Unité 1024, Centre National de la Recherche Scientifique, Unité Mixte de Recherche 8197, F-75005 Paris, France

The neuronal K/Cl transporter KCC2 exports chloride ions and thereby influences the efficacy and polarity of GABA signaling in the brain. KCC2 is also critical for dendritic spine morphogenesis and the maintenance of glutamatergic transmission in cortical neurons. Because KCC2 plays a pivotal role in the function of central synapses, it is of particular importance to understand the cellular and molecular mechanisms underlying its regulation. Here, we studied the impact of membrane diffusion and clustering on KCC2 function. KCC2 forms clusters in the vicinity of both excitatory and inhibitory synapses. Using quantum-dot-based single-particle tracking on rat primary hippocampal neurons, we show that KCC2 is slowed down and confined at excitatory and inhibitory synapses compared with extrasynaptic regions. However, KCC2 escapes inhibitory synapses faster than excitatory synapses, reflecting stronger molecular constraints at the latter. Interfering with KCC2–actin interactions or inhibiting F-actin polymerization releases diffusion constraints on KCC2 at excitatory but not inhibitory synapses. Thus, F-actin constrains KCC2 diffusion at excitatory synapses, whereas KCC2 is confined at inhibitory synapses by a distinct mechanism. Finally, increased neuronal activity rapidly increases the diffusion coefficient and decreases the dwell time of KCC2 at excitatory synapses. This effect involves NMDAR activation, Ca^{2+} influx, KCC2 S940 dephosphorylation and calpain protease cleavage of KCC2 and is accompanied by reduced KCC2 clustering and ion transport function. Thus, activity-dependent regulation of KCC2 lateral diffusion and clustering allows for a rapid regulation of chloride homeostasis in neurons.

Introduction

Fast synaptic transmission mediated by GABA type A and glycine receptors relies primarily on chloride (Cl^-) ion fluxes through ligand-gated ion channels. Thus, the maintenance of intraneuronal chloride homeostasis is crucial to preserve inhibitory synaptic efficacy. Synaptic responses mediated by $GABA_A$ and glycine receptors are principally depolarizing in immature neurons and hyperpolarizing at mature stages. The progressive hyperpolarization of the reversal potential of glycine and GABA-activated currents relies on the developmental upregulation of the neuronal K^+/Cl^- cotransporter KCC2, which extrudes intracellular chloride under resting conditions in many species (Rivera et al., 1999; Vanhatalo et al., 2005) and brain regions (Li et al., 2002; Vinay and Jean-Xavier, 2008). Although KCC2 primarily influences GABAergic transmission in cortical neurons, its aggregation in dendritic spines at excitatory synapses (Gulyás et al., 2001; Gauvain et al., 2011; Chamma et al., 2012) suggests a possible interaction with glutamate signaling. Recent studies indicate that KCC2 is critical for dendritic spine formation (Li et al., 2007; Fiumelli et al., 2013) and the function of excitatory synapses (Gauvain et al., 2011). This regulation is independent from KCC2 transport function but instead involves its interaction with the submembrane actin cytoskeleton, most probably via the adaptor protein 4.1N (Li et al., 2007; Gauvain et al., 2011). Given the pivotal role of KCC2 in both glycine/GABAergic and glutamatergic synaptic transmission, it is of critical importance to understand the cellular and molecular mechanisms underlying its regulation.

KCC2 expression and transport function are downregulated by neuronal activity under both physiological (Kaila et al., 1997; Woodin et al., 2003; Fiumelli et al., 2005; Wang et al., 2006a,b; Kitamura et al., 2008; Lee et al., 2011) and pathological conditions, such as excitotoxicity or seizures (Reid et al., 2001; Rivera et al., 2002, 2004; Huberfeld et al., 2007; Pathak et al., 2007; Wake et

Received Dec. 27, 2012; revised Aug. 20, 2013; accepted Aug. 20, 2013.

Author contributions: J.C.P. and S.L. designed research; I.C., M.H., Q.C., E.E., and I.M. performed research; M.R. contributed unpublished reagents/analytic tools; I.C., M.H., Q.C., and E.E. analyzed data; I.C., J.C.P., and S.L. wrote the paper.

This work was supported by Institut National de la Santé et de la Recherche Médicale (Avenir program to J.C.P.), the Fondation pour la Recherche Médicale (J.C.P. and S.L.), the city of Paris (program grant to J.C.P.), and the Fondation pour la Recherche sur le Cerveau (S.L.). I.C., M.H., and Q.C. were recipients of doctoral fellowships from the Université Pierre et Marie Curie. We thank J. Nabekura for kindly providing the original pEGFP–IRES–KCC2 full-length construct, D. Choquet for the homer1c–GFP construct, A. Triller for the gephyrin–mRFP construct, P. Bregestovski for the chloride sensor CFP–YFP construct, and R. M. Mège for the chicken NCAM-120 construct and primary antibody.

The authors declare no competing financial interests.

Correspondence should be addressed to Sabine Lévi, Institut National de la Santé et de la Recherche Médicale, Université Pierre et Marie Curie, Unité Mixte de Recherche en Santé 839, 17 rue du Fer a Moulin, F-75005 Paris, France. E-mail: sabine.levi@inserm.fr.

DOI:10.1523/JNEUROSCI.5889-12.2013

 0270-6474/13/3315488-16$15.00/0

al., 2007; Li et al., 2008; Shimizu-Okabe et al., 2011). These conditions are associated with a depolarizing shift in the reversal potential of GABA responses (E_{GABA}) that may enhance the gain of recently active excitatory synapses in physiological conditions or contribute to alter the excitation/inhibition balance under pathological conditions. A loss of KCC2 expression and subsequent intracellular chloride accumulation has been associated with interictal activities in the hippocampus of human patients suffering mesial temporal lobe epilepsy (Huberfeld et al., 2007). However, in some neurons, KCC2 expression does not correlate with E_{GABA}, suggesting that KCC2 transport function might be altered independently of its expression level (Huberfeld et al., 2007). Altered KCC2 oligomerization and clustering in hippocampal neurons leads to loss of KCC2 activity with no change in membrane expression (Watanabe et al., 2009), suggesting that rapid regulation of KCC2 at the plasma membrane may be at play to affect KCC2 function.

Here, we studied the membrane dynamics and clustering of KCC2 in hippocampal neurons and examined how these processes are modulated by normal and pathological excitatory activities. Our results suggest activity-dependent modulation of the membrane diffusion of KCC2 participates in rapid, activity-dependent regulation of chloride homeostasis in neurons.

Materials and Methods

DNA constructs. The KCC2–Flag construct was generated by insertion of three Flag sequences (DYKDHDGDYKDHHIDYKDDDD) between the unique NsiI and NheI restriction sites in the second predicted extracellular loop of KCC2. An NsiI–NheI DNA fragment containing three Flag sequences was inserted in the proper reading frame between NsiI and NheI sites engineered by site-directed mutagenesis at position 631 of the rat pEGFP–IRES–KCC2 full-length (GenBank accession number U55816) construct (gift from Junichi Nabekura, Kyushu University, Fukuoka, Japan). The EGFP–IRES sequence was deleted from the construct for multiple transfection experiments with gephyrin–mRFP and homer1c–GFP chimera. Rat KCC2–C-terminal domain (CTD; amino acids 637–1116) was cloned into the pEGFP–IRES vector between XbaI and EcoRV restriction sites for bicistronic expression of KCC2–CTD and EGFP. The CTD was generated using PCR with appropriate oligonucleotides from rat pEGFP–IRES–KCC2 construct as described previously (Gauvain et al., 2011). KCC2–Flag constructs with S940 residue mutated in aspartate (S940D) or alanine (S940A) were generated with Clontech In-Fusion HD Cloning kit (Ozyme). Chicken NCAM-120 construct was provided by René Marc Mège [Institut National de la Santé et de la Recherche Médicale (INSERM), Paris, France]. To generate shRNA targeting rat 4.1N, a previously described small hairpin oligonucleotide sequence shown to reduce 4.1N expression by >80% (Lin et al., 2009) was inserted in a pGeneClip hMGFP vector (Promega). Rat nontarget and KCC2-specific shRNA sequences were obtained from SABiosciences (Qiagen) as described previously (Gauvain et al., 2011). All constructs were sequenced by Beckman Coulter Genomics.

Neuronal culture. Primary cultures of hippocampal neurons were prepared as described previously (Goslin et al., 1998) with some modifications of the protocol. Briefly, hippocampi were dissected from embryonic day 18 or 19 Sprague Dawley rats of either sex. Tissue was then trypsinized (0.25% v/v) and mechanically dissociated in 1× HBSS (Invitrogen) containing 10 mM HEPES (Invitrogen). Neurons were plated at a density of 2.3×10^4 cells/cm^2 onto 18-mm-diameter glass coverslips (Assistent) precoated with 80 μg/ml poly-D,L-ornithine (Sigma-Aldrich) in plating medium composed of MEM (Sigma) supplemented with horse serum (10% v/v; Invitrogen), L-glutamine (2 mM), and Na^+ pyruvate (1 mM) (Invitrogen). After attachment for 2–3 h, cells were incubated in maintenance medium that consists of Neurobasal medium supplemented with B27 (1×), L-glutamine (2 mM), and antibiotics (Invitrogen) for up to 3 weeks at 37°C in a 5% CO_2 humidified incubator. Each week, one-fifth of the culture medium volume was renewed.

Transfection. Neuronal transfections with KCC2–IRES–GFP, KCC2–Flag, KCC2–CTD (Gauvain et al., 2011), KCC2–Flag–S940D, KCC2–Flag–S940A, the shRNA sequence against rat 4.1N mRNA (4.1N shRNA) and nontarget shRNA sequence (NT shRNA), the shRNA sequence against rat KCC2 mRNA and nontarget shRNA sequence (Gauvain et al., 2011), chicken NCAM-120, gephyrin–mRFP (Hanus et al., 2006; gift from A. Triller, École Normale Supérieure, INSERM, Paris, France), and homer1c–GFP (Bats et al., 2007; gift from D. Choquet, Centre National de la Recherche Scientifique, Bordeaux, France) were done at 13–14 d *in vitro* (DIV) using Lipofectamine 2000 (Invitrogen) or Transfectin (Bio-Rad), according to the instructions of the manufacturers (DNA/lipofectant ratio of 1:3 μg/μl), with 1 μg of plasmid DNA per 20 mm well. The following ratios of plasmid DNA were used in cotransfection experiments: 0.5:0.25:0.25 μg for KCC2–Flag/KCC2–Flag–S940D/KCC2–Flag–S940A/NCAM-120:homer1c–GFP:gephyrin–mRFP; 0.75:0.25 μg for KCC2–Flag/eGFP:eGFP; 0.75:0.25 μg for KCC2–Flag:KCC2–CTD:eGFP; and 0.3:0.3:0.2:0.2 μg for 4.1N shRNA/NT shRNA:KCC2–Flag:homer1c–GFP:gephyrin–mRFP. Experiments were performed 7–10 d after transfection.

To test whether insertion of the Flag tag may compromise KCC2 function, COS cells were transfected with the cyan–yellow fluorescent protein (CFP-YFP) chloride sensor (Markova et al., 2008; gift from P. Bregestovski, INSERM, Marseille, France) using nanofectin (PAA Laboratories) according to the instructions of the manufacturer (DNA/nanofectin ratio of 1:2 μg/μl), with 10 μg of plasmid DNA per 100 mm well. The chloride sensor was transfected either alone (for calibration) or in combination with recombinant KCC2–Flag or KCC2–WT with a ratio of 0.5:0.5 μg.

Chloride sensor calibration and imaging. To calibrate the CFP–YFP chloride sensor in COS cells, extracellular and intracellular chloride were equilibrated using the K^+/H^+ ionophore nigericin and the Cl/OH antiporter tributyltin (Krapf et al., 1988; Trapp et al., 1996; Marandi et al., 2002; Metzger et al., 2002) as described previously (Markova et al., 2008; Waseem et al., 2010). Cells were superfused with a solution containing nigericin (10 μM; Sigma), tributyltin chloride (10 μM; Sigma) and the following (in mM): 2 $CaCl_2$, 2 K-gluconate, 3 $MgCl_2$, 10 HEPES, 20 glucose, and 0–140 NaCl/Na-gluconate, pH 7.4. Cells were imaged at 31°C in a temperature-controlled open chamber (BadController V; Luigs & Neumann) mounted onto an Olympus IX71 inverted microscope equipped with a 60× objective [1.42 numerical aperture (NA); Olympus]. CFP and YFP were detected using Lambda DG-4 monochromator (Sutter Instruments) coupled to the microscope through an optic fiber with appropriate filters (excitation, D436/10× and HQ485/15×; dichroic, 505DCXR; emission, HQ510lp; CFP and YFP filters from Chroma Technology). Images were acquired with an ImagEM EMCCD camera (Hamamatsu Photonics) and MetaFluor software (Roper Scientific). Images were obtained with an integration time of 10 ms and a frequency of 0.07 Hz. The mean fluorescence intensity of each region of interest was measured on the last 10 images of the acquisition session. Mean background fluorescence (measured from a nonfluorescent area) was subtracted and the ratio F_{440}/F_{480} was determined.

Peptide treatment and pharmacology. The following peptides and drugs were used: myristoylated dynamin inhibitory peptide (50 μM; Tocris Bioscience), TTX (1 μM; Latoxan), NBQX (10 μM; Ascent Scientific), NMDA (50 μM; Ascent Scientific), D,L-AP-5 (100 μM; Ascent Scientific), 4-aminopyridine (4-AP; 100 μM; Sigma), [(RS)-α-Methyl-4-carboxyphenylglycine] (*R*,*S*-MCPG) (500 μM; Ascent Scientific), EGTA (1.8 mM; Sigma), and PD150606 [(Z)-3-(4-Iodophenyl)-2-mercapto-2-propenoic acid] (30 μM; Tocris Bioscience). EGTA was prepared in NaOH (18 mM), TTX in 2% citric acid (v/v), PD150606 in DMSO (0.03% v/v; Sigma), NBQX, D,L-AP-5, and *R*,*S*-MCPG in equimolar concentrations of NaOH, and NMDA, dynamin inhibitory peptide, and 4-AP in H_2O. Actin filaments were depolymerized with latrunculin A (5 μM; Sigma) dissolved in DMSO (0.1% v/v). For single-particle tracking (SPT) experiments, neurons were preincubated in the presence of appropriate drugs at 31°C for 10 min in imaging medium (see below for composition) after quantum dot (QD) labeling. They were then used within 40 min. For cluster imaging and electrophysiology, drugs were added directly to the culture medium for the indicated duration in a CO_2 incubator

set at 37°C. Cells were then transferred to a recording chamber in imaging medium and used within 30 min. To test the reversibility of 4-AP, cells were treated for 10 min with 4-AP, washed, and incubated for 10 or 30 min in imaging medium in the absence of drugs before Flag immunostaining. The imaging medium consisted of phenol red-free MEM supplemented with glucose (33 mM; Sigma) and HEPES (20 mM), glutamine (2 mM), Na-pyruvate (1 mM), and B27 (1×) from Invitrogen.

Immunocytochemistry. The total (membrane plus intracellular) pools of KCC2–Flag (Fig. 1*B*,*C*) or endogenous KCC2 (Fig. 1*D*) were revealed with immunocytochemistry in fixed and permeabilized cells, whereas the membrane pool of KCC2–Flag (all other experiments) was assessed with live cell staining. Cells were fixed for 15 min at room temperature (RT) in paraformaldehyde (PFA; 4% w/v; Sigma) and sucrose (20% w/v; Sigma) solution in 1× PBS. Cells were then washed in PBS and incubated for 30 min at RT in bovine serum albumin (BSA; 3% w/v; Sigma) and goat serum (GS; 20% v/v; Invitrogen) in PBS to block nonspecific staining. Neurons were then incubated for 1 h with mouse primary antibody against Flag (1:400; Sigma) or rabbit antibody against KCC2 (1:400; Sigma) in PBS supplemented with GS (3% v/v). After washes, cells were incubated for 45 min at RT with Cy3- or Cy5- conjugated goat anti-mouse antibody (1.9 μg/ml; Jackson ImmunoResearch) or Cy3-conjugated goat anti-rabbit antibody (1.9 μg/ml; Jackson ImmunoResearch) in PBS–BSA–GS blocking solution, washed, and mounted on slides with mowiol 4-88 (48 mg/ml; Sigma). For live cell staining, neurons were washed in imaging medium and incubated for 20 min at 4°C with mouse primary antibody against Flag (1:400–1:500; Sigma) in imaging medium in the absence or presence of the appropriate drugs. After washes with imaging medium, cells were fixed for 15 min with PFA and processed for immunodetection of Flag as above. Sets of neurons compared for quantification were labeled and imaged simultaneously.

Fluorescence image acquisition and analyses. Images of Figure 1 were scanned on a Leica SP5 confocal microscope using the LAS-AF program (Leica). Images were acquired using either a 40×/1.25 NA objective (stacks of 16–35 images acquired with an interval of 0.4 μm, voxel size of 273 nm, and optical zoom of 1.4) or a 100×/1.44 NA objective (stacks of 26–48 images acquired with an interval of 0.1 μm, voxel size of 38 nm, and optical zoom of 4). The other images of this study were acquired using a 63× objective (1.3 NA) on a Leica DM6000 upright epifluorescence microscope with a 12-bit cooled CCD camera (Micromax; Roper Scientific) run by MetaMorph software (Roper Scientific). Exposure time was determined on bright control cells to avoid pixel saturation. All images from a given culture were then acquired with the same exposure time and acquisition parameters. Quantifications were performed on images acquired with standard light microscopy using MetaMorph software (Roper Scientific). For each image, a region of interest was chosen. For KCC2–Flag cluster analyses, images were first flatten background filtered (kernel size, $3 \times 3 \times 2$) to enhance cluster outlines, and a user-defined intensity threshold was applied to select clusters and avoid their coalescence. Thresholded KCC2 cluster images were binarized, and binarized regions were outlined and transferred onto raw data to determine the mean KCC2–Flag cluster number, area, fluorescence intensity, and the mean fluorescence intensity per pixel within clusters. The dendritic surface area of the region of interest was measured to determine the number of clusters per 10 μm^2. For quantifications of KCC2–Flag clusters at excitatory or inhibitory synapses, only KCC2 clusters comprising at least three pixels and apposed on at least one pixel with homer1c–GFP or gephyrin–mRFP clusters were considered. For quantifications of the proportion of KCC2–Flag clusters at synapses versus extrasynaptic sites (Fig. 1*F*), binarized regions of excitatory or inhibitory synapses were merged to identify both types of synapses. Excitatory and inhibitory synapses are not equally distributed along dendrites, with excitatory synapses accounting for the vast majority of the total synaptic population. To take this bias into account, the relative abundance of KCC2 at each synapse subtype (Fig. 1*G*) was calculated by plotting the ratio of the total surface of synaptic KCC2 clusters at a given type of synapses (excitatory or inhibitory) over the total surface area occupied by either type of synapses.

Electrophysiology. Neurons were superfused with a solution containing (in mM) 125 NaCl, 20 D-glucose, 10 HEPES, 4 $MgCl_2$, 2 KCl, and 1 $CaCl_2$, pH 7.4, in a recording chamber (BadController V; Luigs & Neumann) maintained at 31°C on an upright microscope (BX51WI; Olympus). Neurons were whole-cell patch clamped with a borosilicate glass pipette containing (in mM) 104 K-gluconate, 25.4 KCl, 10 HEPES, 10 EGTA, 2 MgATP, 0.4 Na_3GTP, and 1.8 $MgCl_2$, pH 7.4, and maintained at a holding potential of −60 mV. Photolysis of caged GABA was used to elicit GABA currents at somatic or dendritic locations. Rubi-GABA (15 μM; Ascent Scientific) was added to the extracellular solution, with 2 mM kynurenate (Sigma), 3 μM CGP52432 (3-[[(3,4-dichlorophenyl)-methyl] amino]propyl](diethoxymethyl)phosphinic acid) (Tocris Bioscience), and 1 μM TTX. Rubi-GABA was photolyzed using a digitally modulated, diode laser beam set at 405 nm (Omicron Deepstar; Photon Lines) delivered through a single-path photolysis head (Prairie Technologies). The diameter of the laser beam was set to 3–5 μm and directed to the soma or distal dendrites of the recorded neurons. Photolysis was induced by a 5 ms pulse at 5–10 mW on the soma or 10 ms at 30–40 mW on distal dendrites (100 μm from the soma). Voltage steps of 10 mV for 3.5 s each ranging from −75 to −25 mV were applied to the cell at least 5 min after break in. Laser pulses were delivered at 2.2 s after the onset of the voltage step to allow for stabilization of the holding current. Current–voltage (*I–V*) relationships were computed from peak amplitudes of a series of GABA-evoked currents recorded at increasing holding potentials and repeated twice for each location (soma and dendrite). Voltages were corrected for liquid junction potential (−14.1 mV) and voltage drop across the series resistance of the pipette. Under these experimental conditions, the expected E_{GABA} predicted by the Nernst equation was −40 mV.

Live cell staining for single-particle imaging. Neurons were stained as described previously (Bannai et al., 2006). Briefly, cells were incubated for 5 min at 37°C with primary antibodies against Flag (mouse, 1:300; Sigma) or extracellular epitopes of NCAM-120 (rabbit, 1:40,000; gift from R. M. Mège), washed, and incubated for 5 min at 37°C with biotinylated Fab secondary antibodies (goat anti-mouse, 1:1000; goat anti-chicken, 1:2000; Jackson ImmunoResearch) in imaging medium. After washes, cells were incubated for 1–2 min with streptavidin-coated QDs emitting at 605 nm (0.5–1 nM; Invitrogen) in borate buffer (50 mM) supplemented with sucrose (200 mM).

QD imaging. Cells were imaged at 31°C in a temperature-controlled open chamber mounted onto an Olympus IX71 inverted microscope equipped with a 60× objective (1.42 NA; Olympus). GFP, mRFP, and QDs were detected using Lambda DG-4 monochromator coupled to the microscope through an optic fiber with appropriate filters (excitation, HQ470/40, D540/25, and D455/70; dichroic, Q495LP, 565DCLP, and 500DCXR; emission, HQ525/50, D605/55, and HQ605/20; GFP and mRFP filters from Chroma Technology; QD filters from Omega Optical). gephyrin–mRFP, homer1c–GFP images, and QD real-time recordings were acquired with ImagEM EMCCD camera and MetaView software (Roper Scientific). Real-time fluorescence images were obtained with an integration time of 30 ms with 1200 consecutive frames. Cells were imaged within 40 min after appropriate drug preincubation.

SPT and analyses. Single QDs were identified by their blinking property, i.e., their random alternation between emitting and non-emitting states (Alivisatos et al., 2005). Single QD tracking and reconstruction of trajectories over the recording were performed with homemade software (MATLAB; MathWorks) as described previously (Bonneau et al., 2005). The center of the fluorescence spots was determined with a spatial accuracy of ~10 nm by cross-correlating the image with a Gaussian fit of the point-spread function (for details, see Triller and Choquet, 2008). Spots were classified as synaptic when they overlapped with gephyrin–mRFP or homer1c–GFP clusters. mRFP and GFP images were first median filtered (kernel size, $3 \times 3 \times 1$) to enhance cluster outlines. Then, a user-defined intensity threshold was applied to select clusters and avoid their coalescence, and a binary mask was generated. Trajectories were considered synaptic when overlapping with the mask or extrasynaptic for spots two pixels (440 nm) away from the border of the mask (Dahan et al., 2003). Values of the mean square displacement (MSD) plot versus time were calculated for each trajectory by applying the following relationship:

$$\mathrm{MSD}(n\tau) = \frac{1}{N-n}\sum_{i=1}^{N-n}[(x((i+n)\tau) - x(i\tau))^2 + (y((i+n)\tau) - y(i\tau))^2]$$

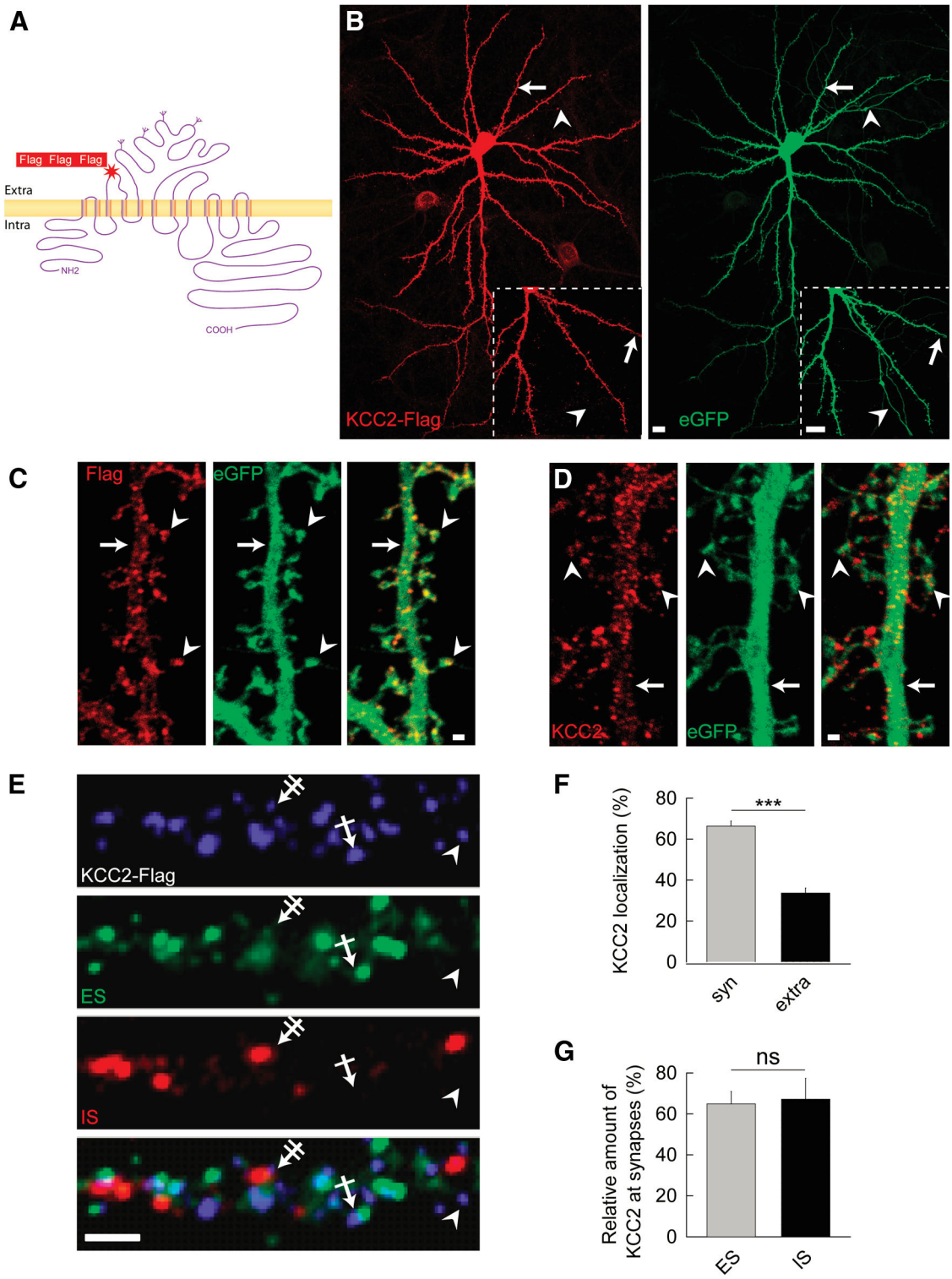

Figure 1. Recombinant, Flag-tagged KCC2 transporter is targeted to the somatodendritic neuron cell surface and preferentially accumulates at synapses. ***A***, Scheme showing the site of insertion of the three Flag sequence in the second extracellular loop between transmembrane segments 3 and 4. ***B***, Flag-tag staining (red) in permeabilized hippocampal neurons (22 DIV) transfected with KCC2–Flag and eGFP (green). Insets, Higher magnification of the regions of interest in ***B***. Scale bars, 10 μm. KCC2–Flag immunoreactivity is somatodendritic (arrow) and absent from axons (arrowhead). ***C***, ***D***, Flag (red, ***C***) or KCC2 (red, ***D***) staining in neurons transfected with KCC2–Flag plus eGFP (***C***) or eGFP alone (***D***). Scale bar, 1 μm. Flag-tagged KCC2 forms numerous clusters in dendritic shafts (arrow) and spines (arrowheads) as the endogenous KCC2 protein. ***E–G***, KCC2–Flag clusters at synapses. ***E***, KCC2–Flag surface staining (blue) in neurons cotransfected with homer1c–GFP (green) and gephyrin–mRFP (red), two markers of excitatory (ES) and inhibitory (IS) synapses. Note that some KCC2–Flag clusters partially overlaid homer1c–GFP clusters (crossed arrow) or gephyrin–mRFP clusters (double crossed arrow), whereas others are associated with the extrasynaptic membrane (arrowhead). Scale bar, 2 μm. ***F***, Quantification of the proportion of KCC2–Flag membrane clusters at synapses (syn) compared with extrasynaptic membrane (extra), showing a preferential localization of KCC2 in the vicinity of synapses ($n = 40$; 3 cultures; $^{***}p < 10^{-4}$). ***G***, Comparable proportion of KCC2 at excitatory (ES) and inhibitory (IS) synapses ($n = 40$; 3 cultures).

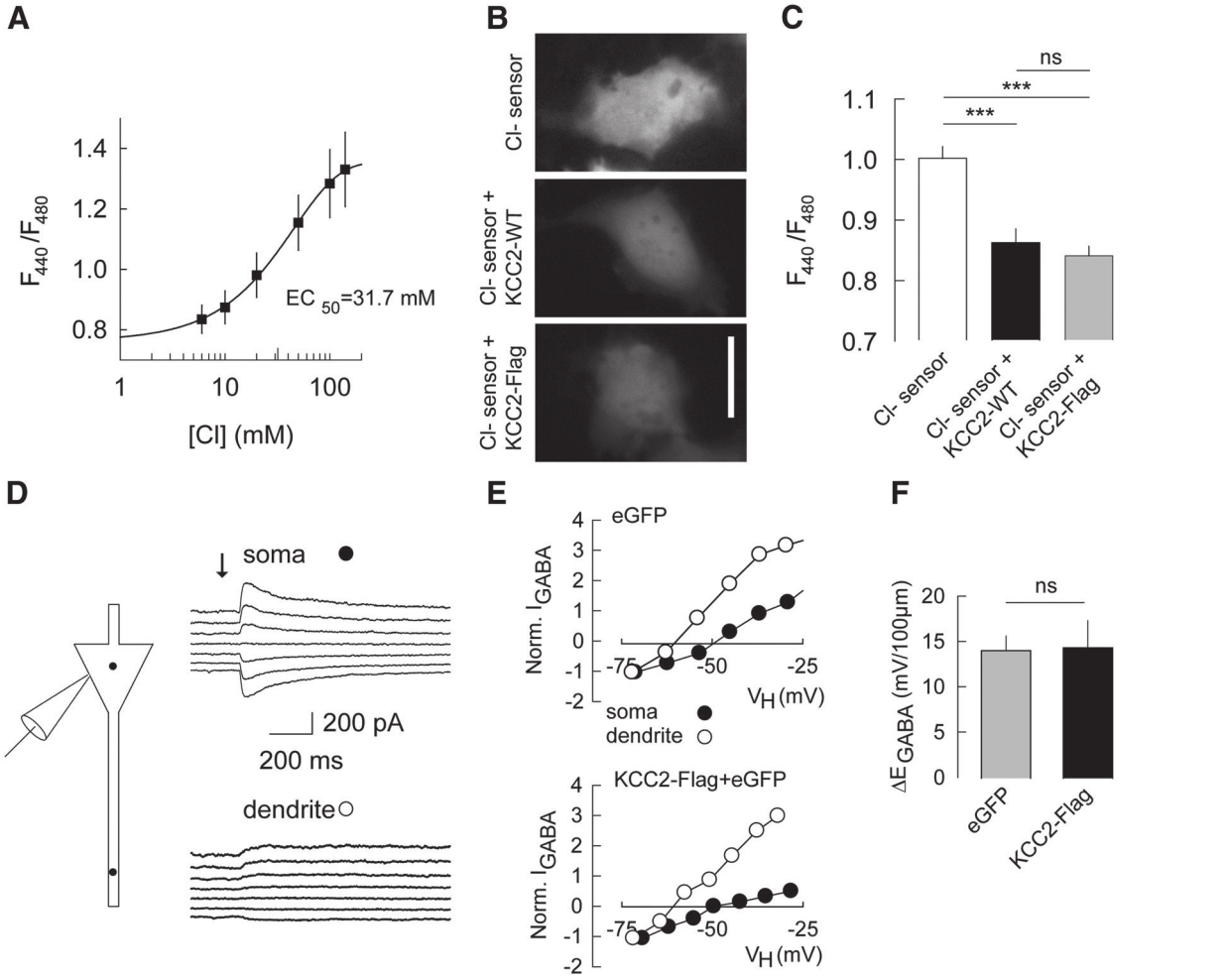

Figure 2. Recombinant KCC2–Flag is functional, and its expression does not perturb chloride extrusion in neurons. ***A***, Calibration of the CFP–YFP chloride sensor ($n = 12$ for each chloride concentration, 3 cultures). ***B***, ***C***, Live cell ratiometric chloride imaging in COS cells transfected with the CFP–YFP chloride sensor (Cl^- sensor) alone or in combination with WT (KCC2–WT) or Flag-tagged KCC2 (KCC2–Flag). ***B***, Images show the F_{440}/F_{480} fluorescence ratio. Scale bar, 20 μm. ***C***, Quantifications showing significant (***$p < 10^{-3}$) decrease in the CFP/YFP ratio in cells expressing the Cl^- sensor in combination with KCC2–WT or KCC2–Flag versus cells expressing the chloride sensor alone. Cl^- sensor, $r = 1.0 \pm 0.02$, $n = 51$; KCC2–WT, $r = 0.86 \pm 0.03$, $n = 53$; KCC2–Flag, $r = 0.83 \pm 0.02$, $n = 53$, four cultures. No significant difference between cells expressing WT or Flag-tagged KCC2 ($p = 7 \times 10^{-2}$) demonstrating that Flag-tag insertion in the second predicted extracellular loop does not compromise KCC2 function. ***D–F***, No effect of KCC2–Flag expression on chloride export estimated from the somatodendritic E_{GABA} gradient. ***D***, ***E***, Representative currents at voltage steps ranging from −75 to −25 mV during Rubi-GABA uncaging at somatic and dendritic sites (***D***) and normalized *I–V* relationships (***E***). Note the leftward shift in *I–V* relationships of dendritic versus somatic GABA currents. ***F***, Mean somatodendritic E_{GABA} gradient from seven (eGFP) and nine (KCC2–Flag) cells.

(Saxton and Jacobson, 1997), where τ is the acquisition time, N is the total number of frames, and n and i are positive integers, with n determining the time increment. For simple, two-dimensional Brownian mobility, the MSD as a function of time is linear with a slope of $4D$, where D is the diffusion constant. If the MSD as a function of time tends to a constant value L, the diffusion is confined in a domain of size L. Diffusion coefficients (D) were calculated by fitting the first four points without origin of the MSD versus time curves with the following equation: $\mathrm{MSD}(n\tau) = 4Dn\tau + b$, where b is a constant reflecting the spot localization accuracy. The area in which diffusion is confined can be estimated by fitting the MSD as a function of time with the following formula:

$$\mathrm{MSD}(ndt) = \frac{L^2}{3}\left(1 - \exp\left(-\frac{12Dndt}{L^2}\right)\right) + 4D_{\mathrm{mac}}ndt,$$

where L^2 is the confined area in which diffusion is restricted, and D_{mac} is the diffusion coefficient on a long timescale (Kusumi et al., 1993). The size of the confinement domain was defined as the side of a square in which diffusion is confined (Kusumi et al., 1993). For details, see Ehrensperger et al. (2007)). Synaptic dwell time (DT) was defined as the duration of detection of QDs at synapses on a recording divided by the number of exits as detailed previously (Charrier et al., 2006; Ehrensperger et al., 2007). DTs ≤5 frames (150 ms) were not retained.

Statistics. Means are shown ±SEM, and median D values are indicated with their interquartile range (IQR, 25–75%). Means were compared using the nonparametric, Mann–Whitney rank-sum test unless stated otherwise using SigmaStat software (SPSS). Cumulative distributions and median D values were compared using the Kolmogorov–Smirnov test under StatView (SAS). Differences were considered significant for p values <5%.

Results

Normal membrane traffic and function of Flag-tagged KCC2 in neurons

QD-based SPT experiments require that antibodies coupled to fluorescent probes bind to the membrane protein of interest. In the absence of a reliable antibody targeting an extracellular epitope of KCC2, we designed a recombinant KCC2 transporter Flag-tagged (KCC2–Flag) within its second predicted extracellu-

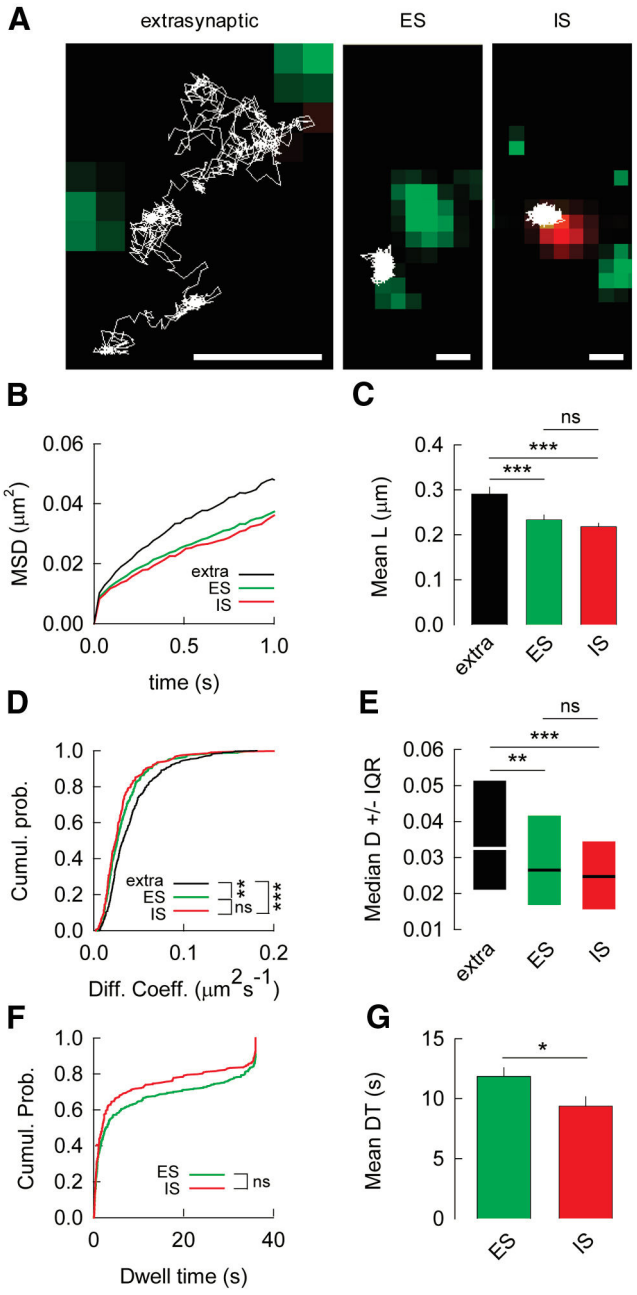

Figure 3. Membrane dynamics of the KCC2 transporter studied with QD-based SPT. ***A***, Representative trajectories (white) of QD-bound Flag-tagged recombinant KCC2 in extrasynaptic membrane (1014 frames, $D = 3 \times 10^{-2}\ \mu m^2 s^{-1}$), at excitatory synapses (1002 frames, $D = 2 \times 10^{-2}\ \mu m^2 s^{-1}$), and at inhibitory synapses (773 frames, $D = 4 \times 10^{-2}\ \mu m^2 s^{-1}$). QD trajectories (white) were overlaid with fluorescent clusters of recombinant homer1c–GFP (green) and gephyrin–mRFP (red) to identify excitatory (ES) and inhibitory (IS) synapses, respectively. Scale bars, 1 μm. ***B***, Time-averaged MSD functions of extrasynaptic QDs (black), QDs at excitatory synapses (green), and QDs at inhibitory synapses (red). The MSD versus time relationship for extrasynaptic trajectories shows a steeper initial slope, suggesting that trajectories were less confined. ***C***, Decreased size of the confinement domain L for synaptic QDs showing increased confinement ($^{***}p < 10^{-3}$). ***D***, ***E***, Cumulative probabilities (***D***) and median values ± 25–75% IQR (***E***) of QD diffusion coefficients D in extrasynaptic membrane (black) or at excitatory (green) or inhibitory (red) synapses. Note the reduced diffusion at synapses ($^{**}p = 2 \times 10^{-3}$, $^{***}p < 10^{-3}$). ***F***, Cumulative probability plots of KCC2–Flag DTs are shifted toward higher values at excitatory synapses ($p = 6 \times 10^{-2}$). ***G***, Mean DTs at excitatory synapses (green) and at inhibitory synapses (red) showing increased DT of KCC2–Flag at excitatory synapses ($^{*}p < 5 \times 10^{-2}$).

Table 1. Diffusion properties of KCC2–Flag at excitatory and inhibitory synapses

Location	Median D ($10^{-2}\ \mu m^2 s^{-1}$)	Mean L (nm)	Mean DT (s)
ES	2.7 (281)	237.39 ± 12.66 (212)	11.9 ± 0.8 (380)
IS	2.5 (202)	221.03 ± 8.90 (142)	9.4 ± 0.8 (288)
Extra	3.3 (367)	299.62 ± 18.27 (279)	n.d.

Quantifications from 49 cells and five independent experiments. Numbers in parentheses indicate the numbers of QDs analyzed. ES, QDs at excitatory synapses; IS, QDs at inhibitory synapses; Extra, QDs at extrasynaptic sites; n.d., not determined. Mean L and DT values are shown ±SEM.

lar loop between transmembrane domains 3 and 4 (see Materials and Methods; Fig. 1*A*). We first examined whether the insertion of the Flag tag may alter membrane targeting and cellular distribution of KCC2. Primary cultures of hippocampal neurons were transfected at 14 DIV with the recombinant KCC2–Flag transporter and eGFP and processed at 22 DIV for immunolabeling on fixed and permeabilized cells using an anti-Flag antibody. KCC2–Flag was targeted to the somatodendritic domain (Fig. 1*B*) and excluded from axons (Fig. 1*B*), as observed for the endogenous transporter (data not shown; Williams et al., 1999; Gulyás et al., 2001; Hübner et al., 2001; Vale et al., 2005; Blaesse et al., 2006; Szabadics et al., 2006; Takayama and Inoue, 2006; Belenky et al., 2008; Bartho et al., 2009; Baldi et al., 2010). At the subcellular level, KCC2–Flag formed numerous clusters in dendritic shafts and spines (Fig. 1*C*), similar to the endogenous transporter (Fig. 1*D*; Lee et al., 2007; Watanabe et al., 2009; Gauvain et al., 2011). Live cell Flag immunolabeling to selectively stain KCC2–Flag at the surface revealed that the recombinant transporter was targeted to the plasma membrane (Fig. 1*E*). These results indicate that the Flag-tagged transporter traffics normally to the somatodendritic membrane and that the recombinant protein is present in large amounts at the cell surface.

We showed previously with confocal microscopy that endogenous KCC2 clusters are detected in the vicinity of excitatory and inhibitory synapses (Chamma et al., 2012), and electron microscopy studies indicate that its localization might be perisynaptic and/or postsynaptic (Gulyás et al., 2001; Bartho et al., 2004; Blaesse et al., 2006; Takayama and Inoue, 2006). Therefore, we evaluated the abundance of surface KCC2–Flag clusters at synapses in neurons cotransfected with GFP-coupled homer1c and mRFP-coupled gephyrin to label excitatory and inhibitory synapses, respectively (Hanus et al., 2006; Ehrensperger et al., 2007). KCC2 clusters were considered synaptically located when overlapping with homer1c–GFP or gephyrin–mRFP clusters and extrasynaptic when localized at least two pixels (286 nm) away from synaptic markers. Surface KCC2–Flag clusters showed partial colocalization with synaptic markers and were also detected in extrasynaptic regions (Fig. 1*E*). Quantifications revealed that 66.4 ± 2.5% surface KCC2–Flag clusters were localized at synapses (i.e., independent of their localization at excitatory or inhibitory synapses; see Materials and Methods; Fig. 1*F*), showing a preferential association of the transporter with synaptic compartments. The apparent preferential synaptic localization of KCC2–Flag was not attributable to a sampling bias because synapses occupy only 11.5 ± 1.0% ($n = 14$) of total dendritic surface. Furthermore, a similar proportion of surface KCC2–Flag clusters localized at glutamatergic and GABAergic synapses (see Materials and Methods; Fig. 1*G*). Thus, KCC2–Flag accumulates at both excitatory and inhibitory synapses.

To test whether insertion of the Flag tag may compromise KCC2 function, we measured chloride extrusion in COS cells using ratiometric fluorescence imaging of a CFP–YFP chloride sensor (Markova et al., 2008; Waseem et al., 2010). We first cali-

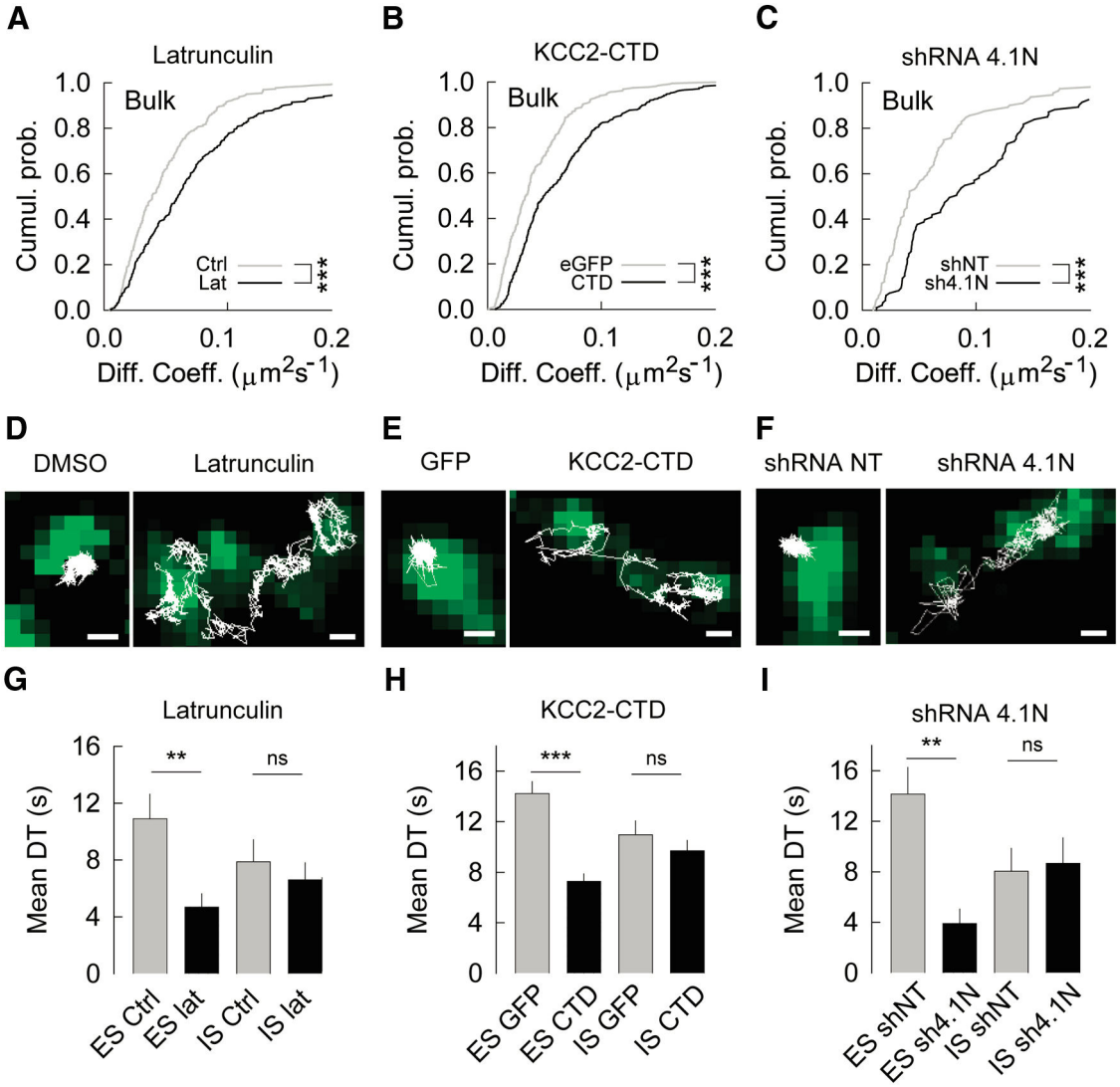

Figure 4. F-actin depolymerization and KCC2–actin binding interference increase the lateral diffusion of KCC2. ***A–C***, Cumulative probability plots of diffusion coefficients (for bulk population of QDs) of KCC2–Flag in control conditions (gray in ***A***) or during application of latrunculin A (black in ***A***), in neurons transfected with eGFP (gray in ***B***), KCC2–CTD (black in ***B***), nontarget shRNA (gray in ***C***), and shRNA against 4.1N (black in ***C***). Note the increase (***$p < 10^{-4}$) in KCC2–Flag diffusion coefficients during actin depolymerization, KCC2–CTD overexpression, or 4.1N suppression. ***D–F***, Examples of KCC2–Flag trajectories in control (***D***; 827 frames, $D = 4 \times 10^{-2}\ \mu m^2 s^{-1}$) versus latrunculin A application (***D***; 944 frames, $D = 9 \times 10^{-2}\ \mu m^2 s^{-1}$), or in neurons transfected with eGFP (***E***; 974 frames, $D = 4 \times 10^{-2}\ \mu m^2 s^{-1}$) versus KCC2–CTD (***E***; 554 frames, $D = 9 \times 10^{-2}\ \mu m^2 s^{-1}$), or in nontarget shRNA (***F***; 494 frames, $D = 4 \times 10^{-2}\ \mu m^2 s^{-1}$) versus 4.1N shRNA (***F***; 380 frames, $D = 13 \times 10^{-2}\ \mu m^2 s^{-1}$) expressing neurons. QD trajectories were overlaid with fluorescent clusters of recombinant homer1c–GFP (green) to identify excitatory synapses. Scale bars, 0.5 μm. Note the increase in surface exploration and faster escape of KCC2 from excitatory synapses (green). ***G–I***, Significant reduction in KCC2–Flag DT at excitatory synapses (ES) but not at inhibitory synapses (IS) after actin depolymerization with latrunculin (IS, $p = 0.9$), reduced KCC2 actin binding with KCC2–CTD overexpression or 4.1N suppression (***G***, **$p = 3 \times 10^{-3}$; ***H***, ***$p < 10^{-4}$; ***I***, **$p = 1.2 \times 10^{-3}$). Ctrl, Control; lat, latrunculin.

Table 2. Effects of F-actin depolymerization and interference with actin binding on KCC2 mobility at excitatory and inhibitory synapses

	Condition					
Location	Control	Latrunculin A	eGFP	CTD	NT shRNA	4.1N shRNA
Bulk median D ($10^{-2}\ \mu m^2 s^{-1}$)	4.3 (258, 24, 3)	6.5 (302, 35, 3)	3.4 (312, 24, 3)	5.0 (369, 35, 3)	4.2 (93, 19, 2)	8.3 (111, 25, 2)
ES mean DT	10.4 ± 1.5 (83, 24, 3)	4.6 ± 0.9 (111, 35, 3)	14.2 ± 1.0 (262, 18, 5)	7.3 ± 0.6 (407, 28, 5)	14.2 ± 2.2 (53, 19, 2)	3.9 ± 1.2 (56, 25, 2)
IS mean DT	8.0 ± 1.5 (68, 24, 3)	6.7 ± 1.2 (103, 24, 3)	11.0 ± 1.1 (159, 18, 5)	9.7 ± 0.8 (278, 28, 5)	8.1 ± 1.8 (54, 19, 2)	8.7 ± 2.1 (45, 25, 2)

Numbers in parentheses indicate the numbers of QDs, cells, and cultures analyzed. ES, QDs at excitatory synapses; IS, QDs at inhibitory synapses. Mean values are shown ± SEM.

brated the probe in our system using a nigericin–tributyltin paradigm (see Materials end Methods; Krapf et al., 1988; Trapp et al., 1996; Marandi et al., 2002; Metzger et al., 2002). In agreement with previous work (Markova et al., 2008; Waseem et al., 2010), the CFP/YFP fluorescence ratio was tightly correlated with chloride concentration with maximal sensitivity in the physiological (10–100 mM) range (Fig. 2*A*). COS cells were then transfected with the CFP–YFP probe alone or together with either wild-type (WT) or Flag-tagged KCC2 constructs (Fig. 2*B*,*C*). We observed a significant decrease in the CFP/YFP ratio in cells expressing

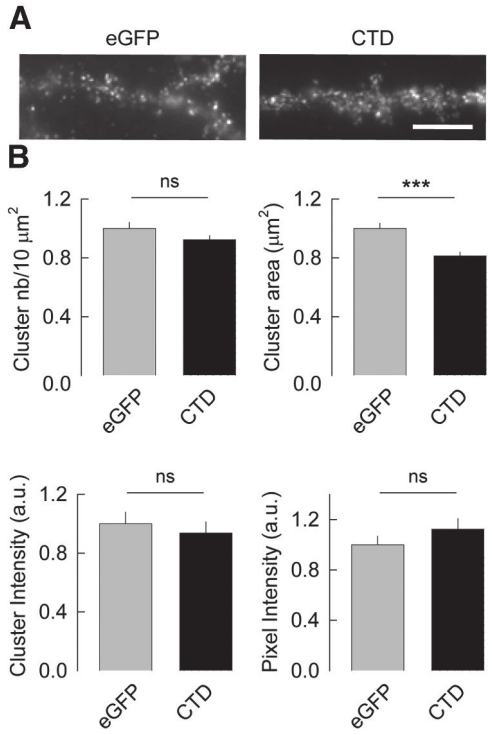

Figure 5. Effects of overexpression of the CTD of KCC2 on its clustering. ***A***, KCC2–Flag remains clustered at the surface of hippocampal neurons after KCC2–CTD overexpression. Scale bar, 10 μm. ***B***, Summary plots of the effect of KCC2–CTD overexpression on the number of KCC2–Flag clusters per 10 μm^2, cluster size, mean fluorescence intensity per cluster, and mean fluorescence intensity per pixel within clusters. Values were normalized to the corresponding control values. eGFP, $n = 36$; KCC2–CTD, $n = 34$; three cultures; $^{***}p < 10^{-3}$.

either forms of KCC2 compared with cells transfected with the chloride probe alone (~15%; Fig. 2*B*,*C*). However, no significant difference was detected between cells expressing WT or Flag-tagged KCC2 (Mann–Whitney test, $p = 7 \times 10^{-2}$; Fig. 2*B*,*C*). These results demonstrate that Flag-tag insertion in the second predicted extracellular loop does not compromise KCC2 function, in agreement with previous work (Zhao et al., 2008; Acton et al., 2012).

We next asked whether expression of exogenous KCC2–Flag may increase KCC2 expression level and alter chloride extrusion properties in transfected neurons. We found that KCC2–Flag expression did not significantly increase the mean KCC2 fluorescence intensity (eGFP, $1.0 \pm 9.2 \times 10^{-2}$, $n = 22$; KCC2–Flag plus eGFP, $1.3 \pm 14.0 \times 10^{-2}$, $n = 25$; two cultures; $p = 9.4 \times 10^{-2}$; data not shown). To compare KCC2 function in neurons expressing KCC2–Flag with cells expressing endogenous KCC2, we measured the somatodendritic gradient of E_{GABA} using local photolysis of caged GABA (Khirug et al., 2005; Gauvain et al., 2011). In neurons expressing KCC2–Flag and eGFP, we measured a gradient of 14.4 ± 3.0 mV/100 μm between somatic and dendritic E_{GABA} (Fig. 2*D*–*F*). This gradient was not significantly different in neurons transfected with eGFP alone (14.1 ± 1.6 mV/100 μM; Fig. 2*D*–*F*). We conclude that exogenous expression of KCC2–Flag does not significantly increase expression and function of KCC2. Altogether, our data report that recombinant KCC2–Flag is a suitable tool to study cell and membrane trafficking of the transporter in neurons without perturbing neuronal chloride homeostasis.

Constrained diffusion of KCC2 at glutamatergic and GABAergic synapses

Neurons were cotransfected at 14 DIV with KCC2–Flag, homer1c–GFP, and gephyrin–mRFP, surface labeled at 22–25 DIV with Flag antibodies, and subsequently labeled with specific intermediate biotinylated Fab fragments and streptavidin-coated QDs (see Materials and Methods). The cell surface exploration of KCC2–Flag was analyzed from 36 s recording sequences. As shown in Figure 3*A*, surface exploration of QDs was restricted to smaller areas at synapses compared with extrasynaptic membranes. In some cases, QDs rapidly exchanged between extrasynaptic and synaptic compartments or escaped synaptic areas and further explored neighboring synapses (data not shown). Quantitative analysis performed on whole populations of trajectories confirmed reduced surface exploration of KCC2–Flag at excitatory and inhibitory synapses. MSD versus time plots showed a steeper slope for extrasynaptic trajectories (Fig. 3*B*), indicative of lower confinement. Accordingly, the mean size of the confinement domain (L) was increased by ~1.3-fold in extrasynaptic membranes compared with synaptic membranes (Fig. 3*C*). Furthermore, synaptic QDs were significantly (0.8-fold) less mobile than extrasynaptic QDs, as detected from cumulative probability plots of diffusion coefficients and median diffusion coefficient D values (Fig. 3*D*,*E*). Thus, KCC2–Flag shows reduced lateral mobility and increased diffusion constraints at excitatory and inhibitory synapses compared with extrasynaptic regions. However, diffusion coefficients and the size of confinement domains of KCC2–Flag were similar at both types of synapses (Fig. 3*C*,*E*). In contrast, the DT of KCC2–Flag was 1.3-fold longer at excitatory compared with inhibitory synapses (Fig. 3*F*,*G*), suggestive of a faster escape from inhibitory synapses. The median D values, mean L, and DT values of KCC2 in the extrasynaptic membrane at excitatory or inhibitory synapses are summarized in Table 1. We conclude that KCC2–Flag undergoes stronger diffusion constraints at excitatory synapses compared with inhibitory synapses.

Effects of altered KCC2–actin interactions on lateral diffusion, clustering, and transport function of KCC2–Flag

The intracellular CTD of KCC2 interacts with the actin cytoskeleton through the neuronal actin-linker protein 4.1N (Li et al., 2007). Such interaction may then hinder the lateral diffusion of KCC2 in the plasma membrane. Therefore, we examined the impact of KCC2–actin interactions on the lateral diffusion and clustering of KCC2. For this purpose, we induced F-actin depolymerization using latrunculin A (10 min at 5 μM; Allison et al., 2000), prevented KCC2 interaction with cytosolic partners by overexpressing its CTD (KCC2–CTD; Li et al., 2007; Gauvain et al., 2011), or specifically disrupted KCC2 interaction with 4.1N using RNA interference against 4.1N (Lin et al., 2009). We then examined the impact of these manipulations on KCC2 membrane dynamics. Bulk diffusion of KCC2–Flag (i.e., independent of synaptic vs extrasynaptic localization) was increased by ~1.5-fold during actin depolymerization, KCC2–CTD overexpression, or 4.1N suppression (Fig. 4*A*–*C*). In all three conditions, increased exploratory behavior of both extrasynaptic and synaptic trajectories was observed. However, facilitated synaptic escape of KCC2–Flag was specific of excitatory synapses (Fig. 4*D*–*F*). Consequently, KCC2–Flag DT at excitatory synapses was reduced by a 2.3-, 2.0-, and 3.6-fold during latrunculin treatment, KCC2–CTD overexpression, or 4.1N suppression (Fig. 4*G*–*I*). In contrast, none of these experimental conditions significantly altered KCC2 DT at inhibitory synapses (Fig. 4*G*–*I*). Median D values for

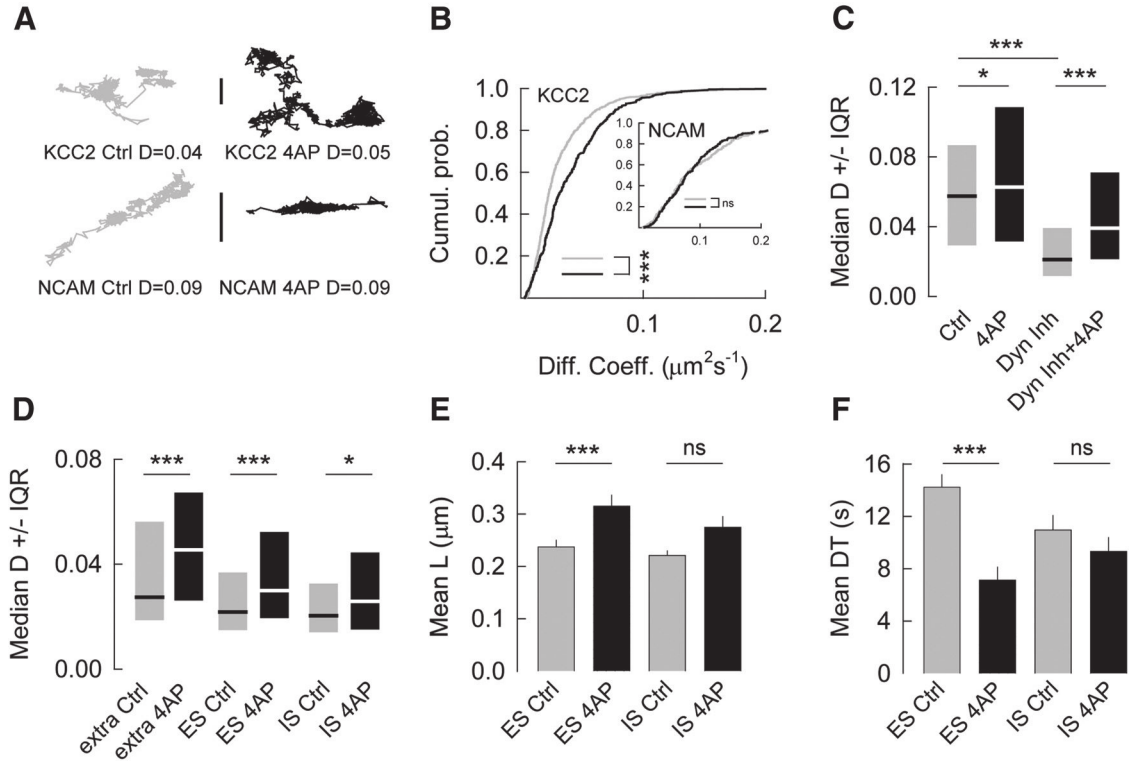

Figure 6. Elevated neuronal activity increases the membrane dynamics of KCC2 at excitatory synapses. ***A***, Examples of trajectories of QD-coupled KCC2–Flag and NCAM-120 in the absence (1049 and 708 frames) or presence of 4-AP (1155 and 825 frames). Scale bar, 0.5 μm. ***B***, Cumulative probabilities of diffusion coefficients (for bulk population of QDs) associated with KCC2–Flag (control, $n = 507$; 4-AP, $n = 430$, 4 cultures) or NCAM-120 (inset; control, $n = 241$; 4-AP, $n = 228$, 2 cultures) in the absence (gray) or presence (black) of 4-AP. Note the selective increase in KCC2 diffusion after 4-AP treatment (***$p < 10^{-3}$). ***C***, Median QD diffusion coefficient D values ± 25–75% IQR (for bulk population of QDs) measured in the absence (left) or presence (right) of the membrane-permeant dynamin inhibitory peptide (dynamin inh) in control (gray) or 4-AP (black) conditions. Slowing down of KCC2 (***$p < 10^{-4}$) in the presence of endocytosis blocker in basal activity conditions. In the same culture, 4-AP increased KCC2 mobility in the absence (*$p = 3 \times 10^{-2}$) or presence (***$p < 10^{-4}$) of the dynamin inhibitory peptide. ***D–F***, Median diffusion coefficients ± 25–75% IQR (***D***), mean confinement domain L (***E***), and mean DT (***F***) of KCC2–Flag in the extrasynaptic region (extra), at excitatory (ES) or inhibitory (IS) synapses, in the absence (gray) or presence (black) of 4-AP. Acute 4-AP treatment increased KCC2 diffusion coefficients in all membrane compartments (*$p = 2 \times 10^{-2}$; ***$p = 5 \times 10^{-4}$), whereas it selectively reduced confinement and DT at excitatory synapses (***$p < 10^{-3}$). Ctrl, Control.

Table 3. Effects of 4-AP on KCC2 lateral diffusion parameters

Location	Median D (10^{-2} $\mu m^2 s^{-1}$)	Mean L (nm)	Mean DT (s)
Control			
ES	2.2 (193)	237.4 ± 12.7 (212)	14.2 ± 1.0 (262)
IS	2.1 (157)	221.1 ± 8.90 (142)	11.0 ± 1.1 (159)
Extra	2.8 (157)	n.d.	n.d.
4-AP (100 μM, 10 min)			
ES	3.0 (160)	315.3 ± 20.80 (144)	7.2 ± 0.6 (141)
IS	2.6 (133)	274.8 ± 20.5 (117)	9.4 ± 1.1 (163)
Extra	4.5 (137)	n.d.	n.d.

Quantifications from 49 (control) and 36 (4-AP) cells and four independent experiments. Numbers in parentheses indicate the numbers of QDs analyzed. ES, QDs at excitatory synapses; IS, QDs at inhibitory synapses; Extra, QDs at extrasynaptic sites; n.d., not determined. Mean values are shown ± SEM.

bulk population of QDs and mean synaptic DT values in control versus altered KCC2–actin interaction are reported in Table 2. These results highlight specific KCC2–actin binding properties at excitatory synapses.

Increased lateral mobility of transmembrane proteins is often correlated with decreased clustering (Triller and Choquet, 2008). Therefore, we examined whether preventing KCC2 interactions with intracellular partners using KCC2–CTD overexpression actually reduced KCC2 clustering in hippocampal neurons. In control conditions, KCC2–Flag formed numerous clusters along the dendrites of transfected neurons (Fig. 5*A*). Overexpression of KCC2–CTD did not affect the density of clusters on dendritic membranes (Fig. 5*B*). However, the size of the clusters was reduced by 1.6-fold (Fig. 5*B*) with no reduction in either the mean fluorescence intensity of KCC2–Flag clusters (Fig. 5*B*) or the mean fluorescence intensity per pixel within clusters (Fig. 5*B*), showing only moderate effect of KCC2-CTD overexpression on KCC2 clustering. Consistent with this conclusion, overexpression of KCC2–CTD did not affect Cl^- transport function, as observed previously (Gauvain et al., 2011). The somatodendritic E_{GABA} gradient was not significantly different in neurons cotransfected with KCC2–CTD and KCC2–Flag (14.8 ± 2.0 mV/100 μM, $n = 12$) compared with KCC2–Flag alone (14.7 ± 2.8 mV/100 μM, $n = 7$, $p = 0.6$; data not shown). Thus, altering KCC2 interaction with intracellular partners releases diffusion constraints to KCC2 without compromising its clustering or function.

Increased diffusion and reduced clustering and transport function of KCC2 upon enhanced neuronal activity

KCC2 function is downregulated by neuronal activity (Kaila et al., 1997; Reid et al., 2001; Rivera et al., 2002, 2004; Woodin et al., 2003; Fiumelli et al., 2005; Wang et al., 2006b,c; Pathak et al., 2007; Wake et al., 2007; Kitamura et al., 2008; Li et al., 2008; Lee et al., 2011; Shimizu-Okabe et al., 2011). Whether this reflects reduced intrinsic transport function or reduced membrane expression of the transporter remains unclear. Therefore, we asked whether increased neuronal activity may induce an alteration of KCC2 membrane diffusion. We examined this issue by comparing the membrane dynamics of recombinant KCC2–Flag in the

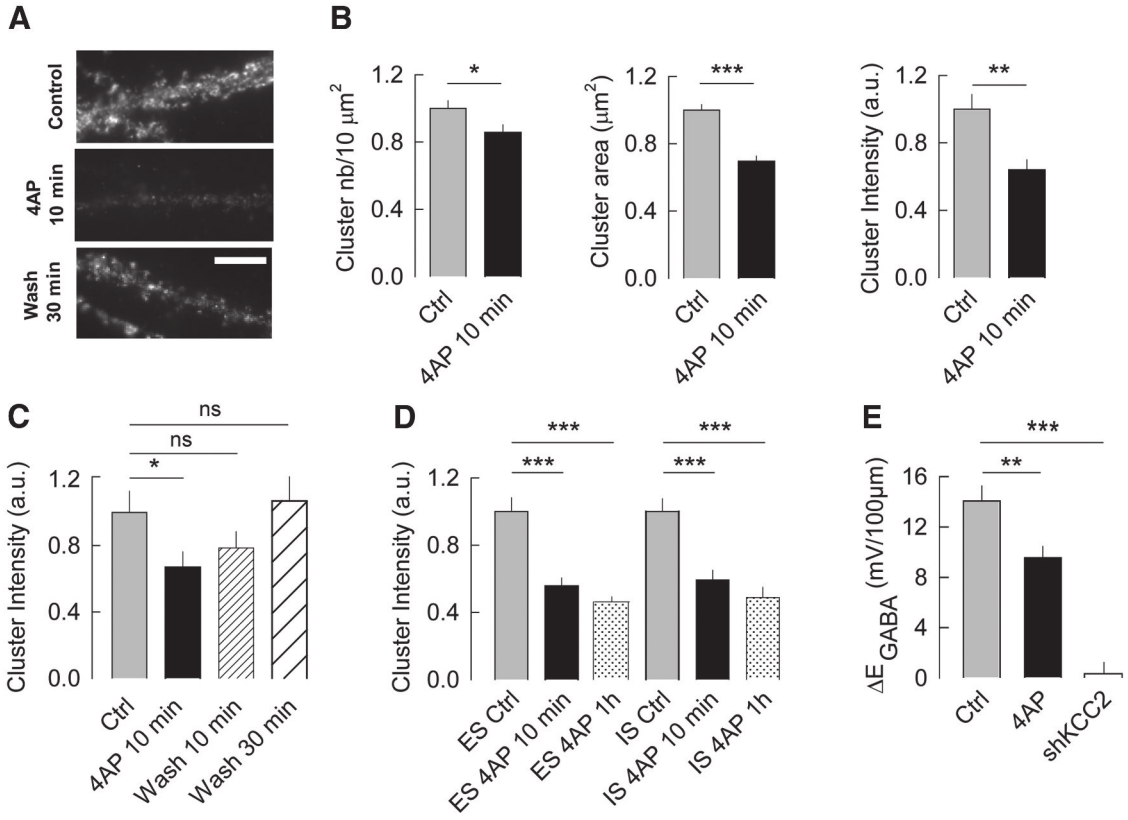

Figure 7. Increased neuronal activity disperses KCC2 clusters and reduces chloride export. ***A***, Flag surface staining in hippocampal neurons (23 DIV) expressing recombinant KCC2–Flag in the absence (Control) or presence of 4-AP for 10 min and after a 30 min washout (Wash). Scale bar, 10 μm. Note the loss of KCC2 clusters after 10 min exposure to 4-AP and the recovery of clusters 30 min after drug washout. ***B***, Quantifications showing significant reduction in the number of KCC2–Flag clusters per 10 μm^2 (left), cluster size (middle), and cluster intensity (right) after 10 min of 4-AP. Values were normalized to the corresponding control values. Control, $n = 26$; 4-AP at 10 min, $n = 31$; three cultures; $^*p = 3 \times 10^{-2}$, $^{**}p = 2 \times 10^{-3}$, $^{***}p < 10^{-3}$. ***C***, The mean fluorescence intensity of KCC2–Flag clusters was reduced by 30% in neurons exposed for 10 min to 4-AP (black) compared with untreated cells (gray). The mean cluster intensity started to increase 10 min (fine hatched) after drug removal to return to control values 30 min (large hatched) later. Values were normalized to the corresponding control values. Control, $n = 22$; 4-AP at 10 min, $n = 26$; 4-AP washout at 10 min, $n = 25$; 4-AP washout at 30 min, $n = 22$; two cultures; $^*p = 3 \times 10^{-2}$. ***D***, Effect of 4-AP on the mean fluorescence intensity of KCC2 aggregates at excitatory (ES) and inhibitory (IS) synapses showing dispersion of KCC2 clusters at either type of synapses after 10 min (black) or 1 h (black dots) exposure to 4-AP compared with control conditions (gray). Values were normalized to the corresponding control. Excitatory synapses: control, $n = 38$; 4-AP at 10 min, $n = 31$; 4-AP at 1 h, $n = 31$; inhibitory synapses: control, $n = 39$; 4-AP at 10 min, $n = 31$; 4-AP at 1 h, $n = 32$; four cultures; $^{***}p < 10^{-3}$. ***E***, 4-AP reduces the chloride ion transport capacity of treated neurons. Reduced somatodendritic E_{GABA} gradient in neurons exposed to 4-AP (black) versus neurons maintained in control (gray) conditions (control, 14.0 ± 1.2, $n = 12$; 4-AP, 9.5 ± 0.9, $n = 16$; *t* test, $^{**}p = 5.0 \times 10^{-3}$). In comparison, KCC2 shRNA (white) reduced by 98% the somatodendritic E_{GABA} gradient (0.3 ± 0.9, $n = 5$; *t* test, $^{***}p < 10^{-3}$). Ctrl, Control.

absence or presence of the potassium channel blocker 4-AP (100 μM). 4-AP treatment leads to a rapid and robust increase in synaptic activity that persists during the application of the drug with no major depolarization (Bouthour et al., 2011). We found that 4-AP increased the exploratory behavior (Fig. 6*A*) and diffusion coefficients of bulk KCC2–Flag populations (Fig. 6*B*). This effect was specific to KCC2 and did not reflect a reduced membrane viscosity because it was not associated with a significant change in the exploratory behavior (Fig. 6*A*) or lateral diffusion of the membrane-associated, cell adhesion molecule NCAM-120 (Fig. 6*B*).

KCC2 internalization and degradation participate in the rapid downregulation of chloride homeostasis by excitation (Lee et al., 2010, 2011). We then asked whether the activity-dependent regulation of KCC2 membrane dynamics was dependent on endocytosis. We examined the impact of 4-AP on the lateral mobility of recombinant KCC2–Flag while pharmacologically blocking endocytosis using bath application of myristoylated QVPSRPNRAP dynamin inhibitory peptide (Marks and McMahon, 1998). Under basal activity conditions, blockade of endocytosis significantly slowed down KCC2 (by 2.8-fold; Fig. 6*C*; see Table 4). This effect was accompanied by a significant (1.9-fold) increase in the mean fluorescence intensity of membrane KCC2–Flag clusters 20 min after blocking endocytosis (Mann–Whitney test, $p < 5.0 \times 10^{-2}$; control, 18 cells; dynamin inhibitor, 17 cells, two cultures; data not shown). The enhanced KCC2 clustering during endocytosis blockade suggests the transporter undergoes a rapid turnover from the cell membrane at steady state, in agreement with published work (Rivera et al., 2004; Lee et al., 2007). Furthermore, our results also reveal a tight correlation between membrane dynamics, clustering, and withdrawal of the transporter. During blockade of dynamin-dependent endocytosis, the amount of surface KCC2 increased, leading to an increase in the clustering and confinement of the transporter. In these conditions, however, 4-AP was still able to increase KCC2 mobility (by 1.9-fold; Fig. 6*C*; see Table 4). Thus, activity-dependent regulation of KCC2 membrane dynamics does not depend on and actually precedes its endocytosis from plasma membrane.

We then analyzed the effects of 4-AP on the diffusion behavior of KCC2 at excitatory and inhibitory synapses. 4-AP application increased KCC2–Flag diffusion by 1.6-, 1.4-, and 1.4-fold in the extrasynaptic membrane, at excitatory synapses and inhibitory synapses, respectively (Fig. 6*D*). This 4-AP-induced increase in diffusion was associated with a 1.3-fold decrease in KCC2 con-

finement at excitatory synapses but not at inhibitory synapses (Fig. 6*E*). Consistent with these observations, 4-AP induced a (twofold) faster escape of KCC2–Flag from excitatory synapses than from inhibitory synapses (Fig. 6*F*). These data are summarized in Table 3. Thus, KCC2 shows lower confinement and faster escape from excitatory but not inhibitory synaptic domains during increased neuronal activity.

We next analyzed the impact of increased neuronal activity on the membrane clustering of KCC2. Application of 4-AP rapidly reduced the membrane-associated KCC2–Flag immunoreactivity (Fig. 7*A*). Indeed, a 10 min exposure to 4-AP reduced the mean number (by 0.9-fold) of membrane-associated KCC2–Flag clusters as well as the size (by 0.7-fold) and fluorescence intensity (by 0.6-fold) of the remaining clusters compared with untreated cells (Fig. 7*B*). The dispersal of KCC2–Flag clusters was totally reversible within 30 min of 4-AP washout (Fig. 7*A*, *C*). The effect of 4-AP on KCC2 clustering was similar at both excitatory and inhibitory synapses (Fig. 7*D*). Application of 4-AP reduced by approximately twofold the mean fluorescence intensity of KCC2–Flag clusters at both excitatory and inhibitory synapses (Fig. 7*D*). The effect of 4-AP on KCC2–Flag clusters was independent of a remodeling of the postsynaptic scaffold because the size of homer1c–GFP and gephyrin–mRFP clusters remained unchanged after 10 min or 1 h of 4-AP (control, $n = 25$; 4-AP at 10 min, $n = 15$; 4-AP at 1 h, $n = 21$; two cultures; 4-AP at 10 min vs control, $p = 0.8$ and 0.2 at excitatory and inhibitory synapses, respectively; 4-AP at 1 h vs control, $p = 0.1$ and 0.5 at excitatory and inhibitory synapses, respectively, Mann–Whitney test; data not shown). However, the loss of KCC2–Flag clusters was accompanied by an alteration of the transport function of KCC2. Indeed, the somatodendritic E_{GABA} gradient was reduced by 32% in neurons exposed to 4-AP compared with control (Fig. 7*E*). In comparison, suppression of KCC2 expression by RNA interference reduced E_{GABA} somatodendritic gradient by 98% (Fig. 7*E*), in agreement with our previous work (Gauvain et al., 2011). Therefore, we conclude that enhanced neuronal activity increases the lateral diffusion of KCC2, leading to reduced membrane clustering and chloride extrusion.

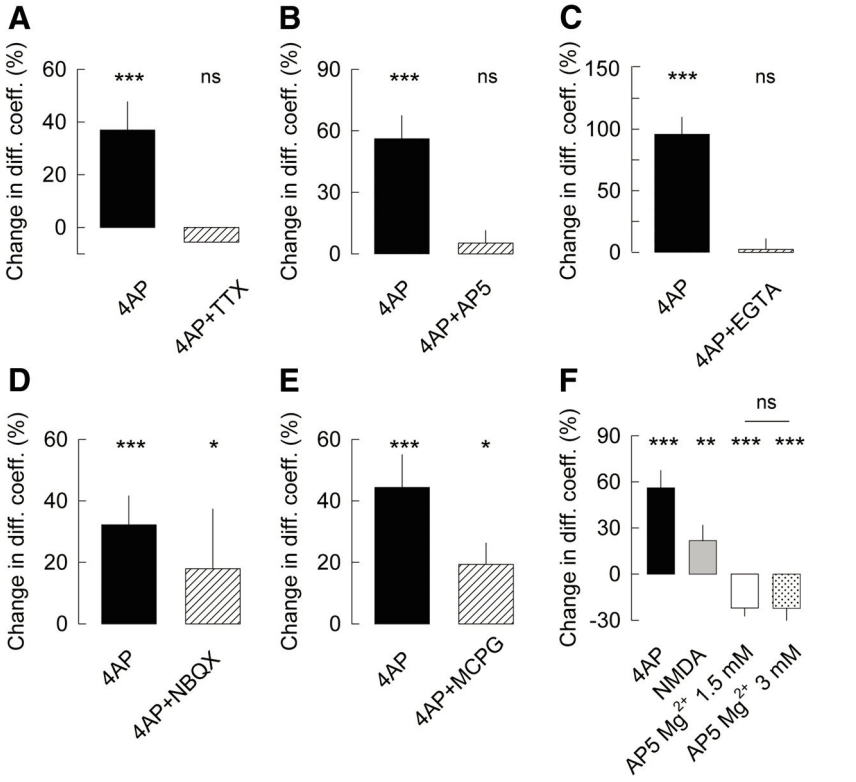

Figure 8. NMDAR activation and calcium influx mediate the 4-AP-induced upregulation of KCC2 diffusion. ***A–E***, The increase in KCC2 diffusion coefficients (calculated for bulk population of QDs) after 4-AP (black) was reversed by (hatched bars) TTX (***A***, $***p < 10^{-3}$), D,L-AP-5 (***B***, $***p < 10^{-3}$), or EGTA (***C***, $***p < 10^{-3}$) but not NBQX (***D***, $*p = 1 \times 10^{-2}$) or *R*,*S*-MCPG (***E***, $*p = 1 \times 10^{-2}$). ***F***, The effect of 4-AP on KCC2 acceleration (black) was partially mimicked by NMDA application (gray, $**p = 9 \times 10^{-3}$). Note also that D,L-AP-5 slows down KCC2 at steady state in conditions of both low (white) and high (black dots) external Mg^{2+} concentration (1.5 mM Mg^{2+}, $n = 223$; AP-5 plus 1.5 mM Mg^{2+}, $n = 174$; $***p < 10^{-4}$; 3 mM Mg^{2+}, $n = 116$; AP-5 plus 3 mM Mg^{2+}, $n = 135$; $***p < 10^{-4}$; AP-5 plus 1.5 mM Mg^{2+} versus AP-5 plus 3 mM Mg^{2+}, $p = 0.5$; 1 culture). In all histograms, values are expressed as percentage of change in diffusion coefficients and statistics compared with drugs versus appropriate controls.

Molecular mechanisms underlying the activity-dependent regulation of KCC2 diffusion and clustering

To identify the molecular mechanisms involved in activity-induced increase of KCC2 diffusion, we compared the effects of 4-AP in the presence or absence of the sodium channel blocker TTX (1 μM; Fig. 8*A*), the NMDAR antagonist AP-5 (100 μM; Fig. 8*B*), the Ca^{2+} chelator EGTA (1.8 mM; Fig. 8*C*), the AMPAR antagonist NBQX (10 μM; Fig. 8*D*), or the group I/group II mGluR antagonist *R*,*S*-MCPG (500 μM; Fig. 8*E*). TTX, AP-5, and EGTA completely abolished the effects of 4-AP on the diffusion of KCC2–Flag (Fig. 8*A–C*). In contrast, NBQX and *R*,*S*-MCPG did not prevent 4-AP-induced acceleration of KCC2–Flag (Fig. 8*D*,*E*). Furthermore, acute application of NMDA (50 μM) increased the exploratory behavior and diffusion of KCC2 (Fig. 8*F*), showing that direct activation of NMDARs mimics the effect of 4-AP on KCC2 diffusion. These results demonstrate that 4-AP leads to an increased diffusion of KCC2 through action potential-dependent, synaptic activation of NMDARs and subsequent Ca^{2+} influx.

Interestingly, application of AP-5 alone reduced the diffusion of the recombinant transporter below that observed in control conditions (Fig. 8*F*), suggesting that NMDAR activation may regulate KCC2 mobility under basal activity. This effect of AP-5 was similar in the presence of high (3 mM) or low (1.5 mM) extracellular $[Mg^{2+}]$ (Fig. 8*F*). This suggests that, at steady state, NMDAR-dependent control of KCC2 diffusion may involve tonic activity of receptors with low Mg^{2+} sensitivity, possibly containing the NR2C and/or NR2D subunits (Feldmeyer and Cull-Candy, 1996). We conclude that NMDAR activation and subsequent Ca^{2+} influx release diffusion constraints to KCC2 diffusion both at steady state and during sustained neuronal activity.

Dephosphorylation of KCC2 serine residue at position 940 in the intracellular CTD of KCC2 (S940) is required for activity-dependent calcium-induced downregulation of KCC2 membrane stability (Lee et al., 2011). Thus, we tested the involvement of this residue in the activity-induced regulation of KCC2 diffusion and clustering. We generated KCC2–Flag constructs with

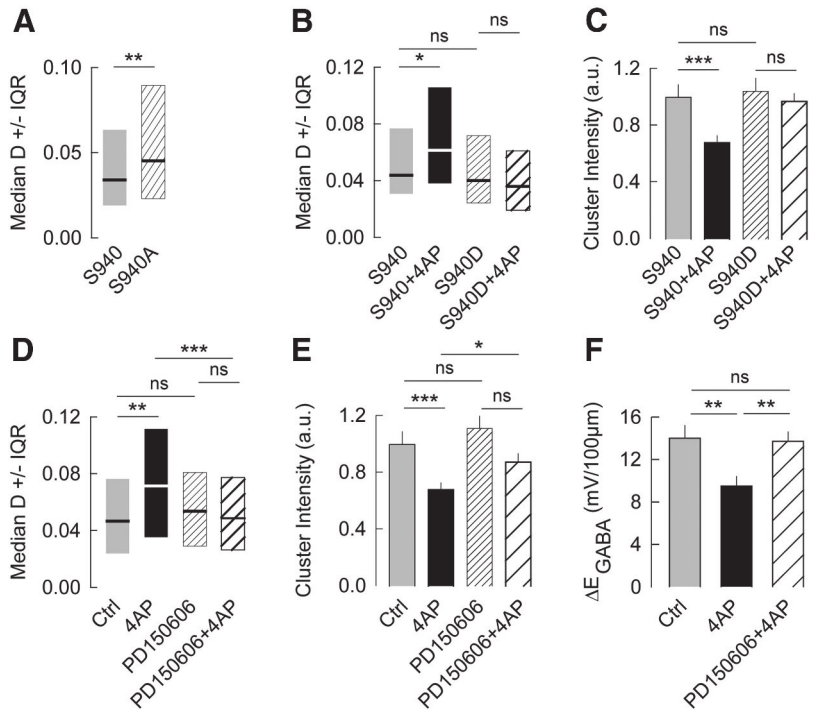

Figure 9. S940 dephosphorylation and calpain cleavage contribute to the 4-AP-mediated regulation of KCC2 diffusion, clustering, and function. ***A–C***, Dephosphorylation of S940 is required for activity-dependent regulation of KCC2 diffusion. ***A***, Median QD diffusion coefficient *D* values ± 25–75% IQR (for bulk population of QDs) of KCC2–S940 (gray) and KCC2–S940A (pattern) in basal activity conditions, showing increased mobility of the dephosphorylated KCC2–S940A transporter (**$p = 2 \times 10^{-3}$). ***B***, ***C***, Median QD diffusion coefficients values ± 25–75% IQR (for bulk population of QDs; ***B***) and mean cluster fluorescence intensity (***C***) of KCC2–S940 (plain) and phospho-mimetic KCC2–S940D (pattern) in the absence (gray and fine pattern) or presence (black and coarse pattern) of 4-AP. Comparable diffusion behavior and clustering of KCC2–S940D and KCC2–S940. Note that 4-AP selectively reduced diffusion constraints (*$p = 2 \times 10^{-2}$) and clustering (***$p < 10^{-3}$) of KCC2–S940 but not of KCC2–S940D. ***C***, KCC2–S940, $n = 32$; KCC2–S940D, $n = 30$; KCC2–S940 plus 4-AP, $n = 31$; KCC2–S940D plus 4-AP, $n = 28$; three cultures. ***D–F***, Median QD diffusion coefficient *D* values ± 25–75% IQR (for bulk population of QDs; ***D***), mean cluster fluorescence intensity (***E***) of KCC2–Flag, and somatodendritic gradient of E_{GABA} (***F***) in the absence (plain) or presence (pattern) of the calpain protease inhibitor PD150606, in control (gray and fine pattern) versus 4-AP (black and large pattern) conditions. No effect of calpain activity blockade in basal activity conditions. The 4-AP-induced increase in KCC2 diffusion (***D***, **$p = 2 \times 10^{-3}$) and decrease in clustering (***E***, ***$p < 10^{-3}$) and function (***F***, **$p = 5 \times 10^{-3}$, *t* test) was reversed by calpain inhibitor (***D***, ***$p < 10^{-3}$; ***E***, *$p = 2 \times 10^{-2}$; ***F***, **$p = 6 \times 10^{-3}$, *t* test). ***E***, Control, $n = 32$; PD150606, $n = 34$; 4-AP $n = 31$; 4-AP plus PD150606, $n = 27$; three cultures. ***F***, Control, $n = 12$; 4-AP, $n = 16$; 4-AP plus PD150606, $n = 9$.

S940 residue mutated in either aspartate (S940D) or alanine (S940A) to mimic KCC2 S940 phosphorylated or dephosphorylated states, respectively. Under basal activity conditions, KCC2–S940A was 1.4-fold faster than the WT recombinant transporter (Fig. 9*A*). In contrast, the mobility and clustering of the KCC2–S940D transporter did not differ significantly from that of the WT KCC2–Flag (Fig. 9*B*,*C*). These results indicate that the majority of membrane KCC2 is phosphorylated on S940 under basal activity conditions, as suggested previously (Lee et al., 2011). However, S-to-D mutation on 940 residue prevented the 4-AP-induced increase in KCC2 lateral diffusion for bulk population of QDs (Fig. 9*B*; Table 4), as well as for extrasynaptic and synaptic QDs (Table 5). Furthermore, expression of the KCC2–S940D transporter precluded the 4-AP-induced increase in KCC2 cluster dispersal (Fig. 9*C*). Thus, activity-dependent regulation of KCC2 diffusion and clustering involves dephosphorylation of its S940 residue.

KCC2–CTD cleavage by calcium-activated calpain protease has been shown to contribute to the downregulation of KCC2 activity (Puskarjov et al., 2012; Zhou et al., 2012). Neuronal exposure to the calpain inhibitor PD150606 did not significantly alter KCC2 lateral diffusion or clustering (Fig. 9*D*,*E*), indicating that membrane-inserted KCC2 is not cleaved under basal activity conditions. However, calpain inhibition entirely blocked the activity-induced increase in KCC2–Flag diffusion, decreased in clustering, and reduced function (Fig. 9*D–F*). Tables 4 and 5 summarize the median *D* values of QDs in the absence or presence of the various drugs and mutations that target the molecular mechanisms underlying the effect of 4-AP. Our results indicate that the relief in diffusion constraints and subsequent dispersal of KCC2 clusters during increased neuronal activity rely on protein cleavage by intracellular, calcium-activated calpain.

Discussion

In this study, we investigated the membrane dynamics and clustering of KCC2 under basal and sustained neuronal activity in hippocampal neurons. Our work demonstrates that KCC2 membrane expression can be rapidly regulated by synaptic activity through changes in lateral diffusion. KCC2 is enriched in the vicinity of both excitatory and inhibitory synapses. In resting conditions, KCC2 is more confined at synapses compared with extrasynaptic regions. Restriction of KCC2 diffusion at excitatory, but not inhibitory synapses relies on its tethering to the actin cytoskeleton via the adaptor protein 4.1N. However, this structural interaction with F-actin is not essential for KCC2 clustering per se, suggesting that other mechanisms may be at play to cluster KCC2 in neuronal membranes. Finally, NMDAR activation and subsequent Ca^{2+} influx rapidly increase KCC2 lateral diffusion presumably through S940 dephosphorylation and calpain-dependent cleavage of KCC2–CTD. This effect is correlated to a reversible dispersal of KCC2 membrane clusters and reduced chloride export. Thus, lateral diffusion and clustering of KCC2 are key mechanisms that rapidly and reversibly regulate KCC2 membrane expression and function through glutamate signaling.

Consistent with its synaptic aggregation, KCC2 diffusion was restricted in the vicinity of synapses compared with extrasynaptic regions. Importantly, KCC2 DT at excitatory synapses was longer than at inhibitory synapses, suggestive of different molecular constraints to the diffusion of KCC2 at these sites. KCC2 was shown to be involved in both the morphogenesis of dendritic spines (Li et al., 2007; Fiumelli et al., 2013) and the efficacy of glutamatergic transmission (Gauvain et al., 2011) through structural interactions with the actin cytoskeleton likely involving 4.1N. Therefore, we tested the hypothesis that restricted diffusion of KCC2 at excitatory synapses relies on its interaction with actin. Inhibition of F-actin polymerization using latrunculin A, overexpression of KCC2–CTD as a dominant negative of its intracellular interactions, or knockdown of its intracellular partner 4.1N (Li et al., 2007) by RNA interference selectively induced the escape of KCC2 from

Table 4. Molecular mechanisms underlying 4-AP-dependent regulation of KCC2 lateral diffusion

	Median D (10^{-2} $\mu m^2 s^{-1}$) for bulk population of QDs			
	Control	4-AP	Drug/mutant	Drug/mutant + 4-AP
Dynamin inhibitor	5.8 (202, 14, 2)	6.3 (249, 10, 2)	2.1 (193, 10, 2)	3.9 (200, 7, 2)
TTX	4.6 (318, 26, 3)	6.3 (303, 21, 3)	5.1 (324, 14, 3)	4.8 (230, 16, 3)
AP-5	2.9 (391, 29, 3)	4.0 (325, 24, 3)	2.3 (322, 17, 3)	2.2 (344, 20, 3)
EGTA	3.4 (165, 17, 3)	6.6 (181, 19, 3)	3.6 (157, 17, 3)	3.7 (213, 20, 3)
NBQX	3.6 (366, 31, 4)	4.4 (360, 24, 4)	3.2 (220, 22, 4)	4.1 (335, 18, 4)
R,*S*-MCPG	3.4 (308, 25, 3)	4.2 (319, 19, 3)	2.8 (246, 15, 3)	3.6 (308, 16, 3)
S940A	3.4 (270, 18, 3)	n.d.	4.6 (234, 14, 3)	n.d.
S940D	4.1 (158, 13, 2)	6.2 (191, 9, 2)	4.1 (256, 12, 2)	3.7 (214, 11, 2)
PD150606	4.7 (180, 13, 2)	7.1 (197, 9, 2)	5.4 (216, 10, 2)	4.9 (198, 9, 2)

Numbers in parentheses indicate the numbers of QDs, cells, and cultures analyzed. n.d., Not determined.

Table 5. The KCC2–S940D mutant and PD150606 calpain inhibitor prevented the 4-AP-induced increased mobility of synaptic and extrasynaptic KCC2–Flag transporters

	Median D (10^{-2} $\mu m^2 s^{-1}$)					
	Extra		ES		IS	
	Ctrl	4AP	Ctrl	4AP	Ctrl	4AP
S940D	4.1 (176)	4.1 (190)	2.9 (68)	2.3 (81)	2.8 (98)	2.3 (78)
PD150606	4.5 (139)	4.8 (118)	4.1 (72)	3.4 (44)	3.6 (85)	2.7 (53)

Numbers in parentheses indicate the numbers of QDs analyzed. The number of cells and cultures analyzed are as in Table 4. In all cases, there was no statistical significance between control and 4-AP conditions. Ctrl, Control; Extra, QDs at extrasynaptic sites; ES, QDs at excitatory synapses; IS, QDs at inhibitory synapses.

excitatory but not inhibitory synapses. Thus, KCC2 diffusion at excitatory and inhibitory synapses might not be hindered by the same intracellular interactions. F-actin is known to be enriched in dendritic spines but not on dendritic shafts in which inhibitory synapses are formed. Therefore, F-actin enrichment could account for the selective impact of cytoskeleton manipulations on KCC2 diffusion at excitatory synapses. The involvement of actin tethering on the hindering of KCC2 diffusion at excitatory synapses may have important implications regarding KCC2 function in dendritic spines. In a former study, we showed that KCC2 contributes to a diffusion barrier in dendritic spines through its structural interaction with the actin cytoskeleton, thereby restricting translocation of transmembrane proteins, including GluA1-containing AMPARs (Gauvain et al., 2011). Thus, release of actin-tethered KCC2 at excitatory synapses during enhanced neuronal activity could act to facilitate protein translocation in dendritic spines and thereby contribute to synaptic plasticity (Czöndör et al., 2012; Czöndör and Thoumine, 2013).

Increased lateral mobility of transmembrane proteins is often correlated with cluster dispersal (Bannai et al., 2009; Muir et al., 2010; Bouthour et al., 2011). Thus, we investigated whether the formation of KCC2 clusters was dependent on interactions of KCC2–CTD with intracellular partners by overexpressing this domain as a dominant negative. Surprisingly, KCC2 clusters were not dispersed during KCC2–CTD overexpression. This contrasts with the results obtained by Watanabe et al. (2009) showing reduced clustering of a KCC2 deletion mutant lacking the intracellular 1089–1116 sites. This discrepancy may be explained by differences in the methodology. Indeed, the experimental procedure used by Watanabe et al. did not permit to discriminate between cytoplasmic and membrane-inserted transporters, whereas we selectively stained the membrane pool of KCC2. We propose that deletion of the KCC2 1089–1116 sites may increase the intracellular pool of KCC2, thus hindering detection of membrane-inserted clusters. Lipid rafts are membrane microdomains enriched in cholesterol and sphingolipids (Simons and Toomre, 2000) and may participate in KCC2 clustering. Like the other CCC family members KCC3, KCC4 (Fujii et al., 2008), NKCC1, and Na^+-Cl^- cotransporter (Welker et al., 2008), KCC2 is associated with lipid rafts (Hartmann et al., 2009; Watanabe et al., 2009), and disruption of those by cholesterol depletion disperses KCC2 clusters in cultured hippocampal neurons (Watanabe et al., 2009). Thus, KCC2 clustering per se does not seem to rely on its interaction with the actin cytoskeleton, but subcellular localization of KCC2-containing rafts might depend on actin tethering through KCC2–CTD. Similarly to the serotonin transporter (Chang et al., 2012), KCC2 may remain confined to membrane rafts after relaxation of actin-associated molecular constraints. Actin-untethering may then relieve diffusion constraints onto KCC2-containing lipid rafts. KCC2 clustering may also involve an oligomerization process. KCC2 is known to multimerize into dimers, trimers, or tetramers (Blaesse et al., 2006; Simard et al., 2007; Uvarov et al., 2009). Preventing phosphorylation of Y1087 residue disrupts oligomerization and clustering of KCC2, suggesting a tight link between these two mechanisms (Watanabe et al., 2009). Thus, one or several molecular mechanisms may be at play to contribute to KCC2 aggregation. Our findings of different diffusion constraints of KCC2 at excitatory versus inhibitory synapses further support this hypothesis.

KCC2 clustering may serve to localize and concentrate the transporter to membrane subdomains, such as excitatory or inhibitory synapses. Clustering may also represent a mechanism for rapid alteration of KCC2 function. In fact, KCC2 dispersal after disruption of membrane rafts is correlated with a loss of function in hippocampal neurons (Watanabe et al., 2009), whereas aggregation in cholesterol-enriched membrane rafts upregulates KCC2 function. In our experiments, however, overexpression of the CTD of KCC2 did not alter KCC2 transport function, suggesting that aggregation but not actin tethering of KCC2 may be essential for its function.

Our results suggest that a transient increase in synaptic activity may then permit a rapid and local regulation of KCC2 diffusion/clustering and therefore function at excitatory and/or inhibitory synapses. Rapid activity-induced dephosphorylation of S940 and phosphorylation of Y903/1087 leads to reduced membrane stability of KCC2 through increased endocytosis and targeting to lysosomal degradation (Lee et al., 2010, 2011). KCC2–CTD cleavage by calcium-activated calpain protease also contributes to the downregulation of KCC2 activity (Puskarjov et al., 2012; Zhou et al., 2012). We showed that increasing neuronal activity—leading to NMDAR activation and subsequent Ca^{2+} influx, dephosphorylation of KCC2 S940, and calpain cleavage of its CTD—rapidly increases the lateral mobility of KCC2 while reducing its clustering and chloride export activity in neurons. Interestingly, the effect of increased activity on KCC2 diffusion was prevented by either calpain inhibitor or expression of phospho-mimetic KCC2–S940D mutant. Because S940 is located on the C-terminal tail of the transporter, which is cleaved by calpain, we propose that dephosphorylation of S940 may be a prerequisite for calpain cleavage of membrane-associated transporter and lead to KCC2 endocytosis and subsequent recycling or degradation. Activity-induced reduction of clustering may then be an inter-

mediate mechanism affecting KCC2 function. Increased neuronal activity leading to changes in KCC2 phosphorylation states may lead to a dispersion of the clusters and freely moving transporters may then become available for internalization and lysosomal degradation.

NMDAR-induced increase in KCC2 lateral mobility and cluster dispersal may have important implications for the efficacy of GABA signaling. The rapid, activity-dependent disruption of KCC2 diffusion and clustering impacts GABAergic transmission through reduced extrusion of chloride ions. This regulation, together with the NMDAR-dependent increase in $GABA_AR$ diffusion and cluster dispersal (Bannai et al., 2009; Muir et al., 2010; Niwa et al., 2012), may then act to decrease the efficacy of GABAergic synapses and in turn facilitate long-term potentiation of excitatory synapses. Furthermore, KCC2 function is reduced under pathological conditions associated with enhanced neuronal activity, thereby contributing to an altered balance of excitation to inhibition that may contribute to excitotoxicity or anomalous synchronous activities underlying seizures (Reid et al., 2001; Rivera et al., 2002, 2004; Huberfeld et al., 2007; Pathak et al., 2007; Wake et al., 2007; Li et al., 2008; Shimizu-Okabe et al., 2011). Activity-driven dispersal of KCC2 clusters may then be one of the first molecular mechanisms favoring the emergence of these anomalous activities. Thus, favoring the membrane stability of KCC2 clusters might provide a new therapeutic strategy for the prevention of several neurological disorders, such as epilepsy, neuropathic pain, and posttraumatic spasticity.

References

Acton BA, Mahadevan V, Mercado A, Uvarov P, Ding Y, Pressey J, Airaksinen MS, Mount DB, Woodin MA (2012) Hyperpolarizing GABAergic transmission requires the KCC2 C-terminal ISO domain. J Neurosci 32:8746–8751. CrossRef Medline

Alivisatos AP, Gu W, Larabell C (2005) Quantum dots as cellular probes. Annu Rev Biomed Eng 7:55–76. CrossRef Medline

Allison DW, Chervin AS, Gelfand VI, Craig AM (2000) Postsynaptic scaffolds of excitatory and inhibitory synapses in hippocampal neurons: maintenance of core components independent of actin filaments and microtubules. J Neurosci 20:4545–4554. Medline

Báldi R, Varga C, Tamás G (2010) Differential distribution of KCC2 along the axo-somato-dendritic axis of hippocampal principal cells. Eur J Neurosci 32:1319–1325. CrossRef Medline

Bannai H, Lévi S, Schweizer C, Dahan M, Triller A (2006) Imaging the lateral diffusion of membrane molecules with quantum dots. Nat Protoc 1:2628–2634. CrossRef Medline

Bannai H, Lévi S, Schweizer C, Inoue T, Launey T, Racine V, Sibarita JB, Mikoshiba K, Triller A (2009) Activity-dependent tuning of inhibitory neurotransmission based on GABAAR diffusion dynamics. Neuron 62:670–682. CrossRef Medline

Barthó P, Payne JA, Freund TF, Acsády L (2004) Differential distribution of the KCl cotransporter KCC2 in thalamic relay and reticular nuclei. Eur J Neurosci 20:965–975. CrossRef Medline

Bartho P, Curto C, Luczak A, Marguet SL, Harris KD (2009) Population coding of tone stimuli in auditory cortex: dynamic rate vector analysis. Eur J Neurosci 30:1767–1778. CrossRef Medline

Bats C, Groc L, Choquet D (2007) The interaction between Stargazin and PSD-95 regulates AMPA receptor surface trafficking. Neuron 53:719–734. CrossRef Medline

Belenky MA, Yarom Y, Pickard GE (2008) Heterogeneous expression of gamma-aminobutyric acid and gamma-aminobutyric acid-associated receptors and transporters in the rat suprachiasmatic nucleus. J Comp Neurol 506:708–732. CrossRef Medline

Blaesse P, Guillemin I, Schindler J, Schweizer M, Delpire E, Khiroug L, Friauf E, Nothwang HG (2006) Oligomerization of KCC2 correlates with development of inhibitory neurotransmission. J Neurosci 26:10407–10419. CrossRef Medline

Bonneau S, Dahan M, Cohen LD (2005) Single quantum dot tracking based on perceptual grouping using minimal paths in a spatiotemporal volume. IEEE Trans Image Process 14:1384–1395. CrossRef Medline

Bouthour W, Leroy F, Emmanuelli C, Carnaud M, Dahan M, Poncer JC, Lévi S (2012) A human mutation in Gabrg2 associated with generalized epilepsy alters the membrane dynamics of GABAA receptors. Cereb Cortex 22:1542–1553. CrossRef Medline

Chamma I, Chevy Q, Poncer JC, Lévi S (2012) Role of the neuronal K-Cl co-transporter KCC2 in inhibitory and excitatory neurotransmission. Front Cell Neurosci 6:5. CrossRef Medline

Chang JC, Tomlinson ID, Warnement MR, Ustione A, Carneiro AM, Piston DW, Blakely RD, Rosenthal SJ (2012) Single molecule analysis of serotonin transporter regulation using antagonist-conjugated quantum dots reveals restricted, p38 MAPK-dependent mobilization underlying uptake activation. J Neurosci 32:8919–8929. CrossRef Medline

Charrier C, Ehrensperger MV, Dahan M, Lévi S, Triller A (2006) Cytoskeleton regulation of glycine receptor number at synapses and diffusion in the plasma membrane. J Neurosci 26:8502–8511. CrossRef Medline

Czöndör K, Mondin M, Garcia M, Heine M, Frischknecht R, Choquet D, Sibarita JB, Thoumine OR (2012) Unified quantitative model of AMPA receptor trafficking at synapses. Proc Natl Acad Sci U S A 109:3522–3527. CrossRef Medline

Czöndör K, Thoumine O (2013) Biophysical mechanisms regulating AMPA receptor accumulation at synapses. Brain Res Bull 93:57–68. CrossRef Medline

Dahan M, Lévi S, Luccardini C, Rostaing P, Riveau B, Triller A (2003) Diffusion dynamics of glycine receptors revealed by single-quantum dot tracking. Science 302:442–445. CrossRef Medline

Ehrensperger MV, Hanus C, Vannier C, Triller A, Dahan M (2007) Multiple association states between glycine receptors and gephyrin identified by SPT analysis. Biophys J 92:3706–3718. CrossRef Medline

Feldmeyer D, Cull-Candy S (1996) Functional consequences of changes in NMDA receptor subunit expression during development. J Neurocytol 25:857–867. CrossRef Medline

Fiumelli H, Cancedda L, Poo MM (2005) Modulation of GABAergic transmission by activity via postsynaptic Ca^{2+}-dependent regulation of KCC2 function. Neuron 48:773–786. CrossRef Medline

Fiumelli H, Briner A, Puskarjov M, Blaesse P, Belem BJ, Dayer AG, Kaila K, Martin JL, Vutskits L (2013) An ion transport-independent role for the cation-chloride cotransporter KCC2 in dendritic spinogenesis in vivo. Cereb Cortex 23:378–388. CrossRef Medline

Fujii T, Takahashi Y, Itomi Y, Fujita K, Morii M, Tabuchi Y, Asano S, Tsukada K, Takeguchi N, Sakai H (2008) K^+-Cl^- cotransporter-3a up-regulates Na^+,K^+-ATPase in lipid rafts of gastric luminal parietal cells. J Biol Chem 283:6869–6877. CrossRef Medline

Gauvain G, Chamma I, Chevy Q, Cabezas C, Irinopoulou T, Bodrug N, Carnaud M, Lévi S, Poncer JC (2011) The neuronal K-Cl cotransporter KCC2 influences postsynaptic AMPA receptor content and lateral diffusion in dendritic spines. Proc Natl Acad Sci U S A 108:15474–15479. CrossRef Medline

Goslin K, Asmussen H, Banker G (1998) Rat hippocampal neurons in low-density culture. Cambridge, MA: Massachusetts Institute of Technology.

Gulyás AI, Sík A, Payne JA, Kaila K, Freund TF (2001) The KCl cotransporter, KCC2, is highly expressed in the vicinity of excitatory synapses in the rat hippocampus. Eur J Neurosci 13:2205–2217. CrossRef Medline

Hanus C, Ehrensperger MV, Triller A (2006) Activity-dependent movements of postsynaptic scaffolds at inhibitory synapses. J Neurosci 26:4586–4595. CrossRef Medline

Hartmann AM, Blaesse P, Kranz T, Wenz M, Schindler J, Kaila K, Friauf E, Nothwang HG (2009) Opposite effect of membrane raft perturbation on transport activity of KCC2 and NKCC1. J Neurochem 111:321–331. CrossRef Medline

Huberfeld G, Wittner L, Clemenceau S, Baulac M, Kaila K, Miles R, Rivera C (2007) Perturbed chloride homeostasis and GABAergic signaling in human temporal lobe epilepsy. J Neurosci 27:9866–9873. CrossRef Medline

Hübner CA, Stein V, Hermans-Borgmeyer I, Meyer T, Ballanyi K, Jentsch TJ (2001) Disruption of KCC2 reveals an essential role of K-Cl cotransport already in early synaptic inhibition. Neuron 30:515–524. CrossRef Medline

Kaila K, Lamsa K, Smirnov S, Taira T, Voipio J (1997) Long-lasting GABA-mediated depolarization evoked by high-frequency stimulation in pyramidal neurons of rat hippocampal slice is attributable to a network-

driven, bicarbonate-dependent K^+ transient. J Neurosci 17:7662–7672. Medline

Khirug S, Huttu K, Ludwig A, Smirnov S, Voipio J, Rivera C, Kaila K, Khiroug L (2005) Distinct properties of functional KCC2 expression in immature mouse hippocampal neurons in culture and in acute slices. Eur J Neurosci 21:899–904. CrossRef Medline

Kitamura A, Ishibashi H, Watanabe M, Takatsuru Y, Brodwick M, Nabekura J (2008) Sustained depolarizing shift of the GABA reversal potential by glutamate receptor activation in hippocampal neurons. Neurosci Res 62: 270–277. CrossRef Medline

Krapf R, Berry CA, Verkman AS (1988) Estimation of intracellular chloride activity in isolated perfused rabbit proximal convoluted tubules using a fluorescent indicator. Biophys J 53:955–962. CrossRef Medline

Kusumi A, Sako Y, Yamamoto M (1993) Confined lateral diffusion of membrane receptors as studied by single particle tracking (nanovid microscopy). Effects of calcium-induced differentiation in cultured epithelial cells. Biophys J 65:2021–2040. CrossRef Medline

Lee HH, Walker JA, Williams JR, Goodier RJ, Payne JA, Moss SJ (2007) Direct protein kinase C-dependent phosphorylation regulates the cell surface stability and activity of the potassium chloride cotransporter KCC2. J Biol Chem 282:29777–29784. CrossRef Medline

Lee HH, Jurd R, Moss SJ (2010) Tyrosine phosphorylation regulates the membrane trafficking of the potassium chloride co-transporter KCC2. Mol Cell Neurosci 45:173–179. CrossRef Medline

Lee HH, Deeb TZ, Walker JA, Davies PA, Moss SJ (2011) NMDA receptor activity downregulates KCC2 resulting in depolarizing GABA(A) receptor-mediated currents. Nat Neurosci 14:736–743. CrossRef Medline

Li H, Tornberg J, Kaila K, Airaksinen MS, Rivera C (2002) Patterns of cation-chloride cotransporter expression during embryonic rodent CNS development. Eur J Neurosci 16:2358–2370. CrossRef Medline

Li H, Khirug S, Cai C, Ludwig A, Blaesse P, Kolikova J, Afzalov R, Coleman SK, Lauri S, Airaksinen MS, Keinänen K, Khiroug L, Saarma M, Kaila K, Rivera C (2007) KCC2 interacts with the dendritic cytoskeleton to promote spine development. Neuron 56:1019–1033. CrossRef Medline

Li X, Zhou J, Chen Z, Chen S, Zhu F, Zhou L (2008) Long-term expressional changes of Na^+-K^+-Cl^- co-transporter 1 (NKCC1) and K^+-Cl^- co-transporter 2 (KCC2) in CA1 region of hippocampus following lithium-pilocarpine induced status epilepticus (PISE). Brain Res 1221:141–146. CrossRef Medline

Lin DT, Makino Y, Sharma K, Hayashi T, Neve R, Takamiya K, Huganir RL (2009) Regulation of AMPA receptor extrasynaptic insertion by 4.1N, phosphorylation and palmitoylation. Nat Neurosci 12:879–887. CrossRef Medline

Marandi N, Konnerth A, Garaschuk O (2002) Two-photon chloride imaging in neurons of brain slices. Pflugers Arch 445:357–365. CrossRef Medline

Markova O, Mukhtarov M, Real E, Jacob Y, Bregestovski P (2008) Genetically encoded chloride indicator with improved sensitivity. J Neurosci Methods 170:67–76. CrossRef Medline

Marks B, McMahon HT (1998) Calcium triggers calcineurin-dependent synaptic vesicle recycling in mammalian nerve terminals. Curr Biol 8:740–749. CrossRef Medline

Metzger F, Repunte-Canonigo V, Matsushita S, Akemann W, Diez-Garcia J, Ho CS, Iwasato T, Grandes P, Itohara S, Joho RH, Knöpfel T (2002) Transgenic mice expressing a pH and Cl^- sensing yellow-fluorescent protein under the control of a potassium channel promoter. Eur J Neurosci 15:40–50. CrossRef Medline

Muir J, Arancibia-Carcamo IL, MacAskill AF, Smith KR, Griffin LD, Kittler JT (2010) NMDA receptors regulate GABAA receptor lateral mobility and clustering at inhibitory synapses through serine 327 on the gamma2 subunit. Proc Natl Acad Sci U S A 107:16679–16684. CrossRef Medline

Niwa F, Bannai H, Arizono M, Fukatsu K, Triller A, Mikoshiba K (2012) Gephyrin-independent GABA(A)R mobility and clustering during plasticity. PLoS One 7:e36148. CrossRef Medline

Pathak HR, Weissinger F, Terunuma M, Carlson GC, Hsu FC, Moss SJ, Coulter DA (2007) Disrupted dentate granule cell chloride regulation enhances synaptic excitability during development of temporal lobe epilepsy. J Neurosci 27:14012–14022. CrossRef Medline

Puskarjov M, Ahmad F, Kaila K, Blaesse P (2012) Activity-dependent cleavage of the K-Cl cotransporter KCC2 mediated by calcium-activated protease calpain. J Neurosci 32:11356–11364. CrossRef Medline

Reid KH, Li GY, Payne RS, Schurr A, Cooper NG (2001) The mRNA level of the potassium-chloride cotransporter KCC2 covaries with seizure susceptibility in inferior colliculus of the post-ischemic audiogenic seizure-prone rat. Neurosci Lett 308:29–32. CrossRef Medline

Rivera C, Voipio J, Payne JA, Ruusuvuori E, Lahtinen H, Lamsa K, Pirvola U, Saarma M, Kaila K (1999) The K^+/Cl^- co-transporter KCC2 renders GABA hyperpolarizing during neuronal maturation. Nature 397: 251–255. CrossRef Medline

Rivera C, Li H, Thomas-Crusells J, Lahtinen H, Viitanen T, Nanobashvili A, Kokaia Z, Airaksinen MS, Voipio J, Kaila K, Saarma M (2002) BDNF-induced TrkB activation down-regulates the K^+-Cl^- cotransporter KCC2 and impairs neuronal Cl^- extrusion. J Cell Biol 159:747–752. CrossRef Medline

Rivera C, Voipio J, Thomas-Crusells J, Li H, Emri Z, Sipilä S, Payne JA, Minichiello L, Saarma M, Kaila K (2004) Mechanism of activity-dependent downregulation of the neuron-specific K-Cl cotransporter KCC2. J Neurosci 24:4683–4691. CrossRef Medline

Saxton MJ, Jacobson K (1997) Single-particle tracking: applications to membrane dynamics. Annu Rev Biophys Biomol Struct 26:373–399. CrossRef Medline

Shimizu-Okabe C, Tanaka M, Matsuda K, Mihara T, Okabe A, Sato K, Inoue Y, Fujiwara T, Yagi K, Fukuda A (2011) KCC2 was downregulated in small neurons localized in epileptogenic human focal cortical dysplasia. Epilepsy Res 93:177–184. CrossRef Medline

Simard CF, Bergeron MJ, Frenette-Cotton R, Carpentier GA, Pelchat ME, Caron L, Isenring P (2007) Homooligomeric and heterooligomeric associations between K^+-Cl^- cotransporter isoforms and between K^+-Cl^- and Na^+-K^+-Cl^- cotransporters. J Biol Chem 282:18083–18093. CrossRef Medline

Simons K, Toomre D (2000) Lipid rafts and signal transduction. Nat Rev Mol Cell Biol 1:31–39. CrossRef Medline

Szabadics J, Varga C, Molnár G, Oláh S, Barzó P, Tamás G (2006) Excitatory effect of GABAergic axo-axonic cells in cortical microcircuits. Science 311:233–235. CrossRef Medline

Takayama C, Inoue Y (2006) Developmental localization of potassium chloride co-transporter 2 in granule cells of the early postnatal mouse cerebellum with special reference to the synapse formation. Neuroscience 143:757–767. CrossRef Medline

Trapp S, Lückermann M, Brooks PA, Ballanyi K (1996) Acidosis of rat dorsal vagal neurons in situ during spontaneous and evoked activity. J Physiol 496:695–710. Medline

Triller A, Choquet D (2008) New concepts in synaptic biology derived from single-molecule imaging. Neuron 59:359–374. CrossRef Medline

Uvarov P, Ludwig A, Markkanen M, Soni S, Hübner CA, Rivera C, Airaksinen MS (2009) Coexpression and heteromerization of two neuronal K-Cl cotransporter isoforms in neonatal brain. J Biol Chem 284:13696–13704. CrossRef Medline

Vale C, Caminos E, Martinez-Galán JR, Juiz JM (2005) Expression and developmental regulation of the K^+-Cl^- cotransporter KCC2 in the cochlear nucleus. Hear Res 206:107–115. CrossRef Medline

Vanhatalo S, Palva JM, Andersson S, Rivera C, Voipio J, Kaila K (2005) Slow endogenous activity transients and developmental expression of K^+-Cl^- cotransporter 2 in the immature human cortex. Eur J Neurosci 22:2799–2804. CrossRef Medline

Vinay L, Jean-Xavier C (2008) Plasticity of spinal cord locomotor networks and contribution of cation-chloride cotransporters. Brain Res Rev 57: 103–110. CrossRef Medline

Wake H, Watanabe M, Moorhouse AJ, Kanematsu T, Horibe S, Matsukawa N, Asai K, Ojika K, Hirata M, Nabekura J (2007) Early changes in KCC2 phosphorylation in response to neuronal stress result in functional down-regulation. J Neurosci 27:1642–1650. CrossRef Medline

Wang L, Kitai ST, Xiang Z (2006a) Activity-dependent bidirectional modification of inhibitory synaptic transmission in rat subthalamic neurons. J Neurosci 26:7321–7327. CrossRef Medline

Wang W, Gong N, Xu TL (2006b) Downregulation of KCC2 following LTP contributes to EPSP-spike potentiation in rat hippocampus. Biochem Biophys Res Commun 343:1209–1215. CrossRef Medline

Wang W, Wang H, Gong N, Xu TL (2006c) Changes of K^+-Cl^- cotransporter 2 (KCC2) and circuit activity in propofol-induced impairment of long-term potentiation in rat hippocampal slices. Brain Res Bull 70:444–449. CrossRef Medline

Waseem T, Mukhtarov M, Buldakova S, Medina I, Bregestovski P (2010) Genetically encoded Cl-Sensor as a tool for monitoring of Cl-dependent pro-

cesses in small neuronal compartments. J Neurosci Methods 193:14–23. CrossRef Medline

Watanabe M, Wake H, Moorhouse AJ, Nabekura J (2009) Clustering of neuronal K^+-Cl^- cotransporters in lipid rafts by tyrosine phosphorylation. J Biol Chem 284:27980–27988. CrossRef Medline

Welker P, Böhlick A, Mutig K, Salanova M, Kahl T, Schlüter H, Blottner D, Ponce-Coria J, Gamba G, Bachmann S (2008) Renal Na^+-K^+-Cl^- cotransporter activity and vasopressin-induced trafficking are lipid raft-dependent. Am J Physiol Renal Physiol 295:F789–F802. CrossRef Medline

Williams JR, Sharp JW, Kumari VG, Wilson M, Payne JA (1999) The neuron-specific K-Cl cotransporter, KCC2. Antibody development and initial characterization of the protein. J Biol Chem 274:12656–12664. CrossRef Medline

Woodin MA, Ganguly K, Poo MM (2003) Coincident pre- and postsynaptic activity modifies GABAergic synapses by postsynaptic changes in Cl^- transporter activity. Neuron 39:807–820. CrossRef Medline

Zhao B, Wong AY, Murshid A, Bowie D, Presley JF, Bedford FK (2008) Identification of a novel di-leucine motif mediating K(+)/Cl(-) cotransporter KCC2 constitutive endocytosis. Cell Signal 20:1769–1779. CrossRef Medline

Zhou HY, Chen SR, Byun HS, Chen H, Li L, Han HD, Lopez-Berestein G, Sood AK, Pan HL (2012) *N*-methyl-D-aspartate receptor- and calpain-mediated proteolytic cleavage of K^+-Cl^- cotransporter-2 impairs spinal chloride homeostasis in neuropathic pain. J Biol Chem 287:33853–33864. CrossRef Medline

III. Role of the neuronal K-Cl co-transporter KCC2 in inhibitory and excitatory neurotransmission.

During my PhD I had the opportunity to participate in the writing of a review on KCC2 function at inhibitory and excitatory synapses published in “Frontiers in cellular neuroscience”

frontiers in
CELLULAR NEUROSCIENCE

REVIEW ARTICLE
published: 21 February 2012
doi: 10.3389/fncel.2012.00005

Role of the neuronal K-Cl co-transporter KCC2 in inhibitory and excitatory neurotransmission

Ingrid Chamma*[1,2,3], *Quentin Chevy*[1,2,3], *Jean Christophe Poncer*[1,2,3]* and *Sabine Lévi*[1,2,3]

[1] *INSERM, UMR-839, Paris, France*
[2] *Université Pierre et Marie Curie, Paris, France*
[3] *Institut du Fer à Moulin, Paris, France*

Edited by:
Enrico Cherubini, International School for Advanced Studies, Italy

Reviewed by:
Melanie A. Woodin, University of Toronto, Canada
Enrica M. Petrini, Italian Institute of Technology, Italy

***Correspondence:**
Sabine Lévi and Jean Christophe Poncer, INSERM UMR-839/UPMC, Institut du Fer à Moulin, Plasticity in Cortical Networks and Epilepsy, 17 rue du Fer à Moulin, 75005 Paris, France.
e-mail: sabine.levi@inserm.fr; jean-christophe.poncer@inserm.fr

The K-Cl co-transporter KCC2 plays multiple roles in the physiology of central neurons and alterations of its function and/or expression are associated with several neurological conditions. By regulating intraneuronal chloride homeostasis, KCC2 strongly influences the efficacy and polarity of the chloride-permeable γ-aminobutyric acid (GABA) type A and glycine receptor (GlyR) mediated synaptic transmission. This appears particularly critical for the development of neuronal circuits as well as for the dynamic control of GABA and glycine signaling in mature networks. The activity of the transporter is also associated with transmembrane water fluxes which compensate solute fluxes associated with synaptic activity. Finally, KCC2 interaction with the actin cytoskeleton appears critical both for dendritic spine morphogenesis and the maintenance of glutamatergic synapses. In light of the pivotal role of KCC2 in the maturation and function of central synapses, it is of particular importance to understand the cellular and molecular mechanisms underlying its regulation. These include development and activity-dependent modifications both at the transcriptional and post-translational levels. We emphasize the importance of post-translational mechanisms such as phosphorylation and dephosphorylation, oligomerization, cell surface stability, clustering and membrane diffusion for the rapid and dynamic regulation of KCC2 function.

Keywords: KCC2, neuronal activity, excitatory and inhibitory synapses, post-translational regulation

INTRODUCTION

Fast synaptic transmission relies on ion fluxes through ligand-gated channels. Therefore, the maintenance of transmembrane ionic gradients is critical to preserve synaptic efficacy. The electroneutral KCC2 co-transporter is the major chloride (Cl^-) extruder in mature neurons (Payne et al., 1996; Williams et al., 1999; Karadsheh and Delpire, 2001; Uvarov et al., 2005). Unlike other KCC family members known to regulate cell volume in non-neuronal cells (Zeuthen and MacAulay, 2002; Zeuthen, 2010), KCC2 has been mostly studied for its role in maintaining low intracellular chloride concentration $[Cl^-]_i$ in neurons [reviewed in (Ben-Ari, 2002; Blaesse et al., 2009)]. $[Cl^-]_i$ influences the efficacy and polarity of synaptic transmission mediated by γ-aminobutyric acid (GABA) type A receptors (GABAARs) and glycine receptors (GlyRs) which both flux chloride ions. The spatio-temporal regulation of KCC2 mRNA and protein expression levels orchestrates the developmental shift in synaptic glycinergic and GABAergic transmission from depolarizing to hyperpolarizing or shunting in many but not all species (Rivera et al., 1999; Vanhatalo et al., 2005) and brain regions (Li et al., 2002; Vinay and Jean-Xavier, 2008). GABAA receptor-mediated depolarization appears as a critical determinant of early network activities (Cherubini et al., 2011), circuit formation (Ben-Ari, 2002; Akerman and Cline, 2006), neuronal migration (Bortone and Polleux, 2009), and synapse maturation (Aguado et al., 2003). Recent studies also indicate a critical role of KCC2 in both the formation (Li et al., 2007) and functional maintenance (Gauvain et al., 2011) of glutamatergic synapses. These mechanisms appear independent of KCC2 function but instead involve KCC2 interaction with submembrane cytoskeleton.

KCC2 expression and function are tightly regulated by neuronal activity (Fiumelli and Woodin, 2007). This regulation involves trophic factors such as brain-derived neurotrophic factor (BDNF), neuronal intrinsic activity or the activity of excitatory synapses (Kaila et al., 1997; Rivera et al., 2002, 2004; Woodin et al., 2003; Fiumelli et al., 2005; Wang et al., 2006a–c; Kitamura et al., 2008; Lee et al., 2011). In some conditions, neuronal activity may either upregulate KCC2 to strengthen synaptic inhibition in a homeostatic manner or, on the contrary, downregulate KCC2 possibly to enhance the gain of recently active excitatory synapses. In several pathological conditions associated with enhanced excitation, suppression of KCC2 is often observed and may contribute to further alter the balance of excitation and inhibition, leading to excitotoxicity, or anomalous activities such as seizures (Reid et al., 2001; Rivera et al., 2002, 2004; Huberfeld et al., 2007; Pathak et al., 2007; Wake et al., 2007; Li et al., 2008b; Shimizu-Okabe et al., 2011). Therefore, KCC2 appears to mediate a crosstalk between excitatory and inhibitory transmission. It is, therefore, crucial to understand the mechanisms that control its expression and activity. Neuronal activity modulates KCC2 activity through both transcriptional and post-translational modifications. Whereas transcriptional mechanisms may be involved

in regional, developmental, and regulation of KCC2 activity in pathological conditions, post-translational mechanisms of KCC2 regulation occurs in a time scale compatible with a control by fast synaptic transmission (Woodin et al., 2003; Wang et al., 2006b; Fiumelli and Woodin, 2007; Wake et al., 2007; Kitamura et al., 2008; Chorin et al., 2011; Lee et al., 2011). Several recent and comprehensive reviews have addressed the biology of cation-chloride co-transporters (CCCs) both in neuronal (Blaesse et al., 2009) and non-neuronal cells (Gamba, 2005). Here, we will review the recent literature more specifically on (1) the subcellular distribution of KCC2 in relation with excitatory and inhibitory synapses, (2) its basic properties as well as its function at inhibitory and excitatory synapses, (3) its regulation during development and by neuronal activity. We will discuss the cellular and molecular mechanisms underlying its regulation.

STRUCTURE AND DIVERSITY OF KCC2 CO-TRANSPORTERS

The K-Cl co-transporter KCC2 is one of the nine cation chloride co-transporters encoded by the Slc12a one to nine genes [for review see (Gamba, 2005)]. Four KCC co-transporters have been identified so far (KCC1–4). KCC2 is the only KCC isoform exclusively expressed in central neurons (Payne et al., 1996; Williams et al., 1999; Karadsheh and Delpire, 2001; Uvarov et al., 2005). The lack of KCC2 mRNA expression in non-neuronal cells relies on binding of the neuron-restrictive silencer factor (NRSF) to the neuron-restrictive silencer element (NRSE) in KCC2 gene promoter (Uvarov et al., 2005). Two transcription factors up- or down-regulate KCC2 mRNA levels (Uvarov et al., 2006). The transcription factor early growth response 4 (Egr4 or NGFI-C) is a neuron-specific immediate early gene that enhances KCC2 expression (Uvarov et al., 2006). In contrast, the REST transcriptional repressor complex inhibits KCC2 mRNA level by binding to two repressor elements (RE-1) in the KCC2 gene (Yeo et al., 2009). The KCC2 mRNA is expressed with a gradual temporal increase from spinal cord and brainstem to higher brain structures (Li et al., 2002; Stein et al., 2004). Alternative splicing of the KCC2 gene (Slc12a5) gives rise to two KCC2 isoforms, KCC2a and KCC2b (Uvarov et al., 2007). The KCC2a transcript is expressed at low-level between E14-P60 (Uvarov et al., 2007). In contrast, the KCC2b mRNA is up-regulated by 10- and 35-fold in hippocampus and neocortex between E17 and P14 (Uvarov et al., 2007). Similarly to the transcripts, KCC2a protein shows only moderate changes during postnatal development, whereas KCC2b expression is strongly up-regulated (Uvarov et al., 2009). Therefore, KCC2a prevails in neonatal brain whereas KCC2b predominates in adult (Uvarov et al., 2009). KCC2b differs from KCC2a by an extra 40 amino acid residue in its *N*-terminal part that carries a putative binding site for the Ste20-related proline alanine-rich (SPAK) and oxidative stress response-1 (OSR1) kinases (Uvarov et al., 2007).

The KCC2 protein is a glycoprotein with a predicted topology of 12 membrane spanning segments flanked by two cytoplasmic carboxy- and amino-terminal domains of long and short size, respectively (Payne et al., 1996). The intracellular regions represent half of the total size of the molecule and are known so far to be the targets of several kinases and one phosphatase that regulate the function of the co-transporter (**Figure 1**). KCC2 carries putative phosphorylation sites for the Src-family tyrosine kinase [residues Tyr903, Tyr1087, (Lee et al., 2010)], the serine/threonine With no lysine kinase (Wnk) family (Wnk3, (Kahle et al., 2005); Wnk1 at residues Thr906, Thr1006, (Rinehart et al., 2009); Wnk2, (Rinehart et al., 2011), and the Ca^{2+}/phospholipid-dependent protein kinase C (PKC) (residues Thr34, Ser728, Thr787, Ser940, Ser1034, (Payne et al., 1996; Lee et al., 2007). Among the five putative PKC-dependent phosphorylation sites, the Ser940 residue is the major site of PKC phosphorylation in neurons (Lee et al., 2007). This site is specific of the KCC2 transporter (Payne et al., 1996) and can be dephosphorylated by the protein phosphatase 1 (PP1) (Lee et al., 2011).

KCC2 can exist as monomers (∼140 kDa), dimers (∼270 kDa), trimers (∼400 kDa), or tetramers (∼500 kDa) (Blaesse et al., 2006; Uvarov et al., 2009). Immunoblots and co-immunoprecipitation studies from brain extracts reported various oligomeric states of KCC2: KCC2a-KCC2a and KCC2b-KCC2b homo-dimers, KCC2a-KCC2b, and KCC2-KCC4 hetero-dimers (Blaesse et al., 2006; Simard et al., 2007; Uvarov et al., 2009). Although KCC oligomerization domains have not been identified so far, the carboxy-terminal domain appears to be required for oligomerization (Casula et al., 2001; Simard et al., 2004). Thus, truncation of KCC1 in its carboxy-terminus (up to residue 805) fails to oligomerize (Casula et al., 2001). KCC2 oligomers also associate through di-sulfide bounds (Uvarov et al., 2009), as described for other CCCs (Moore-Hoon and Turner, 2000; Blaesse et al., 2006).

CELLULAR AND SUBCELLULAR DISTRIBUTION IN NEURONS

REGIONAL EXPRESSION

KCC2a and KCC2b transcripts are expressed in mature neurons throughout the CNS including all layers of the cortex, neurons of the brainstem, thalamus, olfactory bulb, and spinal cord, CA1–CA4 pyramidal neurons of the hippocampus, granular layer, and cerebellar Purkinje neurons (Payne et al., 1996; Uvarov et al., 2007). Most published immunochemical data on KCC2 have been obtained with antibodies against a carboxy-terminal region of KCC2 common to both KCC2a and KCC2b isoforms (residues 932–1043, commercialized by Sigma, Millipore, AbCam, Life Span. . .). KCC2a and KCC2b isotype specific antibodies were recently generated: KCC2a, amino-terminal residues DPESRRHSVADPRRLPREDVK, (Uvarov et al., 2009); KCC2b, amino-terminal residues CEDGDGGANPGDGN, (Hubner et al., 2001). Finally, an antibody against the second extracellular loop of KCC2 (IFKAEDASGEAAAML residues) was obtained and characterized in Gagnon et al. (2007) but failed to yield specific staining in our hands. Since KCC2b prevails in adults, immunofluorescence (IF) data from adult tissue predominantly reveals the distribution of this isoform. KCC2 is detected in neurons of the cerebellum (Williams et al., 1999; Takayama and Inoue, 2006), all relay nuclei of the thalamus (Bartho et al., 2004), retina (Vardi et al., 2000; Vu et al., 2000; Gavrikov et al., 2006; Zhang et al., 2006; Li et al., 2008a), lateral superior olive (LSO) of the brainstem (Blaesse et al., 2006), neocortex (DeFazio et al., 2000; Szabadics et al., 2006), somatosensory cortex (Takayama and Inoue, 2006, 2010), hippocampus (Rivera et al., 1999; Gulyas et al., 2001), spinal cord (Hubner et al., 2001; Stil et al., 2009),

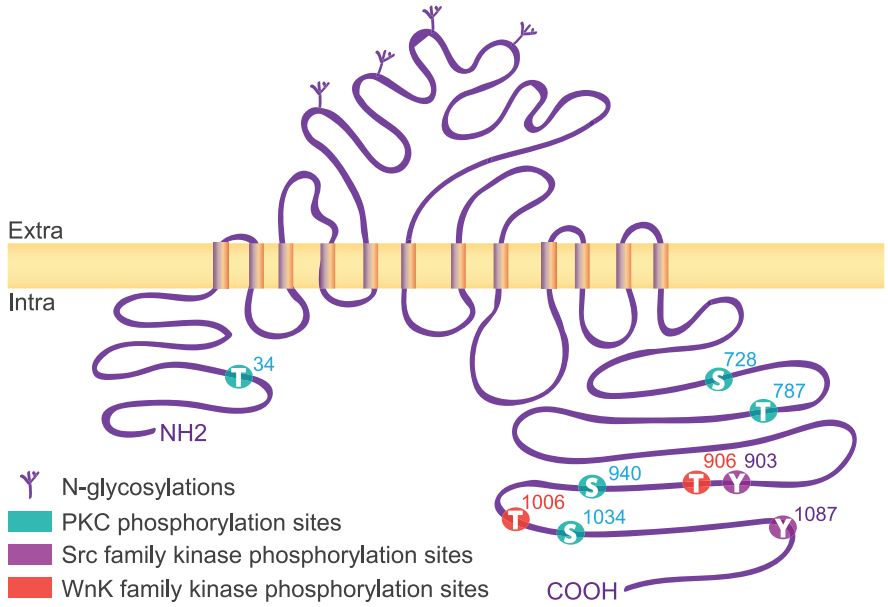

FIGURE 1 | Structure of KCC2. The rat KCC2 co-transporter is a large size (~140 kDa) protein with a predicted topology of 12 membrane spanning segments, a N-linked glycosylated extracellular domain between transmembrane domains 5 and 6, and is flanked by two cytoplasmic carboxy- and amino-terminal domains of 104 and 481 amino acids, respectively. As indicated, the intracellular regions are the targets of several kinases that regulate the function of the co-transporter.

cochlear nucleus (Vale et al., 2005; Yang et al., 2008), and hypothalamic suprachiasmatic nucleus (SCN) (Belenky et al., 2008).

CELLULAR COMPARTMENTALIZATION

KCC2 is restricted to the somato-dendritic compartment and excluded from the axon (Hubner et al., 2001; Szabadics et al., 2006; Bartho et al., 2009) including the initial segment (AIS) (Gulyas et al., 2001; Baldi et al., 2010). KCC2 immunoreactivity is usually evenly distributed along the somato-dendritic axis of neurons of the thalamus (Bartho et al., 2009), the granular layer of the cerebellum (Takayama and Inoue, 2006) and dentate gyrus granule cells (Baldi et al., 2010). However, in OFF bipolar cells and starburst cells of the retina, KCC2 is confined in distal dendrites (Vardi et al., 2000; Gavrikov et al., 2006). Similarly, in hippocampal CA1 pyramidal neurons, KCC2 may preferentially accumulate at GABAergic synapses formed onto distal rather than proximal dendrites (Baldi et al., 2010).

INTRACELLULAR VS. MEMBRANE DISTRIBUTION

Intracellular KCC2 labeling is found at a higher level in immature than in mature neurons. KCC2 decorates the membrane of transport vesicles in dendrites of P2 hippocampal neurons (Gulyas et al., 2001). In contrast, only little cytoplasmic KCC2 is detected in mature hippocampal neurons (Gulyas et al., 2001) as well as neurons of the cochlear nucleus (Vale et al., 2005) and isocortex (Szabadics et al., 2006). In the adult brain, organelles including Golgi apparatus and endoplasmic reticulum do not show KCC2 labeling (Takayama and Inoue, 2006) except in neurons of the SCN (Belenky et al., 2008). Instead, most KCC2 protein is found associated with the plasma membrane both in somatic and dendritic compartments (Williams et al., 1999; Gulyas et al., 2001; Hubner et al., 2001; Vale et al., 2005; Blaesse et al., 2006; Szabadics et al., 2006; Takayama and Inoue, 2006; Belenky et al., 2008; Bartho et al., 2009; Baldi et al., 2010). KCC2 exhibits a high turnover rate. It was shown that the membrane pool of KCC2 is partially (Rivera et al., 2004) or totally (Lee et al., 2007) replaced within 10 min under basal conditions.

SYNAPTIC LOCALIZATION

At the synaptic level, KCC2 is not found within presynaptic boutons except in terminals of the retinal ON bipolar cells (Vardi et al., 2000) and developing photoreceptor cells (Zhang et al., 2006). KCC2-coupled immunogold particles decorate the perisynaptic area of postsynaptic neuronal cell (Gulyas et al., 2001; Bartho et al., 2004; Blaesse et al., 2006; Takayama and Inoue, 2006). Consistent with a major role of the transporter in chloride homeostasis and GABA signaling (see below), KCC2 is found in the postsynaptic membrane near symmetrical inhibitory synapses in brainstem (Blaesse et al., 2006), SCN (Belenky et al., 2008), and spinal cord (Hubner et al., 2001). However, KCC2 also accumulates at or near excitatory synapses formed by cerebellar mossy fiber terminals onto granule cells (Takayama and Inoue, 2006), at terminals formed between the cortico-geniculate fibers and thalamic relay nuclei neurons (Bartho et al., 2004), at synapses in the brainstem (Blaesse et al., 2006) and at glutamatergic synapses in spine heads of principal cells of the hippocampus (Gulyas et al., 2001; Gauvain et al., 2011).

We have studied the subcellular distribution of KCC2 in cultured hippocampal neurons. In line with previous observations (Lee et al., 2007; Watanabe et al., 2009; Gauvain et al., 2011), KCC2 membrane distribution was usually punctate. Using confocal fluorescence microscopy, we found that KCC2

clusters decorate the cell body (**Figures 2A,B**), dendritic shafts (**Figure 2C**) and spines (**Figures 2A–D2**) of mature neurons (29 days *in vitro*). Optical sectioning through a dendrite highlighted the preferential membrane localization of the transporter (**Figures 2D2,D3**). On average, KCC2 IF was about 50% higher near cell surface compared with cytoplasm, reflecting a preferential membrane or sub-membrane localization of the transporter. The fluorescence intensity of KCC2 aggregates in spines was about threefold higher than in cytoplasm and twofold higher than on dendritic shaft, demonstrating KCC2 enrichment in spines. KCC2 clustering was also dependent on spine maturation and was maximal in mushroom-type spines, intermediate in stubby spines and absent in filopodia-like structures. KCC2 expression in relation with excitatory and inhibitory synapses was evaluated in hippocampal neurons co-immunolabeled with the glutamate and GABA receptor anchoring proteins PostSynaptic Density protein 95 kD (PSD95) and gephyrin (**Figures 2E1–G**). KCC2 clusters were found both near inhibitory (**Figures 2E1–E3,G**) and

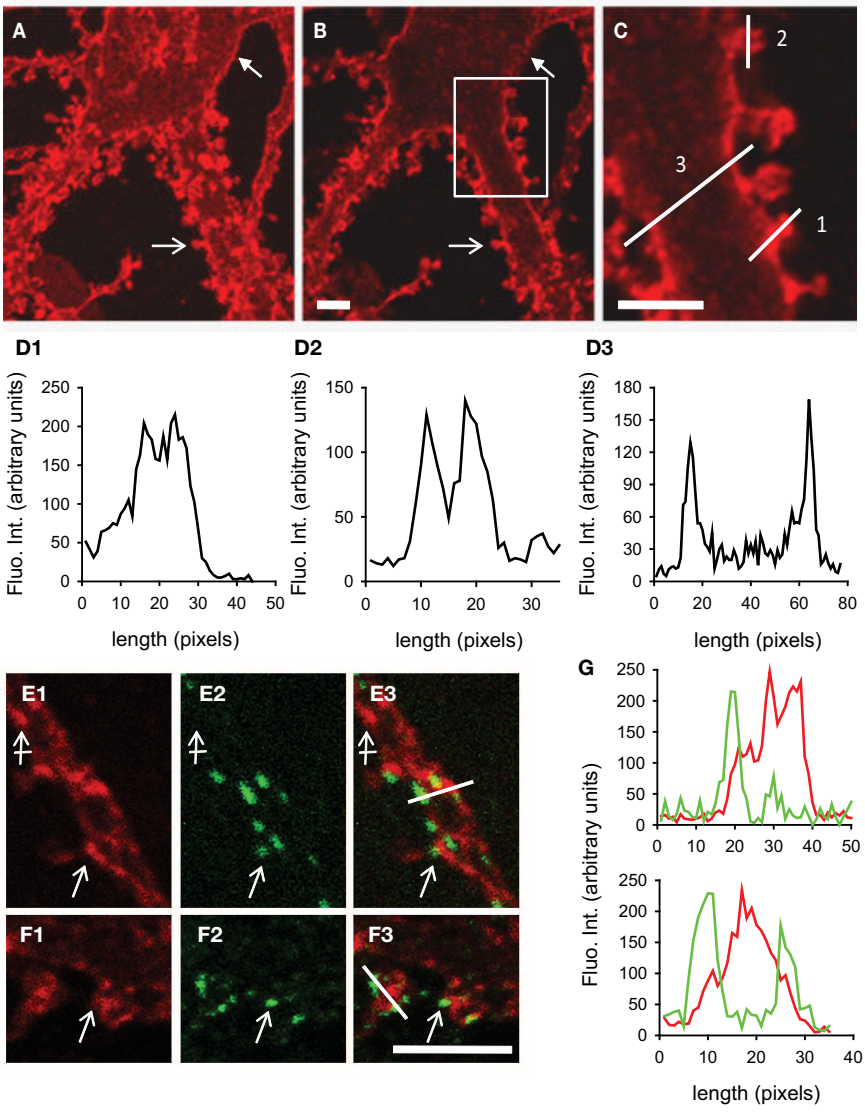

FIGURE 2 | KCC2 clustering in rat hippocampal neurons at 29DIV. (A) Maximum intensity projection of confocal optical sections showing KCC2 at the periphery of somata (filled arrow) and in spines (empty arrow). **(B,C)** optical sectioning from the same neuron as in **(A)**. Boxed region in **(B)** is shown enlarged in **(C)**. Adapted from Gauvain et al. (2011) with permission. Scale bars, 5 μm. **(D)** Fluorescence intensity in arbitrary units per pixel along the lines drawn in **(C)** showing enrichment of KCC2 in dendritic spines **(D1)**, preferential plasma membrane localization of KCC2 in dendritic spines **(D2)** and shafts **(D3)** as compared with the cytoplasm. **(E1–F3)** Dual labeling of KCC2 (red in **E1, E3, F1, F3**) and the GABA and glutamate receptor anchoring proteins gephyrin (green in **E2, E3**) or PSD-95 (green in **F2, F3**). Scale bars, 5 μm. KCC2 forms many clusters on dendritic shafts and spines (empty arrows). Clusters are found at distance from synapses (crossed arrow) as well as near gephyrin-labeled inhibitory synapses (empty arrow in **E1–3**) and PSD95-stained excitatory PSD (empty arrow in **F1–3**). **(G)** Fluorescence intensity in arbitrary units per pixel along the lines drawn in **(E3)** and **(F3)** showing juxtaposition but no colocalization of KCC2 (red) with gephyrin (green, top) or PSD95 (green, bottom).

excitatory (**Figure 2F1–F3,G**) synapses formed on dendrites as well as on the extrasynaptic membrane. However, although concentrated in spines, the co-transporter did not preferentially accumulate within the postsynaptic differentiation (PSD). Instead, it was often localized at the periphery of the PSD (**Figure 2G**). Quantification also revealed the absence of specific KCC2 accumulation at inhibitory synapses (**Figure 2G**). Thus, KCC2 appears to aggregate in close vicinity rather than within synapses, suggesting the existence of specific molecular anchoring mechanisms acting to influence KCC2 clustering.

BASIC PROPERTIES OF THE KCC2 CO-TRANSPORTER

ION CO-TRANSPORT

KCC2 is a secondary active transporter, i.e., it uses the energy of the electrochemical K^+gradient to transport Cl^-. The electrochemical plasma membrane K^+ gradient is generated by the primary active transporter Na-K ATPase (**Figure 3**). KCC2 colocalizes and structurally interacts with the α2 subunit of the Na-K ATPase (Ikeda et al., 2004). Therefore, an alteration of KCC2 membrane expression may impact the Na-K ATPase distribution and/or activity and vice versa. KCC2 functions near thermodynamic equilibrium since the equilibrium potential of K^+ (E_K) is close to the resting membrane potential (RMP) (V_m) (Payne, 1997; Payne et al., 2003). KCC2 can function in either direction depending on the external concentration of K^+ $[K^+]_o$. Even a moderate increase in $[K^+]_o$ may thus reverse Cl^- transport through KCC2. This action may allow K^+ buffering when its extracellular concentration is increased upon sustained neuronal activity (Thompson and Gahwiler, 1989b; Payne, 1997).

WATER TRANSPORT AND THE CONTROL OF CELL VOLUME

Glutamate and GABA/glycine synaptic signaling usually lead to a net influx of Na^+ and/or Ca^{2+} cations and Cl^- anions, respectively. These movements of ions are accompanied by water inflow acting to maintain intracellular osmolarity. Massive water influx may consequently lead to neuronal swelling (Collingridge and Lester, 1989) and, if not compensated, to cell death. Since neurons lack aquaporins (Amiry-Moghaddam and Ottersen, 2003; Andrew et al., 2007) they may use an alternative mechanism to face osmotic challenges. CCCs have been extensively studied in this context of osmotic and volume regulation first in erythrocytes and epithelial cells, two non-neuronal cell types facing large osmotic challenges (Zeuthen and MacAulay, 2002; Hoffmann et al., 2009). It is well established that CCCs function is directly or indirectly coupled to water transport (Zeuthen and MacAulay, 2002; Zeuthen, 2010). Water flows in the same direction as ions to counteract osmotic changes due to CCC activity. The electroneutral Na^+–K^+–$2Cl^-$ NKCC1 co-transporter accumulates intracellular chloride using the electrochemical gradient for Na^+ and K^+ produced by the Na-K ATPase (Gamba, 2005; Blaesse et al., 2009). Both NKCC1 and KCC2 co-transport ions and water and cooperate to maintain ionic and water homeostasis in neurons. It has been estimated that NKCC1 activity triggers a net inflow of 590 water molecules for $1K^+$, $1Na^+$, $2Cl^-$ transported ions. Conversely, KCC2 activity results in the extrusion of 500 water molecules per of $1K^+$ and $1Cl^-$ transported ions [reviewed in (MacAulay and Zeuthen, 2010)]. Consistent with the role of KCC2 in water transport in neurons, experiments using digital holographic microscopy recently revealed that *N*-methyl-D-aspartate (NMDA) receptor activation in neurons triggers water influx through both NMDAR and NKCC1 while delayed activation of KCC2 compensates this influx by mediating a net outflow of water (Jourdain et al., 2011).

The functional properties of NKCC1 and KCC2 co-transporters are reciprocally regulated by serine/threonine phosphorylation. The Wnk kinase family acts as an osmosensor which can lead to reciprocal regulation of NKCC1 and KCC2 in the central nervous system (Kahle et al., 2010). Upon hyperosmotic challenge or in conditions of low $[Cl^-]_i$, activation of Wnk1/3 leads to phosphorylation and activation of NKCC1 through OSR1/SPAK Ste20-type kinases and direct inhibition of KCC2 through phosphorylation of KCC2 Thr906 and Thr1006

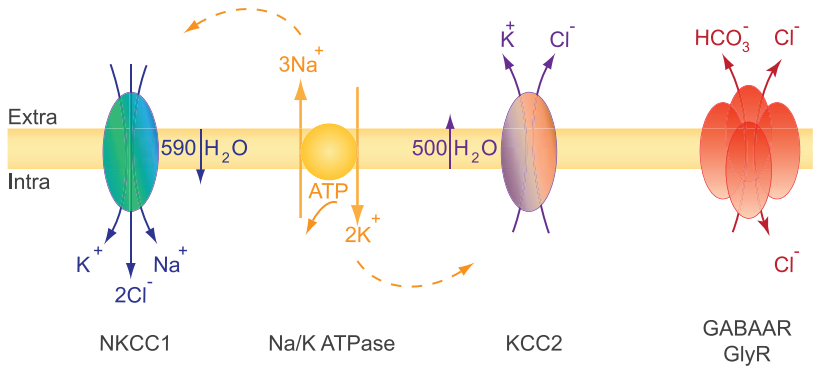

FIGURE 3 | Ions and water transport properties of the co-transporters NKCC1 and KCC2. The secondary active transporters NKCC1 and KCC2 use the energy of the electrochemical Na^+ and K^+ gradients generated by the primary active transporter Na-K ATPase to trigger a net inflow of $1K^+$, $1Na^+$, $2Cl^-$, and a net outflow of $1K^+$, $1Cl^-$ ions, respectively. The activity of each transporter is associated with water influx (NKCC1) or efflux (KCC2). NKCC1 and KCC2 are reciprocally expressed and regulated during development. NKCC1 predominates in early development while KCC2 is the main Cl^- extruder in mature neurons. This expression profile impacts both cell volume regulation and the efficacy and polarity of GlyR and $GABA_AR$ mediated synaptic transmission (see text).

(Gagnon et al., 2006; Rinehart et al., 2009). This results in a net water influx which compensates for cell shrinking due to the hyperosmotic challenge. This process is known as a Regulatory Volume Increase (RVI). Conversely, under hypo-osmotic conditions, activation of KCC2 and inhibition of NKCC1 leads to a Regulatory Volume Decrease (RVD) acting to compensate cell swelling.

INTERACTIONS WITH THE ACTIN CYTOSKELETON

Apart from their ion transport function, several ion channels, pumps, transporters, and exchangers appear to act as cytoskeletal anchors of the plasma membrane [reviewed in (Denker and Barber, 2002)]. Together with other integral membrane proteins, several ion transport proteins anchor actin filaments to the plasma membrane via interactions with the linker proteins of the ankyrin and 4.1 families. A particularly well studied example of such interaction has been described in erythrocytes, where the anion exchanger 1 (AE1) plays a critical role in docking actin cytoskeleton to plasma membrane via ankyrin and 4.1R, thereby influencing cell shape (Jons and Drenckhahn, 1992). KCC2 immunoprecipitation assays recently revealed that the carboxy-terminal domain of KCC2 (KCC2 CTD) directly interacts with 4.1N, a neuronal member of the 4.1 protein family (Li et al., 2007). 4.1N, like other 4.1 family members, possesses a 4.1 Ezrin Radixin Moesin (FERM) domain that binds a variety of transmembrane proteins and a spectrin/actin interaction domain (Baines et al., 2009). Therefore, KCC2 is expected to interact with the submembrane actin cytoskeleton. Such interaction may have multiple implications including (1) to regulate KCC2 clustering and thereby its membrane stability and/or activity, (2) to constrain KCC2 localization to specific membrane microdomains, (3) to control the local organization of actin filaments with downstream effects on subcellular morphology (Mohandas et al., 1992; Cancedda et al., 2007; Li et al., 2007; Gauvain et al., 2011), (4) to regulate cell migration (Wei et al., 2011) and (5) to affect the osmoregulatory response since actin is part of the osmotic sensor of the cell (Mills et al., 1994). These major functions of the KCC2 co-transporter are likely at play in all neuronal compartments where it is expressed. Nevertheless, they may be of particular significance at synapses where they appear to influence synaptic structure and maturation as well as efficacy.

FUNCTIONAL IMPACT OF KCC2 ON SYNAPTIC SIGNALING

FUNCTION IN SYNAPTOGENESIS

Numerous studies have revealed a critical role of KCC2 in synaptogenesis. Early overexpression of recombinant KCC2 in immature hippocampal neurons increases the density of GABAergic terminals, the number of postsynaptic GABAAR clusters as well as the frequency and amplitude of GABAAR-mediated mIPSCs (Chudotvorova et al., 2005). Conversely, the frequency of mIPSCs is reduced in hypomorphic KCC2 mice (Tornberg et al., 2005), suggesting KCC2 is required for the functional maturation of GABAergic synapses. However, the role of KCC2 in the formation of glutamatergic synapses is more controversial. The controversy may result from differences in preparations and experimental methodologies. For instance, early overexpression of KCC2 in *Xenopus laevis* embryos reduced the amplitude and frequency of mEPSCs in tectal neurons (Akerman and Cline, 2006) suggesting elevated $[Cl^-]_i$ may be required for functional maturation of excitatory synapses. Instead, overexpression of KCC2 had no effect on the density of vesicular glutamate transporter isoform 1 (VGlut1)-immunopositive terminals or mEPSC amplitude or frequency in cultured hippocampal neurons (Chudotvorova et al., 2005). This observation, however, contrasts with the effects of the genetic ablation of KCC2 which leads to a reduced number of functional excitatory synapses in immature hippocampal neurons (Li et al., 2007). Finally, in striking contrast with these data, Khalilov et al. (2011) reported a sixfold increase in the density of synaptophysin immunoreactive terminals and increased frequency of spontaneous IPSCs and EPSCs as well as enhanced network activity in CA3 hippocampal neurons from $KCC2^{-/-}$ E18.5 mouse embryos. These discrepancies may result from the timing of both KCC2 manipulations and functional observations and suggest KCC2 differentially modulates synaptogenesis in a very specific time window.

KCC2 may influence synaptogenesis through an ion-transport-independent mechanism (Li et al., 2007; Khalilov et al., 2011). However, the effects of KCC2 on the development of retinotectal circuits rely on a modulation of GABA signaling through shifting transmembrane chloride gradients (Akerman and Cline, 2006). Thus, depolarizing GABA signals may cooperate with NMDAR-mediated transmission to promote the maturation of glutamatergic synapses and the establishment of the balance of excitation and inhibition in developing circuits [for review see (Ben-Ari et al., 2007)].

FUNCTIONNAL IMPACT ON GABA AND GLYCINE SIGNALING

Here, we will present a synthetic view of the well-known impact of KCC2 on inhibitory synaptic transmission and will refer to recent and complete reviews (Ben-Ari, 2002; Ben-Ari et al., 2007; Blaesse et al., 2009). The KCC2-mediated K-Cl co-transport critically determines the electrochemical gradient of chloride ions in neurons. Therefore, a major impact of KCC2 function is on the efficacy or even the polarity of synaptic GABAergic and glycinergic transmissions which both rely on chloride fluxes.

Both GABAARs and GlyRs are primarily permeable to chloride and, to a lesser extent, bicarbonate ions (Bormann et al., 1987). Although these signals are classically considered as 'inhibitory', their polarity and functional impact are dependent on (1) the transmembrane gradients in chloride and bicarbonate ions and (2) the local RMP. Thus, GABAAR-mediated currents are hyperpolarizing only when E_{GABA} (the reversal potential of GABAAR currents, which depends on both E_{Cl} and E_{HCO3}) is hyperpolarized to RMP. Since, under physiological conditions, E_{HCO3} is depolarized as compared to RMP [around −12 mV, (Staley et al., 1995)], a rise in $[Cl]_i$ may be sufficient to depolarize E_{GABA} above RMP, leading to depolarizing actions of GABAAR-mediated currents. This may occur, for instance, during sustained GABAergic activity leading to intraneuronal chloride accumulation (Thompson and Gahwiler, 1989a). It should be noted however, that depolarizing glycine or GABAAR-mediated currents may still be functionally inhibitory due to the electrical shunt of the membrane input resistance generated by the opening of these receptors (Staley and Mody, 1992).

Although measuring $[Cl^-]_i$ in neurons remains a technical challenge potentially subject to many pitfalls (Bregestovski et al., 2009), several studies converge to suggest it may range relatively high values during early postnatal development [25–40 mM; refs in (Blaesse et al., 2009)]. This likely reflects the expression and activity of the NKCC1 transporter which acts to accumulate chloride in neurons and the expression of which precedes that of KCC2 (Plotkin et al., 1997; Hubner et al., 2001). Elevated internal chloride concentration depolarize E_{GABA} above RMP and predicts depolarizing actions of GABA acting on GABAARs in immature neurons. Although this view has been taken for granted for many years (Ben-Ari, 2002), it was recently challenged by experiments suggesting both RMP and E_{GABA} may be strongly dependent on the energy supply to immature neurons, which may be inappropriate in experimental conditions used to measure these variables (Rheims et al., 2009; Ruusuvuori et al., 2010; Tyzio et al., 2011). Nevertheless, several actions of GABA have been associated with membrane depolarization due to low KCC2 function and high intracellular chloride in immature neurons. Those include the generation of population activities such as giant depolarizing potentials (GDPs) *in vitro* (see Ben-Ari, 2002), the maturation of retinotectal circuits (Akerman and Cline, 2006) and cortical interneuron migration (Bortone and Polleux, 2009) *in vivo*.

It is generally agreed that an increase in KCC2 function correlates with a progressive hyperpolarization of E_{GABA} reflecting a reduction of $[Cl^-]_i$ in mature neurons to about 5 mM (Khirug et al., 2008; Tyzio et al., 2008). This developmental switch in chloride electrochemical gradient occurs in almost all brain structures and organisms analyzed, but with variation in the spatio-temporal developmental course (Ben-Ari, 2002). It should be noted however that steady-state $[Cl^-]_i$ is an average and shows intercellular and intracellular variability. GABAAR-mediated currents impinging onto neighboring neurons or even onto different subcellular compartments onto a given neurons may, therefore, be very different. In particular, $[Cl^-]_i$ may differ up to two to threefold between the somatic and dendritic compartments (Duebel et al., 2006) or even from one dendritic branch to the other (Waseem et al., 2010). Similarly, an axo-somatic gradient of E_{GABA} has been reported which may range up to 15–20 mV (Szabadics et al., 2006; Khirug et al., 2008). Thus, GABAAR-mediated currents are usually depolarizing on axon terminals [e.g., (Ruiz et al., 2003); see (Kullmann et al., 2005)] or AISs [(Szabadics et al., 2006; Khirug et al., 2008); but see (Glickfeld et al., 2009)] and hyperpolarizing on somato-dendritic compartments [(Banke and McBain, 2006; Tyzio et al., 2006; Khirug et al., 2008); but see (Tyzio et al., 2008)]. This axo-somatic gradient likely reflects the differential subcellular distribution of KCC2 and NKCC1 (Khirug et al., 2008). In addition, local, activity-dependent alteration of $[Cl^-]_i$ along a single dendrite is correlated with a transient and local shift in E_{GABA} (Dallwig et al., 1999; Staley and Proctor, 1999; Kuner and Augustine, 2000; Isomura et al., 2003; Jedlicka et al., 2011), the dynamics of which likely depends on KCC2 function [see (Doyon et al., 2011)]. Thus, KCC2 dynamically regulates the efficacy of GABA signaling through a local control over $[Cl^-]_i$. Therefore, modulation of KCC2 function may not only impact the steady-state efficacy of GABA signaling through GABAARs but also its dynamic operation. This may occur for instance upon repetitive neuronal activity (Fiumelli and Woodin, 2007) as well as in several pathological conditions which have been shown to both suppress KCC2 expression and affect the efficacy of GABA signaling. These include epilepsy (Cohen et al., 2002; Huberfeld et al., 2007), spinal cord injury (Boulenguez et al., 2010), neuropathic pain (Coull et al., 2003) and others (see Kahle et al., 2008).

FUNCTION AT EXCITATORY SYNAPSES

Although KCC2 primarily influences GABAergic transmission in cortical neurons, its accumulation in dendritic spines near excitatory synapses (Gulyas et al., 2001) suggests a possible interaction with glutamatergic signaling. Most excitatory synapses onto cortical neurons are formed onto dendritic spines which appear concomitantly with the up-regulation of KCC2 during early postnatal development (Rivera et al., 1999; Yuste and Bonhoeffer, 2004). In the absence of KCC2 expression in knock-out animals, spine morphogenesis is largely compromised in immature neurons, leading to anomalously long, filopodia-like protrusions (Li et al., 2007). This defect in spine maturation is associated with a reduced number of functional excitatory synapses as detected by a decreased density of synaptic clusters of the glutamate receptor anchoring proteins PSD95 and Homer and reduced mEPSC frequency. Importantly, this effect can be rescued by expression of a non-functional, *N*-terminal deficient KCC2 and mimicked by expression of the KCC2 CTD (Li et al., 2007). This observation suggests that KCC2 influences spine morphogenesis and functional maturation through a mechanism independent of its ion transport function.

KCC2 CTD directly interacts with the neuronal FERM-domain actin-binding protein 4.1N (Li et al., 2007). F-actin constitutes the main cytoskeleton of dendritic spines and its dynamic organization is known to play a critical role in spine morphogenesis (Tada and Sheng, 2006). In particular, submembrane actin dynamics have been shown to be essential during spine head formation and the transition from filopodium to dendritic spine (Hotulainen et al., 2009). Thus, KCC2–4.1N interaction may contribute to organize submembrane actin cytoskeleton in developing dendritic spines. Consistent with this hypothesis, overexpression of 4.1N FERM domain to prevent KCC2–4.1N interaction is sufficient to prevent spine morphogenesis in hippocampal neurons (Li et al., 2007).

Remodeling of the actin cytoskeleton not only impacts spinogenesis but also affects excitatory synaptic function (Hotulainen and Hoogenraad, 2010). Actin-depolymerizing factors, in particular, induce changes in synaptic function that may reflect changes in glutamate receptor membrane diffusion (Rust et al., 2010). We recently reported that chronic suppression of KCC2 after spine formation does not compromise spine maintenance in mature (>24 DIV) hippocampal neurons (Gauvain et al., 2011). Instead, it is associated with a reduction in the efficacy of excitatory synapses and aggregation of the GluA1 subunit in dendritic spines. Again, this effect is independent of a loss of KCC2 function since it is mimicked by overexpressing the KCC2 CTD but not by application of a selective KCC2 antagonist. Using single particle tracking (SPT) techniques, we showed that suppression of KCC2 expression induced an increase in the lateral diffusion

of rapidly moving, likely extrasynaptic AMPA receptors (Tardin et al., 2003; Petrini et al., 2009) in dendritic spines but not on dendritic shafts. Immobile (likely postsynaptic) receptors were also unaffected. Thus, KCC2 interaction with intracellular partners is essential to spine morphogenesis but not maintenance, and contributes to hinder lateral diffusion of AMPA receptors within dendritic spines, thereby influencing synaptic efficacy (**Figure 4**). A loss of KCC2 clusters in dendritic spines induced by sustained excitatory synaptic activity or under pathological conditions may then induce a rapid homeostatic adjustment of synaptic receptor content and efficacy by acting on the lateral diffusion of AMPA receptors.

Finally, although KCC2 is not necessary for dendritic spine maintenance in mature neurons, its suppression leads to increased spine head volume, an effect that is mimicked by chronic application of a KCC2 antagonist (Gauvain et al., 2011). As described above, KCC function is essential to volume regulation in many cell types (Gamba, 2005). Since KCC2 is the only CCC leading to solute and water extrusion under isotonic conditions (MacAulay et al., 2004; Jourdain et al., 2011), it likely contributes to osmotic regulation in dendritic spines, in particular to counteract cation influx through postsynaptic receptors. These observations predict that changes in KCC2 aggregation or function by synaptic activity may induce activity-dependent modulation of spine volume through local regulation of transmembrane solute and water efflux.

REGULATION OF KCC2 EXPRESSION AND FUNCTION

The expression level and/or transport activity of KCC2 are up-regulated during development (Kahle et al., 2005; Vale et al., 2005; Rinehart et al., 2009; Ludwig et al., 2011a,b). In mature neurons, the activity-dependent regulation of KCC2 contributes to the plasticity of inhibitory synapses under both physiological and pathological conditions. In some conditions, the activity-dependent up-regulation of KCC2 may counteract synaptic excitation by strengthening GABA signaling (Banke and Gegelashvili, 2008; Chorin et al., 2011) whereas in some pathological conditions, KCC2 down-regulation may promote excitotoxicity (Hershfinkel et al., 2009) or seizure (Reid et al., 2001; Rivera et al., 2002, 2004; Huberfeld et al., 2007; Pathak et al., 2007; Wake et al., 2007; Li et al., 2008b; Shimizu-Okabe et al., 2011). Thus, activity-dependent regulation of KCC2 participates in the adjustment of the excitatory-inhibitory balance in neuronal networks.

DEVELOPMENTAL UP-REGULATION OF KCC2

In developing hippocampal neurons, KCC2 expression is increased by the trophic factors neurturin (Ludwig et al., 2011a,b) and BDNF (Ludwig et al., 2011b). BDNF and Neurturin activate similar intracellular cascades that include the src homology two domain containing transforming protein/FGF receptor substrate 2 (Shc/FRS-2). This in turn triggers the extracellular signal-regulated kinase 1/2 (ERK1/2) and the mitogen-activated protein kinase (MAPK) pathway. This effect induces enhanced Egr4 expression and Egr4-dependent activation of KCC2b promoter (Ludwig et al., 2011b). Functional activation of KCC2 also requires oligomerization and/or phosphorylation/dephosphorylation of the co-transporter. Blaesse et al. (2006) showed that membrane expression and mature glycosylation pattern were not sufficient to ensure KCC2-mediated Cl^- extrusion in immature rat LSO neurons. At P3, KCC2 is mainly expressed as a monomeric form in plasma membrane, whereas in more mature neurons (P30) in which Cl^- extrusion was effective, KCC2 was found as oligomers (dimers, trimers, and tetramers). A direct link between oligomerization and ion transport by KCCs is supported by the observation that truncation of KCC1 carboxy-terminal domain prevents both oligomerization and chloride transport (Casula et al., 2001). Phosphorylation and dephosphorylation also play a critical role in KCC2 activation during development. Khirug et al. (2005) observed that the broad-spectrum kinase inhibitor staurosporine, leads to a rapid (5 min) negative shift in EGABA in immature hippocampal cultured neurons.

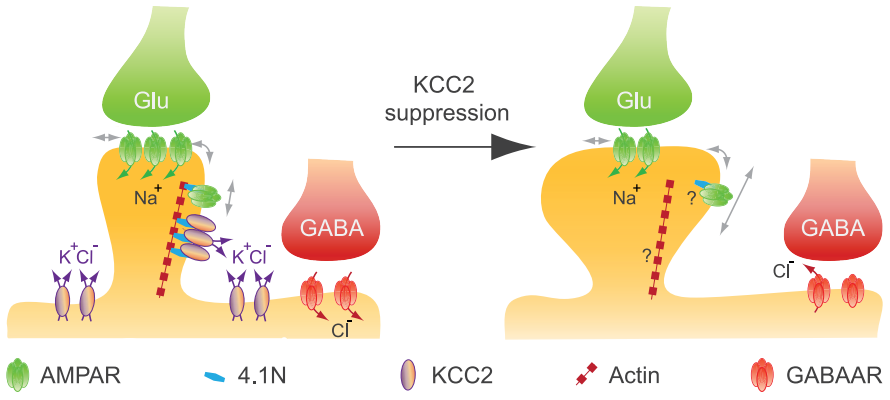

FIGURE 4 | KCC2 controls spine volume and efficacy of glutamatergic AMPAR-mediated synaptic transmission in mature neurons. KCC2 suppression in mature neurons indicates that KCC2 is not required for spine maintenance, while it contributes to both spine head volume regulation and the efficacy of excitatory synapses by physically constraining AMPAR GluA1 subunit in spine head, likely through its interaction with submembrane actin cytoskeleton [adapted from Gauvain et al. (2011)]. A loss of KCC2 clusters induced by sustained excitatory synaptic activity or under pathological conditions may induce a rapid homeostatic adjustment of the efficacy of AMPAR mediated synaptic transmission as well as a reduction in the efficacy of $GABA_AR$-dependent synaptic transmission.

Although this work did not identify the kinase(s) involved or their target(s) (i.e., KCC2 itself and/or molecular partners), KCC2 can be activated by dephosphorylation of Threonine residues. Residues Thr906 and Thr1006 in the CTD of KCC2 are phosphorylated by Wnk1 at birth and dephosphorylated in adult neurons (Rinehart et al., 2009). These phosphorylated residues appear critical for KCC2 function since Wnk1 phosphorylation of KCC2 in mature neurons causes a loss of transport function (Kahle et al., 2005; Rinehart et al., 2009). Although phosphorylation of Ser940 has not been analyzed during development, this residue is phosphorylated in mature hippocampal neurons (Lee et al., 2007), and PKC activation enhances KCC2 function (Banke and Gegelashvili, 2008) through direct phosphorylation of Ser940 (Lee et al., 2007). Therefore, PKC-dependent phosphorylation of Ser940 may also contribute to the developmental or activity-dependent activation of KCC2. Finally, the developmental activation of KCC2 function requires tyrosine kinase activity. Thus, inhibitors of tyrosine phosphorylation such as genistein or lavendustin A impair KCC2 activity in mature hippocampal neurons (Kelsch et al., 2001). KCC2 appears to be a direct target of tyrosine kinases as tyrosine phosphorylation shows a marked increase during postnatal development in cochlear nucleus neurons (Vale et al., 2005). Consistent with this observation, dephosphorylation of Tyr1087 abolishes KCC2 activity in mature neurons (Wake et al., 2007; Watanabe et al., 2009). In conclusion, functional activation of KCC2 during postnatal development appears to rely on dephosphorylation of Thr906 and Thr1006, PKC-dependent phosphorylation of Ser940, and tyrosine kinase phosphorylation of Tyr1087 (**Table 1**).

ACTIVITY-DEPENDENT REGULATION

Neuronal activity dynamically up- or down-regulates KCC2 activity. Rapid up-regulation of KCC2 activity is induced upon activation of group I metabotropic GluRs (mGluRs) and Zn^{2+} extracellular signaling. Tonic activation of both mGluR1 and mGluR5 has been shown to enhance synaptic strength at GABAergic inputs onto CA3 pyramidal neurons through hyperpolarization of E_{GABA} (Banke and Gegelashvili, 2008). This effect may involve synaptic co-release of Zn^{2+} from mossy fibers and subsequent activation of the metabotropic zinc-sensing receptor G-protein coupled receptor 39 (mZnR/GPR39) which in turn causes a hyperpolarizing shift in E_{GABA} by enhancing KCC2 activity and surface expression in CA3 neurons in hippocampal slices (Chorin et al., 2011). mZnR activation triggers Ca^{2+} release from intracellular stores via group I mGluRs, activation of the ERK1/2 pathway and PKC phosphorylation of KCC2 (Banke and Gegelashvili, 2008; Besser et al., 2009; Sindreu et al., 2011). In this context, it is remarkable that synaptic accumulation of Zn^{2+} in mossy fiber terminals and KCC2 activity in pyramidal neurons follow a similar developmental time course (Rivera et al., 1999; Nitzan et al., 2002; Lee et al., 2005; Liguz-Lecznar et al., 2005), suggesting Zn^{2+} signaling may participate in the developmental up-regulation of KCC2 (Chorin et al., 2011). Interestingly however, Zn^{2+} appears to operate a bi-directional control over KCC2 activity. In contrast to extracellular Zn^{2+}, a rise in intracellular Zn^{2+} under pathological conditions such as oxygen-glucose deprivation inhibits KCC2 function resulting in a depolarizing shift in E_{GABA} (Hershfinkel et al., 2009).

KCC2 activity is down-regulated in a variety of physiological and pathological conditions, usually associated with enhanced neuronal activity. These include long term potentiation (Wang et al., 2006b), repetitive pairing of pre- and post-synaptic activities (Woodin et al., 2003), repetitive postsynaptic spiking (Fiumelli et al., 2005), rebound burst activity (Wang et al., 2006a), tetanic stimulation (Kaila et al., 1997), NMDA receptor activation (Kitamura et al., 2008), and epileptic activity (Reid et al., 2001; Rivera et al., 2002, 2004; Huberfeld et al., 2007; Pathak et al., 2007; Wake et al., 2007; Li et al., 2008b; Shimizu-Okabe et al., 2011). All these conditions cause a depolarizing shift in E_{GABA} through reduced KCC2 function and/or expression.

The activity-dependent down-regulation of KCC2 mRNA level involves the BDNF-TrkB signaling and the combination of the Shc/FRS-2 and the phospholipase Cγ (PLCγ) signaling cascades (Rivera et al., 2004). This in turn activates the transcription factor cAMP response element-binding protein (CREB) through phosphorylation (Rivera et al., 2004). At the post-translational level, down-regulation of KCC2 usually relies on Ca^{2+} signaling and involve either Ca^{2+} influx through NMDA receptors (Kitamura et al., 2008; Lee et al., 2011) or L type Ca^{2+} channel (Fiumelli et al., 2005) or Ca^{2+}-induced-Ca^{2-} release from intracellular stores (Fiumelli et al., 2005). Although Ca^{2+} was initially suggested to activate a PKC-dependent phosphorylation of either KCC2 itself or some associated molecules that will in turn inactivate the transporter (Fiumelli et al., 2005), this seems somewhat unlikely since PKC-dependent phosphorylation of KCC2 on Ser940 enhances rather than reduces its activity (Lee et al.,

Table 1 | Phosphorylation/dephosphorylation states of KCC2 at immature or mature stages of development and in conditions of increased activity.

	Immature	Mature	Mature activity-dependent down regulation
Thr906 and Thr1006	Phosphorylated by Wnk kinases (Rinehart et al., 2009)	Dephosphorylated (Rinehart et al., 2009)	?
Tyr1087	Dephosphorylated (Vale et al., 2005)	Phosphorylated (Vale et al., 2005; Wake et al., 2007; Watanabe et al., 2009)	Phosphorylation/Dephosphorylation of Tyr903 Tyr1087 (Wake et al., 2007; Lee et al., 2010)
Ser940	?	Phosphorylated by PKC (Lee et al., 2007)	Dephosphorylated by PP1 (Lee et al., 2011)

2007; Banke and Gegelashvili, 2008). Instead, activity-dependent reduction of KCC2 activity may involve dephosphorylation of Ser940 (Lee et al., 2011) and perhaps phosphorylation of Tyr903/1087 residues (Wake et al., 2007; Lee et al., 2010). NMDAR-dependent Ca^{2+} influx causes PP1 dephosphorylation of KCC2 residue Ser940 (Lee et al., 2011). Thus, PKC-dependent phosphorylation of Ser940 enhances (Lee et al., 2007) while the PP1-mediated dephosphorylation of Ser940 inhibits KCC2 activity (Lee et al., 2011). Lee et al. (2011), therefore, proposed that KCC2 function is controlled by the balance between PKC and PP1 activities. The involvement of residues Tyr903/1087 in the down-regulation of KCC2 by activity is supported by the observation that pilocarpine-induced status epilepticus increases the phosphorylation of KCC2 residues Tyr903/1087 (Lee et al., 2010). However, hyperexcitability induced by BDNF or low external Mg^{2+} as well as oxidative stress all lead to tyrosine dephosphorylation of KCC2 (Wake et al., 2007). Interestingly, in these experiments, tyrosine phosphorylation of KCC2 could only be unmasked once phosphatase activity was blocked. Thus, neuronal activity appears to recruit both kinases and phosphatases, the relative activity of which determines KCC2 phosphorylation state. It is remarkable that developmental up-regulation and activity-dependent down-regulation of KCC2 involve a reciprocal regulation of its phosphorylation (**Table 1**).

REGULATION OF KCC2 BY OLIGOMERIZATION, CLUSTERING AND LATERAL DIFFUSION

Membrane expression and glycosylation of KCC2 precede the onset of KCC2 function and the hyperpolarizing shift in E_{GABA} during postnatal development (Kelsch et al., 2001; Khirug et al., 2005; Vale et al., 2005; Blaesse et al., 2006). In addition, enhanced neuronal activity affects KCC2 at the mRNA and protein expression levels within 1–6 h (Rivera et al., 2002, 2004; Wang et al., 2006c; Wake et al., 2007; Ludwig et al., 2011b) whereas activity-dependent regulation of KCC2 function occurs within minutes (Woodin et al., 2003; Wang et al., 2006b; Fiumelli and Woodin, 2007; Wake et al., 2007; Kitamura et al., 2008; Chorin et al., 2011; Lee et al., 2011). Therefore, regulation of KCC2 function in neurons appears to occur at several, partly interdependent levels and the rapid, activity-dependent modulation of the transporter likely occurs predominantly through post-translational modifications. Activity-induced dephosphorylation of Ser940 and phosphorylation of Tyr903/1087 leads to reduced membrane stability of KCC2 through increased endocytosis and targeting to lysosomal degradation (Lee et al., 2010, 2011). However, the loss of KCC2 activity as detected by increased $[Cl^-]_i$ precedes the removal of KCC2 from cell surface (Wake et al., 2007; Watanabe et al., 2009). Conversely, Zn^{2+}-dependent increase in KCC2 function is observed before the increase in membrane expression (Chorin et al., 2011). These observations suggest that other intermediate mechanisms may be at play to affect KCC2 function independent of its membrane expression level.

As mentioned above, KCC2 oligomerizes and forms clusters at plasma membrane. It is, therefore, tempting to hypothesize that oligomerization and clustering could represent the molecular substrate for such rapid alterations of KCC2 function. So far, only one study has investigated the impact of oligomerization and clustering on KCC2 activity (Watanabe et al., 2009). This study shows that a perturbation of KCC2 oligomerization and clustering by tyrosine kinase inhibitors correlates with a loss of function but no change in membrane expression in hippocampal neurons. Besides, heterologous GT1–7 cells expressing a recombinant KCC2 with either Tyr1087 residue mutated to aspartate (Y1087D) or a deletion of the 28 amino acids distal to the tyrosine phosphorylation site fails to oligomerize and form clusters as wild type KCC2 does (Watanabe et al., 2009). These results support a role for oligomerization and clustering in the regulation of KCC2 function. They also indicate that phosphorylation of Tyr1087 and the carboxyl-terminus of KCC2 play a critical role in oligomerization and clustering.

The mechanisms of KCC2 clustering remain elusive and may involve cholesterol-enriched lipid rafts (Watanabe et al., 2009). Indirect binding of KCC2 to actin through 4.1N interaction (Li et al., 2007) suggests clustering may also involve scaffolding molecules as described for postsynaptic neurotransmitter receptors. Identification of these molecular partners will be of particular importance since the availability of the submembrane scaffold that anchors and stabilizes transmembrane proteins can be rapidly up- or down-regulated by activity (Bruneau et al., 2009) and could be at play to locally control KCC2 aggregation and function.

Lateral diffusion in and outside synapses plays a key role in the activity-dependent regulation of receptor number at synapses (Triller and Choquet, 2008). This raises the question of the impact of lateral diffusion in the control of KCC2 clustering. The mobility of recombinant Flag-tagged KCC2 was analyzed using SPT (Dahan et al., 2003; Bannai et al., 2006). The surface recombinant Flag-tagged KCC2 transporter were labeled with an antibody raised against Flag and subsequently labeled with an intermediate biotinylated Fab fragment and streptavidin-coated quantum dot (QD). QD trajectories were overlaid with fluorescent images of recombinant homer1c-GFP and gephyrin-mRFP clusters in order to identify excitatory and inhibitory synapses, respectively. Trajectories were at/near synapses when overlapping ± 2 pixels (440 nm) with homer1c-GFP and gephyrin-mRFP clusters or extrasynaptic for spots further away (Dahan et al., 2003). As shown in **Figure 5**, KCC2 exploratory behavior (**Figure 5A**) and mobility (**Figure 5B**) is reduced and its confinement (**Figure 5C**) increased in close vicinity of excitatory and inhibitory synapses.

As shown with confocal microscopy (**Figure 2**) and with electron microscopy (Gulyas et al., 2001; Bartho et al., 2004; Blaesse et al., 2006; Takayama and Inoue, 2006), KCC2 is localized at the periphery of the postsynaptic density. Thus, the QDs located in close vicinity of synapses (**Figure 5A**) may correspond to perisynaptic QDs. However, several technical limitations do not permit to strictly separate QDs in the core of the synapse from QDs in the near vicinity of the postsynaptic differentiation (i.e., perisynaptic QDs). Indeed, the optical resolution of the wide field microscope does not permit to precisely segregate the two compartments. Second, due to their large size (20–30 nm), QDs have difficulties to enter the core of the synapse (Groc et al., 2007). Anyway, the extrasynaptic vs. synaptic/perisynaptic diffusion behavior of KCC2 is reminiscent of what was found for neurotransmitter receptors with confined movement of the

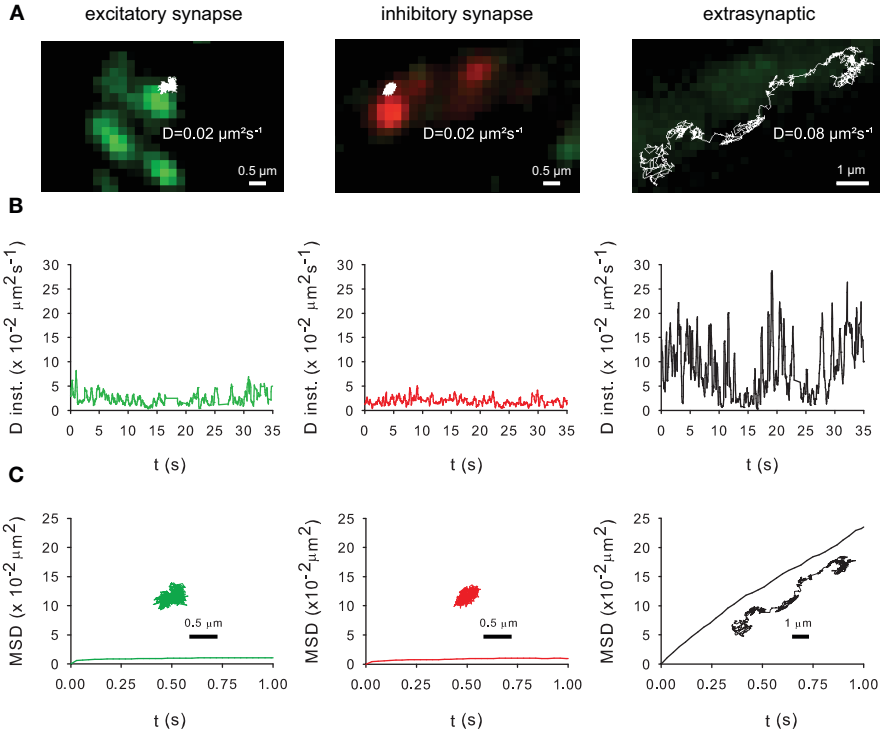

FIGURE 5 | Membrane dynamics of the KCC2 transporter studied with Single Particle Tracking. (A) Representative trajectories of Quantum Dot-bound Flag tagged recombinant KCC2 reconstructed from 35 s recording sequences ($\Delta t = 0.03$ s). QD trajectories were overlaid with fluorescent images of recombinant homer1c-GFP (green) and gephyrin-mRFP (red) clusters in order to identify excitatory and inhibitory synapses, respectively. Note that extrasynaptic QD-bound KCC2 explored larger area of membrane than synaptic/perisynaptic ones. Scale bars for synaptic/perisynaptic and extrasynaptic trajectories, 0.5 µm and 1 µm, respectively. **(B)** Instantaneous diffusion coefficients of the trajectories shown in **(A)**. Note the reduction in diffusion coefficient values and fluctuations for synaptic/perisynaptic QDs as compared with the extrasynaptic QD. **(C)** Time-averaged MSD functions of the trajectories shown in **(A)**. Extrasynaptic and synaptic QDs display linear and negatively bent MSD curves, characteristic of random walk and confined movement, respectively. In all graphs: green and red curves, trajectories at/near excitatory and inhibitory synapses, respectively; black, extrasynaptic trajectory.

protein at/near synapses and free diffusion in extrasynaptic area [ref in (Triller and Choquet, 2008)]. More work is now required to examine whether KCC2 membrane dynamics and clustering are modulated by normal and pathological neuronal activities. A regulation of KCC2 diffusion/clustering might locally affect the net function of KCC2-mediated chloride extrusion. This will be particularly relevant for the regulation of GABA signaling which may be modulated at the subcellular level (Foldy et al., 2010).

CONCLUSIONS AND PERSPECTIVES

The neuronal KCC2 transporter has long been considered only with respect to its function of chloride transport and its subsequent influence on GABA/glycine signaling. It is now becoming clear that KCC2 function in neurons extends beyond the mere transport of ions across the plasma membrane. In particular, KCC2 turns out to play a major role in the maturation and functional maintenance of excitatory synapses where it regulates the density of AMPAR in spines, most likely through actin binding property via 4.1N protein. Interestingly, 4.1N is required for activity-induced exocytosis of GluA1 subunit of AMPAR during long term potentiation (Lin et al., 2009). More work is, therefore, needed to fully characterize the contribution of KCC2/4.1N complexes in AMPAR traffic and long term synaptic plasticity. Another emerging field is that of KCC2 membrane traffic and its regulation by activity. Where does KCC2 exocytosis take place and is it regulated by neuronal activity? If so, this may represent a way to rapidly adjust KCC2 membrane expression and function. We propose that lateral diffusion and clustering of the transporter participate in the rapid regulation of its function. More work is needed to identify the scaffolding molecules that anchor KCC2 to the submembrane cytoskeleton. Whether KCC2 membrane diffusion undergoes a "diffusion trap" mechanism similar to postsynaptic neurotransmitter receptors and whether such mechanism may contribute to the activity-dependent modulation of KCC2 also remain to be established. In this context, it is noteworthy that similar cellular (cell surface stability, clustering, and perhaps lateral diffusion) and molecular (phosphorylation/dephosphorylation) mechanisms are at play to regulate KCC2 and GABAAR at the cell surface [for GABAAR regulation, see (Luscher et al., 2011)]. This raises questions about potential interactions of KCC2 and GABAAR and of their role in the coordinated regulation of GABA/glycine synaptic signaling.

REFERENCES

Aguado, F., Carmona, M. A., Pozas, E., Aguilo, A., Martinez-Guijarro, F. J., Alcantara, S., Borrell, V., Yuste, R., Ibanez, C. F., and Soriano, E. (2003). BDNF regulates spontaneous correlated activity at early developmental stages by increasing synaptogenesis and expression of the K^+/Cl^- co-transporter KCC2. *Development* 130, 1267–1280.

Akerman, C. J., and Cline, H. T. (2006). Depolarizing GABAergic conductances regulate the balance of excitation to inhibition in the developing retinotectal circuit *in vivo*. *J. Neurosci.* 26, 5117–5130.

Amiry-Moghaddam, M., and Ottersen, O. P. (2003). The molecular basis of water transport in the brain. *Nat. Rev. Neurosci.* 4, 991–1001.

Andrew, R. D., Labron, M. W., Boehnke, S. E., Carnduff, L., and Kirov, S. A. (2007). Physiological evidence that pyramidal neurons lack functional water channels. *Cereb. Cortex* 17, 787–802.

Baines, A. J., Bennett, P. M., Carter, E. W., and Terracciano, C. (2009). Protein 4.1 and the control of ion channels. *Blood Cells Mol. Dis.* 42, 211–215.

Baldi, R., Varga, C., and Tamas, G. (2010). Differential distribution of KCC2 along the axo-somato-dendritic axis of hippocampal principal cells. *Eur. J. Neurosci.* 32, 1319–1325.

Banke, T. G., and Gegelashvili, G. (2008). Tonic activation of group I mGluRs modulates inhibitory synaptic strength by regulating KCC2 activity. *J. Physiol.* 586, 4925–4934.

Banke, T. G., and McBain, C. J. (2006). GABAergic input onto CA3 hippocampal interneurons remains shunting throughout development. *J. Neurosci.* 26, 11720–11725.

Bannai, H., Lévi, S., Schweizer, C., Dahan, M., and Triller A. (2006). Imaging the lateral diffusion of membrane molecules with quantum dots. *Nat. Protoc.* 1, 2628–2634.

Bartho, P., Curto, C., Luczak, A., Marguet, S. L., and Harris, K. D. (2009). Population coding of tone stimuli in auditory cortex: dynamic rate vector analysis. *Eur. J. Neurosci.* 30, 1767–1778.

Bartho, P., Payne, J. A., Freund, T. F., and Acsady, L. (2004). Differential distribution of the KCl cotransporter KCC2 in thalamic relay and reticular nuclei. *Eur. J. Neurosci.* 20, 965–975.

Belenky, M. A., Yarom, Y., and Pickard, G. E. (2008). Heterogeneous expression of gamma-aminobutyric acid and gamma-aminobutyric acid-associated receptors and transporters in the rat suprachiasmatic nucleus. *J. Comp. Neurol.* 506, 708–732.

Ben-Ari, Y. (2002). Excitatory actions of gaba during development: the nature of the nurture. *Nat. Rev. Neurosci.* 3, 728–739.

Ben-Ari, Y., Gaiarsa, J. L., Tyzio, R., and Khazipov, R. (2007). GABA: a pioneer transmitter that excites immature neurons and generates primitive oscillations. *Physiol. Rev.* 87, 1215–1284.

Besser, L., Chorin, E., Sekler, I., Silverman, W. F., Atkin, S., Russell, J. T., and Hershfinkel, M. (2009). Synaptically released zinc triggers metabotropic signaling via a zinc-sensing receptor in the hippocampus. *J. Neurosci.* 29, 2890–2901.

Blaesse, P., Airaksinen, M. S., Rivera, C., and Kaila, K. (2009). Cation-chloride cotransporters and neuronal function. *Neuron* 61, 820–838.

Blaesse, P., Guillemin, I., Schindler, J., Schweizer, M., Delpire, E., Khiroug, L., Friauf, E., and Nothwang, H. G. (2006). Oligomerization of KCC2 correlates with development of inhibitory neurotransmission. *J. Neurosci.* 26, 10407–10419.

Bormann, J., Hamill, O. P., and Sakmann, B. (1987). Mechanism of anion permeation through channels gated by glycine and gamma-aminobutyric acid in mouse cultured spinal neurones. *J. Physiol.* 385, 243–286.

Bortone, D., and Polleux, F. (2009). KCC2 expression promotes the termination of cortical interneuron migration in a voltage-sensitive calcium-dependent manner. *Neuron* 62, 53–71.

Boulenguez, P., Liabeuf, S., Bos, R., Bras, H., Jean-Xavier, C., Brocard, C., Stil, A., Darbon, P., Cattaert, D., Delpire, E., Marsala, M., and Vinay, L. (2010). Down-regulation of the potassium-chloride cotransporter KCC2 contributes to spasticity after spinal cord injury. *Nat. Med.* 16, 302–307.

Bregestovski, P., Waseem, T., and Mukhtarov, M. (2009). Genetically encoded optical sensors for monitoring of intracellular chloride and chloride-selective channel activity. *Front. Mol. Neurosci.* 2, 15. doi: 10.3389/neuro.02.015.2009

Bruneau, E. G., Esteban, J. A., and Akaaboune, M. (2009). Receptor-associated proteins and synaptic plasticity. *FASEB J.* 23, 679–688.

Cancedda, L., Fiumelli, H., Chen, K., and Poo, M. M. (2007). Excitatory GABA action is essential for morphological maturation of cortical neurons *in vivo*. *J. Neurosci.* 27, 5224–5235.

Casula, S., Shmukler, B. E., Wilhelm, S., Stuart-Tilley, A. K., Su, W., Chernova, M. N., Brugnara, C., and Alper, S. L. (2001). A dominant negative mutant of the KCC1 K-Cl cotransporter: both N^- and C^- terminal cytoplasmic domains are required for K-Cl cotransport activity. *J. Biol. Chem.* 276, 41870–41878.

Cherubini, E., Griguoli, M., Safiulina, V., and Lagostena, L. (2011). The depolarizing action of GABA controls early network activity in the developing hippocampus. *Mol. Neurobiol.* 43, 97–106.

Chorin, E., Vinograd, O., Fleidervish, I., Gilad, D., Herrmann, S., Sekler, I., Aizenman, E., and Hershfinkel, M. (2011). Upregulation of KCC2 activity by zinc-mediated neurotransmission via the mZnR/GPR39 receptor. *J. Neurosci.* 31, 12916–12926.

Chudotvorova, I., Ivanov, A., Rama, S., Hubner, C. A., Pellegrino, C., Ben-Ari, Y., and Medina, I. (2005). Early expression of KCC2 in rat hippocampal cultures augments expression of functional GABA synapses. *J. Physiol.* 566, 671–679.

Cohen, I., Navarro, V., Clemenceau, S., Baulac, M., and Miles, R. (2002). On the origin of interictal activity in human temporal lobe epilepsy *in vitro*. *Science* 298, 1418–1421.

Collingridge, G. L., and Lester, R. A. (1989). Excitatory amino acid receptors in the vertebrate central nervous system. *Pharmacol. Rev.* 41, 143–210.

Coull, J. A., Boudreau, D., Bachand, K., Prescott, S. A., Nault, F., Sik, A., De Koninck, P., and De Koninck, Y. (2003). Trans-synaptic shift in anion gradient in spinal lamina I neurons as a mechanism of neuropathic pain. *Nature* 424, 938–942.

Dahan, M., Lévi, S., Luccardini, C., Rostaing, P., Riveau, B., and Triller, A. (2003). Diffusion dynamics of glycine receptors revealed by single-quantum dot tracking. *Science* 302, 442–445.

Dallwig, R., Deitmer, J. W., and Backus, K. H. (1999). On the mechanism of GABA-induced currents in cultured rat cortical neurons. *Pflugers Arch.* 437, 289–297.

DeFazio, R. A., Keros, S., Quick, M. W., and Hablitz, J. J. (2000). Potassium-coupled chloride cotransport controls intracellular chloride in rat neocortical pyramidal neurons. *J. Neurosci.* 20, 8069–8076.

Denker, S. P., and Barber, D. L. (2002). Ion transport proteins anchor and regulate the cytoskeleton. *Curr. Opin. Cell Biol.* 14, 214–220.

Doyon, N., Prescott, S. A., Castonguay, A., Godin, A. G., Kroger, H., and De Koninck, Y. (2011). Efficacy of synaptic inhibition depends on multiple, dynamically interacting mechanisms implicated in chloride homeostasis. *PLoS Comput. Biol.* 7, e1002149. doi: 10.1371/journal.pcbi.1002149

Duebel, J., Haverkamp, S., Schleich, W., Feng, G., Augustine, G. J., Kuner, T., and Euler, T. (2006). Two-photon imaging reveals somatodendritic chloride gradient in retinal ON-type bipolar cells expressing the biosensor Clomeleon. *Neuron* 49, 81–94.

Fiumelli, H., Cancedda, L., and Poo, M. M. (2005). Modulation of GABAergic transmission by activity via postsynaptic Ca2+-dependent regulation of KCC2 function. *Neuron* 48, 773–786.

Fiumelli, H., and Woodin, M. A. (2007). Role of activity-dependent regulation of neuronal chloride homeostasis in development. *Curr. Opin. Neurobiol.* 17, 81–86.

Foldy, C., Lee, S. H., Morgan, R. J., and Soltesz, I. (2010). Regulation of fast-spiking basket cell synapses by the chloride channel ClC-2. *Nat. Neurosci.* 13, 1047–1049.

Gagnon, K. B., England, R., and Delpire, E. (2006). Volume sensitivity of cation-Cl^- cotransporters is modulated by the interaction of two kinases: Ste20-related proline-alanine-rich kinase and WNK4. *Am. J. Physiol. Cell Physiol.* 290, C134–C142.

Gagnon, K. B., Fyffe, R. E., Adragna, N. C., and Lauf, P. K. (2007). Characterization of an extracellular epitope antibody to the neuronal K-Cl cotransporter, KCC2. *Clin. Exp. Pharmacol. Physiol.* 34, 566–573.

Gamba, G. (2005). Molecular physiology and pathophysiology of electroneutral cation-chloride cotransporters. *Physiol. Rev.* 85, 423–493.

Gauvain, G., Chamma, I., Chevy, Q., Cabezas, C., Irinopoulou, T., Bodrug, N., Carnaud, M., Levi, S., and Poncer, J. C. (2011). The neuronal K-Cl cotransporter KCC2 influences postsynaptic AMPA receptor content and lateral diffusion in dendritic spines. *Proc. Natl. Acad. Sci. U.S.A.* 108, 15474–15479.

Gavrikov, K. E., Nilson, J. E., Dmitriev, A. V., Zucker, C. L., and Mangel, S. C. (2006). Dendritic compartmentalization of chloride cotransporters underlies directional responses of starburst amacrine cells in retina. *Proc. Natl. Acad. Sci. U.S.A.* 103, 18793–18798.

Glickfeld, L. L., Roberts, J. D., Somogyi, P., and Scanziani, M. (2009). Interneurons hyperpolarize pyramidal cells along their entire somatodendritic axis. *Nat. Neurosci.* 12, 21–23.

Groc, L., Lafourcade, M., Heine, M., Renner, M., Racine, V., Sibarita, J. B., Lounis, B., Choquet, D., and Cognet, L. (2007). Surface trafficking of neurotransmitter receptor: comparison between single-molecule/quantum dot strategies. *J. Neurosci.* 27, 12433–12437.

Gulyas, A. I., Sik, A., Payne, J. A., Kaila, K., and Freund, T. F. (2001). The KCl cotransporter, KCC2, is highly expressed in the vicinity of excitatory synapses in the rat hippocampus. *Eur. J. Neurosci.* 13, 2205–2217.

Hershfinkel, M., Kandler, K., Knoch, M. E., Dagan-Rabin, M., Aras, M. A., Abramovitch-Dahan, C., Sekler, I., and Aizenman, E. (2009). Intracellular zinc inhibits KCC2 transporter activity. *Nat. Neurosci.* 12, 725–727.

Hoffmann, E. K., Lambert, I. H., and Pedersen, S. F. (2009). Physiology of cell volume regulation in vertebrates. *Physiol. Rev.* 89, 193–277.

Hotulainen, P., and Hoogenraad, C. C. (2010). Actin in dendritic spines: connecting dynamics to function. *J. Cell Biol.* 189, 619–629.

Hotulainen, P., Llano, O., Smirnov, S., Tanhuanpaa, K., Faix, J., Rivera, C., and Lappalainen, P. (2009). Defining mechanisms of actin polymerization and depolymerization during dendritic spine morphogenesis. *J. Cell Biol.* 185, 323–339.

Huberfeld, G., Wittner, L., Clemenceau, S., Baulac, M., Kaila, K., Miles, R., and Rivera, C. (2007). Perturbed chloride homeostasis and GABAergic signaling in human temporal lobe epilepsy. *J. Neurosci.* 27, 9866–9873.

Hubner, C. A., Stein, V., Hermans-Borgmeyer, I., Meyer, T., Ballanyi, K., and Jentsch, T. J. (2001). Disruption of KCC2 reveals an essential role of K-Cl cotransport already in early synaptic inhibition. *Neuron* 30, 515–524.

Ikeda, K., Onimaru, H., Yamada, J., Inoue, K., Ueno, S., Onaka, T., Toyoda, H., Arata, A., Ishikawa, T. O., Taketo, M. M., Fukuda, A., and Kawakami, K. (2004). Malfunction of respiratory-related neuronal activity in Na^+, K^+-ATPase alpha2 subunit-deficient mice is attributable to abnormal Cl^- homeostasis in brainstem neurons. *J. Neurosci.* 24, 10693–10701.

Isomura, Y., Sugimoto, M., Fujiwara-Tsukamoto, Y., Yamamoto-Muraki, S., Yamada, J., and Fukuda, A. (2003). Synaptically activated Cl^- accumulation responsible for depolarizing GABAergic responses in mature hippocampal neurons. *J. Neurophysiol.* 90, 2752–2756.

Jedlicka, P., Deller, T., Gutkin, B. S., and Backus, K. H. (2011). Activity-dependent intracellular chloride accumulation and diffusion controls GABA(A) receptor-mediated synaptic transmission. *Hippocampus* 21, 885–898.

Jons, T., and Drenckhahn, D. (1992). Identification of the binding interface involved in linkage of cytoskeletal protein 4.1 to the erythrocyte anion exchanger. *EMBO J.* 11, 2863–2867.

Jourdain, P., Pavillon, N., Moratal, C., Boss, D., Rappaz, B., Depeursinge, C., Marquet, P., and Magistretti, P. J. (2011). Determination of transmembrane water fluxes in neurons elicited by glutamate ionotropic receptors and by the cotransporters KCC2 and NKCC1: a digital holographic microscopy study. *J. Neurosci.* 31, 11846–11854.

Kahle, K. T., Rinehart, J., De Los Heros, P., Louvi, A., Meade, P., Vazquez, N., Hebert, S. C., Gamba, G., Gimenez, I., and Lifton, R. P. (2005). WNK3 modulates transport of Cl^- in and out of cells: implications for control of cell volume and neuronal excitability. *Proc. Natl. Acad. Sci. U.S.A.* 102, 16783–16788.

Kahle, K. T., Rinehart, J., and Lifton, R. P. (2010). Phosphoregulation of the Na-K-2Cl and K-Cl cotransporters by the WNK kinases. *Biochim. Biophys. Acta*. 1802, 1150–1158.

Kahle, K. T., Staley, K. J., Nahed, B. V., Gamba, G., Hebert, S. C., Lifton, R. P., and Mount, D. B. (2008). Roles of the cation-chloride cotransporters in neurological disease. *Nat. Clin. Pract. Neurol.* 4, 490–503.

Kaila, K., Lamsa, K., Smirnov, S., Taira, T., and Voipio, J. (1997). Long-lasting GABA-mediated depolarization evoked by high-frequency stimulation in pyramidal neurons of rat hippocampal slice is attributable to a network-driven, bicarbonate-dependent K^+ transient. *J. Neurosci.* 17, 7662–7672.

Karadsheh, M. F., and Delpire, E. (2001). Neuronal restrictive silencing element is found in the KCC2 gene: molecular basis for KCC2-specific expression in neurons. *J. Neurophysiol.* 85, 995–997.

Kelsch, W., Hormuzdi, S., Straube, E., Lewen, A., Monyer, H., and Misgeld, U. (2001). Insulin-like growth factor 1 and a cytosolic tyrosine kinase activate chloride outward transport during maturation of hippocampal neurons. *J. Neurosci.* 21, 8339–8347.

Khalilov, I., Chazal, G., Chudotvorova, I., Pellegrino, C., Corby, S., Ferrand, N., Gubkina, O., Nardou, R., Tyzio, R., Yamamoto, S., Jentsch, T. J., Hubner, C. A., Gaiarsa, J. L., Ben-Ari, Y., and Medina, I. (2011). Enhanced synaptic activity and epileptiform events in the embryonic KCC2 deficient hippocampus. *Front. Cell. Neurosci.* 5, 23. doi: 10.3389/fncel.2011.00023

Khirug, S., Huttu, K., Ludwig, A., Smirnov, S., Voipio, J., Rivera, C., Kaila, K., and Khiroug, L. (2005). Distinct properties of functional KCC2 expression in immature mouse hippocampal neurons in culture and in acute slices. *Eur. J. Neurosci.* 21, 899–904.

Khirug, S., Yamada, J., Afzalov, R., Voipio, J., Khiroug, L., and Kaila, K. (2008). GABAergic depolarization of the axon initial segment in cortical principal neurons is caused by the Na-K-2Cl cotransporter NKCC1. *J. Neurosci.* 28, 4635–4639.

Kitamura, A., Ishibashi, H., Watanabe, M., Takatsuru, Y., Brodwick, M., and Nabekura, J. (2008). Sustained depolarizing shift of the GABA reversal potential by glutamate receptor activation in hippocampal neurons. *Neurosci. Res.* 62, 270–277.

Kullmann, D. M., Ruiz, A., Rusakov, D. M., Scott, R., Semyanov, A., and Walker, M. C. (2005). Presynaptic, extrasynaptic and axonal GABAA receptors in the CNS: where and why? *Prog. Biophys. Mol. Biol.* 87, 33–46.

Kuner, T., and Augustine, G. J. (2000). A genetically encoded ratiometric indicator for chloride: capturing chloride transients in cultured hippocampal neurons. *Neuron* 27, 447–459.

Lee, H., Chen, C. X., Liu, Y. J., Aizenman, E., and Kandler, K. (2005). KCC2 expression in immature rat cortical neurons is sufficient to switch the polarity of GABA responses. *Eur. J. Neurosci.* 21, 2593–2599.

Lee, H. H., Deeb, T. Z., Walker, J. A., Davies, P. A., and Moss, S. J. (2011). NMDA receptor activity downregulates KCC2 resulting in depolarizing GABA(A) receptor-mediated currents. *Nat. Neurosci.* 14, 736–743.

Lee, H. H., Jurd, R., and Moss, S. J. (2010). Tyrosine phosphorylation regulates the membrane trafficking of the potassium chloride co-transporter KCC2. *Mol. Cell. Neurosci.* 45, 173–179.

Lee, H. H., Walker, J. A., Williams, J. R., Goodier, R. J., Payne, J. A., and Moss, S. J. (2007). Direct protein kinase C-dependent phosphorylation regulates the cell surface stability and activity of the potassium chloride cotransporter KCC2. *J. Biol. Chem.* 282, 29777–29784.

Li, B., Mckernan, K., and Shen, W. (2008a). Spatial and temporal distribution patterns of Na-K-2Cl cotransporter in adult and developing mouse retinas. *Vis. Neurosci.* 25, 109–123.

Li, H., Khirug, S., Cai, C., Ludwig, A., Blaesse, P., Kolikova, J., Afzalov, R., Coleman, S. K., Lauri, S., Airaksinen, M. S., Keinanen, K., Khiroug, L., Saarma, M., Kaila, K., and Rivera, C. (2007). KCC2 interacts with the dendritic cytoskeleton to promote spine development. *Neuron* 56, 1019–1033.

Li, H., Tornberg, J., Kaila, K., Airaksinen, M. S., and Rivera, C. (2002). Patterns of cation-chloride cotransporter expression during embryonic rodent CNS development. *Eur. J. Neurosci.* 16, 2358–2370.

Li, X., Zhou, J., Chen, Z., Chen, S., Zhu, F., and Zhou, L. (2008b). Long-term expressional changes of Na^+ –K^+–Cl^- co-transporter 1 (NKCC1) and K^+–Cl^- co-transporter 2 (KCC2) in CA1 region of hippocampus following lithium-pilocarpine induced status epilepticus (PISE). *Brain Res.* 1221, 141–146.

Liguz-Lecznar, M., Nowicka, D., Czupryn, A., and Skangiel-Kramska, J. (2005). Dissociation of synaptic zinc level and zinc transporter 3 expression during postnatal development and after sensory deprivation in the barrel cortex of mice. *Brain Res. Bull.* 66, 106–113.

Lin, D. T., Makino, Y., Sharma, K., Hayashi, T., Neve, R., Takamiya, K., and Huganir, R. L. (2009). Regulation of AMPA receptor extrasynaptic insertion by 4.1N, phosphorylation and palmitoylation. *Nat. Neurosci.* 12, 879–887.

Ludwig, A., Uvarov, P., Pellegrino, C., Thomas-Crusells, J., Schuchmann, S., Saarma, M., Airaksinen, M. S.,

and Rivera, C. (2011a). Neurturin evokes MAPK-dependent upregulation of Egr4 and KCC2 in developing neurons. *Neural Plast.* 2011, 1–8.

Ludwig, A., Uvarov, P., Soni, S., Thomas-Crusells, J., Airaksinen, M. S., and Rivera, C. (2011b). Early growth response 4 mediates BDNF induction of potassium chloride cotransporter 2 transcription. *J. Neurosci.* 31, 644–649.

Luscher, B., Fuchs, T., and Kilpatrick, C. L. (2011). GABAA receptor trafficking-mediated plasticity of inhibitory synapses. *Neuron* 70, 385–409.

MacAulay, N., Hamann, S., and Zeuthen, T. (2004). Water transport in the brain: role of cotransporters. *Neuroscience* 129, 1031–1044.

MacAulay, N., and Zeuthen, T. (2010). Water transport between CNS compartments: contributions of aquaporins and cotransporters. *Neuroscience* 168, 941–956.

Mills, J. W., Schwiebert, E. M., and Stanton, B. A. (1994). Evidence for the role of actin filaments in regulating cell swelling. *J. Exp. Zool.* 268, 111–120.

Mohandas, N., Winardi, R., Knowles, D., Leung, A., Parra, M., George, E., Conboy, J., and Chasis, J. (1992). Molecular basis for membrane rigidity of hereditary ovalocytosis. A novel mechanism involving the cytoplasmic domain of band 3. *J. Clin. Invest.* 89, 686–692.

Moore-Hoon, M. L., and Turner, R. J. (2000). The structural unit of the secretory Na^+–K^+–$2Cl^-$ cotransporter (NKCC1) is a homodimer. *Biochemistry* 39, 3718–3724.

Nitzan, Y. B., Sekler, I., Hershfinkel, M., Moran, A., and Silverman, W. F. (2002). Postnatal regulation of ZnT-1 expression in the mouse brain. *Brain Res. Dev. Brain Res.* 137, 149–157.

Pathak, H. R., Weissinger, F., Terunuma, M., Carlson, G. C., Hsu, F. C., Moss, S. J., and Coulter, D. A. (2007). Disrupted dentate granule cell chloride regulation enhances synaptic excitability during development of temporal lobe epilepsy. *J. Neurosci.* 27, 14012–14022.

Payne, J. A. (1997). Functional characterization of the neuronal-specific K-Cl cotransporter: implications for K^+o regulation. *Am. J. Physiol.* 273, C1516–C1525.

Payne, J. A., Rivera, C., Voipio, J., and Kaila, K. (2003). Cation-chloride co-transporters in neuronal communication, development and trauma. *Trends Neurosci.* 26, 199–206.

Payne, J. A., Stevenson, T. J., and Donaldson, L. F. (1996). Molecular characterization of a putative K-Cl cotransporter in rat brain. A neuronal-specific isoform. *J. Biol. Chem.* 271, 16245–16252.

Petrini, E. M., Lu, J., Cognet, L., Lounis, B., Ehlers, M. D., and Choquet, D. (2009). Endocytic trafficking and recycling maintain a pool of mobile surface AMPA receptors required for synaptic potentiation. *Neuron* 63, 92–105.

Plotkin, M. D., Snyder, E. Y., Hebert, S. C., and Delpire, E. (1997). Expression of the Na-K-2Cl cotransporter is developmentally regulated in postnatal rat brains: a possible mechanism underlying GABA's excitatory role in immature brain. *J. Neurobiol.* 33, 781–795.

Reid, K. H., Li, G. Y., Payne, R. S., Schurr, A., and Cooper, N. G. (2001). The mRNA level of the potassium-chloride cotransporter KCC2 covaries with seizure susceptibility in inferior colliculus of the post-ischemic audiogenic seizure-prone rat. *Neurosci. Lett.* 308, 29–32.

Rheims, S., Holmgren, C. D., Chazal, G., Mulder, J., Harkany, T., Zilberter, T., and Zilberter, Y. (2009). GABA action in immature neocortical neurons directly depends on the availability of ketone bodies. *J. Neurochem.* 110, 1330–1338.

Rinehart, J., Maksimova, Y. D., Tanis, J. E., Stone, K. L., Hodson, C. A., Zhang, J., Risinger, M., Pan, W., Wu, D., Colangelo, C. M., Forbush, B., Joiner, C. H., Gulcicek, E. E., Gallagher, P. G., and Lifton, R. P. (2009). Sites of regulated phosphorylation that control K-Cl cotransporter activity. *Cell* 138, 525–536.

Rinehart, J., Vazquez, N., Kahle, K. T., Hodson, C. A., Ring, A. M., Gulcicek, E. E., Louvi, A., Bobadilla, N. A., Gamba, G., and Lifton, R. P. (2011). WNK2 kinase is a novel regulator of essential neuronal cation-chloride cotransporters. *J. Biol. Chem.* 286, 30171–30180.

Rivera, C., Li, H., Thomas-Crusells, J., Lahtinen, H., Viitanen, T., Nanobashvili, A., Kokaia, Z., Airaksinen, M. S., Voipio, J., Kaila, K., and Saarma, M. (2002). BDNF-induced TrkB activation down-regulates the K^+–Cl^- cotransporter KCC2 and impairs neuronal Cl^- extrusion. *J. Cell Biol.* 159, 747–752.

Rivera, C., Voipio, J., Payne, J. A., Ruusuvuori, E., Lahtinen, H., Lamsa, K., Pirvola, U., Saarma, M., and Kaila, K. (1999). The K^+/Cl^- co-transporter KCC2 renders GABA hyperpolarizing during neuronal maturation. *Nature* 397, 251–255.

Rivera, C., Voipio, J., Thomas-Crusells, J., Li, H., Emri, Z., Sipila, S., Payne, J. A., Minichiello, L., Saarma, M., and Kaila, K. (2004). Mechanism of activity-dependent downregulation of the neuron-specific K-Cl cotransporter KCC2. *J. Neurosci.* 24, 4683–4691.

Ruiz, A., Fabian-Fine, R., Scott, R., Walker, M. C., Rusakov, D. A., and Kullmann, D. M. (2003). GABAA receptors at hippocampal mossy fibers. *Neuron* 39, 961–973.

Rust, M. B., Gurniak, C. B., Renner, M., Vara, H., Morando, L., Gorlich, A., Sassoe-Pognetto, M., Banchaabouchi, M. A., Giustetto, M., Triller, A., Choquet, D., and Witke, W. (2010). Learning, AMPA receptor mobility and synaptic plasticity depend on n-cofilin-mediated actin dynamics. *EMBO J.* 29, 1889–1902.

Ruusuvuori, E., Kirilkin, I., Pandya, N., and Kaila, K. (2010). Spontaneous network events driven by depolarizing GABA action in neonatal hippocampal slices are not attributable to deficient mitochondrial energy metabolism. *J. Neurosci.* 30, 15638–15642.

Shimizu-Okabe, C., Tanaka, M., Matsuda, K., Mihara, T., Okabe, A., Sato, K., Inoue, Y., Fujiwara, T., Yagi, K., and Fukuda, A. (2011). KCC2 was downregulated in small neurons localized in epileptogenic human focal cortical dysplasia. *Epilepsy Res.* 93, 177–184.

Simard, C. F., Bergeron, M. J., Frenette-Cotton, R., Carpentier, G. A., Pelchat, M. E., Caron, L., and Isenring, P. (2007). Homooligomeric and heterooligomeric associations between K^+–Cl^- cotransporter isoforms and between K^+–Cl^- and Na^+–K^+–Cl^- cotransporters. *J. Biol. Chem.* 282, 18083–18093.

Simard, C. F., Brunet, G. M., Daigle, N. D., Montminy, V., Caron, L., and Isenring, P. (2004). Self-interacting domains in the C terminus of a cation-Cl^- cotransporter described for the first time. *J. Biol. Chem.* 279, 40769–40777.

Sindreu, C., Palmiter, R. D., and Storm, D. R. (2011). Zinc transporter ZnT-3 regulates presynaptic Erk1/2 signaling and hippocampus-dependent memory. *Proc. Natl. Acad. Sci. U.S.A.* 108, 3366–3370.

Staley, K. J., and Mody, I. (1992). Shunting of excitatory input to dentate gyrus granule cells by a depolarizing GABAA receptor-mediated postsynaptic conductance. *J. Neurophysiol.* 68, 197–212.

Staley, K. J., and Proctor, W. R. (1999). Modulation of mammalian dendritic GABA(A) receptor function by the kinetics of Cl^- and $HCO3^-$ transport. *J. Physiol.* 519 Pt 3, 693–712.

Staley, K. J., Soldo, B. L., and Proctor, W. R. (1995). Ionic mechanisms of neuronal excitation by inhibitory GABAA receptors. *Science* 269, 977–981.

Stein, V., Hermans-Borgmeyer, I., Jentsch, T. J., and Hubner, C. A. (2004). Expression of the KCl cotransporter KCC2 parallels neuronal maturation and the emergence of low intracellular chloride. *J. Comp. Neurol.* 468, 57–64.

Stil, A., Liabeuf, S., Jean-Xavier, C., Brocard, C., Viemari, J. C., and Vinay, L. (2009). Developmental up-regulation of the potassium-chloride cotransporter type 2 in the rat lumbar spinal cord. *Neuroscience* 164, 809–821.

Szabadics, J., Varga, C., Molnar, G., Olah, S., Barzo, P., and Tamas, G. (2006). Excitatory effect of GABAergic axo-axonic cells in cortical microcircuits. *Science* 311, 233–235.

Tada, T., and Sheng, M. (2006). Molecular mechanisms of dendritic spine morphogenesis. *Curr. Opin. Neurobiol.* 16, 95–101.

Takayama, C., and Inoue, Y. (2006). Developmental localization of potassium chloride co-transporter 2 in granule cells of the early postnatal mouse cerebellum with special reference to the synapse formation. *Neuroscience* 143, 757–767.

Takayama, C., and Inoue, Y. (2010). Developmental localization of potassium chloride co-transporter 2 (KCC2), GABA and vesicular GABA transporter (VGAT) in the postnatal mouse somatosensory cortex. *Neurosci. Res.* 67, 137–148.

Tardin, C., Cognet, L., Bats, C., Lounis, B., and Choquet, D. (2003). Direct imaging of lateral movements of AMPA receptors inside synapses. *EMBO J.* 22, 4656–4665.

Thompson, S. M., and Gahwiler, B. H. (1989a). Activity-dependent disinhibition. I. Repetitive stimulation reduces IPSP driving force and conductance in the hippocampus *in vitro*. *J. Neurophysiol.* 61, 501–511.

Thompson, S. M., and Gahwiler, B. H. (1989b). Activity-dependent disinhibition. II. Effects of extracellular potassium, furosemide,

and membrane potential on ECl^- in hippocampal CA3 neurons. *J. Neurophysiol.* 61, 512–523.

Tornberg, J., Voikar, V., Savilahti, H., Rauvala, H., and Airaksinen, M. S. (2005). Behavioural phenotypes of hypomorphic KCC2-deficient mice. *Eur. J. Neurosci.* 21, 1327–1337.

Triller, A., and Choquet, D. (2008). New concepts in synaptic biology derived from single-molecule imaging. *Neuron* 59, 359–374.

Tyzio, R., Allene, C., Nardou, R., Picardo, M. A., Yamamoto, S., Sivakumaran, S., Caiati, M. D., Rheims, S., Minlebaev, M., Milh, M., Ferre, P., Khazipov, R., Romette, J. L., Lorquin, J., Cossart, R., Khalilov, I., Nehlig, A., Cherubini, E., and Ben-Ari, Y. (2011). Depolarizing actions of GABA in immature neurons depend neither on ketone bodies nor on pyruvate. *J. Neurosci.* 31, 34–45.

Tyzio, R., Cossart, R., Khalilov, I., Minlebaev, M., Hubner, C. A., Represa, A., Ben-Ari, Y., and Khazipov, R. (2006). Maternal oxytocin triggers a transient inhibitory switch in GABA signaling in the fetal brain during delivery. *Science* 314, 1788–1792.

Tyzio, R., Minlebaev, M., Rheims, S., Ivanov, A., Jorquera, I., Holmes, G. L., Zilberter, Y., Ben-Ari, Y., and Khazipov, R. (2008). Postnatal changes in somatic gamma-aminobutyric acid signalling in the rat hippocampus. *Eur. J. Neurosci.* 27, 2515–2528.

Uvarov, P., Ludwig, A., Markkanen, M., Pruunsild, P., Kaila, K., Delpire, E., Timmusk, T., Rivera, C., and Airaksinen, M. S. (2007). A novel N-terminal isoform of the neuron-specific K-Cl cotransporter KCC2. *J. Biol. Chem.* 282, 30570–30576.

Uvarov, P., Ludwig, A., Markkanen, M., Rivera, C., and Airaksinen, M. S. (2006). Upregulation of the neuron-specific K^+/Cl^- cotransporter expression by transcription factor early growth response 4. *J. Neurosci.* 26, 13463–13473.

Uvarov, P., Ludwig, A., Markkanen, M., Soni, S., Hubner, C. A., Rivera, C., and Airaksinen, M. S. (2009). Coexpression and heteromerization of two neuronal K-Cl cotransporter isoforms in neonatal brain. *J. Biol. Chem.* 284, 13696–13704.

Uvarov, P., Pruunsild, P., Timmusk, T., and Airaksinen, M. S. (2005). Neuronal K^+/Cl^- co-transporter (KCC2) transgenes lacking neurone restrictive silencer element recapitulate CNS neurone-specific expression and developmental up-regulation of endogenous KCC2 gene. *J. Neurochem.* 95, 1144–1155.

Vale, C., Caminos, E., Martinez-Galan, J. R., and Juiz, J. M. (2005). Expression and developmental regulation of the K^+–Cl^- cotransporter KCC2 in the cochlear nucleus. *Hear. Res.* 206, 107–115.

Vanhatalo, S., Palva, J. M., Andersson, S., Rivera, C., Voipio, J., and Kaila, K. (2005). Slow endogenous activity transients and developmental expression of K^+–Cl^- cotransporter 2 in the immature human cortex. *Eur. J. Neurosci.* 22, 2799–2804.

Vardi, N., Zhang, L. L., Payne, J. A., and Sterling, P. (2000). Evidence that different cation chloride cotransporters in retinal neurons allow opposite responses to GABA. *J. Neurosci.* 20, 7657–7663.

Vinay, L., and Jean-Xavier, C. (2008). Plasticity of spinal cord locomotor networks and contribution of cation-chloride cotransporters. *Brain Res. Rev.* 57, 103–110.

Vu, T. Q., Payne, J. A., and Copenhagen, D. R. (2000). Localization and developmental expression patterns of the neuronal K-Cl cotransporter (KCC2) in the rat retina. *J. Neurosci.* 20, 1414–1423.

Wake, H., Watanabe, M., Moorhouse, A. J., Kanematsu, T., Horibe, S., Matsukawa, N., Asai, K., Ojika, K., Hirata, M., and Nabekura, J. (2007). Early changes in KCC2 phosphorylation in response to neuronal stress result in functional downregulation. *J. Neurosci.* 27, 1642–1650.

Wang, L., Kitai, S. T., and Xiang, Z. (2006a). Activity-dependent bidirectional modification of inhibitory synaptic transmission in rat subthalamic neurons. *J. Neurosci.* 26, 7321–7327.

Wang, W., Gong, N., and Xu, T. L. (2006b). Downregulation of KCC2 following LTP contributes to EPSP-spike potentiation in rat hippocampus. *Biochem. Biophys. Res. Commun.* 343, 1209–1215.

Wang, W., Wang, H., Gong, N., and Xu, T. L. (2006c). Changes of K^+–Cl^- cotransporter 2 (KCC2) and circuit activity in propofol-induced impairment of long-term potentiation in rat hippocampal slices. *Brain Res. Bull.* 70, 444–449.

Waseem, T., Mukhtarov, M., Buldakova, S., Medina, I., and Bregestovski, P. (2010). Genetically encoded Cl^-Sensor as a tool for monitoring of Cl-dependent processes in small neuronal compartments. *J. Neurosci. Methods* 193, 14–23.

Watanabe, M., Wake, H., Moorhouse, A. J., and Nabekura, J. (2009). Clustering of neuronal K^+–Cl^- cotransporters in lipid rafts by tyrosine phosphorylation. *J. Biol. Chem.* 284, 27980–27988.

Wei, W. C., Akerman, C. J., Newey, S. E., Pan, J., Clinch, N. W., Jacob, Y., Shen, M. R., Wilkins, R. J., and Ellory, J. C. (2011). The potassium chloride cotransporter 2 (KCC2) promotes cervical cancer cell migration and invasion by an ion transport-independent mechanism. *J. Physiol.* 589, 5349–5359.

Williams, J. R., Sharp, J. W., Kumari, V. G., Wilson, M., and Payne, J. A. (1999). The neuron-specific K-Cl cotransporter, KCC2. Antibody development and initial characterization of the protein. *J. Biol. Chem.* 274, 12656–12664.

Woodin, M. A., Ganguly, K., and Poo, M. M. (2003). Coincident pre- and post-synaptic activity modifies GABAergic synapses by postsynaptic changes in Cl^- transporter activity. *Neuron* 39, 807–820.

Yang, K., Huang, Z. W., Huang, J., Zhang, X. J., and Xiao, B. K. (2008). Expression of the neuron-specific potassium chloride cotransporter KCC2 in adult rat cochlear. *Neurosci. Lett.* 441, 205–209.

Yeo, M., Berglund, K., Augustine, G., and Liedtke, W. (2009). Novel repression of Kcc2 transcription by REST-RE-1 controls developmental switch in neuronal chloride. *J. Neurosci.* 29, 14652–14662.

Yuste, R., and Bonhoeffer, T. (2004). Genesis of dendritic spines: insights from ultrastructural and imaging studies. *Nat. Rev. Neurosci.* 5, 24–34.

Zeuthen, T. (2010). Water-transporting proteins. *J. Membr. Biol.* 234, 57–73.

Zeuthen, T., and MacAulay, N. (2002). Cotransporters as molecular water pumps. *Int. Rev. Cytol.* 215, 259–284.

Zhang, L. L., Fina, M. E., and Vardi, N. (2006). Regulation of KCC2 and NKCC during development: membrane insertion and differences between cell types. *J. Comp. Neurol.* 499, 132–143.

Conflict of Interest Statement: The authors declare that the research was conducted in the absence of any commercial or financial relationships that could be construed as a potential conflict of interest.

Received: 02 December 2011; accepted: 30 January 2012; published online: 21 February 2012.

Citation: Chamma I, Chevy Q, Poncer JC and Lévi S (2012) Role of the neuronal K-Cl co-transporter KCC2 in inhibitory and excitatory neurotransmission. Front. Cell. Neurosci. ***6****:5. doi: 10.3389/fncel.2012.00005*

IV. Odorless Trigeminal Stimulus CO_2 triggers response in the olfactory cortex

The piriform cortex is part of the olfactory cortex and has been involved in odor perception, association and learning. In this journal club, we reviewed a research article investigating the modifications of neuronal activity elicited by non-odorant molecules within the cortex piriform (Carlson et al., 2013). For the first time, the authors observed that $C0_2$, an odorless trigeminal stimulant, leads to an offset response of the piriform cortex neurons. With Esther Klingler, a former PhD student at the Institut du Fer à Moulin, we aimed to summarize and to provide additional insights regarding the spatio-temporal network organization that could udnerlie the offset perception of odorless stimulants by piriform cortex.

Esther Klingler has finished her PhD in September 2014. Her PhD thesis was focusing in part on the development of the piriform cortex and she is now a postdoctoral fellow in the laboratory of Denis Jabaudon in Geneva. Under Esther's leadership, we combined her expertise in piriform cortex and my knowledge in electrophysiology to write this journal club that has been published in the Journal of Neuroscience (Chevy and Klingler, 2014).

Journal Club

Editor's Note: These short, critical reviews of recent papers in the *Journal*, written exclusively by graduate students or postdoctoral fellows, are intended to summarize the important findings of the paper and provide additional insight and commentary. For more information on the format and purpose of the Journal Club, please see http://www.jneurosci.org/misc/ifa_features.shtml.

Odorless Trigeminal Stimulus CO_2 Triggers Response in the Olfactory Cortex

Quentin Chevy* and Esther Klingler*
Institut du Fer à Moulin UMR-S839 (INSERM/UPMC), 75005, Paris, France
Review of Carlson et al.

The olfactory cortex is separated from the outside world by only two synapses, without any relay and filter in the thalamus. The piriform cortex (PCX), part of the olfactory cortex, has been shown to play a role in odor perception, as well as in odor association and learning (Wilson and Sullivan, 2011). Nevertheless, little is known about how olfactory signals coming from the olfactory bulb (OB) are integrated in the olfactory cortex.

The PCX is composed of three layers and can be divided into two regions: the anterior PCX receives more afferents from the OB and has fewer association fibers than the posterior PCX (Bekkers and Suzuki, 2013). The anterior PCX receives not only olfactory signals, but also input from trigeminal nerve (Brand, 2006), which conveys mechanical, thermal, chemical, and/or nociceptive information. At high concentrations, most odorants can elicit intranasal sensations of burning, tingling, or pickling (Doty et al., 1978). Moreover, the odorless trigeminal stimulant, carbon dioxide (CO^2), when presented with low concentration odors, can increase pungency ratings of the odors (Cain and Murphy, 1980). In addition, imaging techniques in humans have shown that even pure trigeminal stimulants, such as CO_2, evoke activity in the PCX (Albrecht et al., 2010). There therefore appears to be interplay between the olfactory and trigeminal systems (Brand, 2006): non-olfactory trigeminal sensations may converge with odor information in the PCX and this convergence may influence odor perception.

In a recent study, Carlson et al. (2013) used multi- and single-unit *in vivo* electrophysiological recordings from anesthetized mice to study integration of olfactory and trigeminal stimulations in the anterior PCX. They compared the activity elicited by odor (low concentration of isopentyl acetate) to that elicited by trigeminal stimuli (CO_2). Low odor concentrations failed to evoke trigeminal sensation and therefore allowed the authors to study responses to olfactory stimuli independently. High odor concentration (4 Torr) or CO_2 allowed them to selectively study responses to trigeminal stimuli.

The authors showed that the activity of 26.3% of recorded PCX neurons was modulated by presentation of CO_2 alone. One-third of these neurons were also activated by odors. Among the neurons responding to isopentyl acetate (11.8% of all neurons), a substantial proportion was also sensitive to CO_2 stimulation (9.2% of all neurons). CO_2-evoked activity was not found in the whole olfactory cortex, however. For example, in the olfactory tubercle (another region of the olfactory cortex), activity in only 3.5% of recorded neurons was modulated by CO_2 presentation. Convergence of inputs to the PCX might explain how the presentation of CO_2 together with a low-concentration odor can change the pungency ratings of the odor.

Carlson et al. (2013) also found that the temporal dynamics of activation in PCX neurons was different for trigeminal versus odor stimulation. Whereas odors triggered an increase in the firing rate during stimulus presentation, the response to trigeminal stimulation occurred at stimulation offset, reaching peak of magnitude ~1 s after the stimulus, independent of CO_2 concentration or stimulus duration.

Carlson et al. (2013) next took advantage of the population of neurons responding with specific temporal dynamics to both odor and trigeminal stimulations to study the ability of odor to elicit intranasal trigeminal sensations. While recording PCX neurons exhibiting both odor and trigeminal-related activity, they applied different concentrations of odor (1–4 Torr of isopentyl acetate) or CO_2 (25–100%). Interestingly, at 4 Torr odor concentration, numerous single units displayed an offset response as found when CO_2 was presented. The authors concluded that the offset response could be generalized to different trigeminal stimuli. More interestingly, these results are the first electrophysiological evidence for a switch from odorant to trigeminal sensation when odors are presented at high concentrations.

While the experiments by Carlson et al. (2013) provided new insights into the temporal and spatial integration of odorant and trigeminal stimulation by the olfactory cortex, they also raise questions regarding the underlying network and the biological relevance of an offset activation

Received Oct. 19, 2013; revised Nov. 16, 2013; accepted Nov. 25, 2013.
The authors declare no competing financial interests.
*Q.C. and E.K. contributed equally to this work.
Correspondence should be addressed to Esther Klingler, Institut du Fer à Moulin UMR-S839 (INSERM/UPMC), 17 rue du Fer à Moulin, 75005 Paris, France. E-mail: esther.klingler@inserm.fr.
DOI:10.1523/JNEUROSCI.4466-13.2014
 0270-6474/14/340341-02$15.00/0

by trigeminal stimulant. Until now, few studies described the electrophysiological activation of the PCX following odor presentation (Bekkers and Suzuki, 2013). It is known that responses in the anterior PCX consist of a burst of activity time-locked to the onset of odor inhalation. Among others, Miura et al. (2012) showed that the activation of the PCX is more strongly correlated to inhalation than to the onset of odor presentation. Strikingly, in some cases, the offset response to trigeminal stimulus seemed also to be synchronized with the inhalation phase of respiration when the stimulus was no longer present (Carlson et al., 2013, their Fig. 3*A*). Whereas the authors showed that CO_2 presentation did not alter respiratory frequency, it would be interesting to study more deeply the putative correlation between trigeminally evoked activity and inhalation.

The response of some PCX neurons to both odor and trigeminal stimuli led Carlson et al. (2013) to propose that the modified pungency rating of odors by CO_2 may be explained by integration processes in the PCX. This interpretation is possible, but it is important to note that the related network is still poorly understood. Trigeminal ganglion neurons are unique among primary sensory neurons in having two axonal branches entering the CNS at widely distant points. The trigeminal nerve projects to the trigeminal nuclei, which in turn project to the amygdala and the thalamus, but some trigeminal collaterals also directly project to the olfactory epithelium (nasal cavity) and to the OB (Brand, 2006). Both these pathways should be activated by CO_2 presentation, and which contributes to activity induced in the PCX by CO_2 and high odor concentration remains unclear. Because the OB receives both direct input from odor sensory neurons and trigeminal input, integration could occur at the OB level, upstream of PCX. It would therefore be valuable to record the response of mitral cells in the OB to trigeminal stimulation.

As discussed above, the trigeminally evoked activity in PCX neurons is an offset response. The physiological relevance and cellular mechanisms underlying this offset response in the PCX remain to be investigated. These may be similar to those proposed to explain the offset response in other sensory systems, including the visual (Bair et al., 2002) and auditory (Kasai et al., 2012) systems. In the case of the auditory system, offset neurons of the inferior colliculus are thought to encode sound duration and the offset response has been proposed to result from postinhibitory rebound excitation dependent on intrinsic membrane properties (Kasai et al., 2012). Further studies using patch-clamp recording of PCX neurons would be necessary to determine whether postinhibitory rebound underlies the offset response in PCX. Moreover, the analyses performed by Carlson et al. (2013) and the low spontaneous activity of PCX neurons did not allow them to detect a putative inhibition during the stimulus that might trigger the offset responses. A more audacious hypothesis is that the low activity in PCX neurons observed upon the presentation of a high odor concentration resulted from an inhibitory activity related to the trigeminal component of the stimulation. From the different electrophysiological recording traces shown by Carlson et al. (2013), one may wonder if we are facing a homogeneous population of neurons. Kasai and colleagues (2012) showed that offset neurons in the auditory system represent a heterogeneous population: some of them were described as pure "offset" neurons (as found in Fig. 3*A*, middle, in Carlson et al., 2013), whereas others displayed both onset and offset activation (as found in Fig. 5*B* in Carlson et al., 2013). Among this last group, Kasai et al. (2012) observed two discharge patterns during the onset period: neurons displayed either a sustained or a phasic activity. It would therefore be of interest to more thoroughly investigate the offset patterns of neurons activated by trigeminal stimulation in the PCX.

In conclusion, Carlson et al. (2013) showed electrophysiological evidence for activation of neurons from the piriform cortex by an odorless trigeminal stimulant. Moreover, they described the pattern of activation of piriform cortex neurons upon this stimulation. Strikingly, whereas response to odor occurred during odor presentation, response to trigeminal stimulants appeared after the stimulus presentation, in the offset period. Importantly, this study gives strong new insights into the modulation of odor perception by trigeminal stimulants and highlights the particular role of the piriform cortex in multisensory integration of information.

References

Albrecht J, Kopietz R, Frasnelli J, Wiesmann M, Hummel T, Lundström JN (2010) The neuronal correlates of intranasal trigeminal function-an ALE meta-analysis of human functional brain imaging data. Brain Res Rev 62:183–196. CrossRef Medline

Bair W, Cavanaugh JR, Smith MA, Movshon JA (2002) The timing of response onset and offset in macaque visual neurons. J Neurosci 22:3189–3205. Medline

Bekkers JM, Suzuki N (2013) Neurons and circuits for odor processing in the piriform cortex. Trends Neurosci 36:429–438. CrossRef Medline

Brand G (2006) Olfactory/trigeminal interactions in nasal chemoreception. Neurosci Biobehav Rev 30:908–917. CrossRef Medline

Cain WS, Murphy CL (1980) Interaction between chemoreceptive modalities of odour and irritation. Nature 284:255–257. CrossRef Medline

Carlson KS, Xia CZ, Wesson DW (2013) Encoding and representation of intranasal CO2 in the mouse olfactory cortex. J Neurosci 33:13873–13881. CrossRef Medline

Doty RL, Brugger WE, Jurs PC, Orndorff MA, Snyder PJ, Lowry LD (1978) Intranasal trigeminal stimulation from odorous volatiles: psychometric responses from anosmic and normal humans. Physiol Behav 20:175–185. CrossRef Medline

Kasai M, Ono M, Ohmori H (2012) Distinct neural firing mechanisms to tonal stimuli offset in the inferior colliculus of mice in vivo. Neurosci Res 73:224–237. CrossRef Medline

Miura K, Mainen ZF, Uchida N (2012) Odor representations in olfactory cortex: distributed rate coding and decorrelated population activity. Neuron 74:1087–1098. CrossRef Medline

Wilson DA, Sullivan RM (2011) Cortical processing of odor objects. Neuron 72:506–519. CrossRef Medline

REFERENCE

LIST

REFERENCE LIST

Abraham, W.C., and Bear, M.F. (1996). Metaplasticity: the plasticity of synaptic plasticity. Trends Neurosci. *19*, 126–130.

Ackermann, M., and Matus, A. (2003). Activity-induced targeting of profilin and stabilization of dendritic spine morphology. Nat. Neurosci. *6*, 1194–1200.

Acton, B. a, Mahadevan, V., Mercado, A., Uvarov, P., Ding, Y., Pressey, J., Airaksinen, M.S., Mount, D.B., and Woodin, M. a (2012). Hyperpolarizing GABAergic transmission requires the KCC2 C-terminal ISO domain. J. Neurosci. *32*, 8746–8751.

Ageta-Ishihara, N., Takemoto-Kimura, S., Nonaka, M., Adachi-Morishima, A., Suzuki, K., Kamijo, S., Fujii, H., Mano, T., Blaeser, F., Chatila, T. a, et al. (2009). Control of cortical axon elongation by a GABA-driven Ca2+/calmodulin-dependent protein kinase cascade. J. Neurosci. *29*, 13720–13729.

Aguado, F., Carmona, M.A., Pozas, E., Aguiló, A., Martínez-Guijarro, F.J., Alcantara, S., Borrell, V., Yuste, R., Ibañez, C.F., and Soriano, E. (2003). BDNF regulates spontaneous correlated activity at early developmental stages by increasing synaptogenesis and expression of the K+/Cl- co-transporter KCC2. Development *130*, 1267–1280.

Ahmad, M., Polepalli, J.S., Goswami, D., Yang, X., Kaeser-Woo, Y.J., Südhof, T.C., and Malenka, R.C. (2012). Postsynaptic complexin controls AMPA receptor exocytosis during LTP. Neuron *73*, 260–267.

Akaneya, Y. (2007). Activity regulates the expression of AMPA receptor subunit GluR4 in developing visual cortex. Eur. J. Neurosci. *25*, 1641–1646.

Akerman, C.J., and Cline, H.T. (2006). Depolarizing GABAergic conductances regulate the balance of excitation to inhibition in the developing retinotectal circuit in vivo. J. Neurosci. *26*, 5117–5130.

Albensi, B.C., Oliver, D.R., Toupin, J., and Odero, G. (2007). Electrical stimulation protocols for hippocampal synaptic plasticity and neuronal hyper-excitability: are they effective or relevant? Exp. Neurol. *204*, 1–13.

Allison, D.W., Gelfand, V.I., Spector, I., and Craig, a M. (1998). Role of actin in anchoring postsynaptic receptors in cultured hippocampal neurons: differential attachment of NMDA versus AMPA receptors. J. Neurosci. *18*, 2423–2436.

Amiry-Moghaddam, M., and Ottersen, O.P. (2003). The molecular basis of water transport in the brain. Nat. Rev. Neurosci. *4*, 991–1001.

Andrew, R.D., and MacVicar, B. a (1994). Imaging cell volume changes and neuronal excitation in the hippocampal slice. Neuroscience *62*, 371–383.

Andrew, R.D., Labron, M.W., Boehnke, S.E., Carnduff, L., and Kirov, S. a (2007). Physiological evidence that pyramidal neurons lack functional water channels. Cereb. Cortex *17*, 787–802.

Andrianantoandro, E., and Pollard, T.D. (2006). Mechanism of actin filament turnover by severing and nucleation at different concentrations of ADF/cofilin. Mol. Cell *24*, 13–23.

Anggono, V., and Huganir, R.L. (2012). Regulation of AMPA receptor trafficking and synaptic plasticity. Curr. Opin. Neurobiol. *22*, 461–469.

Antonov, I., Antonova, I., Kandel, E.R., and Hawkins, R.D. (2003). Activity-dependent presynaptic facilitation and hebbian LTP are both required and interact during classical conditioning in Aplysia. Neuron *37*, 135–147.

Arosio, D., Ricci, F., Marchetti, L., Gualdani, R., Albertazzi, L., and Beltram, F. (2010). Simultaneous intracellular chloride and pH measurements using a GFP-based sensor. Nat. Methods *7*, 516–518.

Ashby, M.C., De La Rue, S. a, Ralph, G.S., Uney, J., Collingridge, G.L., and Henley, J.M. (2004). Removal of AMPA receptors (AMPARs) from synapses is preceded by transient endocytosis of extrasynaptic AMPARs. J. Neurosci. *24*, 5172–5176.

Babiec, W.E., Guglietta, R., Jami, S.A., Morishita, W., Malenka, R.C., and O'Dell, T.J. (2014). Ionotropic NMDA receptor signaling is required for the induction of long-term depression in the mouse hippocampal CA1 region. J. Neurosci. *34*, 5285–5290.

Baines, A.J., Lu, H.-C., and Bennett, P.M. (2014). The Protein 4.1 family: hub proteins in animals for organizing membrane proteins. Biochim. Biophys. Acta *1838*, 605–619.

Banke, T.G., and Gegelashvili, G. (2008). Tonic activation of group I mGluRs modulates inhibitory synaptic strength by regulating KCC2 activity. J. Physiol. *586*, 4925–4934.

Barria, A., and Malinow, R. (2005). NMDA receptor subunit composition controls synaptic plasticity by regulating binding to CaMKII. Neuron *48*, 289–301.

Barria, A., Muller, D., Derkach, V., Griffith, L.C., and Soderling, T.R. (1997). Regulatory phosphorylation of AMPA-type glutamate receptors by CaM-KII during long-term potentiation. Science *276*, 2042–2045.

Barthó, P., Payne, J.A., Freund, T.F., and Acsády, L. (2004). Differential distribution of the KCl cotransporter KCC2 in thalamic relay and reticular nuclei. Eur. J. Neurosci. *20*, 965–975.

Basarsky, T. a, Feighan, D., and MacVicar, B. a (1999). Glutamate release through volume-activated channels during spreading depression. J. Neurosci. *19*, 6439–6445.

Bats, C., Groc, L., and Choquet, D. (2007). The interaction between Stargazin and PSD-95 regulates AMPA receptor surface trafficking. Neuron *53*, 719–734.

Baumgärtel, K., and Mansuy, I.M. (2012). Neural functions of calcineurin in synaptic plasticity and memory. Learn. Mem. *19*, 375–384.

Bayer, K.U., De Koninck, P., Leonard, a S., Hell, J.W., and Schulman, H. (2001). Interaction with the NMDA receptor locks CaMKII in an active conformation. Nature *411*, 801–805.

Bellone, C., and Mameli, M. (2012). mGluR-Dependent Synaptic Plasticity in Drug-Seeking. Front. Pharmacol. *3*, 159.

Ben-Ari, Y. (2002). Excitatory actions of gaba during development: the nature of the nurture. Nat. Rev. Neurosci. *3*, 728–739.

Ben-Ari, Y., Gaiarsa, J.-L., Tyzio, R., and Khazipov, R. (2007). GABA: a pioneer transmitter that excites immature neurons and generates primitive oscillations. Physiol. Rev. *87*, 1215–1284.

Ben-Ari, Y., Woodin, M. a, Sernagor, E., Cancedda, L., Vinay, L., Rivera, C., Legendre, P., Luhmann, H.J., Bordey, A., Wenner, P., et al. (2012). Refuting the challenges of the developmental shift of polarity of GABA actions: GABA more exciting than ever! Front. Cell. Neurosci. *6*, 35.

Benoist, M., Palenzuela, R., Rozas, C., Rojas, P., Tortosa, E., Morales, B., González-Billault, C., Ávila, J., and Esteban, J. a (2013). MAP1B-dependent Rac activation is required for AMPA receptor endocytosis during long-term depression. EMBO J. *32*, 2287–2299.

Berglund, K., Schleich, W., Krieger, P., Loo, L.S., Wang, D., Cant, N.B., Feng, G., Augustine, G.J., and Kuner, T. (2006). Imaging synaptic inhibition in transgenic mice expressing the chloride indicator, Clomeleon. Brain Cell Biol. *35*, 207–228.

Berndt, N., Hoffmann, S., Benda, J., Holzhütter, H.-G., and Holzh, H. (2011). The influence of the chloride currents on action potential firing and volume regulation of excitable cells studied by a kinetic model. J. Theor. Biol. *276*, 42–49.

Berninger, B., Marty, S., Zafra, F., da Penha Berzaghi, M., Thoenen, H., and Lindholm, D. (1995). GABAergic stimulation switches from enhancing to repressing BDNF expression in rat hippocampal neurons during maturation in vitro. Development *121*, 2327–2335.

Billups, D., and Attwell, D. (2002). Control of intracellular chloride concentration and GABA response polarity in rat retinal ON bipolar cells. J. Physiol. *545*, 183–198.

Blaesse, P., and Schmidt, T. (2014). K-Cl cotransporter KCC2-a moonlighting protein in excitatory and inhibitory synapse development and function. Pflugers Arch.

Blaesse, P., Guillemin, I., Schindler, J., Schweizer, M., Delpire, E., Khiroug, L., Friauf, E., and Nothwang, H.G. (2006). Oligomerization of KCC2 correlates with development of inhibitory neurotransmission. J. Neurosci. *26*, 10407–10419.

Blaesse, P., Airaksinen, M.S., Rivera, C., and Kaila, K. (2009). Cation-chloride cotransporters and neuronal function. Neuron *61*, 820–838.

Bliss, T. V, and Lomo, T. (1973). Long-lasting potentiation of synaptic transmission in the dentate area of the anaesthetized rabbit following stimulation of the perforant path. J. Physiol. *232*, 331–356.

Bloodgood, B.L., and Sabatini, B.L. (2005). Neuronal activity regulates diffusion across the neck of dendritic spines. Science *310*, 866–869.

Boehm, J., Ehrlich, I., Hsieh, H., and Malinow, R. (2006). Two mutations preventing PDZ-protein interactions of GluR1 have opposite effects on synaptic plasticity. Learn. Mem. *13*, 562–565.

Bortone, D., and Polleux, F. (2009). KCC2 expression promotes the termination of cortical interneuron migration in a voltage-sensitive calcium-dependent manner. Neuron *62*, 53–71.

Bos, R., Sadlaoud, K., Boulenguez, P., Buttigieg, D., Liabeuf, S., Brocard, C., Haase, G., Bras, H., and Vinay, L. (2013). Activation of 5-HT2A receptors upregulates the function of the neuronal K-Cl cotransporter KCC2. Proc. Natl. Acad. Sci. U. S. A. *110*, 348–353.

Bosch, M., and Hayashi, Y. (2012). Structural plasticity of dendritic spines. Curr. Opin. Neurobiol. *22*, 383–388.

Bosch, M., Castro, J., Saneyoshi, T., Matsuno, H., Sur, M., and Hayashi, Y. (2014). Structural and molecular remodeling of dendritic spine substructures during long-term potentiation. Neuron *82*, 444–459.

Boulenguez, P., Liabeuf, S., Bos, R., Bras, H., Jean-Xavier, C., Brocard, C., Stil, A., Darbon, P., Cattaert, D., Delpire, E., et al. (2010). Down-regulation of the potassium-chloride cotransporter KCC2 contributes to spasticity after spinal cord injury. Nat. Med. *16*, 302–307.

Bregestovski, P., and Bernard, C. (2012). Excitatory GABA: How a Correct Observation May Turn Out to be an Experimental Artifact. Front. Pharmacol. *3*, 65.

Brünig, I., Penschuck, S., Berninger, B., Benson, J., Fritschy, J.M., and Brunig, I. (2001). BDNF reduces miniature inhibitory postsynaptic currents by rapid downregulation of GABA(A) receptor surface expression. Eur. J. Neurosci. *13*, 1320–1328.

Buzsáki, G., Kaila, K., and Raichle, M. (2007). Inhibition and brain work. Neuron *56*, 771–783.

Calabrese, B., Wilson, M.S., and Halpain, S. (2006). Development and regulation of dendritic spine synapses. Physiology *21*, 38–47.

Cane, M., Maco, B., Knott, G., and Holtmaat, a. (2014). The Relationship between PSD-95 Clustering and Spine Stability In Vivo. J. Neurosci. *34*, 2075–2086.

Cantiello, H.F., Prat, A.G., Bonventre, J. V, Cunningham, C.C., Hartwig, J.H., and Ausiello, D.A. (1993). Actin-binding protein contributes to cell volume regulatory ion channel activation in melanoma cells. J. Biol. Chem. *268*, 4596–4599.

Carlson, K.S., Xia, C.Z., and Wesson, D.W. (2013). Encoding and representation of intranasal CO2 in the mouse olfactory cortex. J. Neurosci. *33*, 13873–13881.

Casula, S., Shmukler, B.E., Wilhelm, S., Stuart-Tilley, a K., Su, W., Chernova, M.N., Brugnara, C., and Alper, S.L. (2001). A dominant negative mutant of the KCC1 K-Cl cotransporter: both N- and C-terminal cytoplasmic domains are required for K-Cl cotransport activity. J. Biol. Chem. *276*, 41870–41878.

Cellot, G., and Cherubini, E. (2014). GABAergic signaling as therapeutic target for autism spectrum disorders. Front. Pediatr. *2*, 70.

Chamma, I., Chevy, Q., Poncer, J.C., and Lévi, S. (2012). Role of the neuronal K-Cl co-transporter KCC2 in inhibitory and excitatory neurotransmission. Front. Cell. Neurosci. *6*, 5.

Chamma, I., Heubl, M., Chevy, Q., Renner, M., Moutkine, I., Eugène, E., Poncer, J.C., and Lévi, S. (2013). Activity-dependent regulation of the K/Cl transporter KCC2 membrane diffusion, clustering, and function in hippocampal neurons. J. Neurosci. *33*, 15488–15503.

Chavas, J., and Marty, A. (2003). Coexistence of excitatory and inhibitory GABA synapses in the cerebellar interneuron network. J. Neurosci. *23*, 2019–2031.

Chen, L., Chetkovich, D.M., Petralia, R.S., Sweeney, N.T., Kawasaki, Y., Wenthold, R.J., Bredt, D.S., and Nicoll, R.A. (2000). Stargazin regulates synaptic targeting of AMPA receptors by two distinct mechanisms. Nature *408*, 936–943.

Cherubini, E., Gaiarsa, J.L., and Ben-Ari, Y. (1991). GABA: an excitatory transmitter in early postnatal life. Trends Neurosci. *14*, 515–519.

Chevaleyre, V., and Castillo, P.E. (2003). Heterosynaptic LTD of hippocampal GABAergic synapses: a novel role of endocannabinoids in regulating excitability. Neuron *38*, 461–472.

Chevy, Q., and Klingler, E. (2014). Odorless Trigeminal Stimulus CO2 Triggers Response in the Olfactory Cortex. J. Neurosci. *34*, 341–342.

Choquet, D., and Triller, A. (2013). The dynamic synapse. Neuron *80*, 691–703.

Chorin, E., Vinograd, O., Fleidervish, I., Gilad, D., Herrmann, S., Sekler, I., Aizenman, E., and Hershfinkel, M. (2011). Upregulation of KCC2 Activity by Zinc-Mediated Neurotransmission via the mZnR/GPR39 Receptor. J. Neurosci. *31*, 12916–12926.

Chowdhury, S., Shepherd, J.D., Okuno, H., Lyford, G., Petralia, R.S., Plath, N., Kuhl, D., Huganir, R.L., and Worley, P.F. (2006). Arc/Arg3.1 interacts with the endocytic machinery to regulate AMPA receptor trafficking. Neuron *52*, 445–459.

Choy, R.W.-Y., Park, M., Temkin, P., Herring, B.E., Marley, A., Nicoll, R. a, and von Zastrow, M. (2014). Retromer mediates a discrete route of local membrane delivery to dendrites. Neuron *82*, 55–62.

Chudotvorova, I., Ivanov, A., Rama, S., Hübner, C. a, Pellegrino, C., Ben-Ari, Y., and Medina, I. (2005). Early expression of KCC2 in rat hippocampal cultures augments expression of functional GABA synapses. J. Physiol. *566*, 671–679.

Clayton, G.H., Owens, G.C., Wolff, J.S., and Smith, R.L. (1998). Ontogeny of cation-Cl- cotransporter expression in rat neocortex. Brain Res. Dev. Brain Res. *109*, 281–292.

Cohen, I., Navarro, V., Clemenceau, S., Baulac, M., and Miles, R. (2002). On the origin of interictal activity in human temporal lobe epilepsy in vitro. Science *298*, 1418–1421.

Colledge, M., Dean, R.A., Scott, G.K., Langeberg, L.K., Huganir, R.L., Scott, J.D., and Hughes, H. (2000). Targeting of PKA to glutamate receptors through a MAGUK-AKAP complex. Neuron *27*, 107–119.

Copits, B. a, and Swanson, G.T. (2013). Kainate receptor post-translational modifications differentially regulate association with 4.1N to control activity-dependent receptor endocytosis. J. Biol. Chem. *288*, 8952–8965.

Copits, B. a, Robbins, J.S., Frausto, S., and Swanson, G.T. (2011). Synaptic targeting and functional modulation of GluK1 kainate receptors by the auxiliary neuropilin and tolloid-like (NETO) proteins. J. Neurosci. *31*, 7334–7340.

Copley, S.D. (2012). Moonlighting is mainstream: paradigm adjustment required. Bioessays *34*, 578–588.

Coull, J.A.M., Boudreau, D., Bachand, K., Prescott, S. a, Nault, F., Sík, A., De Koninck, P., and De Koninck, Y. (2003). Trans-synaptic shift in anion gradient in spinal lamina I neurons as a mechanism of neuropathic pain. Nature *424*, 938–942.

Cull-Candy, S., Brickley, S., and Farrant, M. (2001). NMDA receptor subunits: diversity, development and disease. Curr. Opin. Neurobiol. *11*, 327–335.

Cull-Candy, S., Kelly, L., and Farrant, M. (2006). Regulation of Ca2+-permeable AMPA receptors: synaptic plasticity and beyond. Curr. Opin. Neurobiol. *16*, 288–297.

Cummings, J.A., Mulkey, R.M., Nicoll, R.A., and Malenka, R.C. (1996). Ca2+ signaling requirements for long-term depression in the hippocampus. Neuron *16*, 825–833.

Czöndör, K., Mondin, M., Garcia, M., Heine, M., Frischknecht, R., Choquet, D., Sibarita, J.-B., and Thoumine, O.R. (2012). Unified quantitative model of AMPA receptor trafficking at synapses. Proc. Natl. Acad. Sci. U. S. A. *109*, 3522–3527.

Deane, E.C., Ilie, A.E., Sizdahkhani, S., Das Gupta, M., Orlowski, J., and McKinney, R.A. (2013). Enhanced recruitment of endosomal Na+/H+ exchanger NHE6 into Dendritic spines of hippocampal pyramidal neurons during NMDA receptor-dependent long-term potentiation. J. Neurosci. *33*, 595–610.

Debanne, D., and Poo, M.-M. (2010). Spike-timing dependent plasticity beyond synapse - pre- and post-synaptic plasticity of intrinsic neuronal excitability. Front. Synaptic Neurosci. *2*, 21.

Deisseroth, K., and Schnitzer, M.J. (2013). Engineering approaches to illuminating brain structure and dynamics. Neuron *80*, 568–577.

Delpire, E., Days, E., Lewis, L.M., Mi, D., Kim, K., Lindsley, C.W., and Weaver, C.D. (2009). Small-molecule screen identifies inhibitors of the neuronal K-Cl cotransporter KCC2. Proc. Natl. Acad. Sci. U. S. A. *106*, 5383–5388.

Denker, S.P., and Barber, D.L. (2002). Ion transport proteins anchor and regulate the cytoskeleton. Curr. Opin. Cell Biol. *14*, 214–220.

Dent, E.W., Merriam, E.B., and Hu, X. (2011). The dynamic cytoskeleton: backbone of dendritic spine plasticity. Curr. Opin. Neurobiol. *21*, 175–181.

Derkach, V., Barria, A., and Soderling, T.R. (1999). Ca2+/calmodulin-kinase II enhances channel conductance of alpha-amino-3-hydroxy-5-methyl-4-isoxazolepropionate type glutamate receptors. Proc. Natl. Acad. Sci. U. S. A. *96*, 3269–3274.

Ding, J., Ponce-Coria, J., and Delpire, E. (2013). A trafficking-deficient mutant of KCC3 reveals dominant-negative effects on K-Cl cotransport function. PLoS One *8*, e61112.

Dittman, J.S., and Regehr, W.G. (1997). Mechanism and kinetics of heterosynaptic depression at a cerebellar synapse. J. Neurosci. *17*, 9048–9059.

Dong, H., O'Brien, R.J., Fung, E.T., Lanahan, A.A., Worley, P.F., and Huganir, R.L. (1997). GRIP: a synaptic PDZ domain-containing protein that interacts with AMPA receptors. Nature *386*, 279–284.

Dong, H., Zhang, P., Song, I., Petralia, R.S., Liao, D., and Huganir, R.L. (1999). Characterization of the glutamate receptor-interacting proteins GRIP1 and GRIP2. J. Neurosci. *19*, 6930–6941.

Douyard, J., Shen, L.E.I., Huganir, R.L., and Rubio, M.E. (2007). Differential Neuronal and Glial Expression of GluR1 AMPA Receptor Subunit and the Scaffolding Proteins SAP97 and 4 . 1N during Rat Cerebellar Development. J. Comp. Neurol. *156*, 141–156.

Doyon, N., Prescott, S. a., Castonguay, A., Godin, A.G., Kröger, H., and De Koninck, Y. (2011). Efficacy of Synaptic Inhibition Depends on Multiple, Dynamically Interacting Mechanisms Implicated in Chloride Homeostasis. PLoS Comput. Biol. *7*, e1002149.

Duebel, J., Haverkamp, S., Schleich, W., Feng, G., Augustine, G.J., Kuner, T., and Euler, T. (2006). Two-photon imaging reveals somatodendritic chloride gradient in retinal ON-type bipolar cells expressing the biosensor Clomeleon. Neuron *49*, 81–94.

Duguid, I., Sjöström, P.J., and Sjo, P.J. (2006). Novel presynaptic mechanisms for coincidence detection in synaptic plasticity. Curr. Opin. Neurobiol. *16*, 312–322.

Dumitriu, D., Rodriguez, A., and Morrison, J.H. (2011). High-throughput, detailed, cell-specific neuroanatomy of dendritic spines using microinjection and confocal microscopy. Nat. Protoc. *6*, 1391–1411.

Dunham, P.B., and Ellory, J.C. (1981). Passive potassium transport in low potassium sheep red cells: dependence upon cell volume and chloride. J. Physiol. *318*, 511–530.

Dzhala, V., Valeeva, G., Glykys, J., Khazipov, R., and Staley, K. (2012). Traumatic alterations in GABA signaling disrupt hippocampal network activity in the developing brain. J. Neurosci. *32*, 4017–4031.

Dzhala, V.I., Kuchibhotla, K. V, Glykys, J.C., Kahle, K.T., Swiercz, W.B., Feng, G., Kuner, T., Augustine, G.J., Bacskai, B.J., and Staley, K.J. (2010). Progressive NKCC1-dependent neuronal chloride accumulation during neonatal seizures. J. Neurosci. *30*, 11745–11761.

Engert, F., and Bonhoeffer, T. (1999). Dendritic spine changes associated with hippocampal long-term synaptic plasticity. Nature *399*, 66–70.

Espinosa, J.S., and Stryker, M.P. (2012). Development and plasticity of the primary visual cortex. Neuron *75*, 230–249.

Fedulov, V., Rex, C.S., Simmons, D. a, Palmer, L., Gall, C.M., and Lynch, G. (2007). Evidence that long-term potentiation occurs within individual hippocampal synapses during learning. J. Neurosci. *27*, 8031–8039.

Fiumelli, H., and Woodin, M. a (2007). Role of activity-dependent regulation of neuronal chloride homeostasis in development. Curr. Opin. Neurobiol. *17*, 81–86.

Fiumelli, H., Cancedda, L., and Poo, M. (2005). Modulation of GABAergic transmission by activity via postsynaptic Ca2+-dependent regulation of KCC2 function. Neuron *48*, 773–786.

Fiumelli, H., Briner, A., Puskarjov, M., Blaesse, P., Belem, B.J., Dayer, A.G., Kaila, K., Martin, J.-L., and Vutskits, L. (2013). An ion transport-independent role for the cation-chloride cotransporter KCC2 in dendritic spinogenesis in vivo. Cereb. Cortex *23*, 378–388.

Fortin, D. a, Davare, M. a, Srivastava, T., Brady, J.D., Nygaard, S., Derkach, V. a, and Soderling, T.R. (2010). Long-term potentiation-dependent spine enlargement requires synaptic Ca2+-permeable AMPA receptors recruited by CaM-kinase I. J. Neurosci. *30*, 11565–11575.

Foster, K. a, McLaughlin, N., Edbauer, D., Phillips, M., Bolton, A., Constantine-Paton, M., and Sheng, M. (2010). Distinct roles of NR2A and NR2B cytoplasmic tails in long-term potentiation. J. Neurosci. *30*, 2676–2685.

Frost, N. a, Shroff, H., Kong, H., Betzig, E., and Blanpied, T. a (2010). Single-molecule discrimination of discrete perisynaptic and distributed sites of actin filament assembly within dendritic spines. Neuron *67*, 86–99.

Fukazawa, Y., Saitoh, Y., Ozawa, F., Ohta, Y., Mizuno, K., and Inokuchi, K. (2003). Hippocampal LTP is accompanied by enhanced F-actin content within the dendritic spine that is essential for late LTP maintenance in vivo. Neuron *38*, 447–460.

Gagnon, K.B., and Delpire, E. (2013). Physiology of SLC12 transporters: lessons from inherited human genetic mutations and genetically engineered mouse knockouts. Am. J. Physiol. Cell Physiol. *304*, C693–C714.

Gagnon, K.B.E., England, R., and Delpire, E. (2006). Volume sensitivity of cation-Cl- cotransporters is modulated by the interaction of two kinases: Ste20-related proline-alanine-rich kinase and WNK4. Am. J. Physiol. Cell Physiol. *290*, C134–C142.

Gamba, G. (2005). Molecular physiology and pathophysiology of electroneutral cation-chloride cotransporters. Physiol. Rev. *85*, 423–493.

Garbarini, N., and Delpire, E. (2008). The RCC1 domain of protein associated with Myc (PAM) interacts with and regulates KCC2. Cell. Physiol. Biochem. *22*, 31–44.

Gasman, S., Chasserot-Golaz, S., Popoff, M.R., Aunis, D., and Bader, M.F. (1999). Involvement of Rho GTPases in calcium-regulated exocytosis from adrenal chromaffin cells. J. Cell Sci. *112 (Pt 2*, 4763–4771.

Gauvain, G., Chamma, I., Chevy, Q., Cabezas, C., Irinopoulou, T., Bodrug, N., Carnaud, M., Lévi, S., and Poncer, J.C. (2011). The neuronal K-Cl cotransporter KCC2 influences postsynaptic AMPA receptor content and lateral diffusion in dendritic spines. Proc. Natl. Acad. Sci. U. S. A. *108*, 15474–15479.

Gerelsaikhan, T., and Turner, R.J. (2000). Transmembrane topology of the secretory Na+-K+-2Cl- cotransporter NKCC1 studied by in vitro translation. J. Biol. Chem. *275*, 40471–40477.

Gerges, N.Z., Backos, D.S., and Esteban, J. a (2004). Local control of AMPA receptor trafficking at the postsynaptic terminal by a small GTPase of the Rab family. J. Biol. Chem. *279*, 43870–43878.

Glykys, J., Dzhala, V.I., Kuchibhotla, K. V, Feng, G., Kuner, T., Augustine, G., Bacskai, B.J., and Staley, K.J. (2009). Differences in cortical versus subcortical GABAergic signaling: a candidate mechanism of electroclinical uncoupling of neonatal seizures. Neuron *63*, 657–672.

Grandgeorge, M., Lemonnier, E., Degrez, C., and Jallot, N. (2014). The effect of bumetanide treatment on the sensory behaviours of a young girl with Asperger syndrome. BMJ Case Rep. *2014*.

Granger, A.J., Shi, Y., Lu, W., Cerpas, M., and Nicoll, R. a (2013). LTP requires a reserve pool of glutamate receptors independent of subunit type. Nature *493*, 495–500.

Greger, I.H., and Esteban, J. a (2007). AMPA receptor biogenesis and trafficking. Curr. Opin. Neurobiol. *17*, 289–297.

Grimley, J.S., Li, L., Wang, W., Wen, L., Beese, L.S., Hellinga, H.W., and Augustine, G.J. (2013). Visualization of synaptic inhibition with an optogenetic sensor developed by cell-free protein engineering automation. J. Neurosci. *33*, 16297–16309.

Gu, J., Lee, C.W., Fan, Y., Komlos, D., Tang, X., Sun, C., Yu, K., Hartzell, H.C., Chen, G., Bamburg, J.R., et al. (2010). ADF/cofilin-mediated actin dynamics regulate AMPA receptor trafficking during synaptic plasticity. Nat. Neurosci. *13*, 1208–1215.

Gu, L., Kleiber, S., Schmid, L., Nebeling, F., Chamoun, M., Steffen, J., Wagner, J., and Fuhrmann, M. (2014). Long-term in vivo imaging of dendritic spines in the hippocampus reveals structural plasticity. J. Neurosci. *34*, 13948–13953.

Gulyás, A.I., Sík, A., Payne, J.A., Kaila, K., and Freund, T.F. (2001). The KCl cotransporter, KCC2, is highly expressed in the vicinity of excitatory synapses in the rat hippocampus. Eur. J. Neurosci. *13*, 2205–2217.

Hadjikhani, N., Zürcher, N.R., Rogier, O., Ruest, T., Hippolyte, L., Ben-Ari, Y., and Lemonnier, E. (2013). Improving emotional face perception in autism with diuretic bumetanide: A proof-of-concept behavioral and functional brain imaging pilot study. Autism.

Haeckel, A., Ahuja, R., Gundelfinger, E.D., Qualmann, B., and Kessels, M.M. (2008). The actin-binding protein Abp1 controls dendritic spine morphology and is important for spine head and synapse formation. J. Neurosci. *28*, 10031–10044.

Van Harreveld, a, and Fifkova, E. (1975). Swelling of dendritic spines in the fascia dentata after stimulation of the perforant fibers as a mechanism of post-tetanic potentiation. Exp. Neurol. *49*, 736–749.

Hartell, N.A. (2001). Receptors, second messengers and protein kinases required for heterosynaptic cerebellar long-term depression. Neuropharmacology *40*, 148–161.

Hartmann, A.-M., Blaesse, P., Kranz, T., Wenz, M., Schindler, J., Kaila, K., Friauf, E., and Nothwang, H.G. (2009). Opposite effect of membrane raft perturbation on transport activity of KCC2 and NKCC1. J. Neurochem. *111*, 321–331.

Hartmann, A.-M., Tesch, D., Nothwang, H.G., and Bininda-Emonds, O.R.P. (2014). Evolution of the cation chloride cotransporter family: ancient origins, gene losses, and subfunctionalization through duplication. Mol. Biol. Evol. *31*, 434–447.

Harvey, C.D., and Svoboda, K. (2007). Locally dynamic synaptic learning rules in pyramidal neuron dendrites. Nature *450*, 1195–1200.

Harvey, C.D., Yasuda, R., Zhong, H., and Svoboda, K. (2008). The spread of Ras activity triggered by activation of a single dendritic spine. Science *321*, 136–140.

Hayashi, Y., Shi, S.H., Esteban, J.A., Piccini, A., Poncer, J.C., and Malinow, R. (2000). Driving AMPA receptors into synapses by LTP and CaMKII: requirement for GluR1 and PDZ domain interaction. Science *287*, 2262–2267.

Hekmat-Scafe, D.S., Lundy, M.Y., Ranga, R., and Tanouye, M. a (2006). Mutations in the K+/Cl- cotransporter gene kazachoc (kcc) increase seizure susceptibility in Drosophila. J. Neurosci. *26*, 8943–8954.

Henley, J.M., Barker, E. a, and Glebov, O.O. (2011). Routes, destinations and delays: recent advances in AMPA receptor trafficking. Trends Neurosci. *34*, 258–268.

Hering, H., and Sheng, M. (2001). Dendritic spines: structure, dynamics and regulation. Nat. Rev. Neurosci. *2*, 880–888.

Herring, B.E., Shi, Y., Suh, Y.H., Zheng, C.-Y., Blankenship, S.M., Roche, K.W., and Nicoll, R. a (2013). Cornichon proteins determine the subunit composition of synaptic AMPA receptors. Neuron *77*, 1083–1096.

Hershfinkel, M., Kandler, K., Knoch, M.E., Dagan-Rabin, M., Aras, M. a, Abramovitch-Dahan, C., Sekler, I., and Aizenman, E. (2009). Intracellular zinc inhibits KCC2 transporter activity. Nat. Neurosci. *12*, 725–727.

Hewitt, S. a, Wamsteeker, J.I., Kurz, E.U., and Bains, J.S. (2009). Altered chloride homeostasis removes synaptic inhibitory constraint of the stress axis. Nat. Neurosci. *12*, 438–443.

Hirling, H. (2009). Endosomal trafficking of AMPA-type glutamate receptors. Neuroscience *158*, 36–44.

Hofer, S.B., and Bonhoeffer, T. (2010). Dendritic spines: the stuff that memories are made of? Curr. Biol. *20*, R157–R159.

Hoffmann, E.K., Lambert, I.H., and Pedersen, S.F. (2009). Physiology of cell volume regulation in vertebrates. Physiol. Rev. *89*, 193–277.

Holmgren, C.D., Mukhtarov, M., Malkov, A.E., Popova, I.Y., Bregestovski, P., and Zilberter, Y. (2010). Energy substrate availability as a determinant of neuronal resting potential, GABA signaling and spontaneous network activity in the neonatal cortex in vitro. J. Neurochem. *112*, 900–912.

Holtmaat, A.J.G.D., Trachtenberg, J.T., Wilbrecht, L., Shepherd, G.M., Zhang, X., Knott, G.W., and Svoboda, K. (2005). Transient and persistent dendritic spines in the neocortex in vivo. Neuron *45*, 279–291.

Honkura, N., Matsuzaki, M., Noguchi, J., Ellis-Davies, G.C.R., and Kasai, H. (2008). The subspine organization of actin fibers regulates the structure and plasticity of dendritic spines. Neuron *57*, 719–729.

Horn, Z., Ringstedt, T., Blaesse, P., Kaila, K., and Herlenius, E. (2010). Premature expression of KCC2 in embryonic mice perturbs neural development by an ion transport-independent mechanism. Eur. J. Neurosci. *31*, 2142–2155.

Hotulainen, P., Llano, O., Smirnov, S., Tanhuanpää, K., Faix, J., Rivera, C., and Lappalainen, P. (2009). Defining mechanisms of actin polymerization and depolymerization during dendritic spine morphogenesis. J. Cell Biol. *185*, 323–339.

Howard, H.C., Mount, D.B., Rochefort, D., Byun, N., Dupré, N., Lu, J., Fan, X., Song, L., Rivière, J.-B., Prévost, C., et al. (2002). The K-Cl cotransporter KCC3 is mutant in a severe peripheral neuropathy associated with agenesis of the corpus callosum. Nat. Genet. *32*, 384–392.

Huang, Y.Y., Colino, A., Selig, D.K., and Malenka, R.C. (1992). The influence of prior synaptic activity on the induction of long-term potentiation. Science *255*, 730–733.

Huberfeld, G., Wittner, L., Clemenceau, S., Baulac, M., Kaila, K., Miles, R., and Rivera, C. (2007). Perturbed chloride homeostasis and GABAergic signaling in human temporal lobe epilepsy. J. Neurosci. *27*, 9866–9873.

Hübner, C.A., Stein, V., Hermans-Borgmeyer, I., Meyer, T., Ballanyi, K., and Jentsch, T.J. (2001). Disruption of KCC2 reveals an essential role of K-Cl cotransport already in early synaptic inhibition. Neuron *30*, 515–524.

Huganir, R.L., and Nicoll, R. a (2013). AMPARs and synaptic plasticity: the last 25 years. Neuron *80*, 704–717.

Humeau, Y., Reisel, D., Johnson, A.W., Borchardt, T., Jensen, V., Gebhardt, C., Bosch, V., Gass, P., Bannerman, D.M., Good, M.A., et al. (2007). A pathway-specific function for different AMPA receptor subunits in amygdala long-term potentiation and fear conditioning. J. Neurosci. *27*, 10947–10956.

Hyde, T.M., Lipska, B.K., Ali, T., Mathew, S. V, Law, A.J., Metitiri, O.E., Straub, R.E., Ye, T., Colantuoni, C., Herman, M.M., et al. (2011). Expression of GABA signaling molecules KCC2, NKCC1, and GAD1 in cortical development and schizophrenia. J. Neurosci. *31*, 11088–11095.

Ikeda, K., Onimaru, H., Yamada, J., Inoue, K., Ueno, S., Onaka, T., Toyoda, H., Arata, A., Ishikawa, T., Taketo, M.M., et al. (2004). Malfunction of respiratory-related neuronal activity in Na+, K+-ATPase alpha2 subunit-deficient mice is attributable to abnormal Cl- homeostasis in brainstem neurons. J. Neurosci. *24*, 10693–10701.

Inoue, K., Ueno, S., and Fukuda, A. (2004). Interaction of neuron-specific K+-Cl- cotransporter, KCC2, with brain-type creatine kinase. FEBS Lett. *564*, 131–135.

Inoue, K., Yamada, J., Ueno, S., and Fukuda, A. (2006). Brain-type creatine kinase activates neuron-specific K+-Cl- co-transporter KCC2. J. Neurochem. *96*, 598–608.

Isaac, J.T.R., Ashby, M.C., and McBain, C.J. (2007). The role of the GluR2 subunit in AMPA receptor function and synaptic plasticity. Neuron *54*, 859–871.

Ishikawa, M., Otaka, M., Huang, Y.H., Neumann, P.A., Winters, B.D., Grace, A. a, Schlüter, O.M., and Dong, Y. (2013). Dopamine triggers heterosynaptic plasticity. J. Neurosci. *33*, 6759–6765.

Ivakine, E. a, Acton, B. a, Mahadevan, V., Ormond, J., Tang, M., Pressey, J.C., Huang, M.Y., Ng, D., Delpire, E., Salter, M.W., et al. (2013). Neto2 is a KCC2 interacting protein required for neuronal Cl- regulation in hippocampal neurons. Proc. Natl. Acad. Sci. U. S. A. *110*, 3561–3566.

Izeddin, I., Specht, C.G., Lelek, M., Darzacq, X., Triller, A., Zimmer, C., and Dahan, M. (2011). Super-resolution dynamic imaging of dendritic spines using a low-affinity photoconvertible actin probe. PLoS One *6*, e15611.

Jaafari, N., Henley, J.M., and Hanley, J.G. (2012). PICK1 mediates transient synaptic expression of GluA2-lacking AMPA receptors during glycine-induced AMPA receptor trafficking. J. Neurosci. *32*, 11618–11630.

Jedlicka, P., Deller, T., Gutkin, B.S., and Backus, K.H. (2010). Activity-dependent intracellular chloride accumulation and diffusion controls GABA(A) receptor-mediated synaptic transmission. Hippocampus *21*, 885–898.

Jeffery, C.J. (2009). Moonlighting proteins--an update. Mol. Biosyst. *5*, 345–350.

Jeyifous, O., Waites, C.L., Specht, C.G., Fujisawa, S., Schubert, M., Lin, E.I., Marshall, J., Aoki, C., de Silva, T., Montgomery, J.M., et al. (2009). SAP97 and CASK mediate sorting of NMDA receptors through a previously unknown secretory pathway. Nat. Neurosci. *12*, 1011–1019.

Ji, Y., Lu, Y., Yang, F., Shen, W., Tang, T.T.-T., Feng, L., Duan, S., and Lu, B. (2010). Acute and gradual increases in BDNF concentration elicit distinct signaling and functions in neurons. Nat. Neurosci. *13*, 302–309.

Johnson, J.W., and Ascher, P. (1987). Glycine potentiates the NMDA response in cultured mouse brain neurons. Nature *325*, 529–531.

Jones, E.G., and Powell, T.P.S. (1969). Morphological variations in the dendritic spines of the neocortex. J. Cell Sci. *5*, 509–529.

Jourdain, P., Pavillon, N., Moratal, C., Boss, D., Rappaz, B., Depeursinge, C., Marquet, P., and Magistretti, P.J. (2011). Determination of Transmembrane Water Fluxes in Neurons Elicited by Glutamate Ionotropic Receptors and by the Cotransporters KCC2 and NKCC1: A Digital Holographic Microscopy Study. J. Neurosci. *31*, 11846–11854.

Jurado, S., Goswami, D., Zhang, Y., Molina, A.J.M., Südhof, T.C., and Malenka, R.C. (2013). LTP requires a unique postsynaptic SNARE fusion machinery. Neuron *77*, 542–558.

Kahle, K.T., Rinehart, J., de Los Heros, P., Louvi, A., Meade, P., Vazquez, N., Hebert, S.C., Gamba, G., Gimenez, I., and Lifton, R.P. (2005). WNK3 modulates transport of Cl- in and out of cells: implications for control of cell volume and neuronal excitability. Proc. Natl. Acad. Sci. U. S. A. *102*, 16783–16788.

Kahle, K.T., Rinehart, J., and Lifton, R.P. (2010). Phosphoregulation of the Na-K-2Cl and K-Cl cotransporters by the WNK kinases. Biochim. Biophys. Acta *1802*, 1150–1158.

Kahle, K.T., Deeb, T.Z., Puskarjov, M., Silayeva, L., Liang, B., Kaila, K., and Moss, S.J. (2013). Modulation of neuronal activity by phosphorylation of the K-Cl cotransporter KCC2. Trends Neurosci. 1–12.

Kahle, K.T., Merner, N.D., Friedel, P., Silayeva, L., Liang, B., Khanna, A., Shang, Y., Lachance-Touchette, P., Bourassa, C., Levert, A., et al. (2014). Genetically encoded impairment of neuronal KCC2 cotransporter function in human idiopathic generalized epilepsy. EMBO Rep. *15*, 766–774.

Kaila, K., Lamsa, K., Smirnov, S., Taira, T., and Voipio, J. (1997). Long-lasting GABA-mediated depolarization evoked by high-frequency stimulation in pyramidal neurons of rat hippocampal slice is attributable to a network-driven, bicarbonate-dependent K+ transient. J. Neurosci. *17*, 7662–7672.

Kaila, K., Price, T.J., Payne, J.A., Puskarjov, M., and Voipio, J. (2014). Cation-chloride cotransporters in neuronal development, plasticity and disease. Nat. Rev. Neurosci. *15*, 637–654.

Kasai, H., Fukuda, M., Watanabe, S., Hayashi-Takagi, A., and Noguchi, J. (2010). Structural dynamics of dendritic spines in memory and cognition. Trends Neurosci. *33*, 121–129.

Kelsch, W., Hormuzdi, S., Straube, E., Lewen, a, Monyer, H., and Misgeld, U. (2001). Insulin-like growth factor 1 and a cytosolic tyrosine kinase activate chloride outward transport during maturation of hippocampal neurons. J. Neurosci. *21*, 8339–8347.

Kessels, H.W., and Malinow, R. (2009). Synaptic AMPA receptor plasticity and behavior. Neuron *61*, 340–350.

Kessels, H.W., Kopec, C.D., Klein, M.E., and Malinow, R. (2009). Roles of stargazin and phosphorylation in the control of AMPA receptor subcellular distribution. Nat. Neurosci. *12*, 888–896.

Kessels, H.W., Nabavi, S., and Malinow, R. (2013). Metabotropic NMDA receptor function is required for β-amyloid-induced synaptic depression. Proc. Natl. Acad. Sci. U. S. A. *110*, 4033–4038.

Khirug, S., Huttu, K., Ludwig, A., Smirnov, S., Voipio, J., Rivera, C., Kaila, K., and Khiroug, L. (2005). Distinct properties of functional KCC2 expression in immature mouse hippocampal neurons in culture and in acute slices. Eur. J. Neurosci. *21*, 899–904.

Khirug, S., Ahmad, F., Puskarjov, M., Afzalov, R., Kaila, K., and Blaesse, P. (2010). A single seizure episode leads to rapid functional activation of KCC2 in the neonatal rat hippocampus. J. Neurosci. *30*, 12028–12035.

Kim, I.H., Racz, B., Wang, H., Burianek, L., Weinberg, R., Yasuda, R., Wetsel, W.C., and Soderling, S.H. (2013). Disruption of Arp2/3 results in asymmetric structural plasticity of dendritic spines and progressive synaptic and behavioral abnormalities. J. Neurosci. *33*, 6081–6092.

Kiraly, D.D., Eipper-Mains, J.E., Mains, R.E., and Eipper, B. a (2010). Synaptic plasticity, a symphony in GEF. ACS Chem. Neurosci. *1*, 348–365.

Kitamura, A., Ishibashi, H., Watanabe, M., Takatsuru, Y., Brodwick, M., and Nabekura, J. (2008). Sustained depolarizing shift of the GABA reversal potential by glutamate receptor activation in hippocampal neurons. Neurosci. Res. *62*, 270–277.

Ko, J., Kim, S., Valtschanoff, J.G., Shin, H., Lee, J.-R., Sheng, M., Premont, R.T., Weinberg, R.J., and Kim, E. (2003). Interaction between liprin-alpha and GIT1 is required for AMPA receptor targeting. J. Neurosci. *23*, 1667–1677.

Kopec, C.D., Li, B., Wei, W., Boehm, J., and Malinow, R. (2006). Glutamate receptor exocytosis and spine enlargement during chemically induced long-term potentiation. J. Neurosci. *26*, 2000–2009.

Kopec, C.D., Real, E., Kessels, H.W., and Malinow, R. (2007). GluR1 links structural and functional plasticity at excitatory synapses. J. Neurosci. *27*, 13706–13718.

Kornau, H.C., Schenker, L.T., Kennedy, M.B., and Seeburg, P.H. (1995). Domain interaction between NMDA receptor subunits and the postsynaptic density protein PSD-95. Science *269*, 1737–1740.

Korobova, F., and Svitkina, T. (2010). Molecular architecture of synaptic actin cytoskeleton in hippocampal neurons reveals a mechanism of dendritic spine morphogenesis. Mol. Biol. Cell *21*, 165–176.

Koskinen, M., and Hotulainen, P. (2014). Measuring F-actin properties in dendritic spines. Front. Neuroanat. *8*, 74.

Koskinen, M., Bertling, E., and Hotulainen, P. (2012). Methods to measure actin treadmilling rate in dendritic spines. Methods Enzymol. *505*, 47–58.

Kristensen, A.S., Jenkins, M. a, Banke, T.G., Schousboe, A., Makino, Y., Johnson, R.C., Huganir, R., and Traynelis, S.F. (2011). Mechanism of Ca(2+)/calmodulin-dependent kinase II regulation of AMPA receptor gating. Nat. Neurosci. *14*, 727–735.

Krucker, T., Siggins, G.R., and Halpain, S. (2000). Dynamic actin filaments are required for stable long-term potentiation (LTP) in area CA1 of the hippocampus. Proc. Natl. Acad. Sci. U. S. A. *97*, 6856–6861.

Kullmann, D.M., and Lamsa, K.P. (2007). Long-term synaptic plasticity in hippocampal interneurons. Nat. Rev. Neurosci. *8*, 687–699.

Kullmann, D.M., Moreau, A.W., Bakiri, Y., and Nicholson, E. (2012). Plasticity of inhibition. Neuron *75*, 951–962.

Kuner, T., and Augustine, G.J. (2000). A genetically encoded ratiometric indicator for chloride: capturing chloride transients in cultured hippocampal neurons. Neuron *27*, 447–459.

Kuriu, T., Inoue, A., Bito, H., Sobue, K., and Okabe, S. (2006). Differential control of postsynaptic density scaffolds via actin-dependent and -independent mechanisms. J. Neurosci. *26*, 7693–7706.

Kwon, H.-B., and Sabatini, B.L. (2011). Glutamate induces de novo growth of functional spines in developing cortex. Nature *474*, 100–104.

Lamsa, K.P., Heeroma, J.H., Somogyi, P., Rusakov, D. a, and Kullmann, D.M. (2007). Anti-Hebbian long-term potentiation in the hippocampal feedback inhibitory circuit. Science *315*, 1262–1266.

Lauf, P.K., and Theg, B.E. (1980). A chloride dependent K+ flux induced by N-ethylmaleimide in genetically low K+ sheep and goat erythrocytes. Biochem. Biophys. Res. Commun. *92*, 1422–1428.

Lee, S.-J.R., and Yasuda, R. (2009). Spatiotemporal Regulation of Signaling in and out of Dendritic Spines: CaMKII and Ras. Open Neurosci. J. *3*, 117–127.

Lee, H.H.C., Walker, J. a, Williams, J.R., Goodier, R.J., Payne, J. a, and Moss, S.J. (2007). Direct protein kinase C-dependent phosphorylation regulates the cell surface stability and activity of the potassium chloride cotransporter KCC2. J. Biol. Chem. *282*, 29777–29784.

Lee, H.H.C., Jurd, R., and Moss, S.J. (2010a). Tyrosine phosphorylation regulates the membrane trafficking of the potassium chloride co-transporter KCC2. Mol. Cell. Neurosci. *45*, 173–179.

Lee, H.H.C., Deeb, T.Z., Walker, J. a, Davies, P.A., and Moss, S.J. (2011). NMDA receptor activity downregulates KCC2 resulting in depolarizing GABAA receptor-mediated currents. Nat. Neurosci. *14*, 736–743.

Lee, H.-K., Takamiya, K., Han, J.-S., Man, H., Kim, C.-H., Rumbaugh, G., Yu, S., Ding, L., He, C., Petralia, R.S., et al. (2003). Phosphorylation of the AMPA receptor GluR1 subunit is required for synaptic plasticity and retention of spatial memory. Cell *112*, 631–643.

Lee, M.-C., Yasuda, R., and Ehlers, M.D. (2010b). Metaplasticity at single glutamatergic synapses. Neuron *66*, 859–870.

Lee, S.H., Liu, L., Wang, Y.T., and Sheng, M. (2002). Clathrin Adaptor AP2 and NSF Interact with Overlapping Sites of GluR2 and Play Distinct Roles in AMPA Receptor Trafficking and Hippocampal LTD. Neuron *36*, 661–674.

Lee, S.-J.R., Escobedo-Lozoya, Y., Szatmari, E.M., and Yasuda, R. (2009). Activation of CaMKII in single dendritic spines during long-term potentiation. Nature *458*, 299–304.

Lemonnier, E., and Ben-Ari, Y. (2010). The diuretic bumetanide decreases autistic behaviour in five infants treated during 3 months with no side effects. Acta Paediatr. *99*, 1885–1888.

Lemonnier, E., Degrez, C., Phelep, M., Tyzio, R., Josse, F., Grandgeorge, M., Hadjikhani, N., and Ben-Ari, Y. (2012). A randomised controlled trial of bumetanide in the treatment of autism in children. Transl. Psychiatry *2*, e202.

Lerma, J. (2006). Kainate receptor physiology. Curr. Opin. Pharmacol. *6*, 89–97.

Leterrier, C., and Dargent, B. (2014). No Pasaran! Role of the axon initial segment in the regulation of protein transport and the maintenance of axonal identity. Semin. Cell Dev. Biol. *27*, 44–51.

Lewin, N., Aksay, E., and Clancy, C.E. (2012). Computational modeling reveals dendritic origins of GABA(A)-mediated excitation in CA1 pyramidal neurons. PLoS One *7*, e47250.

Li, B., Piriz, J., Mirrione, M., Chung, C., Proulx, C.D., Schulz, D., Henn, F., and Malinow, R. (2011). Synaptic potentiation onto habenula neurons in the learned helplessness model of depression. Nature *470*, 535–539.

Li, H., Khirug, S., Cai, C., Ludwig, A., Blaesse, P., Kolikova, J., Afzalov, R., Coleman, S.K., Lauri, S., Airaksinen, M.S., et al. (2007). KCC2 interacts with the dendritic cytoskeleton to promote spine development. Neuron *56*, 1019–1033.

Li, X., Zhou, J., Chen, Z., Chen, S., Zhu, F., and Zhou, L. (2008). Long-term expressional changes of Na+ -K+ -Cl- co-transporter 1 (NKCC1) and K+ -Cl- co-transporter 2 (KCC2) in CA1 region of hippocampus following lithium-pilocarpine induced status epilepticus (PISE). Brain Res. *1221*, 141–146.

Lin, D.-T., and Huganir, R.L. (2007). PICK1 and phosphorylation of the glutamate receptor 2 (GluR2) AMPA receptor subunit regulates GluR2 recycling after NMDA receptor-induced internalization. J. Neurosci. *27*, 13903–13908.

Lin, D.-T., Makino, Y., Sharma, K., Hayashi, T., Neve, R., Takamiya, K., and Huganir, R.L. (2009). Regulation of AMPA receptor extrasynaptic insertion by 4.1N, phosphorylation and palmitoylation. Nat. Neurosci. *12*, 879–887.

Ling, D.S.F., and Benardo, L.S. (1995). Activity-dependent depression of monosynaptic fast IPSCs in hippocampus: contributions from reductions in chloride driving force and conductance. Brain Res. *670*, 142–146.

Lisman, J. (1989). A mechanism for the Hebb and the anti-Hebb processes underlying learning and memory. Proc. Natl. Acad. Sci. U. S. A. *86*, 9574–9578.

Lisman, J.E. (2009). The pre/post LTP debate. Neuron *63*, 281–284.

Lisman, J., Yasuda, R., and Raghavachari, S. (2012). Mechanisms of CaMKII action in long-term potentiation. Nat. Rev. Neurosci. *13*, 169–182.

Lohmann, C., and Kessels, H.W. (2014). The developmental stages of synaptic plasticity. J. Physiol. *592*, 13–31.

Loo, L.S., Tang, N., Al-Haddawi, M., Dawe, G.S., and Hong, W. (2014). A role for sorting nexin 27 in AMPA receptor trafficking. Nat. Commun. *5*, 3176.

De Los Heros, P., Alessi, D.R., Gourlay, R., Campbell, D.G., Deak, M., Macartney, T.J., Kahle, K.T., and Zhang, J. (2014). The WNK-regulated SPAK/OSR1 kinases directly phosphorylate and inhibit the K+-Cl- co-transporters. Biochem. J. *458*, 559–573.

Lu, D., Yan, H., Othman, T., and Rivkees, S. a (2004). Cytoskeletal protein 4.1G is a binding partner of the metabotropic glutamate receptor subtype 1 alpha. J. Neurosci. Res. *78*, 49–55.

Lu, W., Man, H., Ju, W., Trimble, W.S., MacDonald, J.F., and Wang, Y.T. (2001). Activation of synaptic NMDA receptors induces membrane insertion of new AMPA receptors and LTP in cultured hippocampal neurons. Neuron *29*, 243–254.

Lu, W., Shi, Y., Jackson, A.C., Bjorgan, K., During, M.J., Sprengel, R., Seeburg, P.H., and Nicoll, R. a (2009). Subunit composition of synaptic AMPA receptors revealed by a single-cell genetic approach. Neuron *62*, 254–268.

Ludwig, A., Uvarov, P., Soni, S., Thomas-Crusells, J., Airaksinen, M.S., and Rivera, C. (2011). Early growth response 4 mediates BDNF induction of potassium chloride cotransporter 2 transcription. J. Neurosci. *31*, 644–649.

Luhmann, H.J., Kirischuk, S., and Kilb, W. (2014). Comment on “Local impermeant anions establish the neuronal chloride concentration”. Science *345*, 1130.

Luscher, B., Fuchs, T., and Kilpatrick, C.L. (2011). GABAA receptor trafficking-mediated plasticity of inhibitory synapses. Neuron *70*, 385–409.

Lüscher, C., Houhui, X., Beattie, E.C., Carroll, R.C., Zastrow, M. von, Malenka, R.C., and Nicoll, R.A. (1999). Role of AMPA Receptor Cycling in Synaptic. Neuron *24*, 649–658.

Lüthi, a, Chittajallu, R., Duprat, F., Palmer, M.J., Benke, T. a, Kidd, F.L., Henley, J.M., Isaac, J.T., and Collingridge, G.L. (1999). Hippocampal LTD expression involves a pool of AMPARs regulated by the NSF-GluR2 interaction. Neuron *24*, 389–399.

MacAulay, N., and Zeuthen, T. (2010). Water transport between CNS compartments: contributions of aquaporins and cotransporters. Neuroscience *168*, 941–956.

Mahadevan, V., Pressey, J.C., Acton, B. a, Uvarov, P., Huang, M.Y., Chevrier, J., Puchalski, A., Li, C.M., Ivakine, E. a, Airaksinen, M.S., et al. (2014). Kainate receptors coexist in a functional complex with KCC2 and regulate chloride homeostasis in hippocampal neurons. Cell Rep. *7*, 1762–1770.

Majewska, a, Tashiro, a, and Yuste, R. (2000). Regulation of spine calcium dynamics by rapid spine motility. J. Neurosci. *20*, 8262–8268.

Makino, H., and Malinow, R. (2009). AMPA receptor incorporation into synapses during LTP: the role of lateral movement and exocytosis. Neuron *64*, 381–390.

Makino, H., and Malinow, R. (2011). Compartmentalized versus global synaptic plasticity on dendrites controlled by experience. Neuron *72*, 1001–1011.

Malenka, R.C., and Bear, M.F. (2004). LTP and LTD: an embarrassment of riches. Neuron *44*, 5–21.

Malinow, R., and Tsien, R.W. (1990). Presynaptic enhancement shown by whole-cell recordings of long-term potentiation in hippocampal slices. Nature *346*, 177–180.

Mammen, A.L., Kameyama, K., Roche, K.W., Huganir, R.L., and Ii, C.C.K. (1997). Phosphorylation of the alpha-Amino-3-hydroxy-5-methylisoxazole- 4-propionic Acid Receptor GluR1 Subunit by Calcium / Calmodulin-dependent Kinase II. J. Biol. Chem. *272*, 32528–32533.

Man, H., Sekine-aizawa, Y., and Huganir, R.L. (2007). Regulation of {alpha}-amino-3-hydroxy-5-methyl-4-isoxazolepropionic acid receptor trafficking through PKA phosphorylation of the Glu receptor 1 subunit. Proc. Natl. Acad. Sci. U. S. A. *104*, 3579–3584.

Manser, E., Loo, T.H., Koh, C.G., Zhao, Z.S., Chen, X.Q., Tan, L., Tan, I., Leung, T., and Lim, L. (1998). PAK kinases are directly coupled to the PIX family of nucleotide exchange factors. Mol. Cell *1*, 183–192.

Markova, O., Mukhtarov, M., Real, E., Jacob, Y., and Bregestovski, P. (2008). Genetically encoded chloride indicator with improved sensitivity. J. Neurosci. Methods *170*, 67–76.

Maroteaux, M., and Mameli, M. (2012). Cocaine evokes projection-specific synaptic plasticity of lateral habenula neurons. J. Neurosci. *32*, 12641–12646.

Martina, M., Royer, S., and Paré, D. (2001). Cell-type-specific GABA responses and chloride homeostasis in the cortex and amygdala. J. Neurophysiol. *86*, 2887–2895.

Marty, A., and Llano, I. (2005). Excitatory effects of GABA in established brain networks. Trends Neurosci. *28*, 284–289.

Matsuzaki, M., Ellis-Davies, G.C., Nemoto, T., Miyashita, Y., Iino, M., and Kasai, H. (2001). Dendritic spine geometry is critical for AMPA receptor expression in hippocampal CA1 pyramidal neurons. Nat. Neurosci. *4*, 1086–1092.

Medina, I., Friedel, P., Rivera, C., Kahle, K.T., Kourdougli, N., Uvarov, P., and Pellegrino, C. (2014). Current view on the functional regulation of the neuronal K(+)-Cl(-) cotransporter KCC2. Front. Cell. Neurosci. *8*, 27.

Meng, Y., Zhang, Y., Tregoubov, V., Janus, C., Cruz, L., Jackson, M., Lu, W.Y., MacDonald, J.F., Wang, J.Y., Falls, D.L., et al. (2002). Abnormal spine morphology and enhanced LTP in LIMK-1 knockout mice. Neuron *35*, 121–133.

Mercado, A., Broumand, V., Zandi-Nejad, K., Enck, A.H., and Mount, D.B. (2006). A C-terminal domain in KCC2 confers constitutive K+-Cl- cotransport. J. Biol. Chem. *281*, 1016–1026.

Michishita, M., Ikeda, T., Nakashiba, T., Ogawa, M., Tashiro, K., Honjo, T., Doi, K., Itohara, S., and Endo, S. (2004). Expression of Btcl2, a novel member of Btcl gene family, during development of the central nervous system. Brain Res. Dev. Brain Res. *153*, 135–142.

Miesenböck, G., De Angelis, D.A., and Rothman, J.E. (1998). Visualizing secretion and synaptic transmission with pH-sensitive green fluorescent proteins. Nature *394*, 192–195.

Miles, R., Blaesse, P., Huberfeld, G., Wittner, L., and Kaila, K. (2012). Chloride homeostasis and GABA signaling in temporal lobe epilepsy. Jasper's Basic Mech. Epilepsies 1–13.

Mizoguchi, Y., Ishibashi, H., and Nabekura, J. (2003). The action of BDNF on GABA(A) currents changes from potentiating to suppressing during maturation of rat hippocampal CA1 pyramidal neurons. J. Physiol. *548*, 703–709.

Mizuno, K. (2013). Signaling mechanisms and functional roles of cofilin phosphorylation and dephosphorylation. Cell. Signal. *25*, 457–469.

Mohandas, N., Winardi, R., Knowles, D., Leung, A., Parra, M., George, E., Conboy, J., and Chasis, J. (1992). Molecular Basis for Membrane Rigidity of Hereditary Ovalocytosis. J. Clin. Invest. *89*, 686–692.

Moneron, G., Medda, R., Hein, B., Giske, A., Westphal, V., and Hell, S.W. (2010). Fast STED microscopy with continuous wave fiber lasers. Opt. Express *18*, 1302–1309.

Moniz, S., Matos, P., and Jordan, P. (2008). WNK2 modulates MEK1 activity through the Rho GTPase pathway. Cell. Signal. *20*, 1762–1768.

Monyer, H., Burnashev, N., Laurie, D.J., Sakmann, B., and Seeburg, P.H. (1994). Developmental and regional expression in the rat brain and functional properties of four NMDA receptors. Neuron *12*, 529–540.

Morgans, C.W., and Kopito, R.R. (1993). Association of the brain anion exchanger, AE3, with the repeat domain of ankyrin. J. Cell Sci. *105 (Pt 4*, 1137–1142.

Mott, H.R., Nietlispach, D., Evetts, K.A., and Owen, D. (2005). Structural analysis of the SH3 domain of beta-PIX and its interaction with alpha-p21 activated kinase (PAK). Biochemistry *44*, 10977–10983.

Mount, D.B., Delpire, E., Gamba, G., Hall, A.E., Poch, E., Hoover, R.S., and Hebert, S.C. (1998). The electroneutral cation-chloride cotransporters. J. Exp. Biol. *201*, 2091–2102.

Muñoz-Cuevas, F.J., Athilingam, J., Piscopo, D., and Wilbrecht, L. (2013). Cocaine-induced structural plasticity in frontal cortex correlates with conditioned place preference. Nat. Neurosci. *16*, 1367–1369.

Nabavi, S., Kessels, H.W., Alfonso, S., Aow, J., Fox, R., and Malinow, R. (2013). Metabotropic NMDA receptor function is required for NMDA receptor-dependent long-term depression. Proc. Natl. Acad. Sci. U. S. A. *110*, 4027–4032.

Nägerl, U.V., and Bonhoeffer, T. (2010). Imaging living synapses at the nanoscale by STED microscopy. J. Neurosci. *30*, 9341–9346.

Nägerl, U.V., Willig, K.I., Hein, B., Hell, S.W., and Bonhoeffer, T. (2008). Live-cell imaging of dendritic spines by STED microscopy. Proc. Natl. Acad. Sci. U. S. A. *105*, 18982–18987.

Neuhoff, H., Sassoè-Pognetto, M., Panzanelli, P., Maas, C., Witke, W., and Kneussel, M. (2005). The actin-binding protein profilin I is localized at synaptic sites in an activity-regulated manner. Eur. J. Neurosci. *21*, 15–25.

Nishimune, a, Isaac, J.T., Molnar, E., Noel, J., Nash, S.R., Tagaya, M., Collingridge, G.L., Nakanishi, S., and Henley, J.M. (1998). NSF binding to GluR2 regulates synaptic transmission. Neuron *21*, 87–97.

Nowak, L., Bregestovski, P., Ascher, P., Herbet, A., and Prochiantz, A. (1984). Magnesium gates glutamate-activated channels in mouse central neurones. Nature *307*, 462–465.

Okamoto, K., Bosch, M., and Hayashi, Y. (2009). The roles of CaMKII and F-actin in the structural plasticity of dendritic spines: a potential molecular identity of a synaptic tag? Physiology *24*, 357–366.

Okamoto, K.-I., Nagai, T., Miyawaki, A., and Hayashi, Y. (2004). Rapid and persistent modulation of actin dynamics regulates postsynaptic reorganization underlying bidirectional plasticity. Nat. Neurosci. *7*, 1104–1112.

Okamoto, K.-I., Narayanan, R., Lee, S.H., Murata, K., and Hayashi, Y. (2007). The role of CaMKII as an F-actin-bundling protein crucial for maintenance of dendritic spine structure. Proc. Natl. Acad. Sci. U. S. A. *104*, 6418–6423.

Opazo, P., Labrecque, S., Tigaret, C.M., Frouin, A., Wiseman, P.W., De Koninck, P., and Choquet, D. (2010). CaMKII triggers the diffusional trapping of surface AMPARs through phosphorylation of stargazin. Neuron *67*, 239–252.

Ouyang, Y., Wong, M., Capani, F., Rensing, N., Lee, C.-S., Liu, Q., Neusch, C., Martone, M.E., Wu, J.Y., Yamada, K., et al. (2005). Transient decrease in F-actin may be necessary for translocation of proteins into dendritic spines. Eur. J. Neurosci. *22*, 2995–3005.

Panatier, A., Theodosis, D.T., Mothet, J.-P., Touquet, B., Pollegioni, L., Poulain, D. a, and Oliet, S.H.R. (2006). Glia-derived D-serine controls NMDA receptor activity and synaptic memory. Cell *125*, 775–784.

Papa, M., and Segal, M. (1996). Morphological plasticity in dendritic spines of cultured hippocampal neurons. Neuroscience *71*, 1005–1011.

Park, E., Na, M., Choi, J., Kim, S., Lee, J.-R., Yoon, J., Park, D., Sheng, M., and Kim, E. (2003). The Shank family of postsynaptic density proteins interacts with and promotes synaptic accumulation of the beta PIX guanine nucleotide exchange factor for Rac1 and Cdc42. J. Biol. Chem. *278*, 19220–19229.

Park, M., Penick, E.C., Edwards, J.G., Kauer, J. a, and Ehlers, M.D. (2004). Recycling endosomes supply AMPA receptors for LTP. Science *305*, 1972–1975.

Park, M., Salgado, J.M., Ostroff, L., Helton, T.D., Robinson, C.G., Harris, K.M., and Ehlers, M.D. (2006). Plasticity-induced growth of dendritic spines by exocytic trafficking from recycling endosomes. Neuron *52*, 817–830.

Parnas, D., Haghighi, A.P., Fetter, R.D., Kim, S.W., and Goodman, C.S. (2001). Regulation of postsynaptic structure and protein localization by the Rho-type guanine nucleotide exchange factor dPix. Neuron *32*, 415–424.

Pathak, H.R., Weissinger, F., Terunuma, M., Carlson, G.C., Hsu, F., Moss, S.J., and Coulter, D.A. (2007). Disrupted dentate granule cell chloride regulation enhances synaptic excitability during development of temporal lobe epilepsy. J. Neurosci. *27*, 14012–14022.

Patterson, M.A., Szatmari, E.M., and Yasuda, R. (2010). AMPA receptors are exocytosed in stimulated spines and adjacent dendrites in a Ras-ERK-dependent manner during long-term potentiation. Proc. Natl. Acad. Sci. U. S. A. *107*, 15951–15956.

Payne, J.A. (1997). Functional characterization of the neuronal-specific K-Cl cotransporter: implications for [K+]o regulation. Am. J. Physiol. *273*, C1516–C1525.

Payne, J. a, Rivera, C., Voipio, J., and Kaila, K. (2003). Cation-chloride co-transporters in neuronal communication, development and trauma. Trends Neurosci. *26*, 199–206.

Payne, J. a., Stevenson, T.J., and Donaldson, L.F. (1996). Molecular characterization of a putative K-Cl cotransporter in rat brain. A neuronal-specific isoform. J. Biol. Chem. *271*, 16245–16252.

Pellegrino, C., Gubkina, O., Schaefer, M., Becq, H., Ludwig, A., Mukhtarov, M., Chudotvorova, I., Corby, S., Salyha, Y., Salozhin, S., et al. (2011). Knocking down of the KCC2 in rat hippocampal neurons increases intracellular chloride concentration and compromises neuronal survival. J. Physiol. *589*, 2475–2496.

Perkel, D.J., and Nicoll, R.A. (1993). Evidence for all-or-none regulation of neurotransmitter release: implications for long-term potentiation. J. Physiol. *471*, 481–500.

Petrini, E.M., Lu, J., Cognet, L., Lounis, B., Ehlers, M.D., and Choquet, D. (2009). Endocytic Trafficking and Recycling Maintain a Pool of Mobile Surface AMPA Receptors Required for Synaptic Potentiation. Neuron *63*, 92–105.

Piala, A.T., Moon, T.M., Akella, R., He, H., Cobb, M.H., and Goldsmith, E.J. (2014). Chloride sensing by WNK1 involves inhibition of autophosphorylation. Sci. Signal. *7*, ra41.

Plant, K., Pelkey, K. a, Bortolotto, Z.A., Morita, D., Terashima, A., McBain, C.J., Collingridge, G.L., and Isaac, J.T.R. (2006). Transient incorporation of native GluR2-lacking AMPA receptors during hippocampal long-term potentiation. Nat. Neurosci. *9*, 602–604.

Plotkin, M.D., Snyder, E.Y., Hebert, S.C., and Delpire, E. (1997). Expression of the Na-K-2Cl cotransporter is developmentally regulated in postnatal rat brains: a possible mechanism underlying GABA's excitatory role in immature brain. J. Neurobiol. *33*, 781–795.

Price, G.D., and Trussell, L.O. (2006). Estimate of the chloride concentration in a central glutamatergic terminal: a gramicidin perforated-patch study on the calyx of Held. J. Neurosci. *26*, 11432–11436.

Price, T.J., Cervero, F., Gold, M.S., Hammond, D.L., and Prescott, S. a (2009). Chloride regulation in the pain pathway. Brain Res. Rev. *60*, 149–170.

Pugh, J.R., and Jahr, C.E. (2011). Axonal GABAA receptors increase cerebellar granule cell excitability and synaptic activity. J. Neurosci. *31*, 565–574.

Pugh, J.R., and Jahr, C.E. (2013). Activation of axonal receptors by GABA spillover increases somatic firing. J. Neurosci. *33*, 16924–16929.

Puskarjov, M., Ahmad, F., Kaila, K., and Blaesse, P. (2012). Activity-dependent cleavage of the K-Cl cotransporter KCC2 mediated by calcium-activated protease calpain. J. Neurosci. *32*, 11356–11364.

Puskarjov, M., Seja, P., Heron, S.E., Williams, T.C., Ahmad, F., Iona, X., Oliver, K.L., Grinton, B.E., Vutskits, L., Scheffer, I.E., et al. (2014a). A variant of KCC2 from patients with febrile seizures impairs neuronal Cl- extrusion and dendritic spine formation. EMBO Rep. *15*, 723–729.

Puskarjov, M., Ahmad, F., Khirug, S., Sivakumaran, S., Kaila, K., and Blaesse, P. (2014b). BDNF is required for seizure-induced but not developmental up-regulation of KCC2 in the neonatal hippocampus. Neuropharmacology 3–9.

Raimondo, J. V, Joyce, B., Kay, L., Schlagheck, T., Newey, S.E., Srinivas, S., and Akerman, C.J. (2013). A genetically-encoded chloride and pH sensor for dissociating ion dynamics in the nervous system. Front. Cell. Neurosci. *7*, 202.

Rathje, M., Fang, H., Bachman, J.L., Anggono, V., Gether, U., Huganir, R.L., and Madsen, K.L. (2013). AMPA receptor pHluorin-GluA2 reports NMDA receptor-induced intracellular acidification in hippocampal neurons. Proc. Natl. Acad. Sci. U. S. A. *110*, 14426–14431.

Reisel, D., Bannerman, D.M., Schmitt, W.B., Deacon, R.M.J., Flint, J., Borchardt, T., Seeburg, P.H., and Rawlins, J.N.P. (2002). Spatial memory dissociations in mice lacking GluR1. Nat. Neurosci. *5*, 868–873.

Reymann, K.G., and Frey, J.U. (2007). The late maintenance of hippocampal LTP: requirements, phases, “synaptic tagging”, “late-associativity” and implications. Neuropharmacology *52*, 24–40.

Rheims, S., Holmgren, C.D., Chazal, G., Mulder, J., Harkany, T., Zilberter, T., and Zilberter, Y. (2009). GABA action in immature neocortical neurons directly depends on the availability of ketone bodies. J. Neurochem. *110*, 1330–1338.

Riedl, J., Crevenna, A.H., Kessenbrock, K., Yu, J.H., Neukirchen, D., Bista, M., Bradke, F., Jenne, D., Holak, T.A., Werb, Z., et al. (2008). Lifeact: a versatile marker to visualize F-actin. Nat. Methods *5*, 605–607.

Riekki, R., Pavlov, I., Tornberg, J., Lauri, S.E., Airaksinen, M.S., and Taira, T. (2008). Altered synaptic dynamics and hippocampal excitability but normal long-term plasticity in mice lacking hyperpolarizing GABA A receptor-mediated inhibition in CA1 pyramidal neurons. J. Neurophysiol. *99*, 3075–3089.

Rinehart, J., Maksimova, Y.D., Tanis, J.E., Stone, K.L., Hodson, C. a, Zhang, J., Risinger, M., Pan, W., Wu, D., Colangelo, C.M., et al. (2009). Sites of regulated phosphorylation that control K-Cl cotransporter activity. Cell *138*, 525–536.

Rivera, C., Voipio, J., Payne, J.A., Ruusuvuori, E., Lahtinen, H., Lamsa, K., Pirvola, U., Saarma, M., and Kaila, K. (1999). The K+/Cl- co-transporter KCC2 renders GABA hyperpolarizing during neuronal maturation. Nature *397*, 251–255.

Rivera, C., Li, H., Thomas-Crusells, J., Lahtinen, H., Viitanen, T., Nanobashvili, A., Kokaia, Z., Airaksinen, M.S., Voipio, J., Kaila, K., et al. (2002). BDNF-induced TrkB activation down-regulates the K+-Cl- cotransporter KCC2 and impairs neuronal Cl- extrusion. J. Cell Biol. *159*, 747–752.

Rivera, C., Voipio, J., Thomas-Crusells, J., Li, H., Emri, Z., Sipilä, S., Payne, J. a, Minichiello, L., Saarma, M., and Kaila, K. (2004). Mechanism of activity-dependent downregulation of the neuron-specific K-Cl cotransporter KCC2. J. Neurosci. *24*, 4683–4691.

Rocca, D.L.L., Amici, M., Antoniou, A., Blanco Suarez, E., Halemani, N., Murk, K., McGarvey, J., Jaafari, N., Mellor, J.R.R., Collingridge, G.L.L., et al. (2013). The Small GTPase Arf1 Modulates Arp2/3-Mediated Actin Polymerization via PICK1 to Regulate Synaptic Plasticity. Neuron *79*, 293–307.

Roche, K.W., O’Brien, R.J., Mammen, A.L., Bernhardt, J., and Huganir, R.L. (1996). Characterization of Multiple Phosphorylation Sites on the AMPA Receptor GluR1 Subunit. Neuron *16*, 1179–1188.

Rose, J., Jin, S.-X., and Craig, A.M. (2009). Heterosynaptic molecular dynamics: locally induced propagating synaptic accumulation of CaM kinase II. Neuron *61*, 351–358.

Le Roux, N., Cabezas, C., Böhm, U.L., and Poncer, J.C. (2013). Input-specific learning rules at excitatory synapses onto hippocampal parvalbumin-expressing interneurons. J. Physiol. *591*, 1809–1822.

Rumpel, S., LeDoux, J., Zador, A., and Malinow, R. (2005). Postsynaptic receptor trafficking underlying a form of associative learning. Science *308*, 83–88.

Rust, M.B., Gurniak, C.B., Renner, M., Vara, H., Morando, L., Görlich, A., Sassoè-Pognetto, M., Banchaabouchi, M. Al, Giustetto, M., Triller, A., et al. (2010). Learning, AMPA receptor mobility and synaptic plasticity depend on n-cofilin-mediated actin dynamics. EMBO J. *29*, 1889–1902.

Rutherford, L.C., Nelson, S.B., and Turrigiano, G.G. (1998). BDNF has opposite effects on the quantal amplitude of pyramidal neuron and interneuron excitatory synapses. Neuron *21*, 521–530.

Ruusuvuori, E., Kirilkin, I., Pandya, N., and Kaila, K. (2010). Spontaneous network events driven by depolarizing GABA action in neonatal hippocampal slices are not attributable to deficient mitochondrial energy metabolism. J. Neurosci. *30*, 15638–15642.

Saadi, R.A., He, K., Hartnett, K.A., Kandler, K., Hershfinkel, M., and Aizenman, E. (2012). SNARE-dependent upregulation of potassium chloride co-transporter 2 activity after metabotropic zinc receptor activation in rat cortical neurons in vitro. Neuroscience *210*, 38–46.

Saier, M.H. (2003). Tracing pathways of transport protein evolution. Mol. Microbiol. *48*, 1145–1156.

Sanabria, H., Swulius, M.T., Kolodziej, S.J., Liu, J., and Waxham, M.N. (2009). {beta}CaMKII regulates actin assembly and structure. J. Biol. Chem. *284*, 9770–9780.

Saneyoshi, T., Wayman, G., Fortin, D., Davare, M., Hoshi, N., Nozaki, N., Natsume, T., and Soderling, T.R. (2008). Activity-dependent synaptogenesis: regulation by a CaM-kinase kinase/CaM-kinase I/betaPIX signaling complex. Neuron *57*, 94–107.

Saneyoshi, T., Fortin, D. a, and Soderling, T.R. (2010). Regulation of spine and synapse formation by activity-dependent intracellular signaling pathways. Curr. Opin. Neurobiol. *20*, 108–115.

Seja, P., Schonewille, M., Spitzmaul, G., Badura, A., Klein, I., Rudhard, Y., Wisden, W., Hübner, C. a, De Zeeuw, C.I., and Jentsch, T.J. (2012). Raising cytosolic Cl- in cerebellar granule cells affects their excitability and vestibulo-ocular learning. EMBO J. *31*, 1217–1230.

Sharma, K., Fong, D.K., and Craig, A.M. (2006). Postsynaptic protein mobility in dendritic spines: long-term regulation by synaptic NMDA receptor activation. Mol. Cell. Neurosci. *31*, 702–712.

Shen, K., Teruel, M.N., Connor, J.H., Shenolikar, S., and Meyer, T. (2000a). Molecular memory by reversible translocation of calcium/calmodulin-dependent protein kinase II. Nat. Neurosci. *3*, 881–886.

Shen, L., Liang, F., Walensky, L.D., and Huganir, R.L. (2000b). Regulation of AMPA receptor GluR1 subunit surface expression by a 4. 1N-linked actin cytoskeletal association. J. Neurosci. *20*, 7932–7940.

Shi, S.H., Hayashi, Y., Petralia, R.S., Zaman, S.H., Wenthold, R.J., Svoboda, K., and Malinow, R. (1999). Rapid spine delivery and redistribution of AMPA receptors after synaptic NMDA receptor activation. Science *284*, 1811–1816.

Shi, Y., Suh, Y.H., Milstein, A.D., Isozaki, K., Schmid, S.M., Roche, K.W., and Nicoll, R. a (2010). Functional comparison of the effects of TARPs and cornichons on AMPA receptor trafficking and gating. Proc. Natl. Acad. Sci. U. S. A. *107*, 16315–16319.

Shin, E.-Y., Shin, K.-S., Lee, C.-S., Woo, K.-N., Quan, S.-H., Soung, N.-K., Kim, Y.G., Cha, C.I., Kim, S.-R., Park, D., et al. (2002). Phosphorylation of p85 beta PIX, a Rac/Cdc42-specific guanine nucleotide exchange factor, via the

Ras/ERK/PAK2 pathway is required for basic fibroblast growth factor-induced neurite outgrowth. J. Biol. Chem. *277*, 44417–44430.

Smith, K.R., Davenport, E.C., Wei, J., Li, X., Pathania, M., Vaccaro, V., Yan, Z., and Kittler, J.T. (2014). GIT1 and βPIX Are Essential for GABAA Receptor Synaptic Stability and Inhibitory Neurotransmission. Cell Rep. *9*, 298–310.

Staley, K.J., and Mody, I. (1992). Shunting of excitatory input to dentate gyrus granule cells by a depolarizing GABAA receptor-mediated postsynaptic conductance. J. Neurophysiol. *68*, 197–212.

Staley, K.J., Soldo, B.L., and Proctor, W.R. (1995). Ionic mechanisms of neuronal excitation by inhibitory GABAA receptors. Science *269*, 977–981.

Steinberg, J.P., Takamiya, K., Shen, Y., Xia, J., Rubio, M.E., Yu, S., Jin, W., Thomas, G.M., Linden, D.J., and Huganir, R.L. (2006). Targeted in vivo mutations of the AMPA receptor subunit GluR2 and its interacting protein PICK1 eliminate cerebellar long-term depression. Neuron *49*, 845–860.

Steiner, P., Higley, M.J., Xu, W., Czervionke, B.L., Malenka, R.C., and Sabatini, B.L. (2008). Destabilization of the postsynaptic density by PSD-95 serine 73 phosphorylation inhibits spine growth and synaptic plasticity. Neuron *60*, 788–802.

Stewart, M.G., Medvedev, N.I., Popov, V.I., Schoepfer, R., Davies, H. a, Murphy, K., Dallérac, G.M., Kraev, I. V, and Rodríguez, J.J. (2005). Chemically induced long-term potentiation increases the number of perforated and complex postsynaptic densities but does not alter dendritic spine volume in CA1 of adult mouse hippocampal slices. Eur. J. Neurosci. *21*, 3368–3378.

Strange, K., Singer, T.D., Morrison, R., and Delpire, E. (2000). Dependence of KCC2 K-Cl cotransporter activity on a conserved carboxy terminus tyrosine residue. Am. J. Physiol. Cell Physiol. *279*, C860–C867.

Takahashi, T., Svoboda, K., and Malinow, R. (2003). Experience strengthening transmission by driving AMPA receptors into synapses. Science *299*, 1585–1588.

Takasaki, K., and Sabatini, B.L. (2014). Super-resolution 2-photon microscopy reveals that the morphology of each dendritic spine correlates with diffusive but not synaptic properties. Front. Neuroanat. *8*, 29.

Tanaka, H., and Hirano, T. (2012). Visualization of subunit-specific delivery of glutamate receptors to postsynaptic membrane during hippocampal long-term potentiation. Cell Rep. *1*, 291–298.

Tardin, C., Cognet, L., Bats, C., Lounis, B., and Choquet, D. (2003). Direct imaging of lateral movements of AMPA receptors inside synapses. EMBO J. *22*, 4656–4665.

Tatavarty, V., Kim, E.-J., Rodionov, V., and Yu, J. (2009). Investigating sub-spine actin dynamics in rat hippocampal neurons with super-resolution optical imaging. PLoS One *4*, e7724.

Terashima, A., Pelkey, K. a, Rah, J.-C., Suh, Y.H., Roche, K.W., Collingridge, G.L., McBain, C.J., and Isaac, J.T.R. (2008). An essential role for PICK1 in NMDA receptor-dependent bidirectional synaptic plasticity. Neuron *57*, 872–882.

Thompson, S.M., Deisz, R. a, and Prince, D. a (1988). Outward chloride/cation co-transport in mammalian cortical neurons. Neurosci. Lett. *89*, 49–54.

Tønnesen, J., Katona, G., Rózsa, B., and Nägerl, U.V. (2014). Spine neck plasticity regulates compartmentalization of synapses. Nat. Neurosci. *17*, 678–685.

Tornberg, J., Voikar, V., Savilahti, H., Rauvala, H., and Airaksinen, M.S. (2005). Behavioural phenotypes of hypomorphic KCC2-deficient mice. Eur. J. Neurosci. *21*, 1327–1337.

Traynelis, S.F., Hartley, M., and Heinemann, S.F. (1995). Control of proton sensitivity of the NMDA receptor by RNA splicing and polyamines. Science *268*, 873–876.

Turrigiano, G.G. (2008). The self-tuning neuron: synaptic scaling of excitatory synapses. Cell *135*, 422–435.

Tyzio, R., Cossart, R., Khalilov, I., Minlebaev, M., Hübner, C. a, Represa, A., Ben-Ari, Y., and Khazipov, R. (2006). Maternal oxytocin triggers a transient inhibitory switch in GABA signaling in the fetal brain during delivery. Science *314*, 1788–1792.

Tyzio, R., Allene, C., Nardou, R., Picardo, M. a, Yamamoto, S., Sivakumaran, S., Caiati, M.D., Rheims, S., Minlebaev, M., Milh, M., et al. (2011). Depolarizing actions of GABA in immature neurons depend neither on ketone bodies nor on pyruvate. J. Neurosci. *31*, 34–45.

Tyzio, R., Nardou, R., Ferrari, D.C., Tsintsadze, T., Shahrokhi, A., Eftekhari, S., Khalilov, I., Tsintsadze, V., Brouchoud, C., Chazal, G., et al. (2014). Oxytocin-Mediated GABA Inhibition During Delivery Attenuates Autism Pathogenesis in Rodent Offspring. Science *343*, 675–679.

Urban, N.T., Willig, K.I., Hell, S.W., and Nägerl, U.V. (2011). STED Nanoscopy of Actin Dynamics in Synapses Deep Inside Living Brain Slices. Biophys. J. *101*, 1277–1284.

Uvarov, P., Ludwig, A., Markkanen, M., Rivera, C., and Airaksinen, M.S. (2006). Upregulation of the neuron-specific K+/Cl- cotransporter expression by transcription factor early growth response 4. J. Neurosci. *26*, 13463–13473.

Uvarov, P., Ludwig, A., Markkanen, M., Pruunsild, P., Kaila, K., Delpire, E., Timmusk, T., Rivera, C., and Airaksinen, M.S. (2007). A novel N-terminal isoform of the neuron-specific K-Cl cotransporter KCC2. J. Biol. Chem. *282*, 30570–30576.

Uvarov, P., Ludwig, A., Markkanen, M., Soni, S., Hübner, C. a, Rivera, C., and Airaksinen, M.S. (2009). Coexpression and heteromerization of two neuronal K-Cl cotransporter isoforms in neonatal brain. J. Biol. Chem. *284*, 13696–13704.

Vardi, N., Zhang, L.L., Payne, J.A., and Sterling, P. (2000). Evidence that different cation chloride cotransporters in retinal neurons allow opposite responses to GABA. J. Neurosci. *20*, 7657–7663.

Vicario-Abejón, C., Collin, C., Mckay, R.D.G., Segal, M., and Vicario-abejo, C. (1998). Neurotrophins induce formation of functional excitatory and inhibitory synapses between cultured hippocampal neurons. J. Neurosci. *18*, 7256–7271.

Vicidomini, G., Moneron, G., Han, K.Y., Westphal, V., Ta, H., Reuss, M., Engelhardt, J., Eggeling, C., and Hell, S.W. (2011). Sharper low-power STED nanoscopy by time gating. Nat. Methods *8*, 571–573.

Viitanen, T., Ruusuvuori, E., Kaila, K., and Voipio, J. (2010). The K+-Cl cotransporter KCC2 promotes GABAergic excitation in the mature rat hippocampus. J. Physiol. *588*, 1527–1540.

Vilen, H., Eerikäinen, S., Tornberg, J., Airaksinen, M.S., and Savilahti, H. (2001). Construction of gene-targeting vectors: a rapid Mu in vitro DNA transposition-based strategy generating null, potentially hypomorphic, and conditional alleles. Transgenic Res. *10*, 69–80.

Vinay, L., and Jean-Xavier, C. (2008). Plasticity of spinal cord locomotor networks and contribution of cation-chloride cotransporters. Brain Res. Rev. *57*, 103–110.

Wake, H., Watanabe, M., Moorhouse, A.J., Kanematsu, T., Horibe, S., Matsukawa, N., Asai, K., Ojika, K., Hirata, M., and Nabekura, J. (2007). Early changes in KCC2 phosphorylation in response to neuronal stress result in functional downregulation. J. Neurosci. *27*, 1642–1650.

Wang, D.S., and Shaw, G. (1995). The association of the C-terminal region of beta I sigma II spectrin to brain membranes is mediated by a PH domain, does not require membrane proteins, and coincides with a inositol-1,4,5 triphosphate binding site. Biochem. Biophys. Res. Commun. *217*, 608–615.

Wang, W., Gong, N., and Xu, T.-L. (2006). Downregulation of KCC2 following LTP contributes to EPSP-spike potentiation in rat hippocampus. Biochem. Biophys. Res. Commun. *343*, 1209–1215.

Wang, Y., Dong, Q., Xu, X.-F., Feng, X., Xin, J., Wang, D.-D., Yu, H., Tian, T., and Chen, Z.-Y. (2013). Phosphorylation of cofilin regulates extinction of conditioned aversive memory via AMPAR trafficking. J. Neurosci. *33*, 6423–6433.

Wang, Z., Edwards, J.G., Riley, N., Provance, D.W., Karcher, R., Li, X.-D., Davison, I.G., Ikebe, M., Mercer, J. a, Kauer, J. a, et al. (2008). Myosin Vb mobilizes recycling endosomes and AMPA receptors for postsynaptic plasticity. Cell *135*, 535–548.

Warmuth, S., Zimmermann, I., and Dutzler, R. (2009). X-ray structure of the C-terminal domain of a prokaryotic cation-chloride cotransporter. Structure *17*, 538–546.

Watanabe, M., Wake, H., Moorhouse, A.J., and Nabekura, J. (2009). Clustering of neuronal K+-Cl- cotransporters in lipid rafts by tyrosine phosphorylation. J. Biol. Chem. *284*, 27980–27988.

Wei, W.-C., Akerman, C.J., Newey, S.E., Pan, J., Clinch, N.W. V, Jacob, Y., Shen, M.-R., Wilkins, R.J., and Ellory, J.C. (2011). The potassium-chloride cotransporter 2 promotes cervical cancer cell migration and invasion by an ion transport-independent mechanism. J. Physiol. *589*, 5349–5359.

Weisskopf, M.G., and Nicoll, R.A. (1995). Presynaptic changes during mossy fibre LTP revealed by NMDA receptor-mediated synaptic responses. Nature *376*, 256–259.

Wenthold, R.J., Petralia, R.S., Blahos J, I.I., and Niedzielski, A.S. (1996). Evidence for multiple AMPA receptor complexes in hippocampal CA1/CA2 neurons. J. Neurosci. *16*, 1982–1989.

Wenz, M., Hartmann, A.-M., Friauf, E., and Nothwang, H.G. (2009). CIP1 is an activator of the K+-Cl- cotransporter KCC2. Biochem. Biophys. Res. Commun. *381*, 388–392.

Whitlock, J.R., Heynen, A.J., Shuler, M.G., and Bear, M.F. (2006). Learning induces long-term potentiation in the hippocampus. Science *313*, 1093–1097.

Willard, S.S., and Koochekpour, S. (2013). Glutamate, glutamate receptors, and downstream signaling pathways. Int. J. Biol. Sci. *9*, 948–959.

Williams, J.R., Sharp, J.W., Kumari, V.G., Wilson, M., and Payne, J.A. (1999a). The Neuron-specific K-Cl Cotransporter, KCC2. J. Biol. Chem. *274*, 12656–12664.

Williams, J.R., Sharp, J.W., Kumari, V.G., Wilson, M., and Payne, J.A. (1999b). The neuron-specific K-Cl cotransporter, KCC2. Antibody development and initial characterization of the protein. J. Biol. Chem. *274*, 12656–12664.

Woo, N.-S., Lu, J., England, R., McClellan, R., Dufour, S., Mount, D.B., Deutch, A.Y., Lovinger, D.M., and Delpire, E. (2002). Hyperexcitability and epilepsy associated with disruption of the mouse neuronal-specific K-Cl cotransporter gene. Hippocampus *12*, 258–268.

Woodin, M. a, Ganguly, K., and Poo, M. (2003). Coincident pre- and postsynaptic activity modifies GABAergic synapses by postsynaptic changes in Cl- transporter activity. Neuron *39*, 807–820.

Wyszynski, M., Valtschanoff, J.G., Naisbitt, S., Dunah, A.W., Kim, E., Standaert, D.G., Weinberg, R., and Sheng, M. (1999). Association of AMPA receptors with a subset of glutamate receptor-interacting protein in vivo. J. Neurosci. *19*, 6528–6537.

Xia, J., Zhang, X., Staudinger, J., and Huganir, R.L. (1999). Clustering of AMPA receptors by the synaptic PDZ domain-containing protein PICK1. Neuron *22*, 179–187.

Xie, Z., Srivastava, D.P., Photowala, H., Kai, L., Cahill, M.E., Woolfrey, K.M., Shum, C.Y., Surmeier, D.J., and Penzes, P. (2007). Kalirin-7 controls activity-dependent structural and functional plasticity of dendritic spines. Neuron *56*, 640–656.

Xu, W. (2011). PSD-95-like membrane associated guanylate kinases (PSD-MAGUKs) and synaptic plasticity. Curr. Opin. Neurobiol. *21*, 306–312.

Xu, J.C., Lytle, C., Zhu, T.T., Payne, J. a, Benz, E., and Forbush, B. (1994). Molecular cloning and functional expression of the bumetanide-sensitive Na-K-Cl cotransporter. Proc. Natl. Acad. Sci. U. S. A. *91*, 2201–2205.

Yamada, M.K., Nakanishi, K., Ohba, S., Nakamura, T., Ikegaya, Y., Nishiyama, N., and Matsuki, N. (2002). Brain-derived neurotrophic factor promotes the maturation of GABAergic mechanisms in cultured hippocampal neurons. J. Neurosci. *22*, 7580–7585.

Yang, B., Tadavarty, R., Xu, J.-Y., and Sastry, B.R. (2010). Activity-mediated plasticity of GABA equilibrium potential in rat hippocampal CA1 neurons. Exp. Neurol. *221*, 157–165.

Yang, G., Pan, F., and Gan, W. (2009). Stably maintained dendritic spines are associated with lifelong memories. Nature *462*, 920–924.

Yang, Y., Wang, X., Frerking, M., and Zhou, Q. (2008). Spine expansion and stabilization associated with long-term potentiation. J. Neurosci. *28*, 5740–5751.

Yashiro, K., and Philpot, B.D. (2008). Regulation of NMDA receptor subunit expression and its implications for LTD, LTP, and metaplasticity. Neuropharmacology *55*, 1081–1094.

Yeo, M., Berglund, K., Augustine, G., and Liedtke, W. (2009). Novel repression of Kcc2 transcription by REST-RE-1 controls developmental switch in neuronal chloride. J. Neurosci. *29*, 14652–14662.

Yuste, R. (2013). Electrical compartmentalization in dendritic spines. Annu. Rev. Neurosci. *36*, 429–449.

Zeuthen, T. (2010). Water-transporting proteins. J. Membr. Biol. *234*, 57–73.

Zeuthen, T., and MacAulay, N. (2002). Cotransporters as molecular water pumps. Int. Rev. Cytol. *215*, 259–284.

Zhang, D., Isack, N.R., Glodowski, D.R., Liu, J., Chen, C.C.-H., Xu, X.Z.S., Grant, B.D., and Rongo, C. (2012). RAB-6.2 and the retromer regulate glutamate receptor recycling through a retrograde pathway. J. Cell Biol. *196*, 85–101.

Zhang, H., Webb, D.J., Asmussen, H., and Horwitz, A.F. (2003). Synapse formation is regulated by the signaling adaptor GIT1. J. Cell Biol. *161*, 131–142.

Zhang, J., Wang, Y., Chi, Z., Keuss, M.J., Pai, Y.-M.E., Kang, H.C., Shin, J.-H., Bugayenko, A., Wang, H., Xiong, Y., et al. (2011). The AAA+ ATPase Thorase regulates AMPA receptor-dependent synaptic plasticity and behavior. Cell *145*, 284–299.

Zhang, R., Zhang, S., and Du, J. (2013). KCC2-dependent subcellular E(Cl) difference of ON-OFF retinal ganglion cells in larval zebrafish. Front. Neural Circuits *7*, 103.

Zhao, B., Wong, A.Y.C., Murshid, A., Bowie, D., Presley, J.F., and Bedford, F.K. (2008). Identification of a novel di-leucine motif mediating K(+)/Cl(-) cotransporter KCC2 constitutive endocytosis. Cell. Signal. *20*, 1769–1779.

Zheng, C.-Y., Seabold, G.K., Horak, M., and Petralia, R.S. (2011). MAGUKs, synaptic development, and synaptic plasticity. Neuroscientist *17*, 493–512.

Zhou, H.-Y., Chen, S.-R., Byun, H.-S., Chen, H., Li, L., Han, H.-D., Lopez-Berestein, G., Sood, A.K., and Pan, H.-L. (2012). N-methyl-D-aspartate receptor- and calpain-mediated proteolytic cleavage of K+-Cl- cotransporter-2 impairs spinal chloride homeostasis in neuropathic pain. J. Biol. Chem. *287*, 33853–33864.

Zhu, J.J., Esteban, J. a, Hayashi, Y., and Malinow, R. (2000). Postnatal synaptic potentiation: delivery of GluR4-containing AMPA receptors by spontaneous activity. Nat. Neurosci. *3*, 1098–1106.

Zhu, J.J., Qin, Y., Zhao, M., Van Aelst, L., and Malinow, R. (2002). Ras and Rap control AMPA receptor trafficking during synaptic plasticity. Cell *110*, 443–455.

Zhu, L., Lovinger, D., and Delpire, E. (2005). Cortical neurons lacking KCC2 expression show impaired regulation of intracellular chloride. J. Neurophysiol. *93*, 1557–1568.

Zhu, L., Polley, N., Mathews, G.C., and Delpire, E. (2008). NKCC1 and KCC2 prevent hyperexcitability in the mouse hippocampus. Epilepsy Res. *79*, 201–212.

Ziff, E.B. (2007). TARPs and the AMPA receptor trafficking paradox. Neuron *53*, 627–633.

Zito, K., Scheuss, V., Knott, G., Hill, T., and Svoboda, K. (2009). Rapid functional maturation of nascent dendritic spines. Neuron *61*, 247–258.

Ziv, N.E., and Smith, S.J. (1996). Evidence for a role of dendritic filopodia in synaptogenesis and spine formation. Neuron *17*, 91–102.